Antiviral responses of Xela DS2 and Xela VS2, two newly established *Xenopus laevis* skin epithelial-like cell lines, to viral dsRNA and Frog Virus 3

by

Maxwell Papadopoulos Bui-Marinos

A thesis

presented to the University of Waterloo

in fulfillment of the

thesis requirements for the degree of

Master of Science

in

Biology

Waterloo, Ontario, Canada, 2019

Author's Declaration

I hereby declare that I am the sole author of this thesis and consists of material all of which I authored. This is a true copy of the thesis, including any final revisions, as accepted by my examiners.

I understand that my thesis may be made electronically available to the public.

Statement of Contributions

This thesis is composed of 4 chapters; 1 introductory chapter, 2 data chapters, and 1 concluding discussion chapter. In Chapter 1, Section 1.3 was adapted from a review article that was previously published entitled “Frog skin innate immune defences: sensing and surviving pathogens” by Joseph F. A. Varga, Maxwell P. Bui-Marinos, and Barbara A. Katzenback (Varga et al., 2019). Parts of this review which were adapted into this thesis were written exclusively by the thesis author, Maxwell P. Bui-Marinos. The 2 data chapters, Chapter 2 and Chapter 3, have been prepared in a manuscript as they will be submitted for publication. The names of the authors that will be on each respective manuscript and their contributions are listed below. Writing and analysis for all chapters were written solely by the thesis author, Maxwell P. Bui-Marinos, unless otherwise specified.

Chapter 2

Authors: Maxwell P. Bui-Marinos, Joseph F. A. Varga, Nguyen T. K. Vo, Niels C. Bols, Barbara A. Katzenback

Joseph F. A. Varga – performed Hoescht staining of Xela DS2 and Xela VS2 and wrote the accompanying methods (Section 2.2.8) and figure legend (Fig. 2.3), and helped with manual cell counts for determination of Xela DS2 and Xela VS2 optimal growth conditions as described in Section 2.2.9

Nguyen T. K. Vo and Niels C. Bols – provided guidance, workspace and some materials for the initial establishment of Xela DS2 and Xela VS2 as described in Sections 2.2.2 – 2.2.3

Chapter 3

Authors: Maxwell P. Bui-Marinos, Marie-Claire D. Wasson, Barbara A. Katzenback

Marie-Claire D. Wasson – performed viral titre assays on samples as described in Sections 3.2.8, 3.2.10, and 3.2.14

Abstract

There is a current decline in amphibian populations, wherein the emerging pathogen Frog Virus 3 (FV3) is believed to be a proximate cause. The conservation of frog species is thus important as population declines would yield drastic ecological and environmental impacts. Frog skin is an important interface between the frog's external environment and internal milieu and is the first line of defence against pathogen insult. In mammalian models, the skin epithelial layer acts as an important immunological barrier against pathogens and is capable of recognizing and responding to pathogen-associated molecular patterns (PAMPs) and signal to underlying cells that a threat is present. However, the ability and role of frog skin epithelial cells in recognizing and responding to viral PAMPs and FV3 is unknown. To address this, two cell lines from the dorsal skin (Xela DS2) and ventral skin (Xela VS2) of the African clawed frog (*Xenopus laevis*) were established.

Xela DS2 and Xela VS2 were first characterized then used as models to determine whether frog skin epithelial cells exhibit the ability to sense and respond to extracellular dsRNA. Xela DS2 and Xela VS2 cells have an epithelial-like morphology, express genes associated with epithelial cells, and lack beta-galactosidase associated senescence activity. Cells grew optimally in 70% Leibovitz's L-15 medium supplemented with 15% fetal bovine serum at 26°C. Upon treatment with poly(I:C), an analogue for viral dsRNA and known type I interferon (IFN) inducer, Xela DS2 and Xela VS2 exhibited marked upregulation of key antiviral and proinflammatory transcripts, including Type I IFN and the interferon stimulated gene (ISG), protein kinase R (PKR). This suggests that frog skin epithelial cells may participate in the recognition of extracellular dsRNA and production of local inflammatory signals similar to mammalian models.

Once Xela DS2 and Xela VS2 were established as suitable models for the study of frog skin epithelial cell immunity, they were utilized to better understand the FV3-frog skin epithelial cell interaction. Xela DS2 and Xela VS2 are permissive to FV3 infection and support viral replication as seen by the detection of viral transcripts and increase in viral particles released from infected cells over time. The loss of cellular adherence in response to FV3 is a characteristic cytopathic effect (CPE) in Xela DS2 and Xela VS2. Xela DS2 and Xela VS2 appear incapable of initiating antiviral or proinflammatory programs following infection with FV3 or challenge with UV-inactivated FV3, suggesting that FV3 is likely capable of immunoevasion in these cells. Nonetheless, pre-treatment of Xela DS2 and Xela VS2 with poly(I:C) followed by FV3 challenge was able to completely abrogate FV3-induced CPE and limit viral replication. This data demonstrates that despite FV3 being well equipped with immunoevasive strategies and mechanisms for total shutdown of host macromolecular synthesis, FV3 is unable to break an antiviral state in frog skin epithelial-like cell lines.

Overall, Xela DS2 and Xela VS2 are currently the only known frog skin epithelial-like cell lines capable of sensing and responding to viral PAMPs and FV3. Cell line properties, such as plasticity in temperature growth and response to external stimuli, demonstrate that they are excellent models for the *in vitro* study of impacts from environmental stressors (e.g. pathogen insult, contaminants, temperature, etc.) on frog skin epithelial cells. Their ability to sense and respond to extracellular stimuli will also be useful in further elucidating host-pathogen interactions. With the demonstration that FV3 is unable to break an induced antiviral state in Xela DS2 and Xela VS2, we can now begin to further investigate methods and mechanism of mitigating FV3 infection at the skin epithelial barrier.

Acknowledgements

Firstly, thank you to my supervisor Dr. Barb Katzenback. There is so much I wish to say, I don't even know where to begin. You were the first PI I got to work under, and I am the first student you got to mentor; this has been such a unique experience and you have provided me with so much opportunity that I will not take for granted. I have experienced so much growth and gained a lot of knowledge these past years in so many facets. You would always push me to my limits and force me to not just "do" but to think; I know you do this because you see something in me that I don't—I appreciate that so much. At the same time, you consistently went above and beyond your own expectations as a PI to support me. Your patience and understanding towards me is something I will never forget. Most of all, you never gave up on me and always believed in me. Even if I didn't believe it, you would remind me how great of a student, learner, and person I am. I am immensely grateful and hold not a single regret for having gone on this journey, I could not imagine being in this position with any other PI. I am so fortunate.

Thank you to my committee members Dr. Mungo Marsden and Dr. Stephanie DeWitte-Orr. Although our interactions were limited, I cannot envision a better committee that pushed me to gain such a broad range of knowledge and to be versatile in my understanding and thinking. From Mungo's macroscale outlook in looking at the big picture (and throwing a lot of curveballs), to Stephanie's microscale outlook in being very detail oriented and constantly pushing me to think about how I should communicate my science effectively. I am so thankful for your willingness to sit on my committee.

Next, I would like to thank Dr. Niels Bols and Dr. Nathan Vo for disseminating their vast cell culture knowledge to me, in addition to aiding in the establishment of the cell lines I used for my thesis. I would also like to acknowledge Dr. John Pham for having provided guidance, support and knowledge during my times utilizing the Bols Lab space. Thank you to Joseph Varga for aiding in Hoechst staining and manual cell counts; my hunchback, or lack thereof, thanks you as well. Marie-Claire Wasson, a thousand thank yous for aiding with the viral titre assays. My thesis, honestly, would not be what it is if it was not for your help, commitment, and determination.

Thank you to Dr. Paul Craig and Dr. Brian Dixon for instructing the Animal Physiology and Advanced Immunology courses, respectively. I was not the strongest in Biology when I started my M.Sc., but these courses truly helped me bridge a lot of gaps in my understanding; the knowledge I gained will stick with me for life. Also, Brian, I will never forget the generosity and understanding you provided, thank you. To Dr. Cheryl

Duxbury: thank you for your endless support, encouragement and open-door policy for any discussion; conversations with you were some of my favorite during my time here. The words of wisdom which you parted on me will remain as life lessons.

Thank you to all previous and current Katzenback Lab members. Joseph, Quinn, Heather, Nathanael, and Alex: the support and advice you provided throughout my time here, whether school or life related, are things I will hold dear to me. I wish I had enough space to thank every volunteer or 499 students in my years here, but if it were not for you, I would not have learned so much about what it takes to be a mentor. To the great friends I have made on this journey, Joseph, Rebecca and Quinn: I am already missing the near daily conversations we would have, I have learned so much from each of you. Donya, I did not forget about you; I am fortunate to know someone who goes out of their way to gain understanding and introspection in the ways that you do. Your actions speak volumes, and I have an encyclopedia complete with nothing but appreciation for your support and tough love. With near daily coffee sessions and more, you made all this a little bit more bearable and a lot more memorable. A very special thank you goes out to my friends Leonardo, Aisha, Jean, Kim, Erin and Shanice: I don't think I am myself more than when I am around you. You all ground me, my sanity remains in check since you all allow me to express myself in any way shape or form without feeling even a hint of judgment in the air. Words cannot begin to describe my gratitude and love for you.

Thank you to my family for their constant love and support. Mom and Dad: read the next page. To my siblings Young, Vicki and Yoshi: you all constantly inspire me to work my hardest. I look up to each of you so much, for different reasons, and I am very proud to be able to call you family. The ways you demonstrate your support and encouragement mean the world to me; I have the best siblings anyone could ask for.

Carsen: you were my rock—boulder—mountain for majority of my thesis and showed me a new light after being trapped in the dark for so long. I have nothing but immense gratitude and respect for you. Although the storms have weathered down the mountainous range into flat plains, the Earth has been nourished to support a field of flowers between us. Don't pick too many yet, let's wait until the afterglow.

Finally, to everyone mentioned above: you have all been instrumental in orchestrating my success these past years, whether in terms of my academics or personal growth. I am a very sentimental person, and this thesis/these past years means more to me than just the completion of a degree. May this symphony play on for years to come, and then some.

If you are reading this future Max, thank you for staying strong, you know? Trust, you know. Also, try not to feel too embarrassed re-reading this, these people meant/mean a lot to you.

Dedication

I would like to dedicate this thesis to my parents, Van Bui (“coccinelle – ladybug”) and Dennis Marinos (“pigeon”). Ladybugs are symbolic of luck and prosperity, and pigeons are symbolic of sacrifice. I am beyond lucky for the constant support you both provide since I left the nest. The amount of sacrifices you have both made never goes unnoticed – I would not be where I am today if it wasn’t for you. I will translate your sacrifices into a bounteous harvest; may the road ahead hold love and prosperity. Mom, I am thankful everyday for the times you pushed (and still push) me to be a better person, a wiser thinker, and to have unwavering ambition, drive, and perseverance; you were there with/for me every step of the way. Above all else, the unconditional love and understanding you provide has given me the strength to reach for the stars. Hold my hand and let’s shine together, you deserve to.

Table of Contents

List of Figures

List of Tables

List of Abbreviations

AL-15	amphibian Leibovitz L-15 media
ANOVA	analysis of variance
AP-1	activating protein 1
APBS	amphibian phosphate buffered saline
BLASTn	Basic Local Alignment Search Tool: nucleotide
cDNA	complementary deoxyribonucleic acid
cGAS	cyclic GMP-AMP synthase
COI	cytochrome c oxidase I
CPE	cytopathic effect
DMSO	dimethyl sulfoxide
DNA	deoxynucleic acid
DNase	deoxynucleic nuclease
dNTP	deoxyribonucleotide triphosphate
DPBS	Duelbeco's phosphate buffered saline
dpi	days post infection
dsDNA	double-stranded deoxyribonucleic acid
dsRNA	double-stranded ribonucleic acid
EDTA	ethylenediaminetetraacetic acid
EF1α	elongation factor 1 alpha
EMT	epithelial-mesenchymal transition
EPC	epithelioma papulosum cyprini cell line
FBS	fetal bovine serum
FV3	Frog Virus 3
hpi	hours post infection
ICE	interleukin-1 converting enzyme
IFN	interferon
IκB	inhibitor of kappa B
IL	interleukin

IFNAR	interferon alpha receptor
IRF	interferon regulatory factor
ISG	interferon stimulated gene
ISGF3	interferon stimulated gene factor
ISRE	interferon stimulated response element
JAK	janus kinases
KOac	potassium acetate
L-15	Leibovitz media
LB	Luria-Bertani media
MCP	major capsid protein
MDA5	melanoma differentiation-associated protein 5
MOI	multiplicity of infection
MSA	multiple sequence alignment
Mx	myxovirus resistance protein
NCBI	National Centre for Biotechnology Information
NF-κB	nuclear factor kappa B
NTC	no template control
OAS	2'-5'-oligoadenylate synthase
ORF	open reading fram
PAMP	pathogen-associated molecular pattern
PBS	phosphate buffered saline
PCR	polymerase chain reaction
PFU	plaque forming units
PKR	protein kinase R
PL	peritoneal leukocyte
Poly(I:C)	polyinosinic:polycytidylic acid
PRR	pattern recognition receptor
RIG-I	retinoic acid-inducible gene I
RLR	RIG-I-like receptor

RNA	ribonucleic acid
RNase	ribonucleic nuclease
RT-PCR	reverse transcriptase polymerase chain reaction
RT-qPCR	reverse transcriptase quantitative polymerase chain reaction
SOB	Super optimal broth media
SR	scavenger receptor
ssDNA	single-stranded deoxyribonucleic acid
ssRNA	single-stranded ribonucleic acid
STAT	signal transducer and activator of transcription proteins
STING	stimulator of interferon genes
TAE	Tris, acetic acid, EDTA solution
$TCID_{50}$	median tissue culture infective dose at which 50% of cells are infected
TLR	toll-like receptor
TNF	tumor necrosis factor
UV-FV3	UV inactivated FV3
vIF2α	viral initiation factor 2 alpha
Xela BMW3	*Xenopus laevis* bone marrow cell line
Xela DS2	*Xenopus laevis* dorsal skin epithelial-like cell line
Xela VS2	*Xenopus laevis* ventral skin epithelial-like cell line

Chapter 1: Introduction[1]

1.1. Amphibians – importance and population declines

Over 8,000 amphibian species have been discovered to date, with ~150 new species discovered each year (AmphibiaWeb, 2019). Amphibians are vital to the health of ecosystems, acting as both prey and predator, and play an important role in invertebrate pest control (DuRant and Hopkins, 2008). They also participate in important environmental tasks such as nutrient cycling and further act as sentinels of environmental health and toxicity (Beard et al., 2002; Showell and Conlon, 2009). Frogs, particularly the model organism *Xenopus laevis*, have been used widely in research for understanding physiological and developmental processes (Kay and Peng, 1992) and for the study of human diseases, such as cystic fibrosis (Tucker et al., 1992). Many advancements in human health have been made by studying frog species, such as understanding the impact of toxic compounds on hormone function, or identification and isolation of skin antimicrobial peptides (AMPs) which have broad action against many mammalian pathogens (Hinther et al., 2011; Miyata and Ose, 2012; Showell and Conlon, 2009; Varga et al., 2019). Amphibian species are clearly integral not only to sustain ecological and environmental well-being, but also in the context of being key models for the study of human health.

Currently, 32.5% of global amphibian populations are categorized as vulnerable, endangered, or critically endangered, with 43.2% of amphibian populations experiencing some form of population decline (AmphibiaWeb, 2019; Stuart et al., 2004). Although amphibian population decline etiology is complex, including habitat loss, overexploitation, chemical contaminants, and climate change, emerging infectious diseases, such as Frog Virus

[1] A version of the frog skin structure has been published in Varga, J.F.A., Bui-Marinos, M.P., Katzenback, B.A. 2019. Frog skin innate immune defences: sensing and surviving pathogens. *Front Immunol* 9.

3 (FV3) and *Batrachochytrium dendrobatidis*, are believed to be the proximate cause (Blaustein et al., 2010a; Stuart et al., 2004; Young et al., 2001). Ranaviruses, in general, have been identified in at least 105 amphibian species in 25 countries, with recent evidence of FV3-related mass die-offs in North America (Duffus et al., 2015; Gray et al., 2007; Greer et al., 2005). Varying susceptibility of frog species to FV3 infection has been documented (Duffus et al., 2015), but key symptoms from infection include the formation of skin lesions, swelling, internal hemorrhaging, and induction of necrosis and liquefaction of liver, spleen, renal tubule, hematopoietic tissue and lymphoid tissue (Forzán et al., 2017; Miller et al., 2007; Robert et al., 2005). FV3 infections have high death rates (80-90% mortality) in infected tadpoles, suggesting a predicted negative impact on amphibian numbers by impairing future reproductive capacity (Daszak et al., 2003). FV3 outbreaks adversely affects frog populations with specialized habitats due to low adaptability or populations that have low fecundity (Daszak et al., 2003). The rapid loss of amphibian biodiversity can yield drastic ecological and environmental impacts such as the collapse of predator-prey systems affecting food chain dynamics (Stuart et al., 2004), signalling a critical need to understand frog-FV3-environment interactions in order to further amphibian conservation efforts.

1.2. Frog Virus 3 infection and transmission

Frog Virus 3, the type species of Family *Iridoviridae*, Genus *Ranavirus*, is a large (~200 nm) dsDNA virus containing a 100-106 kb genome composed of 95-100 open reading frames (ORFs), depending on the isolate (Chinchar et al., 2011; Morrison et al., 2014). FV3 exists as an enveloped or naked virion. The enveloped virion enters the host cell through receptor-mediated endocytosis via clathrin-coated pits (Chinchar et al., 2011), with recent studies identifying scavenger receptor-A (SR-A) in mediating FV3 entry (Fig. 1.1A) (Vo et

al., 2019a). The naked virion, either external (Fig. 1.1A) or after internalization (Fig. 1.1B), is believed to fuse with the cell membrane or nuclear membrane, respectively, and inject its genomic content, but this mechanism is poorly understood (Fig 1.1C) (Jancovich et al., 2015). FV3 uses host machinery for replication (Fig. 1.1D), starting with the production of early viral mRNA transcripts by host RNA polymerase II, which is further translated by host machinery to produce a suite of viral proteins that are believed to participate in the shutdown of host macromolecular synthesis and promotion of viral replication (Fig. 1.1E, F) (Jancovich et al., 2015). It has previously been documented that dsRNA is also produced during FV3 replications cycles (Doherty et al., 2016) and can be detected in the intracellular space (Fig. 1.1). After nuclear replication by viral DNA polymerase (Fig. 1.1G), FV3 dsDNA enters the cytosol which may then be used to undergo late viral mRNA transcript production via viral RNA polymerase II (Fig. 1.1H). This leads to the synthesis of viral packaging and capsid proteins (Fig. 1.1I) (Jancovich et al., 2015). Cytosolic DNA also polymerizes to form viral DNA concatemers in preparation of virion assembly. With viral DNA concatemers present in the cytosol, FV3 virion packaging and assembly begins upon capsid protein production (Fig. 1.1J), however this process is not well understood. This assembly creates a crystalline array of active virions which may then bud out from the cell membrane, creating the presence of enveloped FV3 (Fig. 1.1K), wherein naked FV3 is released upon cell death (Jancovich et al., 2015).

A hallmark of FV3 infection, which appears to be conserved among many large dsDNA viruses, is its ability for the complete shutdown of host macromolecular synthesis, regardless if the virus is infective or inactivated through heat or UV treatment, and the presence of proteins which elicit immunoevasion properties (Goorha and Granoff, 1974;

Jancovich et al., 2015; Williams, 1996). While the ability for FV3 to selectively inhibit host machinery is unknown, it is believed that viral proteins may play a role in inhibition of host polymerases and selective translation of viral mRNA transcripts (Fig. 1.1F) (Jancovich et al., 2015). Studies on knockout FV3 mutants for the genes 18K, 52L, 64R and viF2α showed reductions in viral infectivity and replication in *X. laevis* tadpoles (Andino Fde et al., 2015; Chen et al., 2011; Jacques et al., 2017). Nonetheless, the presence of viral polymerases is believed to not only take over host transcription and DNA replication but also be responsible for generating high levels of viral products that outcompete and suppress host macromolecular synthesis (Fig. 1.1F) (Jancovich et al., 2015).

Much of our understanding of frog-FV3 interactions and pathogenesis derives from studying FV3 in the context of the African clawed frog, *Xenopus laevis* and represents a host that is relatively resistant to FV3. FV3-Infected adult *X. laevis* appear symptomatic (slight skin shedding, lethargy) for 3-4 weeks then appear asymptomatic thereafter (Robert et al., 2007). During the symptomatic phase, FV3 infected adult *X. laevis* transmit infectious virus to adult and larval *X. laevis* within 3 hours of exposure through waterborne transmission (Robert et al., 2011). As part of their innate immune response, *X. laevis* increases the total number of peritoneal leukocytes (PL) to fight infection, combined with FV3-induced proinflammatory gene expression (*il-1b* and *tnfa*) in PLs (Morales et al., 2010). FV3 infected adult *X. laevis* mount an adaptive immune response as demonstrated by the ability to develop a memory CD8+ T-cell response, supported by quicker cell proliferation and FV3 clearance upon secondary infection (Morales and Robert, 2007). Although FV3-infected adult *X. laevis* appear asymptomatic and resistant to challenge infection following recovery, low levels of

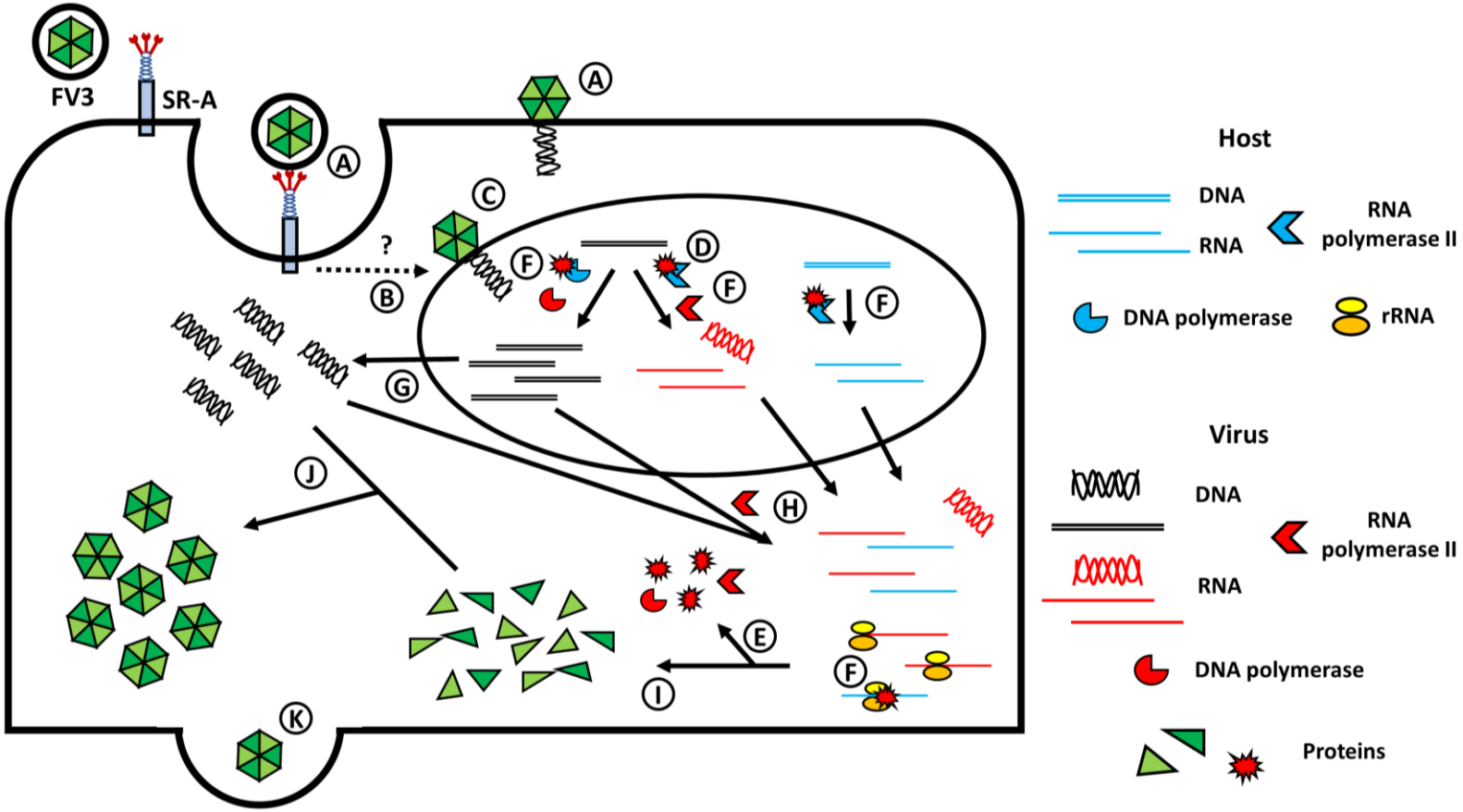

Figure 1.1. Schematic of Frog Virus 3 infection, replication, and suppression in a susceptible host cell. (A) Cellular recognition of enveloped FV3 by SR-A helps to mediate cellular entry, while naked virions fuse with the cell membrane and inject genetic material. (B) After internalization, FV3 interacts with host nucleus and (C) injects viral DNA into the nucleus. (D) Host RNA polymerase II generates early viral mRNA (E) followed by the synthesis of viral proteins. (F) Select proteins are believed to inhibit host machinery, wherein FV3-derived RNA polymerase II generate transcripts to outcompete host translation, and viral DNA polymerase synthesizes viral DNA. (G) Replicated viral DNA enter host cytosolic space (H) where late viral mRNA synthesis allows for the synthesis of (I) viral capsid proteins. (J) Active virions are assembled which then (K) bud from the host membrane to propagate infection. Figure was adapted from (Janovich et al, 2015).

FV3 can be detected in the kidney of recovered *X. laevis*, suggesting a quiescent state of FV3 that permits reactivation of viral replication when the host is immunosuppressed (Robert et al., 2007; Robert et al., 2014). As such, even resistant anuran hosts can play an important role in FV3 transmission, particularly under environmental conditions that may lead to host immunosuppression and FV3 reactivation.

Upon release from infected hosts, FV3 is transmitted through the environment, either through direct contact (e.g. during mating), indirect contact (e.g. water borne transmission) or consumption of infected carcasses (Brunner et al., 2007; Schock et al., 2008). In addition to infected amphibians shedding FV3 into the environment, other frogs, salamanders, fish, and reptiles may be potential reservoirs for FV3, even if the host is not susceptible to infection, potentiating the transmission of FV3 to susceptible hosts (Duffus et al., 2008; Hausmann et al., 2015). Regardless of the transmission route, FV3 must cross either the skin epithelial barrier or the gut epithelial barrier. A key symptom of FV3 infection in susceptible developmental stages of frog species is skin shedding and the formation of skin lesions through epidermal cell necrosis (Forzán et al., 2017; Gray et al., 2009). It is proposed that loss of the skin barrier during FV3 infection allows for increased pathogen entry and ultimately leads to mortality in susceptible hosts, stressing the overall importance of the skin barrier (Chinchar et al., 2011; Varga et al., 2019). Yet, much of the innate immune properties of frog skin remain to be understood outside of antimicrobial peptides.

1.3. Vertebrate skin as the first line of defence

While the structure and certain features of skin is species dependent, the role is generally conserved – skin acts as a the initial protective layer between the environment and the host's internal makeup (Haslam et al., 2014). Though skin composition varies across

species, the organization of skin layers appears consistent: there is an epithelial cell-rich epidermal layer, and lower fibroblastic cell-rich dermal layer (Haslam et al., 2014), wherein both are important in maintaining skin barrier integrity and epithelial cells are the initial interface between the environment and organism.

1.3.1. Structural properties of mammalian epidermis

The two main basic cell types that comprise the skin barrier include epithelial cells comprising the epidermal layer, and fibroblastic cells from connective tissue (Haslam et al., 2014). Specifically, the surface epithelial cells serve as a physical protective barrier through the formation of tight junctions and adherens junctions (Niessen, 2007). Tight junctions are strictly localized to epithelial and endothelial cells and require integral membrane proteins from the claudin and occludin families for formation (Furuse et al., 1998; Furuse et al., 1993). Claudin-1 is expressed across all tissue types and is capable of interacting with other claudin types, such as claudin-3 (Coyne et al., 2003; Furuse et al., 1998). Claudin-3 has no defined expression profile, but claudin-3 presence has previously been identified in mucosal tissue and has been known to increase in expression in malignancies (Coyne et al., 2003; Hewitt et al., 2006). Adherens junctions require the protein cadherin to be functional and has broad range expression across cells including, but not limited to, epithelial cells, fibroblastic cells, and neuronal cells (Matsuyoshi and Imamura, 1997; Yap et al., 1997). Among these, the expression of cadherin-1 (E-cadherin) is known to be specific for epithelial cells (van Roy and Berx, 2008). Meanwhile, skin can possess mesenchyme tissue derived from epithelial cells which have undergone an epithelial to mesenchymal transition (EMT), characterized by the loss of tight junctions and adherens junctions and increased levels of vimentin filament

(Cano et al., 2000; Figiel et al., 2017; Kalluri and Weinberg, 2009). Nonetheless, the cellular junctions formed between epithelial cells is necessary for maintaining surface skin integrity.

Structurally, mammalian cytoskeleton is composed of 3 principal structural units: actin microfilaments, tubulin microtubules, and intermediate filaments (Chu and Weiss, 2002). Of these, there are 6 intermediate filaments, wherein 2 of the 6 include acidic type I and basic type II cytokeratins (Chu and Weiss, 2002). Pairs of cytokeratins appear to be co-expressed in different types of epithelial cells (Chu and Weiss, 2002), wherein all mammalian epithelial cells possess cytokeratins for structural support (Moll et al., 1982). Of the type I cytokeratins, cytokeratin 19 is found in stratified squamous epithelia as well as simple epithelia (Chu and Weiss, 2002). Cytokeratin 14 (type I) and cytokeratin 5 (type II) are a cytokeratin pair which localizes in basal keratinocytes of the epidermis (Chu and Weiss, 2002). Expression and identification of cytokeratins is specific for epithelium and not found in connective tissue (Chu and Weiss, 2002). Yet in connective tissue, fibroblast cells demonstrate a high level of collagen synthesis as well as the intermediate filament vimentin as part of its cytoskeletal structure (Brewer, 1967; Franke et al., 1978). Structurally distinct collagen types are distributed in a specific fashion; collagen type I and collagen type III were found to be distributed and co-regulated in interstitial connective tissues while type II collagen is exclusively found in cartilage (Raghow and Thompson, 1989). In addition to participating in cytoskeletal structure in fibroblast cells, collagen is an important component in extracellular matrix formation (Ricard-Blum, 2011). Distinct cell types express unique genes necessary for its overall function, wherein the presence of cytokeratins is a hallmark of epithelial cell identification.

1.3.2. Frog epidermis

Frog skin supports vital physiological functions including, but not limited to, respiration, ion regulation, water transport, predator defence and immune function (Larsen and Ramløv, 2013; Lillywhite, 2006; Toledo and Jared, 1995). Mucosal glands within frog skin secrete mucus to maintain skin moisture, permeability and elasticity, all of which are necessary for homeostasis (Larsen and Ramløv, 2013; Lillywhite, 2006; Lillywhite and Licht, 1975), while also functioning in pathogen trapping and removal (Cone, 2009; Stannard and O'Callaghan, 2006). In addition, frogs have evolved a specialized glandular network beneath the skin surface that synthesize and secrete a plethora of antimicrobial and toxic substances, thus aiding in the defence against pathogens and predators (Toledo and Jared, 1995). Yet frog skin is particularly vulnerable to cutaneous injury due to the relatively thin and permeable nature of the organ – characteristics necessary to support many of the aforementioned physiological processes. Thus, frog skin is an important first line of defence against harmful agents in the environment.

Frog skin is composed of epidermal and dermal layers, with each layer predominantly consisting of epithelial and fibroblastic cells, respectively (Haslam et al., 2014; Villaro et al., 1998). While it is presumed that features of mammalian epithelial and fibroblast cells are conserved in amphibians, the mucosal nature of frog skin epithelium suggests that frog skin epithelial and fibroblast cells may differ compared to those in non-mucosal skin tissues. For example, while human and mouse skin epidermal cells generally do not produce collagen, epithelial cells from human, mouse, and chick mucosal tissues (i.e. gut, lung, eye) do produce collagen (Birkedal-Hansen et al., 1982; Haslam et al., 2014; Hayashi et al., 1988; Ohji et al., 1994). Although collagen has been identified in whole frog skin (Li et al., 2004;

Purna Sai and Babu, 2001), the exact cellular source is unknown. Furthermore, frog skin is unique in that although it acts as a direct interface to the environment like skin in other organisms, it is also a mucosal tissue like from the gut or lung mucosa (Haslam et al., 2014). As such, this must be kept into consideration if making comparisons to mammalian skin, which is non-mucosal; comparisons to mammalian mucosal tissue may be more appropriate in instances.

The presence of cellular junctions is a key hallmark of epithelial cells in mammalian models, a feature which appears conserved for amphibian species (Farquhar and Palade, 1963, 1965). Tight junction proteins are detected as early as the gastrulation stage and persist until full development (Farquhar and Palade, 1965). The presence of tight junction claudin-1 proteins is crucial during gastrulation in *X. laevis* embryos (Chang et al., 2010), but general observations of tight junction proteins in adult frogs are lacking. In early larvae, tripartite junctional complexes of tight junction, adherens junction, and desmosomes are observed, wherein these complexes appear to lose significant contribution from adherens junctions in larvae approaching metamorphosis and in adult frogs (Farquhar and Palade, 1965). Nonetheless, strong expression of adherens-dependent cadherin protein has been detected in adult *X. laevis* skin (Levi et al., 1991). While the presence and role of gap junctions and desmosomes have been reported in the skin of other vertebrates, the observation of these junctions in frogs has been limited to frog embryos undergoing development, or identification in adult frogs (Munoz et al., 2012; Shahin and Blankemeyer, 1989; Suhrbier and Garrod, 1986; Warner, 1985). Though all cellular junctions have been identified in frogs at different developmental stages, it is important to note that these studies have been limited to *X. laevis* and *R. pipiens* species and thus may not necessarily be representative of all frogs.

Collectively, epithelial cell junctions allow for a continuous epithelial network that is relatively closed to the external environment while remaining open to the basal collagenous-rich dermal layers. As such, maintenance of epithelial cellular junctions is important for barrier integrity, and thus pathogen defence, particularly considering the relatively thin epidermal layer in frogs.

1.4. Cellular pathogen recognition and defense

A recent phenomenon which has been garnering attention is the participation of non-immune cells in recognizing and responding to external stimuli, and further downstream signaling to help initiate an immune response. These include local cell populations around a site of injury or infection, such as epithelial cells, acting as a more immediate responder than relying on the systemic recruitment of immune cells. While the immune role of mammalian epithelial cells, of epidermal and mucosal origin, has been elucidated, efforts in amphibian models are lacking.

1.4.1. Mammalian cellular innate immunity

Mammalian cells produce germ-line encoded pattern recognition receptors (PRRs) that can bind pathogen-associated molecular patterns (PAMPs). Viruses may either contain or produce several viral PAMPs in their replicative cycle such as nucleic acids: double-stranded ribonucleic acid (dsRNA), single-stranded ribonucleic acid (ssRNA), double-stranded deoxyribonucleic acid (dsDNA) and single-stranded deoxyribonucleic acid (ssDNA) (Bartenschlager et al., 2010; Buller and Palumbo, 1991; Chinchar, 2002; Doherty et al., 2016). Viral nucleic acids are released extracellularly upon host cell lysis during infection where they can be recognized by nearby host cells. This recognition may be performed by surface receptors, such as dsRNA recognition by scavenger receptors (SR) which are

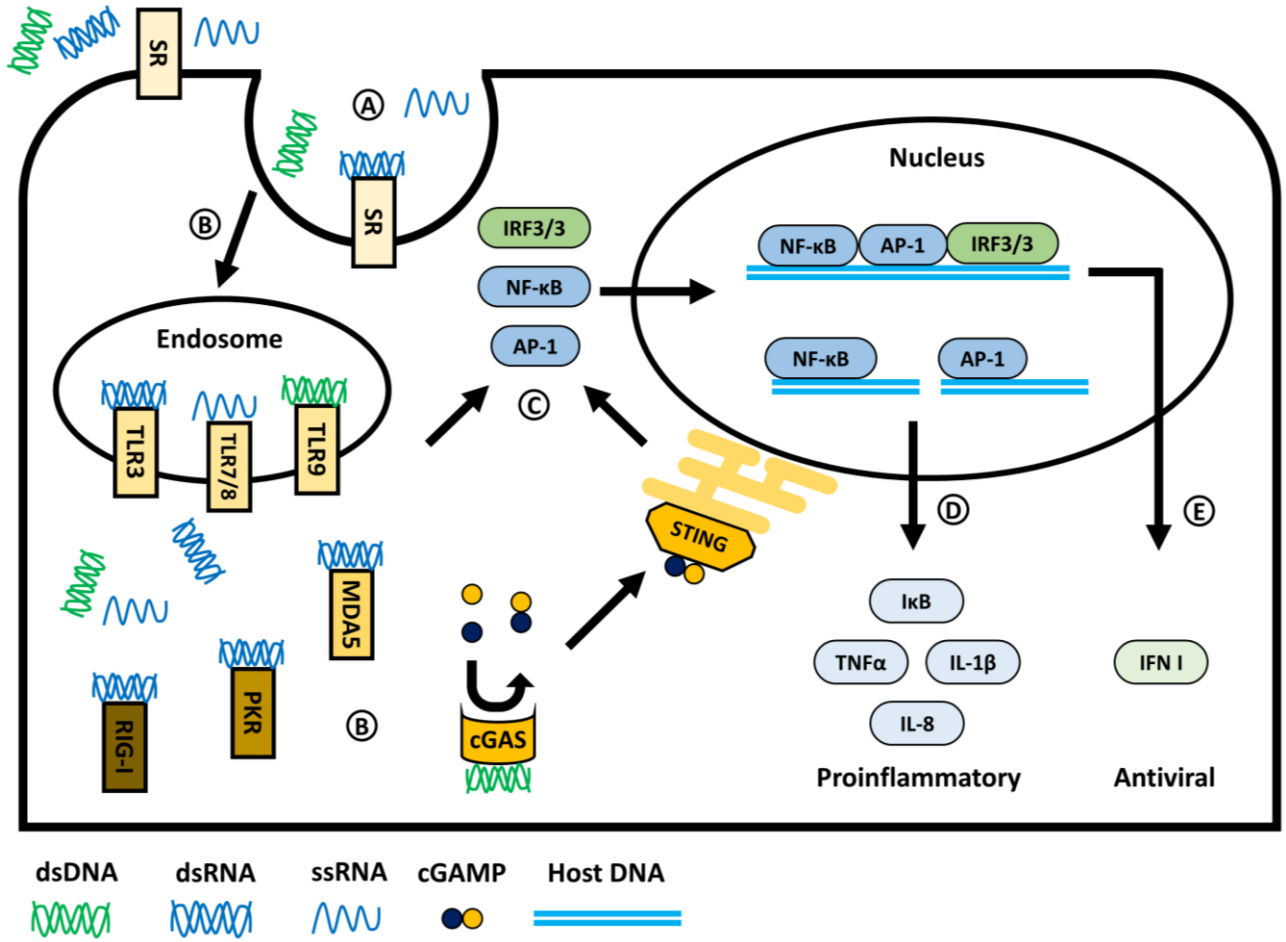

Figure 1.2. Cellular recognition and antiviral response to viral nucleic acids. (A) Detection of exogenous viral nucleic acids or endocytosis-internalization into the host cell, mediated by SRs in the case of dsRNA. (B) Viral nucleic acids are recognized by endosomal TLRs upon endosomal fusion, or free nucleic acids sensed by cytosolic receptors. (C) Regardless of PRR engagement, intracellular signaling pathways converges to activate IRF3/3, NF-κB and AP-1 transcription factors, leading to nuclear translocation and the up-regulation in gene expressions and protein synthesis of (D) proinflammatory cytokines, chemokines, and the inhibitor of NF-κB (IκB) and (E) antiviral molecules.

responsible for trafficking substrates to endosomes (Fig. 1.2A) (Murshid et al., 2015; Yoneyama and Fujita, 2010). Once trafficked to endosomes, viral PAMPs can be sensed by toll-like receptors (TLRs) (Fig. 1.2B) wherein TLR3 senses dsRNA, TLR 7 and TLR 8 sense ssRNA, and TLR9 senses dsDNA (Kawasaki and Kawai, 2014; Yoneyama and Fujita, 2010). Free viral nucleic acids may also be present in the cytosol, through viral delivery or produced during the viral replicative cycle, and can be sensed by cytosolic PRRs (Fig. 1.2B). Cytosolic dsRNA is recognized by protein kinase R (PKR) and the RIG-I-like receptors (RLRs) RIG-I and MDA5 (Wilkins and Gale, 2010; Yoneyama and Fujita, 2010; Zhou et al., 2014). Furthermore, dsDNA is also a viral PAMP commonly found in dsDNA viruses, such as FV3, and can be sensed by cytoplasmic DNA sensors such as the cGAS-STING system (Fig. 1.2B) (Diner et al., 2013), among others. Recognition of viral nucleic acids by these PRRs leads to the initial homodimerization of interferon regulatory factor (IRF) 3 to create the IRF3/3 transcription factor (Bonjardim et al., 2009; Ysebrant de Lendonck et al., 2014), alongside the activation of NF-κB and AP-1 transcription factors (Fig. 1.2C) (De Bosscher et al., 2003). NF-kB and AP-1 induce transcription regulation of proinflammatory cytokines and chemokines such as IL-1β, TNFα, IL-8, and IκB (Fig. 1.2E) (De Bosscher et al., 2003). Meanwhile, the initial activation of Type I IFN gene expression requires the recognition of NF-κB, AP-1 and IRF3/3 transcription factors (Fig. 1.2D) (Bonjardim et al., 2009; Ysebrant de Lendonck et al., 2014). These proteins are responsible for initiating antiviral and proinflammatory activities in the host.

Innate immune responses to viral pathogens are primarily mediated by a class of cytokines called interferons (IFN), important antiviral cytokines involved in inducing an antiviral state in cells and limiting viral replication (Bonjardim et al., 2009). The three classes

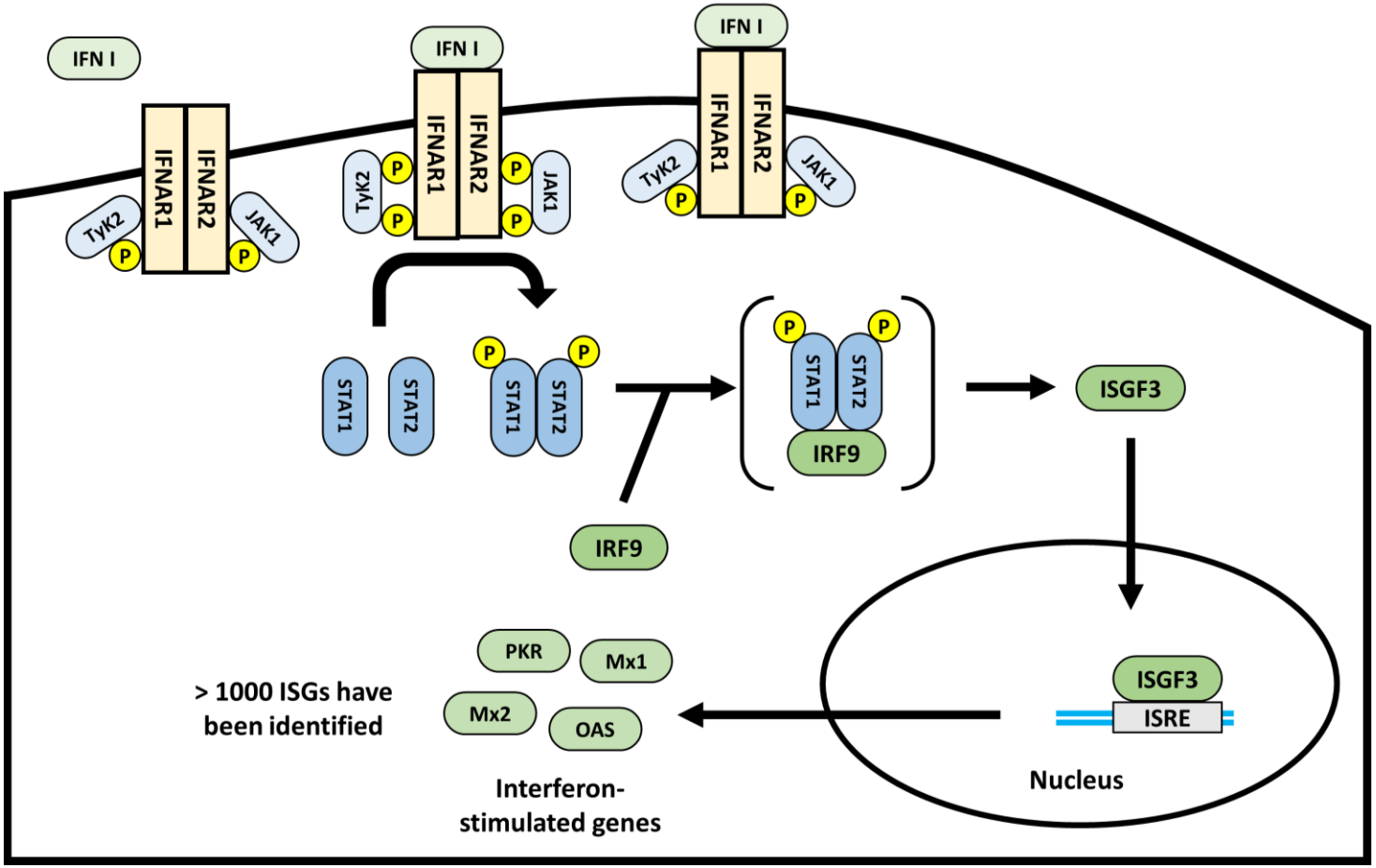

Figure 1.3. Induction of interferon-stimulated genes upon Type I IFN recognition. Cellular recognition of secreted Type I IFN by its cognate receptor, IFNAR1/2, leads to the phosphorylation of STAT1 and STAT2 via JAK proteins, which together create a tripartite complex with IRF9. The formation of this complex yields the transcription factor interferon-stimulated gene factor 3 (ISGF3). ISGF3 then binds to ISREs and allows for the induction and subsequent synthesis of a number of ISGs, such as Mx proteins, PKR, and OAS, proteins necessary for limiting viral replication.

of IFNs include Type I IFN, Type II IFN, and Type III IFN with Type I and Type III IFNs possessing functionally similar antiviral effects (Vilcek, 2003). Notably, while Type I IFN appears to act globally, Type III IFN targets mucosal epithelial cells in a mammalian model (Wack et al., 2015). Once produced and secreted, IFNs can act in an autocrine or paracrine fashion by binding to IFN receptors, activating Janus family kinases (JAK) and signal transducer and activator of transcription (STAT) proteins (Fink and Grandvaux, 2013). In the case of Type I IFN responses, JAK1 and Tyk2 JAK proteins phosphorylate STAT1 and STAT2 proteins, which then form a heterotrimer with IRF9 (Fig. 1.3) (Fink and Grandvaux, 2013). This heterotrimer complex is referred to as the interferon-stimulated gene factor 3 (ISGF3) and is the transcription factor that binds to interferon stimulated response elements (ISREs) to upregulate interferon-stimulated genes (ISGs; Fig. 1.3) (Fink and Grandvaux, 2013; Hayes and Chayama, 2017). Over 1000 ISGs have been identified (Fig. 1.3), wherein previous studies found less than a 2-fold change in ISG induction for over 75% of these (Der et al., 1998).

Antiviral effectors, such as (2'-5')-oligoadenylate synthetase (OAS), PKR, and interferon-inducible GTPase myxovirus-resistance proteins (Mx) (Fig. 1.3), are integral to limiting viral replication and viral dissemination (Alsharifi et al., 2008; Schoggins and Rice, 2011; Sen and Ransohoff, 1993). OAS specifically binds cytosolic viral dsRNA and, through a combination of effects, degrades both viral and host cellular ssRNA, effectively suppressing viral infection (Silverman, 2007). PKR is activated mainly by the presence of dsRNA and its key antiviral effect is to suppress viral replication through translational inhibition (Williams, 1999). Mx genes are divided into two lineages: nuclear protein Mx1 and cytoplasmic protein Mx2 (Haller et al., 2015; Pilla-Moffett et al., 2016). Functionally,

Mx1 inhibits primary transcription occurring in the nucleus performed by viral nucleocapsid-associated viral polymerase, while Mx2 inhibits viruses which replicate exclusively in the cytoplasm (Haller and Kochs, 2011; Pilla-Moffett et al., 2016). IRF7 is also an ISG and, once synthesized, can heterodimerize with IRF3 to generate the IRF3/7 transcription factor to further enhance the expression of Type I IFN and promote cellular antiviral responses (Martins et al., 2015; Ysebrant de Lendonck et al., 2014). Overall, vertebrates rely on the IFN response to elicit antiviral programs to limit and/or eliminate viral infections. A common method used to study Type I IFN responses in cells is through treatment with polyinosinic-polycytidylic acid [poly(I:C)], a viral dsRNA analogue that is also recognized by surface SR-As present on some cell types and trafficked to endosomal TLR3 (Martins et al., 2015; Murshid et al., 2015) to elicit the same set of antiviral mechanisms.

The stimulation of viral nucleic acid sensors also results in the direct or ISG-mediated activation of NF-κB, turning on proinflammatory programs (Alexopoulou et al., 2001; Zamanian-Daryoush et al., 2000). Proinflammatory cytokines, such as TNF and IL-1β, and chemokines, such as IL-8, are key mediators of host inflammatory responses to infection (Dinarello, 2000). TNF is expressed by many cell types and binds to the TNF receptor and yields three key cell signaling events: activation of mitogen-activated protein kinase pathway, induction of NF-κB, and induction of cell death signaling (Locksley et al., 2001; Zelova and Hosek, 2013). TNF can act on other cell types, including epithelial cells, to activate NF-κB and can thereby induce the gene expression of IL-1 (Dinarello, 1996; Dolcet et al., 2005). Alternatively, transcriptional activation of IL-1 can occur in response to engagement of PRRs and downstream activation of NF- κB (Lawrence, 2009). In mammals, IL-1 protein possesses an interleukin-1 converting (ICE) cleavage site, leading to production of IL-1β. In fish and

frogs, a definitive ICE cleavage site is not present in the IL-1 protein and the exact mechanism of how IL-1β is produced from the IL-1 protein is unclear (Covello et al., 2009; Jelaso et al., 1998; Liu et al., 2012). Lastly, the transcription and translation of IL-8 following TLR engagement is essential for inducing chemotaxis of neutrophils to the site of infection and enhancement of their phagocytic capacity (Baggiolini et al., 1989). The combined effects of TNF, IL-1 β, and IL-8 facilitate a proinflammatory response to an array of pathogens. While epithelial cells act as an important physical barrier to pathogen entry, they are also essential in viral detection and activation of underlying innate immune cells through the induction of cellular antiviral mechanisms (Dai et al., 2008; Kopfnagel et al., 2011; Tohyama et al., 2005).

1.4.2. Frog cellular innate immunity and understanding FV3 pathogenesis through *X. laevis*

Despite extensive studies showing that amphibian skin is vital to survival, relatively little focus has been placed on examining the role of frog skin epithelium in sensing and responding external stimuli, such as pathogen attack. This focus is paramount since mucosal epithelia are more prone to pathogen attack, such as that seen in mammalian lung and gut epithelium (Kim et al., 1998; Plotkowski et al., 1993; Ringø et al., 2010; Sperandio et al., 2015). While the ability for mammalian epithelial cells to sense and respond to viral nucleic acids has been documented (Dai et al., 2008; Kopfnagel et al., 2011; Tohyama et al., 2005), the observation of this in frog skin epithelial cells is lacking. While the majority of *X. laevis*-FV3 research has bypassed the skin barrier via intraperitoneal injection of virus into the host (Jacques et al., 2017; Koubourli et al., 2017; Morales et al., 2010; Morales and Robert, 2007), a couple of recent studies in *X. laevis* have investigated the role of Type I IFN and Type III IFN mediated antiviral response in adult and tadpole *X. laevis* skin during FV3 infection

(Wendel et al., 2017; Wendel et al., 2018). Subcutaneous administration of Type I IFN or Type III IFN in *X. laevis* tadpoles, which are highly susceptible to FV3, offered short-term protection against FV3 infection, combined with induced expression of antiviral genes in the skin (Wendel et al., 2017). Furthermore, it appears that Type I IFN and Type III IFN responses may play an integral role in the antiviral response in *X. laevis* skin in adult frogs and tadpoles, respectively (Wendel et al., 2017; Wendel et al., 2018). However, the contribution of frog skin epithelial cells in mediating these antiviral responses remains unknown due to the inherent complexity of whole skin tissue, requiring further introspection into the interaction between FV3 and isolated frog epithelial cells.

1.5. Research scope, objectives, and hypotheses

While extensive studies have been conducted to unveil FV3 pathogenicity and host immune response at the animal level, particularly in *X. laevis*, the role of skin epithelial cells in sensing and responding to pathogens is not well understood. Furthermore, examination of FV3 infection of frog skin epithelial cells remains to be elucidated. It is important to investigate the interaction between frog skin epithelial cells and FV3 as the skin is the first barrier of defense, and one of the modes of FV3 transmission is known to occur through direct skin contact (Lesbarreres et al., 2012). Elucidation of this interaction will prove to be insightful when further exploring how frog skin epithelial cells, whether through natural or induced mechanisms, may aid in attempting to limit viral infection and spread. In part, this remains unexplored due to a lack of model systems available to actively study the frog skin epithelial cell-FV3 interaction.

I investigated two main objectives for my master's thesis to address this knowledge gap. Chapter 2 focused on the establishment, development and characterization of novel *X. laevis*

dorsal and ventral skin epithelial-like cell lines, Xela DS2 and Xela VS2, and their capacity to recognize the extracellular viral dsRNA analogue, poly(I:C). I hypothesize that Xela DS2 and Xela VS2 are epithelial in nature and can recognize and respond to extracellular poly(I:C). Upon establishing Xela DS2 and Xela VS2 as suitable models for studying frog skin epithelial cell antiviral responses, Chapter 3 investigated Xela DS2 and Xela VS2 susceptibility to FV3, their response to FV3 infection, and whether poly(I:C) pre-treatment could induce a functional antiviral state that confers resistance to FV3 infection. Here, I hypothesize that Xela DS2 and Xela VS2 are permissive to FV3 infection and replication, wherein poly(I:C) pre-treatment would confer protective properties due to initial upregulation of antiviral programs.

Chapter 2: Xela DS2 and Xela VS2: two novel skin epithelial-like cell lines from adult African clawed frog (*Xenopus laevis*) and their role in sensing extracellular viral dsRNA

2.1. Introduction

Amphibian skin is a unique organ that participates in barrier function as well as key physiological processes necessary for survival. Although dependent on the species, physiological functions may include osmoregulation, respiration, ion transport, thermoregulation and more (Haslam et al., 2014; Lillywhite, 2006). The skin epithelium serves as a direct interface between an amphibian's internal milieu and external environment, facing constant exposure to changing temperatures, environmental pollutants, and acting as the first line of defence against pathogens (Stuart et al., 2004). Accordingly, skin integrity and barrier function must be continuously maintained and reinforced to limit the effects of subjected environmental insult, including pathogens.

Recent evidence in murine and human models suggest that epithelial cells are more than just bystanders, playing an active role in pathogen sensing and downstream signalling to immune cells (Braff et al., 2005; Hamel et al., 2015; Pasparakis et al., 2014). Epithelial cells express a number of pattern recognition receptors (PRRs) that sense pathogen-associated molecular patterns (PAMPs), leading to the activation of key transcription factors (IRF3/3, NF-κB, AP-1) depending on the PAMP recognized and, mediates the transcriptional regulation of key antiviral and proinflammatory cytokines and chemokines in response to a range of microbes (Artis, 2008; De Bosscher et al., 2003; Ghosh et al., 1998; Tosi, 2005). In the case of viral-associated double-stranded RNA (dsRNA), extracellular dsRNA is trafficked to endosomal TLR3 by SR-As while intracellular dsRNA is recognized by cytosolic RIG-I or MDA5. Recognition of dsRNA by endosomal or cytosolic dsRNA sensors

lead to the activation and homodimerization of IRF3 to initiate host cell antiviral programs through the initial expression of type I and/or type III interferons (IFN). Secreted type I or type III IFNs can then act in an autocrine or paracrine fashion through their cognate IFN receptors (IFNARs) on the infected or neighbouring healthy cells. Binding of IFNAR1/2 leads to the activation of the transcription factor complex ISGF3, comprised of STAT1/STAT2 and IRF9, and binds interferon stimulated response elements (ISREs) to regulate the expression of interferon stimulated genes (ISGs), many which encode for the proteins necessary for mediating antiviral programs in the host (Fink and Grandvaux, 2013; Hayes and Chayama, 2017; Schoggins and Rice, 2011) and includes IRF7, a transcription factor that can heterodimerize with IRF3 to further bolster the induction of type I IFNs in a positive feedback loop (Bonjardim et al., 2009; Ysebrant de Lendonck et al., 2014)..

Despite the documented roles of skin epithelial cells in pathogen sensing and initiation of proinflammatory and antiviral responses in mouse and human models (Gomez et al., 2013; Nestle et al., 2009), very little is known regarding whether frog skin epithelial cells function in a similar fashion. Among frog species studied, the African clawed frog (*Xenopus laevis*) has been established as a model system to investigate the host-pathogen interactions and amphibian immunity (Gantress et al., 2003; Ramsey et al., 2010). However, the contribution of isolated skin epithelial cells to amphibian antiviral immunity remains limited. It is critical to dissect the potential individual role(s) of frog skin epithelial cells in regard to recognizing and responding to viral-associated molecular patterns to improve our understanding of the skin epithelial cell antiviral mechanisms.

Since dsRNA is produced by the majority of viruses at some point during their replicative life cycle (Weber et al., 2006), addition of poly(I:C), a viral dsRNA analogue,

may approximate extracellular dsRNA potentially released from infected cells due to cell lysis and illustrate the potential of frog skin epithelial cells to recognize viral dsRNA *in vivo*. In this chapter, I hypothesized that *X. laevis* skin epithelial cells are capable of recognizing and responding to poly(I:C), a mixture of synthetic dsRNA of various lengths and a known inducer of Type I IFN (Longhi et al., 2009; Poynter and DeWitte-Orr, 2018). Therefore, the first objective of this chapter was to generate *X. laevis* skin epithelial cell lines for use as a model system to study host-pathogen interactions. The second objective was to determine whether these cell lines were capable of recognizing and responding to exogenous poly(I:C) and characterizing the potential response. Herein, I report on the generation and establishment of two skin epithelial-like cell lines from *X. laevis* dorsal and ventral skin, named Xela DS2 and Xela VS2, respectively, their optimal growth conditions, and morphological and molecular characterization. Furthermore, I assessed the expressions of key antiviral genes, proinflammatory cytokines, and chemokine in response to treatment with poly(I:C) over time.

2.2. Methods

2.2.1. Frogs

Tissues from female African clawed frogs (*Xenopus laevis)* were kindly donated by Dr. Mungo Marsden (University of Waterloo, Waterloo, ON). Dr. M. Marsden purchased *X. laevis* from Nasco (Fort Atkinson, Wisconsin, USA) and these frogs were previously used in a breeding colony. Frogs were fed *ad libitum* with *Xenopus* food pellets (Boreal Science) and housed in opaque tanks filled with well water that was replaced twice a week. Frogs were kept at 22^{o}C in the Aquatic Facility of the Biology building, University of Waterloo. Prior to tissue extraction, frogs were euthanized by immersion in a solution of benzocaine (300 mg/L,

initially dissolved in 1 mL 100% ethanol). The frogs were maintained according to the guidelines of the University of Waterloo Animal Care Committee and the Canadian Council of Animal Care (CCAC-Canada).

2.2.2. Media

Leibovitz's L-15 medium (HyClone) was diluted to 70% with cell culture water (Lonza) to adjust for the osmolarity of amphibian cells and will herein be referred to as AL-15. During initial establishment of cell tissue explant cultures, media was comprised of AL-15 supplemented with 20% fetal bovine serum (FBS; HyClone), 200 U/mL penicillin (HyClone), 200 μg/mL streptomycin (HyClone), 50 μg/mL gentamicin sulfate (HyClone) and 1 μg/mL amphotericin B (HyClone), herein referred to as establishment media. Once the primary cultures were established and in the early passage stage (passage 4-6), the continuous skin cell cultures were maintained using AL-15 medium supplemented with 15% FBS, 100 U/mL penicillin, 100 μg/mL streptomycin, and 50 μg/mL gentamicin sulfate. From passage 10 onwards, cells were maintained in AL-15 media supplemented with 15% FBS, without antibiotics, and will be referred to as complete medium. Amphibian phosphate-buffered saline (APBS) was prepared by diluting Dulbecco's phosphate-buffered saline (DPBS; Lonza) to 70% of the original salt concentration with cell culture water and 0.25% Trypsin-EDTA (HyClone) was also diluted to 70% original concentration with cell culture water.

2.2.3. Generation and establishment of continuous skin cultures

Dorsal and ventral skin were dissected from euthanized *X. laevis* under sterile conditions and placed in individual petri dishes containing APBS supplemented with 200 U/mL penicillin, 200 μg/mL streptomycin, and 50 μg/mL gentamicin sulfate. Tissues were

cut into small pieces with a scalpel and washed twice in APBS containing antibiotics prior to placing 4-6 tissue pieces into a 25 cm^2 plug-seal tissue culture treated flask (BioLite, Thermo Scientific) containing 1.5 mL establishment medium to cover the tissue pieces. Primary tissue explant cultures were maintained at 26°C, in the absence of additional CO_2. Medium was changed twice a week for the first three weeks using establishment media, and every 5-7 days afterwards using complete medium. Tissue culture explants were monitored for cell outgrowth. Once tissue explant cultures exhibited significant cell growth, adherent cells were collected by removing complete medium and washing cell cultures with 1× APBS prior to the addition of Trypsin-EDTA. Upon cell detachment, medium containing 20% FBS was added and the cells were sub-cultured into fresh 25 cm^2 plug-seal tissue culture flasks. Two continuous cell cultures were generated from these primary tissue explant cultures, named Xela DS2 and Xela VS2 for dorsal and ventral skin, respectively.

2.2.4. Cell culture maintenance

Early cell cultures were passed every 7 to 10 days at a 1:2 split. Once established (>passage 25 for Xela DS2, >passage 30 for Xela VS2), Xela DS2 and Xela VS2 continuous skin cell cultures were maintained in 75 cm^2 plug-seal tissue-culture treated flasks at 26°C in complete medium without antibiotics. Upon becoming confluent, usually every 3-4 days, cells were split. Briefly, medium was removed from the flask and cells washed with 3-5 mL of APBS. Following removal of the APBS, 2 mL of trypsin-EDTA was added to detach cells from the cell culture vessel. Cell detachment was monitored and complete medium was immediately added following cell detachment to inactivate trypsin. Cells were sub-cultured 1:4 into flasks containing 10 mL of fresh complete medium. Collected cells were used for setting up experiments, wherein a plating efficiency for cell seeding of 79% and 83% was

considered for Xela DS2 and Xela VS2 respectively. The reported cell numbers used in the experiments described below were all corrected for these plating efficiency differences. Cell morphology was monitored over successive passages by capturing phase-contrast images using a Nikon Eclipse TSX-100 microscope (taken at 100× magnification) fitted with a color camera and Picture Project software during early passages and with a Zeiss AxioVert-A1 microscope (taken at 200× magnification) fitted with an Axiocam 503 color camera and Zen 2.0 Lite software during later passages.

2.2.5. Cryopreservation

After harvest from tissue culture vessels, Xela DS2 or Xela VS2 cells were centrifuged at 500 × *g* for 5 min to pellet cells. The supernatant was removed and cells were resuspended to approximately 2 × 10^6 million cells per mL in chilled complete medium containing 10% DMSO (Fisher Scientific). One mL of cell suspension was aliquotted into individual cryogenic tubes (Nunc) and vials placed in a Mr. Frosty freezing container (Thermo Scientific) at -80°C overnight prior to long-term storage in liquid nitrogen.

2.2.6. Hematoxylin-Eosin (H&E) staining

Xela DS2 (passage 74) and Xela VS2 (passage 75) cells were seeded in 6-well plates (BioLite, Thermo Scientific) at cell densities of 300,000 cells/well in 1 mL of complete medium and allowed to adhere overnight at 26°C. The following day, media was removed from the wells and cells were fixed to the tissue culture plate by adding 70% ethanol for 2 min with gentle agitation. The ethanol was aspirated and residual ethanol was allowed to evaporate before cells were rinsed with 1 mL of Scott's Tap Water for 30 s, with agitation. Cells were stained with Hematoxylin Gill 3 solution (VWR) for 5 min with agitation and washed with six exchanges of 1 mL Scott's Tap Water (240 mM $NaHCO_3$, 135 mM $MgSO_4$,

pH 8.0). Cells were counterstained for 15 s with agitation in non-acidified 1% Eosin Y (Fisher Scientific) prior to rinsing cells with 1 mL of an increasing ethanol series (70%, 95%, and 100%). Cells were allowed to air dry prior to capture of brightfield images using a Zeiss AxioVert-A1 microscope fitted with an Axiocam 503 color camera and using Zen 2.0 Lite software

2.2.7. Determination of senescence-associated beta-galactosidase activity

Cells were seeded in a 12-well plate, at cell densities of 50,000 cells/well for Xela DS2 (passage 9 and passage 74) or Xela VS2 (passage 13 and passage 75), and 30,000 cells/well for Xela BMW3 as a positive control (passage 11 and passage 20), in 0.5 mL of complete medium. Cells were allowed to adhere overnight at 26°C prior to being assessed for β-galactosidase activity associated with cellular senescence using a commercially available Senescence Cells Histochemical Staining Kit (Sigma Aldrich). The protocol was followed according to the manufacturer's specifications with the following modification: after adding the staining mixture to each well, plates were incubated at 26°C instead of 37°C. Briefly, complete medium was removed from the adherent cells prior to washing cells twice with 1 mL of cold APBS. Cells were fixed to the wells of the plate with 0.5 mL fixation buffer for 7 min. Fixation solution was aspirated and cells washed 3× with 0.5 mL of APBS. The APBS was aspirated and 0.5 mL of staining solution was applied to each well prior to incubation at 26°C overnight. The following day, the cells were washed with APBS prior to taking cell images with a phase-contrast microscope (Nikon Eclipse TSX-100 at earlier passage, Zeiss AxioVert-A1 at later passage). Digital images were taken of 3-5 fields of view from each well for each cell type. The numbers of β-galactosidase positive (blue) and negative cells (clear) were enumerated from a minimum of 400 cells counted for each cell type. The

numbers of cells positive for senescence-associated β-galactosidase activity were expressed as a percent of the total number of cells enumerated for each cell type examined.

2.2.8. Hoechst staining for Mycoplasma detection

Thirty thousand Xela DS2 (passage 151) and Xela VS2 (passage 135) cells were seeded separately onto sterile cover slips (Baxter) in a 6-well plate in 1 mL of complete medium. The plate was sealed with parafilm and placed overnight at 26°C. The following day, cells adhered to the coverslip were washed with room temperature APBS and fixed immediately with an ice-cold acetic acid and methanol fixative at a 1:3 ratio, respectively, for 20 min at – 20°C. The cells were washed twice with room temperature APBS for 5 min under gentle agitation prior to the addition of 1 mL chilled Hoechst 33342 solution (Fisher) for 5 min, at a 1:2000 dilution in APBS; protected from light. The cells were washed twice with room temperature APBS for 5 min with gentle agitation. Excess liquid was allowed to run off the coverslip before being mounted on a glass slide in a 1:10 ratio of 100 mM Tris solution (pH 8.0) to glycerol. The slides were kept in the dark at room temperature overnight and the coverslips were sealed the following day with nail polish. Images were captured on an inverted fluorescent microscope (Zeiss Axio Vert.A1) under oil immersion at 630× magnification.

2.2.9. Determination of optimal growth conditions

To assess the optimal growth conditions for Xela DS2 and Xela VS2 cell lines, three sets of experiments were performed to examine the effect of temperature, percent FBS supplementation and seeding density on cell growth. For each experiment, Xela DS2 and Xela VS2 cells were harvested from confluent cultures via trypsin treatment. Trypsin was inactivated by the addition of complete medium and removed via centrifugation at 500 × *g*

for 5 min. The resultant cell pellet was resuspended in complete medium. Cell concentration was determined by mixing a subsample of the cell suspension with Trypan Blue (Invitrogen) at a 1:1 ratio and viable cells enumerated using a hemocytometer. Cells were seeded at the desired concentration in duplicate or triplicate wells per time point and treatment.

The first set of experiments aimed to determine the optimal temperature for cell growth. Cells were seeded in a 6-well plate in triplicate at cell densities of 40,000 cells/well for both Xela DS2 (passages 118-120) and Xela VS2 (between passages 123-129), in 1 mL of complete medium. Cells were placed at 26°C overnight to allow cells to adhere. The following day, the number of adherent cells was enumerated from the day 0 treatment wells. To each of the remaining wells, 1 mL of complete medium was added prior to placing the plates at their appropriate experimental temperatures of 14°C, 18°C, 22°C, 26°C, and 30°C. The number of viable adherent cells in each well was enumerated after 2 d, 4 d, 6 d, and 8 d of growth at differing temperatures. This experiment was repeated three independent times.

The second set of experiments examined the effect of varying the percentage of FBS supplementation on cell growth. Cells were seeded in a 6-well plate in triplicate at cell densities of 40,000 cells/well for both Xela DS2 (between passages 118-120) and Xela VS2 (between passages 123-129), in 1 mL of complete medium. After allowing the cells to adhere overnight at 26°C, cells from triplicate wells were enumerated and represent the cell number at day 0. To all other wells, the media was removed and replaced with 2 mL of AL-15 supplemented with either 0%, 2%, 5%, 10%, 15%, or 20% FBS. Plates were placed at 26°C for duration of the experiment. After 4 days and 8 days post addition of media supplemented with varying percentages of FBS, the number of viable adherent cells in each well were enumerated. The experiment was conducted three independent times.

In the last set of experiments, the effect of cell density on cellular growth was examined. Xela DS2 (between passages 92-102) or Xela VS2 (between passages 93-103) cells were seeded in duplicate wells in 1 mL of complete medium at 10,000, 20,000 or 40,000 cells/well of a 6-well plate. Cells were allowed to adhere overnight at 26°C. The following day, cells were harvested for day 0 counts, and to all remaining wells an additional 1 mL of complete medium was added. Cell growth was monitored by enumerating the number of viable adherent cells after 2 d, 4 d, 6 d, and 8 d of incubation at 26°C. The experiment was repeated five times ($N = 5$).

In all experiments, cells were enumerated by first aspirating media, washing cells with 1 mL APBS and then adding 400 µL trypsin to detach cells from the tissue culture plates. Once all cells were detached, an equal volume of complete media was added to inactivate trypsin and the entire cell suspension was collected in a 1.5 mL microcentrifuge tube (Axygen). An additional 400 µL of media was added to the wells to collect any remaining cells and added to the corresponding microcentrifuge tube. Samples were centrifuged for 5 min at 500 × *g* and resuspended in a known volume of complete medium. A subsample of each cell suspension was mixed 1:1 with trypan blue and counted using a hemocytometer.

2.2.10. DNA isolation

Total DNA was isolated from 2×10^6 Xela DS2 or Xela VS2 cells using the TRI reagent method according to the manufacturer's instructions. Briefly, cells were collected by centrifugation at 500 × *g* for 5 min and lysed with 1 mL of TRI reagent (Sigma) by pipetting. Samples were incubated at room temperature for 5 min prior to the addition of 0.2 mL chloroform and vigorous shaking for 15 s. Mixtures were allowed to sit at room temperature

for 5 min prior to centrifugation at 12,000 × *g* for 15 min at 4°C. The top aqueous phase was discarded and 0.3 mL of 100% ethanol added to the remaining interphase and organic phase and mixed by inversion. Samples were left at room temperature for 3 min before centrifugation at 2,000 × *g* for 5 min at 4°C. The supernatant was removed and the DNA pellet was washed 2 × with 1 mL of 0.1 M sodium citrate in 10% ethanol. Between washes, the DNA pellet was allowed to stand in the sodium citrate/ethanol wash solution for 30 min, vortexed and centrifuged at 2,000 × *g* for 5 min at 4°C. The supernatant was removed and the DNA pellet was further washed 2 × with 1.5 mL 75% ethanol. Between washes, the DNA pellet was allowed to stand in the ethanol wash solution for 20 min, vortexed and centrifuged at 2,000 × *g* for 5 min at 4°C. The ethanol was aspirated and the DNA pellet allowed to air dry for approximately 10 minutes before being resuspended in TE (Tris-EDTA) buffer (pH 8.0). Total DNA quantity and purity was determined using a NanoDrop 1000 Spectrophotometer.

2.2.11. DNA barcoding

PCR reaction conditions and barcoding primers for amphibians were adapted from Che et al, 2012. Taxonomic DNA barcoding sequences the 5'-region of cytochrome c oxidase subunit I mitochondrial gene; for amphibians, the forward degenerate primer sequence was 5'-TYTCWACWAAYCAYAAAGAYATCGG-3' and reverse degenerate primer sequence was 5'-ACYTCRGGRTGRCCRAARAATCA-3' (Che et al., 2012). PCR reactions consisted of (final concentrations) PCR reaction buffer containing 2mM $MgCl_2$ (GeneDireX), 200 nM dNTP (GeneDireX), 200 nM sense and antisense primers (Sigma), 0.625 U Taq DNA Polymerase (GeneDireX), and 50 ng DNA template in a 25 µL reaction volume. The cycling conditions were as follows: initial denaturation at 95°C for 10 min; 35

amplification cycles of 94°C for 1 min, annealing at 45°C for 1 min and elongation at 72°C for 1 min; followed by a final extension step at 72°C for 10 min. In tandem with the PCR, a no template control using molecular grade water was used. To each PCR reaction, 5 µL of 6× loading buffer [0.15% xylene cyanol (ICN Biomedicals), 30% v/v glycerol (EMD Chemicals)] was added prior to loading into a 2.0% agarose (VWR) gel containing 1× RedSafe Nucleic Acid Staining Solution (FroggaBio) and electrophoresed in 1× Tris-Acetate-EDTA (TAE) buffer at 140 V for 20 min.

To purify DNA amplicons from agarose gel slices, bands were excised from the gel, placed in a 1.5 mL microcentrifuge tube and frozen at -80°C for 30 min. A hole was punctured in the bottom of a 0.5 mL tube (LifeGene), stuffed with a small amount of glass wool (Acros Organics), and the frozen gel slice added. The 0.5 mL tube containing the gel slice was placed inside a 1.5 mL microcentrifuge tube and centrifuged at 14,500 × *g* for 5 min. To the flow through, 0.1 volumes of 3 M sodium acetate and 1 volume of isopropanol was added. Samples were vortexed before centrifugation at 14,500 × *g* for 15 min. The pellet was washed 2 × with 1 mL of 70% ethanol, vortexed and centrifuged at 14,500 × *g* for 5 min at 4°C between washes. The precipitated DNA amplicons were resuspended in molecular grade water, cloned into the pUCM-T cloning vector (BioBasic) according to manufacturer's instructions, and transformed into chemically competent *Escherichia coli* XL1-Blue by heat shock (1 min, 42°C). Transformed cells were allowed to recover for 1 h at 37°C with shaking at 220 rpm in SOB medium (2% w/v tryptone, 0.5% w/v yeast extract, 8.56 mM NaCl, 2.5 mM KCl, 10 mM $MgCl_2$). Transformed bacteria were plated on LB agar plates containing 100 µg/mL ampicillin (Fisher), 2 mg X-gal (BioBasic) and 2 µmol IPTG (Fisher) at 37°C overnight. The following day, white colonies were selected and the presence of inserts

confirmed by colony PCR using M13 forward (5'-TTGTAAAACCGACGGCCAGTG -3') and reverse (5'-GGAAACAGCTATGACCATGATTACGC -3') primers. Positive colonies were inoculated in 2 mL of LB broth containing 100 µg/mL ampicillin and grown overnight at 37°C with shaking at 220 rpm. The next day, bacteria were collected by centrifugation (10,000 × *g*, 5 min) and plasmids isolated using a modified plasmid isolation protocol. Briefly, bacterial pellets were resuspended in 100 µL of ice-cold 50 mM glucose, 10 mM EDTA, 25 mM Tris, pH 8.0 and vortexed to mix. To this mixture, 200 µL of room temperature 0.2 N NaOH, 1.0% SDS solution was added to the suspension and inverted to mix, followed by the addition of 150 µL of ice-cold 3 M KOac, pH 6.0. Lysates were centrifuged at 15,500 × *g* for 30 min at 4°C. The supernatant was transferred to a new 1.5 mL microcentrifuge tube and incubated with 20 µg RNase A (BioBasic) for 20 min at 37°C. After incubation, 2.5 volumes of isopropanol was added, the solution inverted to mix, and centrifuged at 15,500 × *g* for 30 min at 4°C. The plasmid pellet was washed 2 × with 1 mL of 70% ethanol by vortexing and centrifuging at 15,500 × *g* for 5 min at 4°C between washes. Ethanol was aspirated and the plasmid DNA pellet allowed to air dry before being resuspended in molecular grade water. A minimum of 10 positive clones generated from each cell line were sent to the TCAG Facility at The Centre for Applied Genomics (Toronto, Ontario, Canada) for sequencing. Resulting sequences were subjected to Clustal Omega multiple sequence alignment (MSA) against the complete genome of *X. laevis* mitochondrion (GenBank Accession HM991335.1) to confirm the identity of the amplicons (Appendix A for Xela DS2 MSA, Appendix B for Xela VS2 MSA).

2.2.12. Total RNA isolation and cDNA synthesis

Total RNA was isolated from 1×10^6 Xela DS2 or Xela VS2 cells using the EZ-10 Spin Column Total RNA Minipreps Super Kit (Bio Basic Canada Inc.) according to manufacturer's instructions, with the following modification in order to include an on-column DNaseI digestion: Following the first RW wash step, 30 µL of DNase I solution containing 5 U of DNase I (Thermo Scientific) was added to the spin column for 20 min at room temperature. Afterwards, 500 µL of RW solution was added to the column and left at room temperature for 2-3 min before spin column centrifugation at 6,000 × *g* for 1 min.

Isolation of total RNA from *X. laevis* skin tissues, previously stored at −80°C, was performed using TRI reagent according to the manufacturer's instructions. Briefly, *X. laevis* dorsal and ventral skin were ground to a powder using a mortar and pestle under liquid nitrogen and transferred to a 1.5 mL microtube containing 1 mL of TRI reagent. Tissues were homogenized by passage through a 1 mL syringe fitted with a 25½ gauge needle. Once homogenized, samples were placed on ice for 5 min prior to centrifugation at 12,000 × *g* for 10 min at 4°C to remove particulates. The supernatant was transferred to a new tube to which 0.2 mL chloroform was added and samples shaken vigorously for 15 s. Mixtures were allowed to sit at room temperature for 5 min prior to centrifugation at 12,000 × *g* for 15 min at 4°C. The top aqueous phase was transferred to a new tube containing 0.5 mL isopropanol and mixed by inversion. Samples were left on ice for 10 min followed by centrifugation at 12,000 × *g* for 10 min at 4°C. The supernatant was removed and the RNA pellet was washed 2× with 1 mL of 75% ethanol, vortexed and centrifuged at 12,000 × *g* for 5 min at 4°C between washes. Ethanol was aspirated and the RNA pellet allowed to air dry before being resuspended in molecular grade water. RNA was treated with DNAseI (Fermentas) according

to the manufacturer specifications. Total RNA quantity and purity was determined using a NanoDrop 1000 Spectrophotometer. RNA quality was further assessed by running 1 µg RNA on a 2.0% agarose gel containing 1× RedSafe Nucleic Acid Staining Solution and electrophoresed in 1× TAE buffer at 120 V for 30 min.

RNA was reverse transcribed into cDNA using the SensiFAST cDNA Synthesis Kit (BioLine) according to manufacturer's specifications. Briefly, 500 ng of RNA was mixed with 4 µL of 5× reaction mix in a total volume of 20 µL. The resulting reactions were incubated at 25°C for 10 min, 42°C for 15 min and the reaction inactivated by incubation at 85°C for 5 min. Synthesized cDNA was stored at -20°C until use.

2.2.13. Reverse transcriptase polymerase chain reaction (RT-PCR) for the detection of cell type transcript markers

Primers for *X. laevis* β-actin (*actb*), collagen type I A1 (*col1a1*), collagen type I A2 (*col1a2*), collagen type III (*col3*), cytokeratin 5 (*krt5*), cytokeratin 14 *(krt14*), cytokeratin 19 (*krt19*), vimentin (*vim*), cadherin 1 (*cdh1*), claudin 1 (*cldn1*), claudin 3 (*cldn3*), and occludin (*ocln*) (Table 2.1) were designed using the online PrimerQuest tool from Integrated DNA Technologies (IDT; https://www.idtdna.com/Primerquest/Home/Index). RT-PCR reactions (25 µL reactions) consisted of (final concentrations) PCR reaction buffer containing 2 mM $MgCl_2$, 200 µM dNTP, 200 nM sense and antisense primers (Sigma), 0.625 U Taq DNA polymerase. Reaction template included cDNA generated from isolated *X. laevis* dorsal skin and ventral skin tissue RNA, and cDNA generated from Xela DS2 (between passages 72-88) and Xela VS2 (between passages 73-89) RNA samples. For cell type marker detection (*col1a1*, *col1a2*, *col3*, *krt5*, *krt14*, *krt19*, *vim*, *actb*) the cycling conditions were as follows: initial denaturation at 95°C for 5 min; 35 amplification cycles (*krt5*), 32 amplification cycles

(*col1a1, col1a2, col3, krt14, krt19*), or 26 amplification cycles *(vim, actb)* of 95°C for 45 s, annealing at 55°C for 30 s and elongation at 72°C for 45 s; followed by a final extension step at 72°C for 5 min. For gap junction marker detection (*cdh1, cldn1, cldn3, ocln, actb*) the cycling conditions were as follows: initial denaturation at 95°C for 5 min; 28 amplification cycles (*cdh1, cldn1, cldn3, ocln*), 23 amplification cycles *(actb)* of 95°C for 45 s, annealing at 57°C for 30 s and elongation at 72°C for 45 s; followed by a final extension step at 72°C for 5 min. A no template control was set up for all primer sets, and an RNA only control for each RNA sample was set up using β-actin primers. Both sets of RT-PCR reactions were repeated three times, using cDNA generated from Xela DS2 and Xela VS2 RNA at three different passages. To each RT-PCR reaction, 5 µL of 6× loading buffer (0.15% xylene cyanol, 30% v/v) was added prior to loading into a 2.0% agarose gel containing 1× RedSafe Nucleic Acid Staining Solution and electrophoresed in 1× TAE buffer at 140 V for 20 min. Gels were imaged via ChemiDoc imager using Image Lab program. Bands were excised from the gel, purified, and prepared for sequencing as described in Section 2.2.11. Resulting sequences were subjected to BLASTn (Altschul et al., 1990) analysis to confirm the identity of the amplicons (Appendix C).

2.2.14. Treatment of Xela DS2 and Xela VS2 cells with poly(I:C)

Xela DS2 (between passages 110-116) or Xela VS2 (between passages 111-118) cells were seeded in a 6-well plate at a cell density of 2×10^6 cells per well in 1 mL of complete medium and allowed to adhere overnight at 26°C. At the time of treatment, medium was replaced with 2 mL of fresh complete medium (time-matched controls) or complete medium containing 10 µg/mL polyinosinic-polycytidylic acid [poly(I:C), Sigma Aldrich Catalogue #

Table 2.1. List of primers used for RT-PCR in the identification of Xela DS2 and Xela VS2 cell type.

Gene target	Sequence (5'→3')	Accession Number
actb	**S –** ATCGTGGGGCGCCCCAGGCACC| **AS -** CTCCTTAATGTCACGCACGATTTC	NM_001091337.1
Fibroblast cell markers		
col1a1	**S –** ATTCAACGGACCCTCTGGAC **AS –** ATCTTCAGGTCACGGCAGGT	NM_001087352.1
col1a2	**S –** AGCGTGGCTATCCTGGAAAC **AS -** ATTCACCACCAAAGCCACCA	NM_001087258.1
col3	**S –** CTGGTGGTCGTGGTATTGTT **AS -** TTAGATCCTGGTGGTCCTCTT	NM_001090075.1
Epithelial cell markers		
krt5	**S –** GTCATCAGCTCTGGAGGCAA **AS -** TGCACAGACAATGCTTGAGAG	NM_001085584.1
krt14	**S –** TTTTGACCGGTGGCACTTCT **AS -** CAACTCCCACACTGGACCTG	NM_001166441.1
krt19	**S –** CCAAGTCGGTGGACAAATTA **AS -** CCATAACGGGCTTCTGTTT	NM_001091523.1
Mesenchymal cell marker		
vim	**S -** CTGTCGGAAGCTGCTAATC **AS -** CAACCTGTCCATCTCTTGTC	NM_001087439.1
Epithelial adherens junction marker		
cdh1	**S -** ACAGTGAAGGGTTTGGACTATG **AS -** CACCAGTCAGCTCTGCTTTAT	NM_001172232.1
Epithelial tight junction marker		
cldn1	**S -** CTGGGCTGGATTGGGTTTATAG **AS -** CTACTCCAACCTTTGCCTTCTT	NM_001085976.1
cldn3	**S -** GGATGGATAGGAAGTGTGGTATG **AS -** GTTGACCTGGCAGCTGTATAA	NM_001093931.1
ocln	**S -** CTTCTGGATCGGCTTTCTACAC **AS -** GGCAGACTCTCCTCCTGTATTA	NM_001088474.1

P1530-25MG]. Phase contrast digital images were taken of control and poly(I:C) treated cells at 0 h, 3 h, 6 h, 12 h, and 24 h post treatment using a Leica DMi1 microscope fitted with a MC170 color camera and LASX 4.8 software to assess cell morphology. At each time point, cells from time-matched controls and poly(I:C) treatments were harvested by using a cell scraper to lift adherent cells from the culture vessel surface into suspension. This was collected and centrifuged at 230 × *g* for 10 min, collecting both previously adherent cells as well as cells which lost adherence from poly(I:C) treatment. The supernatant was aspirated and the cell pellet was used for total RNA isolation using the EZ-10 Spin Column Total RNA Minipreps Super Kit as described in Section 2.2.12. Assessments of RNA quantity, purity, and integrity, and subsequent cDNA synthesis, were performed as described in Section 2.2.12. The cDNA samples were stored at -20°C until use in quantitative RT-PCR (qRT-PCR) transcript analysis.

2.2.15. RT- qPCR of Xela DS2 and Xela VS2 poly(I:C) stimulated cells

Primer sequences and accession numbers for *X. laevis* tumor necrosis factor (*tnf*), interleukin-1 (*il1*), interleukin-8 (*il8*), inhibitor of kappa B (*ikb*), type I interferon (*ifn1*), protein kinase R (*pkr*), and myxovirus resistance gene 2 (*mx2*) can be found in Table 2.2; primer efficiencies and R^2 values are also reported. Prior to transcript analysis, gene stability testing was conducted for *actb*, cyclophilin (*cyp*), elongation factor 1-α (*ef1a*), glyceraldehyde 3-phosphate dehydrogenase (*gapdh*), and hypoxanthine-guanine phosphoribosyltransferase (*hgprt*) to determine a stable endogenous control selection. cDNA samples across all trials generated from Section 2.2.12 was pooled together in a time-matched and treatment-matched fashion, then diluted to 1:40 for all reactions. RT-qPCR reactions were prepared in triplicate and consisted of (final concentrations) 250 nM sense and

antisense primer, 5 µL PowerUp SYBR green mix (Thermo Scientific), and 2.5 µL of 1:40 diluted, pooled cDNA at a final reaction volume of 10 µL. All reactions were prepared in a MicroAmp fast optical 96-well reaction plate and optical film (Life Technologies) and run on QuantStudio5 Real-Time PCR System (Thermo Scientific). The cycling conditions were as follows: initial denaturation at 50°C for 2 min, followed by 95°C for 2 min, 40 amplification cycles of denaturation at 95°C for 1 s, and extension at 60°C for 30 s. A melt curve step followed all runs to ensure only a single dissociation peak was present, with initial denaturation at 95°C for 1 s, then dissociation analysis at 60°C for 20 s followed by 0.1°C increments between 60°C and 95°C at 0.1°C/s. Gene stability measures (M-value) were determined for all endogenous control candidates, wherein a lower M-value infers stronger gene stability across time and treatment. The lowest M-value was for *ef1a* at 0.278 and 0.217 for Xela DS2 and Xela VS2, respectively; *ef1a* was thus selected as the endogenous control (Table 2.3). For transcript analysis, cDNA generated from Section 2.2.12 was diluted to 1:20 for all reactions. RT-qPCR reactions were prepared in triplicated and consisted of 500 nM sense and antisense primer, 5 µL PowerUp SYBR green mix, and 2.5 µL of 1:20 diluted cDNA in a final reaction volume of 10 µL. The cycling conditions and melt curve step were performed as previously described. All reactions were prepared in a MicroAmp fast optical 96-well reaction plate and optical film and run on QuantStudio5 Real-Time PCR System. RT-qPCR reactions for transcript analysis were repeated five times, using cDNA generated from experiments outlined in Section 2.2.14 (N = 5). Amplicons from all primer sets used in RT-qPCR reactions were sequenced as described in Section 2.2.11 and resulting sequences were subjected to BLASTn (Altschul et al., 1990) analysis to confirm the identity of the amplicons and amplification of a single gene target (Appendix D).

Table 2.2. List of primers and efficiencies used for RT-qPCR in this study.

Gene target	Sequence (5'→3')	Efficiency (%)	R^2	Accession Number
actb	**S** - GAGCTGCCTGACGGACAAGT **AS** - TACCGCAGGATTCCATACCAA	102.919	0.998	NM_001088953.2
cyp	**S** - TGTGCCAGGGAGGTGACTTC **AS** - CCAGTGTGCTTCAGGGTGAA	104.165	0.998	NM_001089190.1
ef1a	**S** - GTTCATTTACCGCACAGGTTATC **AS** - CGGCGATCAATCTTCTCCTT	97.232	0.998	NM_001087442.1
gapdh	**S** - GGGAATCCTGGGATACACACA **AS** - ATTCAGGGCAATTCCAGCAT	105.677	0.998	NM_001087098.1
hpgrt	**S** - AAGACTTTGCTTGCTATGCTCAAG **AS** - CTGGCCTGTATCCCACACTTC	103.420	0.998	NM_1096766.1
Antiviral targets				
ifn1	**S** - GCTGCTCCTGCTCAGTCTCA **AS** - GAAAGCCTTCAGGATCTGTGTGT	92.719	0.982	KF597522 (Robert, 2015)
mx2	**S** - GGAACGCCGCACTTGCAGAA **AS** - CGATTAATCCTGGCACCTCC	97.232	0.997	XM_018250537.1 (Robert, 2015)
pkr	**S** - GCTCACCGGCGGGATTA **AS** - TTCAACTTTATTCATGCGTGCTATG	105.187	0.998	XM_018261547.1 (Robert, 2015)
Proinflammatory targets				
ikb	**S** - TATCCGCCGTTCATACAAGGA **AS** - GATTTCGTGTTGCTCGGT	86.674	0.999	NM_001093529.1
il1	**S** - CATTCCCATGGAGGGCTACA **AS** - TGACTGCCACTGAGCAGCAT	95.435	0.995	NM_001085605.1 (Robert, 2015)
il8	**S** - CCTATCCATCCCAAGCACATAAA **AS** - GATATCGTCCCCACTTGTCAAAG	92.658	0.998	NM_001097106.1
tnf	**S** - TGTCAGGCAGGAAAGAAGCA **AS** - CAGCAGAGCAAAGAGGATGGT	90.809	0.995	NM_001114778.1 (Robert, 2015)

2.2.16. Statistics

For cell growth experiments, data were analyzed by a two-way analysis of variance (ANOVA) for the relationship between treatment and time with a Tukey's post hoc analysis. Groups were considered statistically significant groups when $p < 0.05$. For RT-qPCR analysis of Xela DS2 and Xela VS2 poly(I:C) stimulated cells, statistical analysis was performed by using a Mann-Whitney test with Bonferroni correction, which considers each time-point (4 total) as an independent test, correcting initial $p < 0.05$ to $p < 0.0125$. As such, statistical significance (*) was determined within each time-point between treated cells and their time matched control wherein significant groups have $p < 0.0125$. Statistical analyses were performed using GraphPad Prism v6 software.

Table 2.3. Candidate endogenous genes for use in RT-qPCR analysis of poly(I:C) treated Xela DS2 and Xela VS2 cells.

Target	Xela DS2 M-Value	Xela VS2 M-Value
actb	0.528	0.266
cyp	0.354	0.226
ef1a	**0.278**	**0.217**
gapdh	0.290	0.348
hgprt	0.367	0.298

2.3. Results

2.3.1. Development of Xela DS2 and Xela VS2 cell lines and cell characteristics

In order to elucidate the contribution of skin epithelial cells to amphibian innate immune responses, I established skin epithelial-like cell lines from the dorsal and ventral skin of *X. laevis*. Within one week of placing *X. laevis* dorsal skin or ventral skin tissue explants in tissue culture flasks, cells were seen migrating out of the tissues (not shown). These cells appeared to have an epithelial-like morphology with simple epithelium structure as seen by a

single layer of polygonal cells with close cell-to-cell contact. Over a period of 3 – 4 months, a flask containing dorsal skin fragments and a flask containing ventral skin fragments, originating from the same animal, produced large islands of adherent single-layered cells surrounding the central mass of tissue and covered ~60-70% of the area in the flask. Trypsin treatment was used to readily detach the cells over subsequent passages, leading to continuous propagation. The resulting cell lines originating from *X. laevis* dorsal skin and ventral skin tissue explants were named Xela DS2 and Xela VS2, respectively. During this time, Xela DS2 and Xela VS2 consistently displayed epithelial-like morphology. At early cell passages of passage 9 for Xela DS2 (Fig. 2.1A) and passage 13 for Xela VS2 (Fig. 2.1E), cells were largely adherent and epithelial-like in morphology (Fig. 2.1A, E). While earlier passages of Xela DS2 and Xela VS2 had slow and patchy growth, later passages of Xela DS2 (Fig. 2.1B) and Xela VS2 (Fig. 2.1F) grew more rapidly and formed confluent monolayers. If cell cultures became over-confluent, cells would begin to lose adherence. Both Xela DS2 and Xela VS2 cell lines are now routinely maintained in complete medium without antibiotics and were split 1:4 every 3-4 days. Xela DS2 and Xela VS2 have been passed >160 times over 4 years since their initial establishment and have been successfully cryopreserved at a variety of passages in complete medium containing 10% DMSO. Xela DS2 and Xela VS2 cell lines were confirmed to be of *X. laevis* origin by sequencing a region of the cytochrome c oxidase I (COI) gene followed by NCBI BLASTn analysis that returned an identical hit for *X. laevis* cytochrome c oxidase subunit I in the mitochondrial genome (GenBank Accession HM991335.1). Clustal Omega multiple sequence alignment (MSA) via EMBL-EBI (Madeira et al., 2019) of the 10 isolated colonies containing Xela DS2 and Xela VS2 COI against *X. laevis* mitochondrial genome is provided in Appendix A.

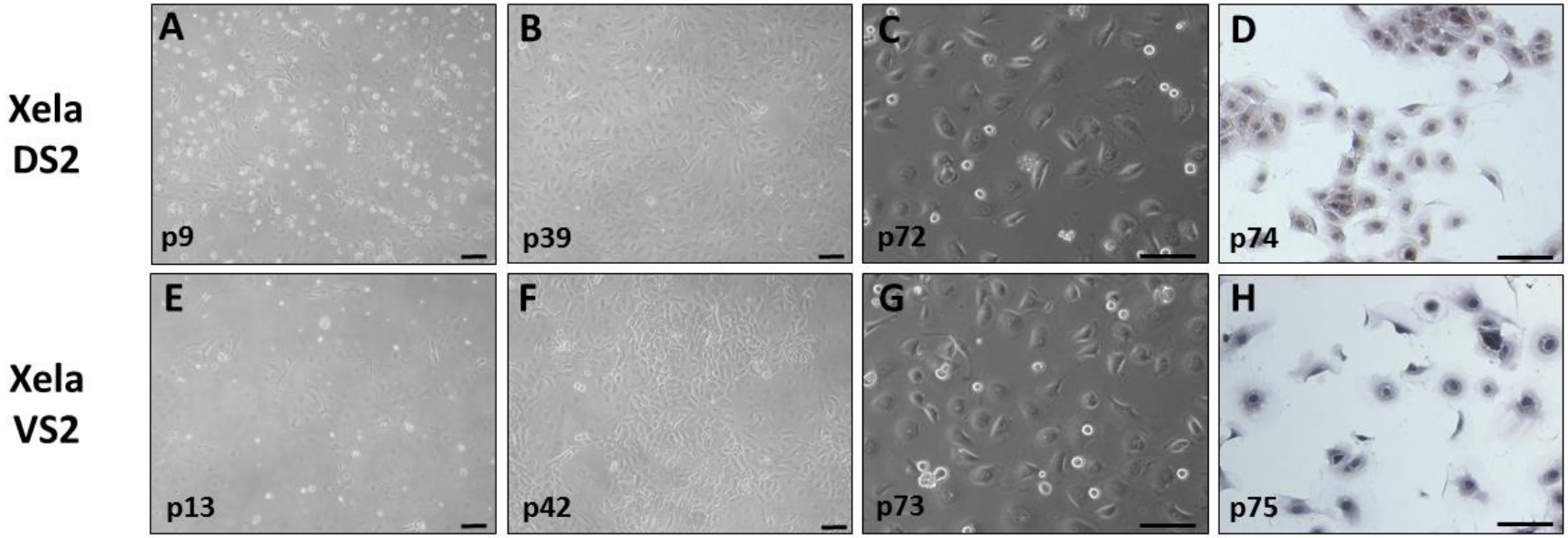

Figure 2.1. Xela DS2 and Xela VS2 cells exhibit epithelial cell-like morphology. Phase-contrast digital images of Xela DS2 cells were taken at passage 9 (A), passage 39 (B), and passage 72 (C), and of Xela VS2 cells at passage 13 (E), passage 42 (F), and passage 73 (G). Bright-field digital images of Hematoxylin and Eosin stained Xela DS2 cells (D) and Xela VS2 cells (H). Scale bars represent a distance of 100 μm.

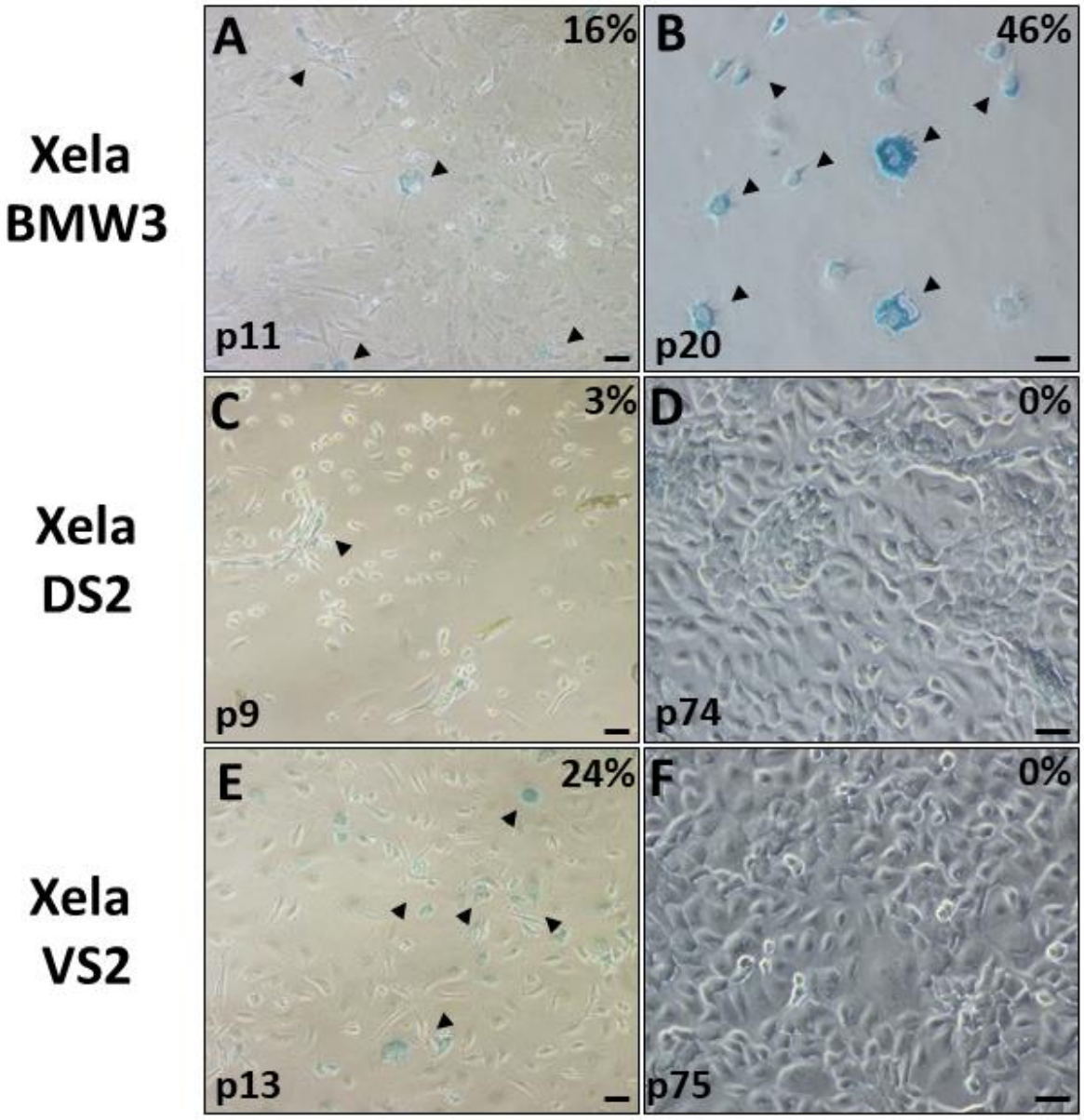

Figure 2.2. Senescence associated β-galactosidase activity of Xela DS2 and Xela VS2 cells from early and established cultures. Xela DS2 and Xela VS2 cells were tested for senescence associated β-galactosidase activity and visualized under phase-contrast microscopy. Cells positive for β-galactosidase activity appear blue. Digital images of Xela BMW3 cells at passage 11 (A), Xela DS2 cells at passage 9 (C), Xela VS2 cells at passage 13 (E), Xela BMW3 cells at passage 20 (B), Xela DS2 cells at passage 74 (D) and Xela VS2 cells at passage 75 (F). Xela BMW3 cells were used as a positive control for β-galactosidase activity. The percent β-galactosidase positive cells is indicated in the top-right hand corner of each image. Scale bars represent a distance of 50 μM.

To characterize cell morphology, cells were stained with Hematoxylin-Eosin. Xela DS2 cells were characterized by oval nuclei and light pink cytoplasm (Fig. 2.1D), while Xela VS2 cells also had oval nuclei but relatively clear to light purple cytoplasm (Fig. 2.1H) and both cell lines appeared epithelial-like with polygonal morphology. At lower cell densities, some Xela DS2 and Xela VS2 cells also appeared crescent-like (Fig. 2.1D, H). Furthermore, at higher cell densities, Xela DS2 and Xela VS2 become compact and had an average cell diameter of approximately 35 μm. Cells from Xela BMW3 continuous cell cultures derived from *X. laevis* bone marrow were used as a positive control for cellular senescence as these cells previously stained positive for β-galactosidase activity (unpublished data). At passage 11 (Fig. 2.2A) and passage 20 (Fig. 2.2B), 16% and 46% of the BMW3 cells appeared blue, respectively, indicative of β-galactosidase activity. At early passages, Xela DS2 (passage 9) and Xela VS2 (passage 13) exhibited 3% and 24% cellular senescence, respectively (Fig. 2.2C, E). However, with successive passages both Xela DS2 (Fig. 2.2D) and Xela VS2 (Fig. 2.2F) cells lost β-galactosidase activity. In addition, Xela DS2 and Xela VS2 were tested for potential mycoplasma contamination by employing the Hoechst staining method. Extranuclear fluorescent foci were not observed in Xela DS2 or Xela VS2 cultures (Fig. 2.3).

2.3.2. Effect of culture conditions on Xela DS2 and Xela VS2 cell growth

Although other *X. laevis* cell lines are routinely cultivated in osmotically adjusted medium containing FBS, the percentage of FBS and incubation temperature varies with the cell line (Pudney et al., 1973; Rafferty, 1969; Sakaguchi et al., 1989). Therefore, I undertook studies to determine the optimal level of serum supplementation and incubation temperature for Xela DS2 and Xela VS2. In general, Xela DS2 and Xela VS2 cell growth occurred in an FBS and time dependant manner. Two-way ANOVA analysis indicated that there is a

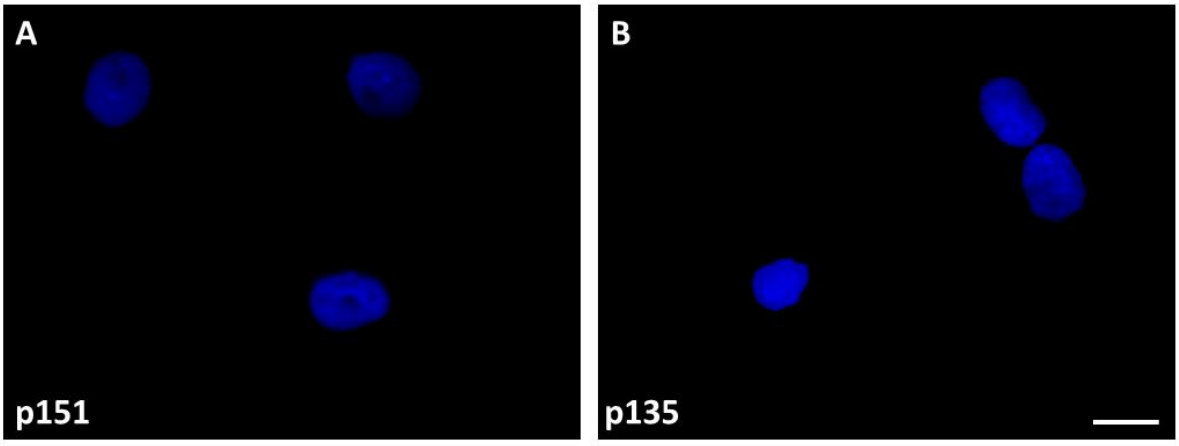

Figure 2.3. Hoechst staining of Xela DS2 and Xela VS2 cells. (A) Xela DS2 at passage 151 (B) Xela VS2 at passage 135. Both cell lines exhibit nuclei with no evidence of fluorescent specks or puncta outside of the nucleus. Magnification, 630× and scale bar is 20 µm.

significant effect due to time ($p < 0.0001$) and FBS treatment ($p < 0.0001$) for both Xela DS2 and Xela VS2. In the absence of FBS supplementation, or with only 2% FBS, no significant differences in cell numbers were observed in Xela DS2 (Fig. 2.4A) or Xela VS2 (Fig. 2.4B) cultures over 8 days at 26°C. However, I noted that Xela DS2 and Xela VS2 cells started to lose adherence to the tissue culture vessel over time when cultured in the absence of FBS; whether this was due to cell death was not assessed. Supplementation of cultures with 5% FBS also did not support statistically significant proliferation of Xela DS2 (Fig. 2.4A) or Xela VS2 cells (Fig. 2.4B), although there were roughly 4-fold as many cells by day 8 of culture for both cell lines. A minimum of 10% FBS was required to promote significant increases in cell numbers in Xela DS2 (Fig. 2.4A) or Xela VS2 (Fig. 2.4B) over 8 days. Indeed, fold change in Xela DS2 (Fig. 2.4A) and Xela VS2 (Fig. 2.4B) cell numbers increased in a dose-dependent manner with FBS supplementation after 8 days, achieving a

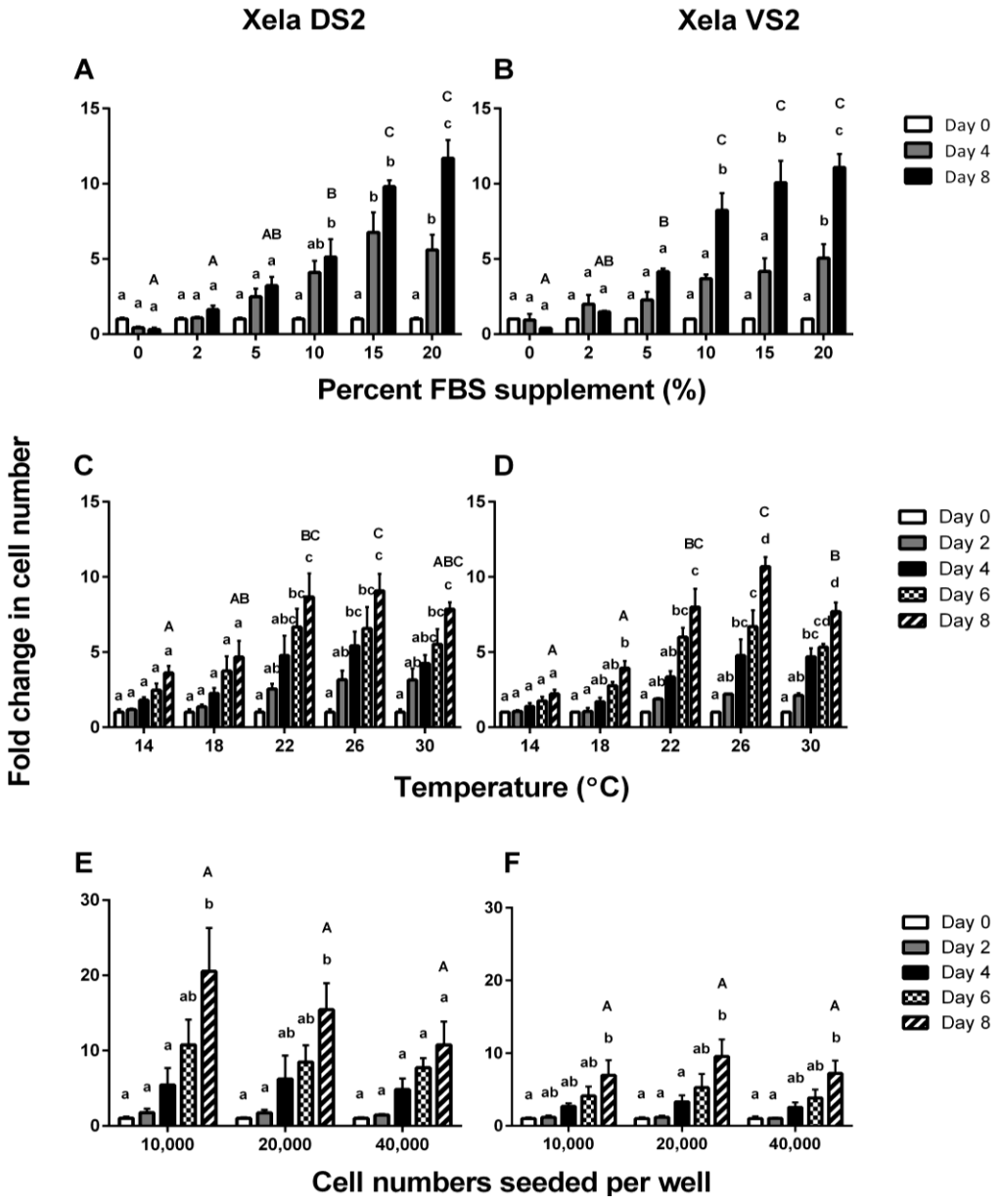

Figure 2.4. Fold change in cell growth for Xela DS2 and Xela VS2 cells under varying conditions. Fold change in Xela DS2 (A) and Xela VS2 (B) cell numbers when seeded at 40,000 cells per well and grown at 26°C in AL-15 medium supplemented with 0%, 2%, 5%, 10%, 15%, 20%, or 30% FBS (n = 3 independent trials). Fold change in Xela DS2 (C) and Xela VS2 (D) cell numbers when seeded at 40,000 cells per well and grown in AL-15 supplemented with 15% FBS at varying temperatures (n = 3 independent trials). Fold change Xela DS2 (E) or Xela VS2 (F) cell numbers after being seeded at varying initial cell densities and grown at 26˚C in AL-15 medium supplemented with 15% FBS (n = 5 independent trials). For all experiments, viable cells were enumerated on the indicated day and expressed as a fold change in cell number relative to the corresponding Day 0 time point. Significant differences were determined by a two-way ANOVA and a Tukey's post-hoc test ($p < 0.05$), wherein like lettering indicates no statistical significance between groups.

maximum ~10-fold increase in cell numbers when cultured in the presence of a minimum of 15% FBS for Xela DS2 (Fig. 2.4A) or 10% FBS for Xela VS2 (Fig. 2.4B). Based on these results, 15% FBS supplementation was chosen for maintenance of, and further experimentation with, Xela DS2 and Xela VS2.

Both Xela DS2 and Xela VS2 showed a time and temperature-dependent increase in cell number. Two-way ANOVA analysis indicated that there was a significant effect due to time ($p < 0.0001$) and incubation temperature ($p = 0.01850$ for Xela DS2, $p < 0.0001$ for Xela VS2) in both Xela DS2 and Xela VS2. Growth of Xela DS2 (Fig. 2.4C) and Xela VS2 (Fig. 2.4D) cells were minimally supported at lower temperatures of 14°C and 18°C after 8 days of cultivation. However, both Xela DS2 (Fig. 2.4C) and Xela VS2 (Fig. 2.4D) demonstrated significant growth over eight days at temperatures above 22°C, with no significant difference in fold change in cell number at 8 days post seeding across the 22°C, 26°C and 30°C for Xela DS2 (Fig. 2.4C) or 22°C and 26°C for Xela VS2 (Fig. 2.4D). Over 8 days of cultivation, Xela DS2 cells exhibited a 9-fold, 9-fold and 8-fold change in cell number when grown at 22°C, 26°C and 30°C (Fig. 2.4C), respectively, while Xela VS2 exhibited an 8-fold, 10.5-fold, and 7.5-fold change in cell number at identical growth temperatures (Fig. 2.4D). While no distinct changes in cellular morphology were noted for Xela DS2 or Xela VS2 at 14°C, 18°C, or 26°C, cells appeared unable to reach well confluency at 30°C as cells began to lose adherence between 6 and 8 days of cultivation (not shown; personal observation). Since Xela DS2 and Xela VS2 appeared to have optimal cell growth over 8 days of cultivation at 26°C, this temperature was selected to maintain the cells and to conduct further studies.

To assess if Xela DS2 or Xela VS2 cells demonstrated contact inhibition, since cells grow in a monolayer and thus have limited space for growth, cells were seeded at 10,000 cells/well, 20,000 cells/well, or 40,000 cells/well in complete medium and cultured for 8 days at 26°C. Two-way ANOVA analysis indicated that there was a significant effect of time ($p < 0.0001$) but not seeding cell density ($p = 0.5607$ for Xela DS2, $p = 0.6700$ for Xela VS2) on the growth of Xela DS2 and Xela VS2. At an initial seeding cell density of 10,000, 20,000, or 40,000 cells per well, Xela DS2 cells (Fig. 2.4E) exhibited a 26-fold, 18-fold, and 12-fold change in cell number over 8 days of cultivation, respectively, albeit not statistically significant from each other. Consistent growth of Xela DS2 was observed at all initial seeding cell densities up to day 4, wherein there was a reduction in the expected levels of fold change in cell numbers in the wells seeded at 20,000 or 40,000 cells per well. Visually, Xela DS2 cells appeared to reach well confluency by day 8 for cells initially seeded at 20,000 cells per well, while confluency appeared to be reached by day 6 for cells initially seeded at 40,000 cells per well. In contrast, Xela VS2 (Fig. 2.4F) exhibited a 7.5-fold, 11-fold, and 8-fold change in cell number after 8 day of culture after initially being seeded at 10,000 cells/well, 20,000 cells/well, or 40,000 cells/well, respectively. Unlike Xela DS2, Xela VS2 cells did not appear to reach confluency by day 8 of cultivation across all seeding cell densities when comparing monolayer morphologies through phase contrast.

2.3.3. Xela DS2 and Xela VS2 express molecular markers of epithelial cells

To characterize the cell type present in Xela DS2 and Xela VS2, the molecular signatures of Xela DS2 and Xela VS2 were investigated and gene targets selected based on those typically expressed in mammalian fibroblast cells, epithelial cells and mesenchymal cells. Genes known to be expressed primarily in fibroblasts include *col1a1*, *col1a2*, and *col3*

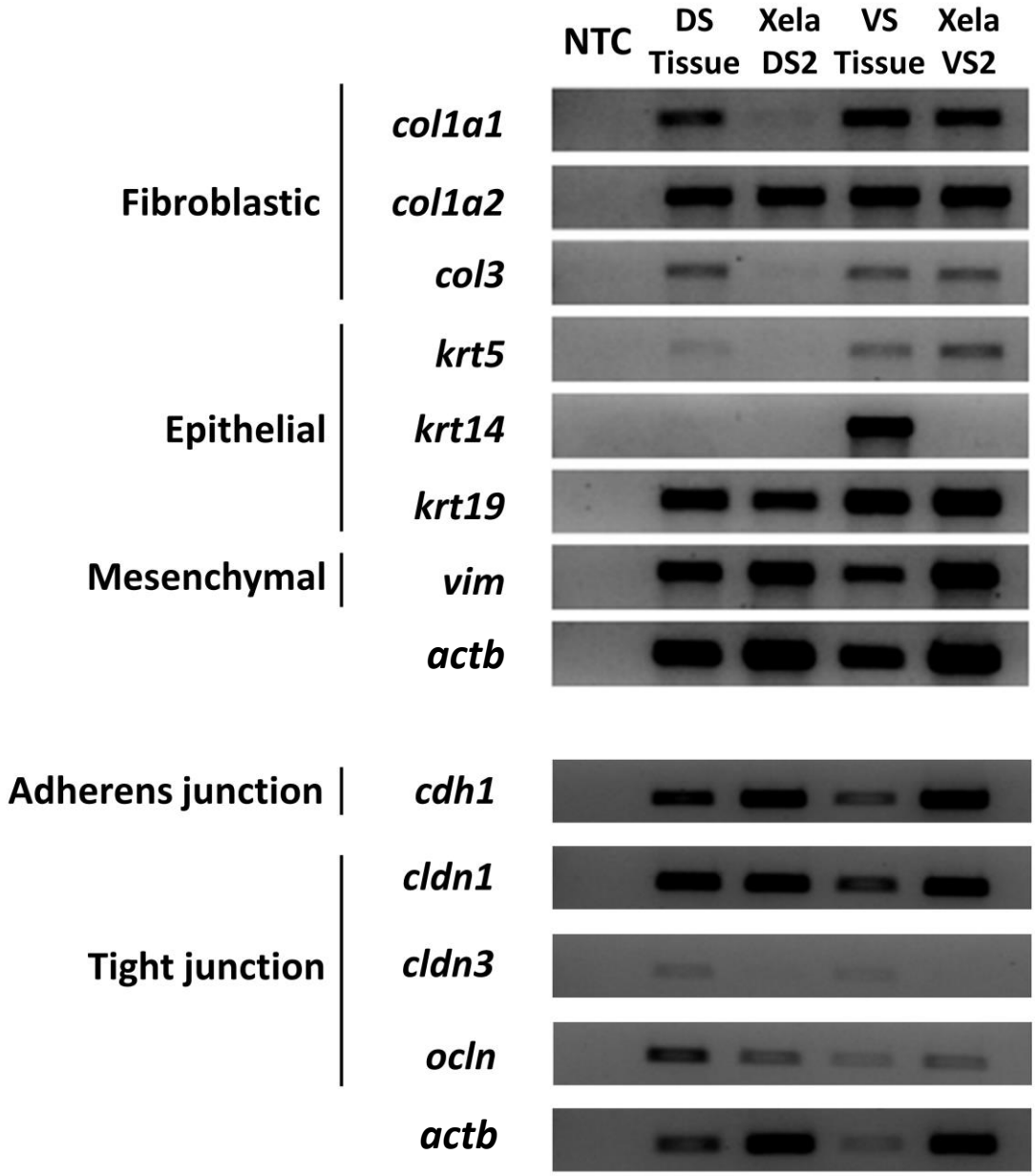

Figure 2.5. Xela DS2 and Xela VS2 have unique molecular signatures characteristic of epithelial cells. Gel electrophoresis from RT-PCR for cell type markers of dorsal skin tissue (DS Tissue), Xela DS2, ventral skin tissue (VS Tissue), and Xela VS2. Gene targets include fibroblastic molecular markers *col1a1*, *col1a2*, *col3*, epithelial molecular markers *krt5*, *krt14*, *krt19*, mesenchymal marker *vim*, and *actb* as an endogenous control. Gel electrophoresis from RT-PCR for epithelial gap junction markers was performed on the same set of samples. Gene targets include adherens junction marker *cdh1*, tight junction markers *cldn1*, *cldn3*, *ocln*, and *actb* as an endogenous control. NTC, no template control (n = 3 independent trials).

which are necessary for extracellular matrix formation (Miskulin et al., 1986; Vuorio et al., 1987). Epithelial cells express an array of cytokeratin for structural support such as *krt5* and *krt14* in epidermal stratified squamous epithelium, or *krt19* in simple epithelium (Chu and Weiss, 2002; Moll et al., 1982). Finally, *vim* was selected as a marker of mesenchymal cells since epithelial cells are known to undergo an epithelial to mesenchymal transition (EMT) in instances (Chaw et al., 2012; Mendez et al., 2010). Dorsal and ventral skin tissues from *X. laevis* expressed all the gene targets examined (Fig. 2.5), with the exception of *krt14* that did not appear to be expressed in dorsal skin tissue. Xela DS2 demonstrated robust expressions of *col1a2*, *krt19*, and *vim*, and barely detectable expressions of *col1a1* and *col3* (Fig. 2.5). Expressions of *krt5* and *krt14* in Xela DS2 were not detected (Fig. 2.5). Xela VS2 expressed *col1a1*, *col1a2*, *col3*, *krt5*, *krt19*, and *vim* genes (Fig. 2.5). However, Xela VS2 did not appear to express *krt14* (Fig. 2.5).

To further ascertain the cell type identities of Xela DS2 and Xela VS2, the expressions of genes involved in encoding for tight and adherens junction proteins, essential to the integrity of the epithelial barrier (Menco, 1980; Villaro et al., 1998), were examined. Tight junctions are strictly localized to epithelial and endothelial cells, requiring claudin and occludin family membrane proteins for formation, while adherens junctions require cadherin family proteins to be functional (Coyne et al., 2003; Yap et al., 1997). Both Xela DS2 and Xela VS2 expressed *cdh1*, *cldn1* and *ocln* genes (Fig. 2.5), wherein *cdh1* is strictly localized to epithelial cells in mammalian systems. The expression of *cldn3* is detected at relatively low levels in frog skin tissue but remains undetected in Xela DS2 or Xela VS2 (Fig. 2.5).

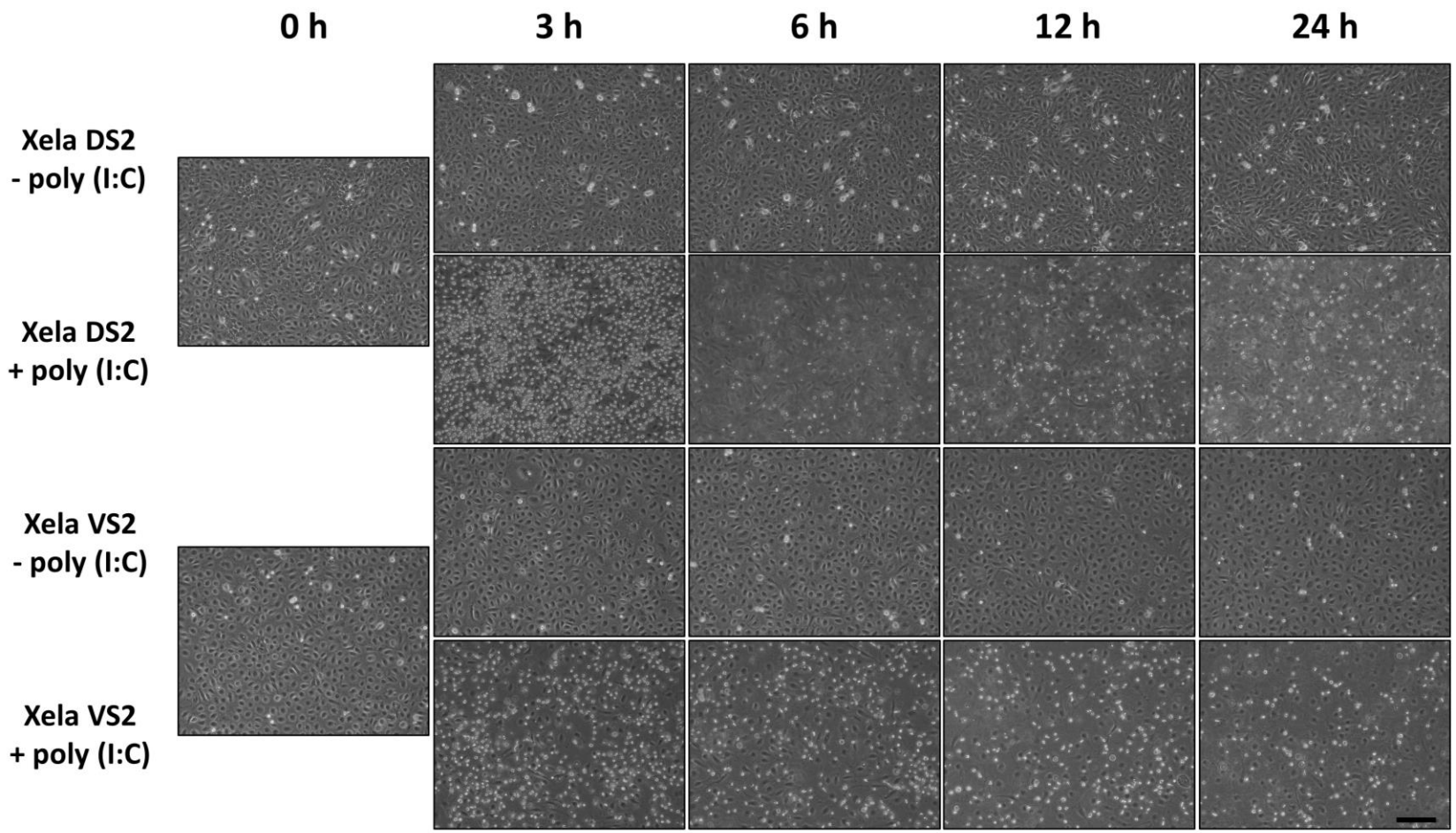

Figure 2.6. Xela DS2 and Xela VS2 cells lose adherence following treatment with poly(I:C). Phase contrast images showing cell morphology of Xela DS2 and Xela VS2 cells in the absence or presence of 10 µg/mL of poly(I:C). Non-treated Xela DS2 or Xela VS2 cells form adherent monolayers with very few non-adherent cells observed. Treatment of Xela DS2 and Xela VS2 cells with poly(I:C) results in cellular loss of adherence as early as 3 h post treatment. Images were taken at 100× magnificent, and scale bar represents a distance of 200 µm.

2.3.4. Effect of poly(I:C) treatment on Xela DS2 and Xela VS2 cell adherence

To assess the potential effects of dsRNA on Xela DS2 and Xela VS2 cell adherence, Xela DS2 and Xela VS2 were treated with 10 µg/mL poly(I:C) at 26°C. Upon treatment of Xela DS2 and Xela VS2 with poly(I:C), a proportion of cells exhibited a loss of adherence to the tissue culture vessel, appearing as suspension cells in the media within 3 h post treatment (Fig. 2.6). Following this initial loss of cell adherence, no further loss of cell attachment was observed over the 24 h treatment period (Fig. 2.6). Sampling of the suspension cells at the 24 h time point revealed the exclusion of trypan blue by these suspension cells, suggesting their membranes were intact and the cells still viable at this time point. Non-treated Xela DS2 and Xela VS2 cells did not exhibit any changes in cell morphology or adherence to the tissue culture vessel over the 24 h time period (Fig. 2.6).

2.3.5. Effect of poly(I:C) treatment on antiviral gene expressions in Xela DS2 and Xela VS2

I next assessed whether poly(I:C) might also be a potent inducer of type I interferon (*ifn1*) in Xela DS2 and Xela VS2. First, it is important to note that *X. laevis ifn1* primers were accessed, and this study conducted, prior to the identification of the expanded *X. laevis* intron-containing and intronless IFNs {Sang, 2016 #419}. As such, while the primer set used for this study has been annotated for identification of type I IFN, the actual amplified target may be within the expanded *X. laevis* Type I IFN family. Xela DS2 showed an initial 3.9 ± 0.7 fold ($p = 0.0079$) increase in *ifn1* transcripts at 3 h post treatment and transcript levels continued to increase in a time-dependent manner, reaching a 7.7 ± 2.6 fold ($p = 0.0079$) increase at 12 h post treatment relative to the time-matched controls (Fig. 2.7A). Although *ifn1* transcript levels were 20.0 ± 9.7 fold ($p = 0.0317$) higher than the time matched non-treated control cells, the relationship is not statistically significant. Xela VS2

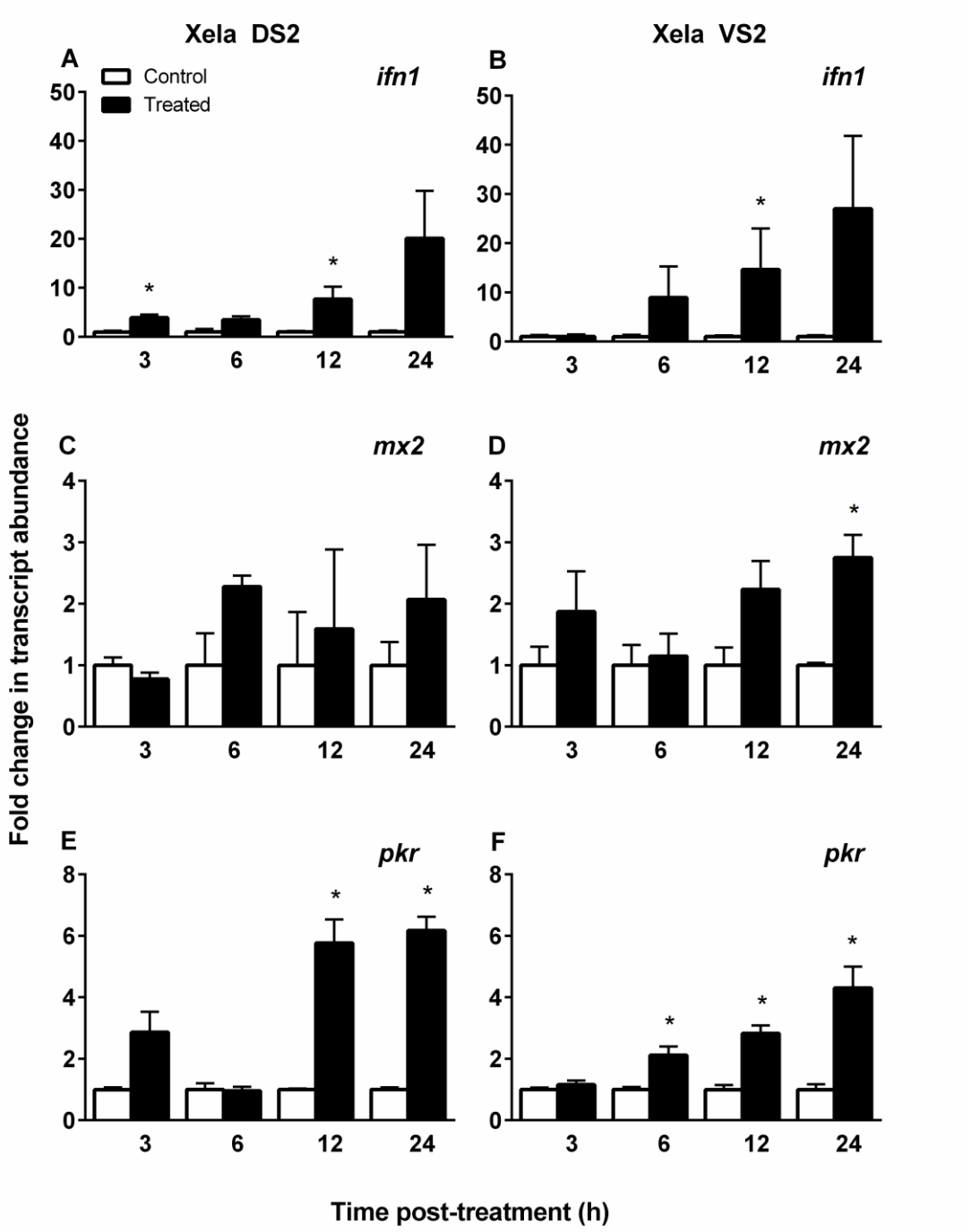

Figure 2.7. Poly(I:C) treatment induces upregulation of type I interferon and interferon stimulated genes in Xela DS2 and Xela VS2. RT-qPCR was performed on cDNA generated from non-treated (control) and poly(I:C) treated Xela DS2 or Xela VS2 cells to determine relative transcript levels of *ifn1* (A, B), *mx2* (C, D), and *pkr*. For all experiments, transcript expression from treated samples was normalized to time matched control, (n = 5 independent trials). Significant differences were determined by a Mann-Whitney test with Bonferroni correction ($p < 0.0125$).

also demonstrated a time-dependent increase in *ifn1* transcript levels over 24 h post poly(I:C) treatment (Fig. 2.7B). At 6 h post poly(I:C) treatment, *ifn1* transcript levels were 8.9 ± 6.3 fold higher than the time matched non-treated control cells (Fig. 2.7B), although not statistically significant ($p = 0.7937$). By 12 h and 24 h post poly(I:C) treatment, *ifn1* mRNA levels in Xela VS2 were 14.6 ± 8.4 fold ($p = 0.0079$) and 27.0 ± 14.8 fold higher ($p = 0.0159$), respectively, than time-matched non-treated controls (Fig. 2.7B). Although the *ifn1* levels are not statistically different from the time-matched controls at 24 h post treatment, the p-value ($p = 0.0159$) is close to the cut-off ($p < 0.0125$).

RT-qPCR was also used to determine transcript levels of the key downstream ISGs, *mx2* and *pkr*, that are important in mediating antiviral programs in host cells in response to type I interferon by limiting viral transcription and viral translation respectively (Haller et al., 2015; Williams, 1999). Over 24 h post treatment with poly(I:C), *mx2* transcript levels did not significantly change in Xela DS2 cells (Fig. 2.7C). Similarly, no significant changes in *mx2* transcript levels occurred in Xela VS2 over the first 12 h post poly(I:C) treatment (Fig. 2.7D). However, by 24 h post treatment, a significant 2.8 ± 0.4 fold ($p = 0.0079$) increase in *mx2* transcripts were observed in Xela VS2 (Fig. 2.7D). In contrast to *mx2* transcript levels, *pkr* transcript levels increased in Xela DS2 (Fig. 2.7E) and Xela VS2 (Fig. 2.7F) cells following poly(I:C) treatment. Xela DS2 showed a significant 5.8 ± 0.8 fold increase ($p = 0.0079$) in *pkr* transcript levels in response to poly(I:C) after 12 h, and this increase in transcript level was similar at 24 h, with a 6.2 ±0.4 fold increase ($p = 0.0079$) above time matched non-treated controls (Fig. 2.7E). Transcripts for *pkr* were also up-regulated in a time-dependent manner in poly(I:C) treated Xela VS2 cells at all time points, reaching a 4.3 ± 0.7 fold increase ($p = 0.0079$) in *pkr* mRNA levels after 24 h post treatment (Fig. 2.7F).

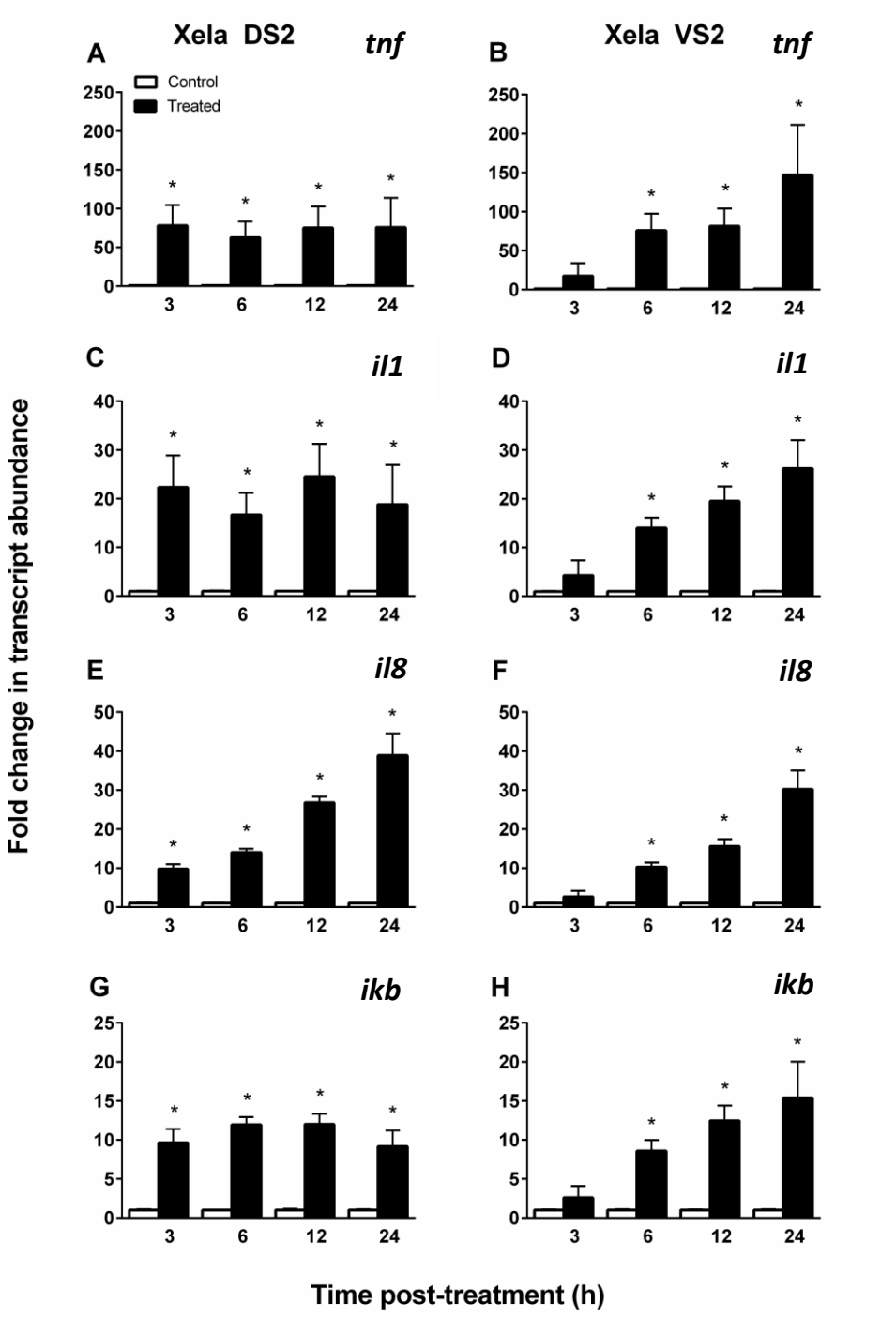

Figure 2.8. Poly(I:C) treatment induces the upregulation of cytokine and chemokine transcript levels in Xela DS2 and Xela VS2. RT-qPCR was performed on cDNA generated from non-treated (control) and poly I:C treated Xela DS2 or Xela VS2 cells to determine relative transcript levels of *tnf* (A, B*), il1* (C, D), *il8* (E, F), *and ikb* (G, H). For all experiments, transcript expression from treated samples was normalized to the time matched control, (n = 5 independent trials). Significant differences were determined by a Mann-Whitney test with Bonferroni correction ($p < 0.0125$).

2.3.6. Treatment of Xela DS2 and Xela VS2 cells with poly(I:C) induces the up-regulation of key proinflammatory cytokines

To determine the whether the sensing of poly(I:C) by frog skin epithelial cells results in promoting a proinflammatory response, RT-qPCR was performed to examine potential changes in proinflammatory transcript levels in Xela DS2 and Xela VS2 in response to poly(I:C) treatment over 24 h. Xela DS2 and Xela VS2 both showed increases in *tnf, il1,* and *il8* proinflammatory transcripts following poly(I:C) treatment (Fig. 2.8). Xela DS2 demonstrated significant increases *tnf* (Fig. 2.8A) and *il1* (Fig. 2.8C) transcript levels of 78.0 ± 26.4 fold ($p = 0.0079$) and 22.3 ± 6.5 fold ($p = 0.0079$), respectively, at 3 h post poly(I:C) treatment, and these increases in transcript levels persisted over the 24 h time period examined. A 75.7 ± 21.7 fold ($p = 0.0079$) increase in *tnf* mRNA levels ($p = 0.0079$; Fig. 2.8B) and a 14.0 ± 0.1 fold ($p = 0.0079$) increase in *il1* mRNA levels ($p = 0.0079$; Fig. 2.8D) were observed at 6 h post poly(I:C) treatment in Xela VS2 cells. Transcript levels of *tnf* and *ilb* remained significantly elevated in Xela VS2 relative to the time-matched, non-treated controls over the entire course of the experiment, with a 146.7 ± 64.7 fold ($p = 0.0079$) increase in *tnf* expression (Fig. 2.8B) and a 26.2 ± 5.8 fold ($p = 0.0079$) increase in *il1* expression (Fig. 2.8D) observed at 24 h post poly(I:C) treatment.

As IL-8 is a potent chemokine and thus instrumental in recruiting innate immune cells (e.g. neutrophils) to the site of inflammation, I measured the relative change in *il8* transcripts in Xela DS2 and Xela VS2 cells in response to poly(I:C) stimulation. Similar to the upregulation of proinflammatory cytokine gene expressions, a time-dependent increase in *il8* transcript levels were observed in Xela DS2 (Fig. 2.8E) and Xela VS2 (Fig. 2.8F) as early as 3 h and 6 h post poly(I:C) treatment, respectively. By 24 h post treatment, *il8* transcript levels reached 38.9 ± 5.6 fold ($p = 0.0079$) and 30.1 ± 4.9 fold ($p = 0.0079$) higher levels in

poly(I:C) treated Xela DS2 (Fig. 2.8E) and Xela VS2 (Fig. 2.8F), respectively, relative to time-matched, non-treated control cells.

Finally, changes in *ikb* expressions in Xela DS2 and Xela VS2 following treatment with poly(I:C) were examined. Xela DS2 showed a significant 9.6 ± 1.8 fold ($p = 0.0079$) increase in *ikb* transcript levels by 3 h post treatment and these transcript levels were sustained throughout the 24 h treatment period (Fig. 2.8G). Similarly, a significant 8.6 ± 1.4 fold increase ($p = 0.0079$) in *ikb* transcript levels were observed in Xela VS2 cells by 6 h post treatment, reaching 15.4 ± 4.6 fold higher transcript levels ($p = 0.0079$), relative to the time-matched controls, by 24 h post treatment (Fig. 2.8H).

2.4. Discussion

2.4.1. Xela DS2 and Xela VS2 are skin epithelial-like cell lines

Xela DS2 and Xela VS2 have been developed from the dorsal and ventral skin of adult African clawed frogs and are the first known skin epithelial-like cell lines to be produced from the adult of this important model organism. Although a number of cell lines have been developed from *X. laevis*, they are mainly derived from embryos (Sakaguchi et al., 1989; Smith et al., 2002) or tadpoles (Anizet et al., 1981; Pudney et al., 1973), with only a handful of cell lines developed from adult frogs, mostly derived from tumors (Rafferty, 1965; Rafferty, 1969; Robert et al., 1994) or restricted to kidney tissue origin such as the A6 (Rafferty, 1969) and XLK-WG (Martin et al., 1998) cell lines. Like other ectothermic vertebrate cell lines (Bols et al., 2017; Rafferty, 1969; Rausch and Simpson, 1988), Xela DS2 and Xela VS2 arose spontaneously through sub-culturing efforts and have been passaged over 160 times within the past four years. Both Xela DS2 and Xela VS2 grow optimally at 26°C; however, they are capable of growth over a much wider temperature range (14°C to

30°C) and thus excellent models for temperature-based research. Although Xela DS2 and Xela VS2 initially exhibited low levels of senescence associated beta-galactosidase activity at early passages, at higher passages beta-galactosidase activity was completely absent. In mammalian cells, beta-galactosidase enzyme activity is usually associated with cellular senescence and is rarely observed in quiescent or immortalized cells (Dimri et al., 1995), permitting beta-galactosidase activity to be used as a general indicator of cellular senescence *in vivo* and *in vitro* (Itahana et al., 2007). The long term and high proliferative capacity, together with the lack of beta galactosidase enzyme activity, supports the immortal nature of Xela DS2 and Xela VS2 cell lines.

Xela DS2 and Xela VS2 cell lines display uniform epithelial-like cell morphology and express epithelial cell associated molecular markers (Chu and Weiss, 2002). Although Xela DS2 and Xela VS2 demonstrate differential *krt5* expression and lack *krt14* expression, both cell lines express *krt19*, a keratin subtype known to be expressed in highly permeable simple epithelium (Chu and Weiss, 2002). This coincides with the characteristic permeable nature of frog skin, as the epidermal layer is relatively thin compared to skin of other organism in order to achieve important physiological functions (Lillywhite, 2006). Furthermore, cytokeratin 19 has been implicated as a marker for skin stem cells that are necessary for continuous regeneration of skin layers and wound healing, and the presence of cytokeratin 19 has been identified in human skin cultures *in vitro* (Michel et al., 1996). Another hallmark of epithelial cells is the formation of cellular junctions, such as adherens and tight junctions. Both Xela DS2 and Xela VS2 express the *cdh1* gene wherein the corresponding cadherin 1 protein, also known as epidermal cadherin, is involved in the formation of adherens junctions specifically between epithelial cells (Proksch et al., 2008;

van Roy and Berx, 2008). These cells also expressed *cldn1* and *ocln* genes that are necessary for the formation of tight junctions between epithelial cells (Furuse et al., 1998; Tsukita and Furuse, 1999) with claudin 1 protein notably known to be important in mammalian epidermal barrier integrity (Furuse et al., 2002). The expression of these cellular junction genes is in accordance with the observed junctions apparent between cells in confluent Xela DS2 and Xela VS2 monolayers when viewed using phase contrast microscopy.

Interestingly, Xela DS2 and Xela VS2 exhibit differential expression of *col* and *vim* molecular markers. Collagen genes are usually expressed by fibroblasts and the production of collagen proteins is important in the formation of the extracellular matrix (Groulx et al., 2011). However, collagen genes are also expressed in epithelial cells (Creely et al., 1988), including mucosal associated epithelial cells (Birkedal-Hansen et al., 1982; Hayashi et al., 1988; Ohji et al., 1994) or epithelial cells undergoing EMT (Hosper et al., 2013; Yang et al., 2013). It is possible that a select population of Xela DS2 and Xela VS2 cells may be undergoing EMT as *vim*, a gene commonly expressed by mesenchymal cells (Chaw et al., 2012; Mendez et al., 2010), was expressed in both cell lines. While my results indicate that Xela DS2 and Xela VS2 differentially express collagen genes, the synthesis and secretion of collagen proteins and formation of extracellular matrixes by these cells lines requires further investigation. Yet, the expression of tight and adherens junction protein transcripts, particularly *cdh1*, is strong evidence to support that Xela DS2 and Xela VS2 are epithelial-like in nature, as cellular junctions are important for maintain epidermal integrity and *cdh1* is known to be localized to epidermal cells (Farquhar and Palade, 1963; Proksch et al., 2008; van Roy and Berx, 2008). Collectively, these results, in conjunction with cell morphology, strongly support that Xela DS2 and Xela VS2 are epithelial-like in origin. Further *in vivo*

detection of these epithelial markers at the protein level is required before Xela DS2 and Xela VS2 can be deemed true epithelial cultures. Nonetheless, the establishment and characterization of Xela DS2 and Xela VS2 represent a key advancement in the generation of *in vitro* model systems for future investigations in amphibian skin epithelial cell biology, including environmental parameters that may impact epithelial cell characteristics such as cellular junctions and transepithelial resistance as a means of determining skin barrier integrity.

2.4.2. Xela DS2 and Xela VS2 are capable of sensing and responding to extracellular dsRNA by initiating antiviral and proinflammatory programs

Poly(I:C) treatment of mammalian epithelial cell cultures resulted in marked upregulation of *TNF*, *IL-1β*, *IL-8*, *IFN1,* and *PKR* gene expressions or protein production (Kinoshita et al., 2009; Kumar et al., 2006). The upregulation of key proinflammatory cytokines *tnf* and *il1* was also observed in the teleost epithelial cell line EPC when treated with poly(I:C) (Holopainen et al., 2012). Xela DS2 and Xela VS2 had an immediate morphological response to poly(I:C) exposure, with many cells losing adherence to the cell culture vessel by 3 h. Both cell lines had marked upregulation in key antiviral genes as well as proinflammatory cytokine transcripts, as expected based on other models studied (Baggiolini et al., 1989; Dinarello, 1996; Zelova and Hosek, 2013). The expression of *il8* in Xela DS2 and Xela VS2 suggests that frog skin epithelial cells may be capable of producing chemotactic factors necessary for the recruitment of immune cells. Xela DS2 and Xela VS2 are thus able to upregulate key antiviral, proinflammatory, and chemokine programs responsible for the initiation and direction of an innate immune response to the site of infection via recruitment of innate immune cells. Furthermore, in mammalian models, Type I IFN binds to its cognate receptor on virus–infected or non-infected neighbouring host cells,

upregulating ISGs (Alsharifi et al., 2008; Schoggins and Rice, 2011) that play an integral role in the inhibition of viral replication and ultimately lead to viral clearance (Sen and Ransohoff, 1993). Although there was no change in *mx2* expression, the increase in *pkr* transcript levels for both Xela DS2 and Xela VS2 likely indicates that these cells are capable of ISG production to further drive host cellular antiviral mechanisms. Overall, my findings suggest potential conservation of the ability for epithelial cells across vertebrates to recognize and respond to dsRNA. The results shown here provide evidence that Xela DS2 and Xela VS2 are capable of sensing extracellular dsRNA, as seen by changes in morphology and upregulation of transcript levels for key genes part of the antiviral and proinflammatory programs. This suggests that frog skin epithelial cells may be more than an inert physical barrier, potentially contributing to an inflammatory response similar to that observed in skin epithelial cells of human and mouse models (Gomez et al., 2013; Nestle et al., 2009). It is important to note, however, that further studies are needed to compare the results obtained using Xela DS2 and Xela VS2 cell lines with frog skin epithelial cell primary cultures as well as comparison to *in vivo* studies.

Sensors of viruses in mammalian skin epithelial cells and teleost cells include Toll-like receptors and scavenger receptors, particularly for their capacity to recognize dsRNA (Dieudonne et al., 2012; Köllisch et al., 2005; Poynter and DeWitte-Orr, 2018). The *X. laevis* genome encodes for TLRs and scavenger receptors, as well as several other mediators of viral infection such as IFN receptors (Ishii et al., 2007; Krause and Pestka, 2005). While there is some evidence to suggest that engagement of such receptors with their cognate ligands or viral nucleic acids generates a typical antiviral response in amphibians (Bird et al., 2002; Krause and Pestka, 2005; Sun et al., 2010), the ability of frog skin epithelial cells to

detect and respond to viral pathogens remains poorly understood. In mammals, frogs and teleosts, class A scavenger receptors bind extracellular poly(I:C) or dsRNA and is believed to traffic extracellular dsRNA to endosomal TLR3 (Matsumoto and Seya, 2008; Poynter and DeWitte-Orr, 2018; Vo et al., 2019b). Although I have not identified the receptor(s) that recognize poly(I:C) on Xela DS2 and Xela VS2, my findings demonstrates that both cell lines are capable of sensing exogenous dsRNA and must express dsRNA-sensing surface PRRs that result in the robust upregulation of antiviral genes and proinflammatory genes in these cells. This may suggest that extracellular dsRNA in aquatic environments may be sensed by frog skin epithelial cells to initiate antiviral defences and confer a level of protection to the host. Finally, while this study examined the expression of an intron-containing IFN, *X. laevis* is known to express a suite of intron and intron-less IFNs (Sang et al., 2016; Wendel et al., 2018) which should be further explored in Xela DS2 and Xela VS2. Frog skin epithelial cells are thus an important first line of defence in sensing pathogens and signalling to underlying immune cells that a threat is present.

Chapter 3: Investigating the role of Xela DS2 and Xela VS2 in recognizing and responding to Frog Virus 3

3.1. Introduction

Emerging infectious diseases, such as Frog Virus 3 (FV3), are believe to be the proximate cause in the current worldwide decline in amphibian populations, with 43% of amphibian species experiencing some form of decline (Daszak et al., 2003; Stuart et al., 2004). FV3 (family *Iridoviridae*, genus *Ranavirus*) is a large double-stranded DNA virus (Chinchar, 2002) and has recently been linked to mass die-offs events in ponds across North America (Gray et al., 2007; Greer et al., 2005). Frogs susceptible to FV3 exposure, such as *R. sylvatica* (Forzán et al., 2017) and *R. catesbeiana* (Miller et al., 2007), exhibit formation of skin lesions, swelling, internal hemorrhage, and while dependent on frog species, FV3 is known to induce necrosis and liquefaction of liver, spleen, renal tubule, hematopoietic tissue and lymphoid tissue (Forzán et al., 2017; Robert et al., 2005).

Transmission of FV3 is believed to occur through direct animal contact, indirectly through the aquatic environment, or through the ingestion of FV3 containing organic material (e.g. cannabolism of infected individuals) (Lesbarreres et al., 2012). In the laboratory, infected adult *X. laevis* can transmit FV3 to healthy adult and larval frogs within 3 h of exposure through waterborne infectivity (Robert et al., 2011). As such, frog skin is an important interface between the frog's internal milieu and the external environment and is likely the first line of defence against direct and indirect sources of environmental FV3. Skin tissue is multi-layered, but unlike in other vertebrae, frog skin has a relatively thin epithelial barrier layer (Varga et al., 2019). Though this aids in the provision of highly permeable frog skin necessary for physiological homeostasis (Lillywhite, 2006; Varga et al., 2019), it may also be disadvantageous as there is physically less barrier for pathogens to cross. Recent

studies in *X. laevis* suggest that Type I IFN responses in skin tissues play an integral role in the FV3 antiviral response wherein subcutaneous administration of Type I IFN into highly susceptible *X. laevis* tadpoles conferred short-term protection from FV3 infection (Wendel et al., 2017; Wendel et al., 2018). While skin is the first interface between a frog and its environment, it is important to also understand the contribution of individual frog skin epithelial cells in mediating a response meant to abrogate FV3 infection, such as participating in the initiation of antiviral programs.

Studies conducted on understanding FV3 viral properties and virus-cell interactions have been done primarily *in vitro*. Albeit being largely performed in mammalian and fish cell lines, FV3 is known to induce a total shutdown of host cellular macromolecular synthesis whether live, heat-inactivated or UV-inactivated (Goorha and Granoff, 1974; Williams, 1996). Investigation of FV3 infection in frog cells *in vitro* has been limited to immune cell (Koubourli et al., 2017; Morales et al., 2010), kidney (Andino Fde et al., 2015), or tadpole (Vo et al., 2019a). To date, no studies have looked at the interaction between FV3 and isolated frog skin epithelial cells. Therefore, the establishment of Xela DS2 and Xela VS2 that are capable of responding to synthetic analogues of viral dsRNA (outlined in Chapter 2) affords an excellent opportunity to investigate the antiviral response of frog skin epithelial cells to FV3 exposure using these two cell lines as a model system. I hypothesized that Xela DS2 and Xela VS2 would be permissive to FV3 infection and be unable to initiate protective cellular antiviral or proinflammatory programs in response to FV3 infection. The first objective of this chapter was to evaluate whether Xela DS2 and Xela VS2 were permissive to FV3 and support viral replication. The second objective was to determine whether these cell lines initiate an antiviral response to FV3. The last objective was to determine if prior

initiation of antiviral programs in Xela DS2 and Xela VS2 would impact cellular cytopathicity and FV3 replication in infected cells. Herein, I report on Xela DS2 and Xela VS2 permissiveness to FV3, their inability to upregulate key antiviral, proinflammatory cytokine and chemokine gene transcripts in response to FV3 challenge, and the effectiveness of prior induction of an antiviral response through pre-treatment of cells with poly(I:C) on limiting FV3 replication.

3.2. Methods

3.2.1. Media

For Xela cell lines, the preparation of complete media and APBS was performed as previously described in Chapter 2 Section 2.2.2. Since viral binding and infection efficiency is hindered at high FBS concentrations (Petricevich et al., 2001), experiments involving FV3 infection of Xela cell lines were performed using AL-15 supplemented with 2% FBS (VWR), herein referred to as Xela low serum media. Epithelioma Papulosum Cyprini (EPC) cells were maintained in L-15 (Wisent Inc.) supplemented with 10% FBS, herein referred to as EPC complete media. For FV3 applications using EPC cells, L-15 supplemented with 2% FBS was used and will be referred to as EPC low serum media.

3.2.2. Cell culture maintenance

The maintenance of Xela DS2 and Xela VS2 was performed as previously described in Chapter 2 Section 2.2.4. For all experiments herein, a plating efficiency of 79% for Xela DS2, 83% for Xela VS2 was taken into account when seeding cells. EPC cells were kindly provided by Dr. Niels Bols at the University of Waterloo. Although it is known that current EPC cell lineages were contaminated with fathead minnow cells, they are still deemed worth retaining as a cell line for the study of aquatic viruses (Winton et al., 2010). EPC cells were

selected since they have been widely used in the study of FV3 and in FV3 propagation (Ariel et al., 2009; Pham et al., 2015). EPC cells were maintained in T-75 cm^2 plug-seal tissue-culture treated flasks containing 10 mL of EPC complete media at 26°C. EPC cells were subcultured 1:4 every 5-7 days as follows: media was removed from the flask and cells washed with 6 mL of 1× PBS. Following the removal of PBS, 2 mL 0.25% trypsin-EDTA (Wisent Inc.) was added to detach cells from the cell culture vessel. Immediately following total cell detachment from the flask, 2 mL of EPC complete media was added to inactive trypsin prior to seeding at 1:4. Cells harvested from flasks were used in experiments by first centrifuging at 300 × *g* for 10 min and resuspension in fresh EPC complete media. EPC cells demonstrated 100% plating efficiency when enumerated the day after seeding.

3.2.2.1. Cryopreservation of EPC cells

Harvested EPC cells were used for cryopreservation as previously described in Chapter 2 Section 2.2.5 with the following changes: EPC cells were centrifuged at 300 × *g* for 10 min, and cells were resuspended to approximately 10-12 × 10^6 million cells per mL in chilled EPC complete media containing 10% DMSO.

3.2.3. Propagation of FV3 in EPC cells

FV3 (Granoff strain, ATCC VR-567) was a kind gift from Dr. Niels Bols at the University of Waterloo. FV3 was propagated in confluent EPC cells, known to be highly permissive to FV3 infection. EPC cells were maintained at 26°C in T-75 cm^2 plug-sealed flasks containing EPC complete media. For FV3 propagation, 1 mL of stock FV3 was diluted in 9 mL of EPC low serum media and the entire volume placed on a confluent flask of EPC cells for 7 days at 26°C. At 7 days post infection (dpi), cell culture media from the flask of infected EPC cells was collected, centrifuged at 1000 × *g* for 10 min, filtered through a 0.22

μm PES filter (FroggaBio), then aliquoted into sterile 1.5 mL microfuge tubes for storage at -80°C. Usually, stock FV3 aliquots were prepared by pooling cell culture media containing FV3 from five T-75 cm^2 flasks, yielding ~ 50 mL of stock FV3.

3.2.4. Determination of FV3 viral titre

To determine viral stock titre, EPC cells were seeded in a 96-well plate (Thermo Scientific) at a final cell density of 100,000 cells/well in 0.1 mL EPC complete media and allowed to adhere overnight at 26°C. The next day, three FV3 stock tubes were removed from the -80°C freezer, pulse vortexed, and serially diluted by a factor of 1:10 up to 11 times (10^{-11}) in EPC low serum media. EPC monolayers were exposed to 0.2 mL of diluted supernatant in octuplicate for 10 days at room temperature, where they were then scored for cytopathic effects (CPE). Viral titre was expressed as the tissue culture infectious dose wherein 50% of cells are infected ($TCID_{50}$/mL), calculated from the plate scoring using the Karber method (Kärber, 1931), further described by (Pham et al., 2011). This protocol was also applied to experimental samples described below, with the following differences: diluted supernatants were added in quadruplicate and incubated for 7 days at room temperature. $TCID_{50}$/mL was multiplied by a factor of 0.7 to determine the approximate FV3 PFU/mL for multiplicity of infection (MOI) calculations (Knudson and Tinsley, 1974).

3.2.5. FV3 infection in early passage Xela DS2 and Xela VS2 cells to assess change in morphology

Xela DS2 (passage 23) and Xela VS2 (passage 25) (N = 1) cells were seeded in a T-25 cm^2 plug-seal tissue-culture treated flasks (Thermo Scientific) at a final cell density of 6 × 10^6 million cells/flask in 2 mL of Xela complete media allowed to adhere overnight at 26°C. The next day, Xela complete media was removed from flasks then cells were treated with 2 mL of Xela low serum media alone (non-infected control), or containing FV3 at MOIs of 0.2,

2 or 20. After 2 h of incubation at 26°C, media was removed and wells washed 3 × 2 mL APBS, prior to the addition of 2 mL of fresh Xela low serum media to all wells. Phase contrast digital images were captured 24 hpi using a Nikon Eclipse TSX-100 fitted with a color camera and Picture Project software.

3.2.6. RT-PCR for the detection of FV3 *mcp* transcripts in infected Xela DS2 and Xela VS2

Xela DS2 (passages 75-90) and Xela VS2 (passages 75-90) (N = 3) cells were seeded into a 6-well plate at a final cell density of 625,000 cells/well in 1 mL Xela complete media and allowed to adhere overnight at 26°C. The next day, cells were treated with 6.25 mL of low serum media alone (non-infected control), or containing FV3 at MOIs of 0.2 or 20, for 2 h at 26°C. Afterwards, media was removed and wells were washed 3 × 1 mL APBS prior to the addition of 2 mL fresh Xela low serum media. Plates were then incubated at 26°C for the duration of the experiment. Cells were collected using a 1000 µL pipette tip as a cell scraper to gently detach adherent cells from wells into suspension at 12 and 24 hpi for cells challenged at MOI of 20, or 1 and 3 dpi for cells challenged with MOI of 0.2 FV3. Cell suspensions were centrifuged at 500 × *g* for 5 min and supernatant aspirated. Cell pellets were washed 1 × 500 µL APBS then centrifuged at 500 × *g* for 5 min to remove trace serum. RNA was isolated from the cell pellets using EZ-10 Spin Column Total RNA Minipreps Super Kit (Bio Basic Canada Inc.) and cDNA synthesized using SensiFAST cDNA Synthesis Kit (BioLine distributed by FroggaBio) as described previously in Chapter 2, Section 2.2.12. RT-PCR reactions consisted of (final concentrations) 2 mM $MgCl_2$, 200 µM dNTP, 200 nM sense primer, 200 nM antisense primer (Sense: 5’-GACTTGGCCACTTATGAC-3’, Antisense: 5’-GTCTCTGGAGAAGAAGAA-3’), 0.625 U Taq DNA Polymerase, and 0.5 µL template made up to 25 µL reaction volumes with molecular grade water. Targets included

major capsid protein (*mcp*) viral transcripts from FV3 (Sense: 5'-GACTTGGCCACTTATGAC-3', Antisense: 5'-GTCTCTGGAGAAGAAGAA-3') (Pham et al., 2015; Robert, 2015), and *X. laevis actb* (see Chapter 2 Table 2.2 for primer information) as an endogenous control. Molecular grade water used as a no template control. Thermocycling conditions were as follows: initial denaturation at 95°C, 5 min; 25 (*actb*) or 35 (*mcp*) amplification cycles of denaturation at 95°C for 45 s, annealing at 55°C for 30 s, and elongation at 72°C for 45 s (*actb*) or 60 s (*mcp*), followed by a final extension step at 72°C for 10 min. To each RT-PCR reaction, 5 µL of 6× loading buffer [0.1% xylene cyanol (ICN Biomedicals), 30% v/v glycerol (EMD Chemicals)) was added prior to loading into a 1.4% agarose (VWR) gel containing 1× RedSafe Nucleic Acid Staining Solution (FroggaBio) and electrophoresed in 1× TAE buffer at 140 V for 20 min. Gels were imaged using a ChemiDoc imager (BioRad) with the Image Lab program.

3.2.7. Alamar blue assay to assess cell adherence over FV3 infection of Xela cells

Xela DS2 and Xela VS2 cells (passages 20-55) were seeded in a 48-well (Bio-Lite) plate at a final cell density of 50,000 cells/well in 0.2 mL Xela complete media and allowed to adhere overnight at 26°C. The next day, media was removed and then cells treated with 0.25 mL of Xela low serum media alone (non-infected control), or containing FV3 at MOIs of 0.002, 0.02, 0.2, 2 or 20 in triplicate wells, alongside triplicate wells containing no cells as a background blank. After 2 h of incubation at 26°C, media was removed and wells washed 3 × 300 µL before the addition of 500 µL of Xela low serum media. FV3-induced CPE was evaluated using an Alamar Blue (Life Technologies Inc) assay as a measurement of attached, viable cells remaining in the well. Alamar Blue is a commercial preparation of resazurin, which gets metabolically converted to a fluorescent compound for detection (Rampersad,

2012). A decrease in the cells' ability to convert resazurin to its fluorescent counterpart means a decrease in cell metabolism, inferring a decrease in cellular health and thus cell viability (Rampersad, 2012). Resazurin assay was performed on 1, 3, 5 7, 10 and 14 dpi. The culture media was removed prior to the addition of 200 μL Alamar Blue solution, diluted 1:20 with APBS, to each well. Plates were incubated for 1 h in the dark and read on a BioTek Synergy H1 plate reader, with excitation wavelength at 535 nm and emission wavelength at 590 nm. Data was expressed as a fold change in fluorescence relative to the blank wells which contained no cells, representing a well wherein there was complete loss of cell adherence.

3.2.8. Determining viral titre upon FV3 infection of Xela DS2 and Xela VS2

Xela DS2 (earlier passages 30-50, later passages 129-139) and Xela VS2 (earlier passages 30-50, later passages 134-139) (N = 3 for early passage cells, N = 4 for later passage cells) cells were seeded in a 12-well plate (Thermo Scientific) at a final cell density of 250,000 cells/well in 0.75 mL complete media and allowed to adhere overnight at 26°C. The next day, cells were collected by trypsin-EDTA from a triplicate set of sample wells, mixed 1:1 with trypan blue (Invitrogen) and counted on a hemocytometer to accurately ascertain the number of cells present to calculate MOI from stock FV3. Complete media was removed from wells then cells were treated with 0.5 mL of low serum media alone (non-infected control) or containing FV3 at a MOI of 20 and 0.2 for early passage cells, or MOI of 20, 2, 0.2, 0.02, and 0.002 for later passage cells. After 2 h of infection at 26°C, media was removed and wells washed 3 × 0.5 mL APBS, prior to the addition of 2.5 mL of fresh low serum media to all wells. For early cell passages, phase contrast digital images and cell culture media were collected on 0 (30 min post-wash), 1, 3, and 5 dpi for MOI of 20 FV3

challenge, and 0, 1, 3, 5, 7, 10, and 14 dpi for MOI of 0.2 FV3 challenge. Images were taken using a Nikon Eclipse TSX-100 fitted with a color camera and Picture Project software for early cell passages. Later cell passage phase contrast digital images and cell culture media were collected on 0, 1, 3, 5, and 7 dpi for all treatments; phase contrast digital images were captured using a Leica DMi1 microscope fitted with a MC170 color camera and LASX 4.8 software. Collected cell culture media was centrifuged at 500 × *g* for 5 min, and supernatants transferred to sterile 1.5 mL microfuge tubes prior to storage at -80°C. Viral titre assay using EPC cells was performed as described in Section 3.2.4 with the following changes: for later passage titres, day 0 samples were serially diluted by a factor of 1:10 up to 4 times (10^{-4}), up to 7 times (10^{-7}) for day 1 samples, and up to 11 times (10^{-11}) for day 3, 5, and 7 samples.

3.2.9. Inactivation of FV3 via UV irradiation

FV3 aliquots, stored in 1.5 mL microfuge tubes, were removed from -80°C and placed in a sealed transfer vessel (beaker with parafilm) lined with paper towel then allowed to thaw at room temperature. A paper towel was soaked with 70% ethanol then placed inside a UV Crosslinker (BioRad) to dry. Afterwards, FV3 aliquots were removed from the transfer vessel, mixed via gentle vortexing, then disinfected with 70% ethanol and left to dry on the paper towel in the UV crosslinker. Once dried, FV3 aliquots received a total of 150 mJ UV energy, a dose which has been previously used to effectively inactivate FV3 (Chinchar et al., 2003). Tubes were placed evenly spaced from one another and in an identical spatial orientation to ensure each aliquot received identical treatment. Aliquots and the UV crosslinker was then disinfected with 70% ethanol, and aliquots stored at -80°C for future use.

3.2.10. Confirmation of UV-inactivation of FV3 using EPC cells via viral transcript detection and viral titre assay

In order to verify UV-FV3 was effectively inactivated and incapable of replication, EPC cells were infected with both FV3 and UV-FV3 to assess viral transcription and titre. To detect the presence of the viral transcripts, EPC cells (passage 420) (N = 1) were seeded in a 6-well plate (Thermo Scientific) at a final cell density of 800,000 cells/well in 1 mL EPC complete media and allowed to adhere overnight at 26°C. After 48 h, cells were exposed to 1 mL of EPC infection media alone (non-infected control), UV-inactivated FV3 (MOI of 2), or FV3 (MOI of 2) in triplicate, for 2 h at 26°C. Afterwards, media containing treatments were removed from EPC monolayers and wells washed 3 × 1 mL APBS prior to the addition of 2 mL fresh EPC infection media. Plates were incubated at 26°C for the duration of the experiment. A 1000 µL pipette tip was used as a cell scraper to lift adherent cells from a single well of each treatment into suspension at 24 hours post infection (hpi). Cell suspensions were centrifuged at 300 × *g* for 10 min and supernatant was removed. Cell pellets were washed 1 × 500 µL PBS then centrifuged at 300 × *g* for 5 min. RNA was isolated from the cell pellets using EZ-10 Spin Column Total RNA Minipreps Super Kit (Bio Basic Canada Inc.) and cDNA synthesized using SensiFAST cDNA Synthesis Kit (BioLine distributed by FroggaBio) as described in Chapter 2 Section 2.2.12. RT-PCR reactions consisted of (final concentrations) 2 mM $MgCl_2$ (GeneDireX), 200 µM dNTP (GeneDireX), 200 nM sense and antisense primers (Sigma), 0.625 U Taq DNA Polymerase (GeneDireX), and 0.5 µL of template made up to 25 µL reaction volumes with molecular grade water. Targets included FV3 *mcp* to evaluate viral transcript production, and EPC *actb* (Sense: 5'-TGAAGATCCTGACCGAGAGA-3', Antisense: 5'-GGATACCGCAAGACTCCATAC-3') as an endogenous control. Molecular grade water used as a no template control.

Thermocycling conditions were as follows: initial denaturation at 95°C, 5 min; 30 (EPC *actb*) or 35 (*mcp*) amplification cycles of denaturation at 95°C for 45 s, annealing at 55°C for 30 s, and elongation at 72°C for 50 s (EPC *actb*) or 60 s (*mcp*), followed by a final extension step at 72°C for 10 min. To each RT-PCR reaction, 5 µL of 6× loading buffer [0.1% xylene cyanol (ICN Biomedicals), 30% v/v glycerol (EMD Chemicals)) was added prior to loading into a 1.4% agarose (VWR) gel containing 1× RedSafe Nucleic Acid Staining Solution (FroggaBio) and electrophoresed in 1× TAE buffer at 140 V for 20 min. Gels were imaged using a ChemiDoc imager (BioRad) with the Image Lab program. Detection of *mcp* was only detected in EPC cells infected with FV3 and not in UV-FV3 treated EPC. To detect the presence of infectious FV3 virions, cell supernatants from all treatments were collected from the remaining duplicate wells at 0 and 7 dpi, centrifuged at 500 × *g* for 5 min, and supernatants transferred to a sterile 1.5 mL microfuge tubes prior to storage at -80°C. Viral titre assays using EPC cells were performed as previously described (Section 3.2.4).

3.2.11. Challenge of Xela DS2 and Xela VS2 with poly(I:C), UV-inactivated FV3, and FV3

Xela DS2 (passages 120-130) and Xela VS2 (passages 125-135) (N = 4 independent trials) were seeded in a 6-well plate (Eppendorf) at a cell density of 625,000 cells/well in 1 mL of Xela complete media and allowed to adhere overnight at 26°C. The next day, the media was removed and cells treated with 0.5 mL of Xela low serum media alone into two wells or containing UV-inactived FV3 (MOI of 2) into one well, and FV3 (MOI of 2) into one well. After 2 h at 26°C, media containing the various treatments was removed, wells washed 3 × 0.5 mL APBS, and replaced with 2 mL of fresh Xela low serum media to one of two Xela low serum treated wells, the UV-FV3 treated well, and FV3-infected well. Immediately after, 2 mL of fresh Xela low serum media containing 1 µg/mL poly(I:C) was

added to the remaining Xela low serum treated well (positive control). Phase-contrast images were taken of all treatments at 0, 6, 24, 48, and 72 h post treatment, which commenced following addition of fresh Xela low serum media, using a Leica DMi1 microscope fitted with a MC170 color camera and LASX 4.8 software to assess cell morphology. At each time point, cell supernatants from all treatments were collected and centrifuged at 500 × *g* for 5 min to collect all cells. The supernatants were transferred to a sterile 1.5 mL microcentrifuge tube at stored at -80°C for later use (see Section 3.2.13). The cell pellet was used for total RNA isolation using the EZ-10 Spin Column Total RNA Minipreps Super Kit as described in Chapter 2 Section 2.2.12 with the following change: cell pellets were suspended in 100 µL lysis solution then mixed 1:1 with 70% ethanol and stored on ice. Meanwhile, remaining adherent cells were washed 1 × 1 mL APBS, followed by the addition of 300 µL lysis solution directly to wells for 1 min on ice, then mixed 1:1 with 70% EtOH. This was then transferred and mixed by inversion with cell pellet lysis extract prior to addition to spin columns. RNA quantity, purity, and integrity, and subsequent cDNA synthesis, were performed as described in Chapter 2 Section 2.2.12. The cDNA samples were stored at -20°C until use in RT-qPCR transcript analysis.

3.2.12. Quantitative RT-PCR

Primer sequences, accession numbers, R^2 and primer efficiency values for *X. laevis* *tnf*, *il1*, *il8*, *ikb*, *ifn1*, *mx2*, *pkr*, *actb*, *cyp*, *ef1a*, *gapdh*, and *hgprt* were previously reported in Table 2.2, Chapter 2 Section 2.2.15. Prior to transcript analysis, gene stability testing was conducted for *actb*, *cyp*, *ef1a*, *gapdh*, and *hgprt* to permit selection of an endogenous control. To perform gene stability testing, cDNA samples across all trials generated from Section 3.2.11 were pooled together in a time-matched and treatment-matched fashion and diluted

1:40 in molecular grade water. RT-qPCR reactions (10 µL volumes) were prepared in triplicated and consisted of (final concentrations) 500 nM sense and antisense primer, 5 µL PowerUp SYBR green mix (Thermo Scientific), and 2.5 µL of diluted cDNA template. Thermocycling conditions were as follows: initial denaturation at 50°C for 2 min, followed by 95°C for 2 min, 40 amplification cycles of denaturation at 95°C for 1 s, and extension at 60°C for 30 s. A melt curve step followed all runs to ensure only a single dissociation peak was present, with initial denaturation at 95°C for 1 s, then dissociation analysis at 60°C for 20 s followed by 0.1°C increments between 60°C and 95°C at 0.1°C/s. Gene stability measures (M-value) were determined for all endogenous control candidates using the Applied Biosystems QuantStudio Analysis software (Table 3.1), wherein a lower M-value infers stronger gene stability across time and treatment. The target selected for the endogenous control was *actb*, with M-value values at 0.428 and 0.424 for Xela DS2 and Xela VS2 respectively.

For transcript analysis, RT-qPCR reactions were prepared in duplicate and consisted of 2.5 µL of 500 nM sense and antisense primers, 5 µL PowerUp SYBR green mix (Thermo Scientific), and 2.5 µL of diluted (1:20) cDNA template. The cycling conditions and dissociation analysis was performed as described above. Reactions were prepared in a MicroAmp fast optical 96-well reaction plates (Life Technologies), sealed with MicroAmp clear optical film (Life Technologies) and run on QuantStudio5 Real-Time PCR System (Thermo Scientific). Four independent trials were conducted using Xela DS2 and Xela VS2 cells at four different passages as described in Section 3.2.11 ($N = 4$).

Table 3.1. Candidate endogenous genes for use in RT-qPCR analysis of FV3 infected Xela DS2 and Xela VS2 cells.

Target	Xela DS2 M-Value	Xela VS2 M-Value
actb	**0.428**	**0.424**
cyp	0.393	0.440
ef1a	0.479	0.600
gapdh	0.434	0.462
hgprt	0.462	0.534

3.2.13. Detection of FV3 *mcp* transcripts in Xela cells to confirm UV-inactivation of FV3

RT-PCR reactions for FV3 *mcp* consisted of buffer containing (final concentrations) 2 mM $MgCl_2$, 200 µM dNTP, 200 nM sense and antisense primers, 0.625 U Taq DNA Polymerase, 1 µL of template in a total volume of 25 µL. Templates consisted of molecular grade water (no template control), cDNA generated from EPC cells infected with FV3 at MOI of 2 after 24 hpi (see Section 3.2.6), or cDNA generated from Xela DS2 or Xela VS2 infected with FV3 at MOI of 2 after 48, and 72 hpi (see Section 3.2.11) (N = 4). Thermocycling conditions were as follows: initial denaturation at 95°C, 5 min; 35 amplification cycles of denaturation at 95°C for 45 s, annealing at 55°C for 30 s, and elongation at 72°C for 60 s, followed by a final extension step at 72°C for 10 min. To each RT-PCR reaction, 5 µL of 6× loading buffer (0.15% xylene cyanol, 30% v/v glycerol) was added prior to loading into a 1.5% Agarose gel containing 1× RedSafe Nucleic Acid Staining Solution and electrophoresed in 1× TAE buffer at 100 V for 30 min. Gels were imaged using a ChemiDoc imager (BioRad) with the Image Lab program..

3.2.14. Viral titre of supernatants from UV-FV3 challenged and FV3-infected Xela DS2 and Xela VS2

Collected cell supernatants from Section 3.2.11 were used to determine FV3 viral titres (N = 4). Viral titre assays using EPC cells were performed as previously described (Section 3.2.4) with the following changes: non-infected and poly(I:C) treated samples were diluted to 10^{-1}, culture media from UV-FV3 challenged samples were diluted to 10^{-2}, and culture media from FV3 challenged samples were diluted to 10^{-7} by a factor of 1:10 in EPC low serum media. $TCID_{50}$/mL was calculated by scoring for CPE after 7 days at 26°C (Kärber, 1931; Pham et al., 2011).

3.2.15. Effect of poly(I:C) treatment and FV3 infection on suspension cell viability

Xela DS2 (passages 135-140) and Xela VS2 (passages 138-143) cells were seeded in a 48-well (Thermo Scientific) plate at a final cell density of 50,000 cells/well in 0.3 mL Xela complete media and allowed to adhere overnight at 26°C. The next day, media was removed, and cells were pre-treated with 160 µL of Xela low serum media containing 0, 10, 50, or 100 ng/mL poly(I:C) for 24 h, in sextuplicate. Following pre-treatment, 90 µL of low serum media alone was added to three of the six replicates for all treatments, or Xela low serum media containing FV3 (MOI of 2) added to the remaining triplicate 0, 10, 50, or 100 ng/mL poly(I:C) pre-treated wells. After incubation at 26°C for 2 h, supernatants from all poly(I:C) pre-treatments without FV3 were collected and while remaining media was removed from all wells, and washed 3× with 0.3 mL APBS prior to the addition of 0.5 mL of fresh Xela low serum media to all wells, placed at 26°C. Collected supernatants (26 h post-treatment) were centrifuged at 500 × g for 5 min, and cell pellets resuspended in 20 µL Xela low serum media. Cell suspensions were mixed 1:1 with trypan blue and live/dead cells enumerated using a hemocytometer under 400× brightfield using a Leica DMi1 microscope. A total of

200 cells were counted in multiple fields of view per-treatment. In addition to monitoring effects of poly(I:C) on suspension cell viability, supernatants were collected from all treatments at 5 dpi, centrifuged at 500 × *g* for 5 min, and pellets were resuspended in 20 µL Xela low serum media. Trypan blue exclusion assay was performed on cell supernatants as previously described. Three independent trials were performed for each set of experiments.

3.2.16. Determining the effect of poly(I:C) pre-treatment on Xela DS2 and Xela VS2 cellular adherence via resazurin assay and cell enumeration of NucBlue Live stained cells

This experiment was conducted in tandem with the experiment described in Section 3.2.15. After 0, 3, 5 dpi, cell culture media was collected across 0, 10, 50, and 100 ng/mL poly(I:C) pre-treated samples, which were infected or non-infected with FV3, then centrifuged at 500 × *g* for 5 min and transferred to sterile 1.5 mL microfuge tubes prior to storage at -80°C for later determination of FV3 titre (see Section 3.2.17). Afterwards, duplicate wells were treated with 200 µL of 440 µM resazurin (Acros Organics) solution dissolved in APBS and a single well treated with 200 µL Xela low serum media containing NucBlue Live reagent (ThermoFisher), which is a Hoechst stain, and incubated in the dark for 1 h. NucBlue Live was prepared by adding 1 drop of reagent per mL of Xela low serum media. Following the 1 h incubation, plates were read on BioTek Cytation5 imaging reader using Gen5 software under the following conditions: duplicate resazurin treated wells were read with excitation wavelength 535 nm and emission wavelength 590 nm, while single NucBlue Live treated wells were fluorescently imaged with excitation wavelength 377 nm and emission wavelength 477 nm to determine representative cell count for each respective treatment. Digital phase contrast images were capture in addition to fluorescent imaging of

NucBlue Live treated cells. Four independent trials were conducted, using cells from different passages for each trial.

3.2.17. Monitoring the potential effect poly(I:C) pre-treatment has on FV3 viral titre in Xela DS2 and Xela VS2

Collected cell supernatants from Section 3.2.16 were used to perform a titre analysis (N = 3). Viral titre assay using EPC cells was performed as previously described (Section 3.2.4) with the following changes: regardless of poly(I:C) pre-treatment, non-FV3 challenged samples were diluted to 10^{-1} while FV3 challenged samples were diluted to 10^{-11} by a factor of 1:10 in EPC low serum media. $TCID_{50}$/mL was calculated from the plate scoring using a modified Karber method (Kärber, 1931; Pham et al., 2011).

3.2.18. Statistics

Alamar blue assay (Section 3.2.7) data were analyzed by a two-way ANOVA test followed by a Tukey's post-hoc test. RT-qPCR (Section 3.2.12) data were analyzed by a two-way ANOVA followed by a Holm-Sidak post-hoc analysis. Viral titres from FV3 infected cells (Section 3.2.14), and poly(I:C) cytotoxicity and FV3 cytopathicity data (Section 3.2.15) were analyzed by a one-way ANOVA, followed by a Tukey's post-hoc test. Effect of poly(I:C) pre-treatment on FV3 replication in Xela DS2 and Xela VS2 (adherence and FV3 titres; Sections 3.2.16 and 3.2.17, respectively) were analyzed by a two-way ANOVA followed by a Tukey's post-hoc test. Statistical analyses were performed using GraphPad Prism v6 software and groups were considered statistically significant when $p < 0.05$.

3.3. Results

3.3.1. Xela DS2 and Xela VS2 are permissive to FV3 and support viral replication

To assess the effect of FV3 challenge on Xela DS2 (passage 23) and Xela VS2 (passage 25) morphology, cells were monitored under phase-contrast after 24 h post infection (hpi) for cytopathic effects (CPE) (Fig. 3.1). Non-infected cells remained adherent to the cell culture vessel, retaining characteristic epithelial cell-to-cell contact (Fig. 3.1). After 24 hpi, there appeared to be no changes in cell morphology in Xela DS2 or Xela VS2 infected with FV3 MOI of 0.2 relative to the non-infected control (Fig. 3.1). Minor CPE are observed in both Xela DS2 and Xela VS2 infected with FV3 at a MOI of 2, wherein cell-to-cell contact and cell density appears to have decreased, accompanied with an apparent increase in non-adherent, suspension cells (Fig. 3.1). CPE was most pronounced in Xela DS2 and Xela VS2 infected with FV3 MOI of 20, wherein cells appear to contract followed by the loss of cell adherence to the cell culture vessel.

To determine whether FV3 is capable of transcription in the host, the presence of *mcp* transcripts in FV3 challenged Xela DS2 and Xela VS2 were examined (Fig. 3.2). Transcripts for FV3 *mcp* were detected at 12 hpi and 24 hpi in both Xela DS2 and Xela VS2 infected with FV3 at a MOI of 20 (Fig. 3.2). In Xela DS2 and Xela VS2 cells infected with FV3 at a lower MOI of 0.2, *mcp* transcripts were detected as early as 1 d post infection (dpi) and *mcp* transcripts appeared to increase at 3 dpi (Fig. 3.2). To further ascertain whether Xela DS2 and Xela VS2 could support FV3 replication and production of infectious virions, viral titre analysis was performed on cell culture media obtained from Xela DS2 and Xela VS2

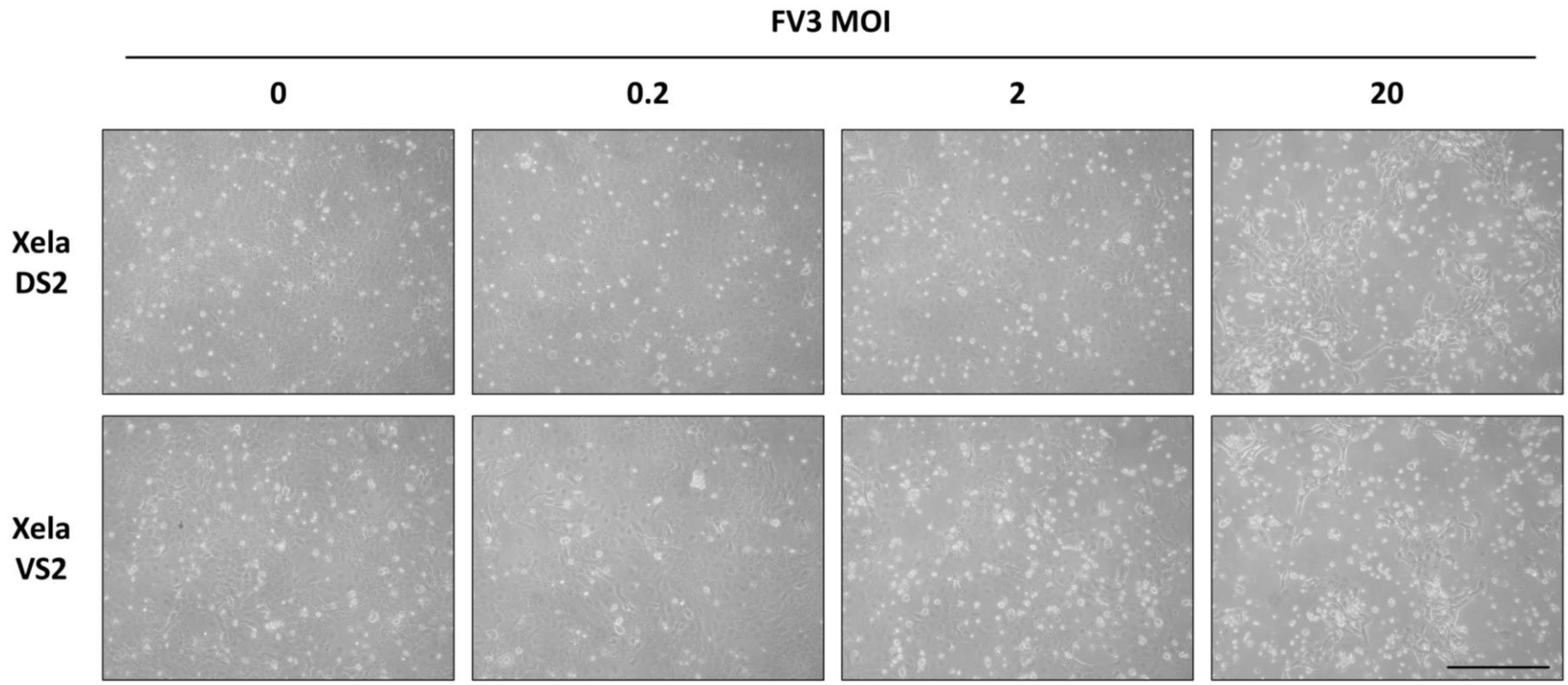

Figure 3.1. Effect of FV3 challenge on early passage Xela DS2 and Xela VS2 morphology. Phase contrast images of early passage Xela DS2 and Xela VS2 following challenge with FV3 at MOI of 0, 0.2, 2, or 20, monitored 24 hpi. Images were taken at 50× magnification using a Nikon Eclipse TSX-100 microscope, scale bar is 500 µM. Images shown are from one independent trial.

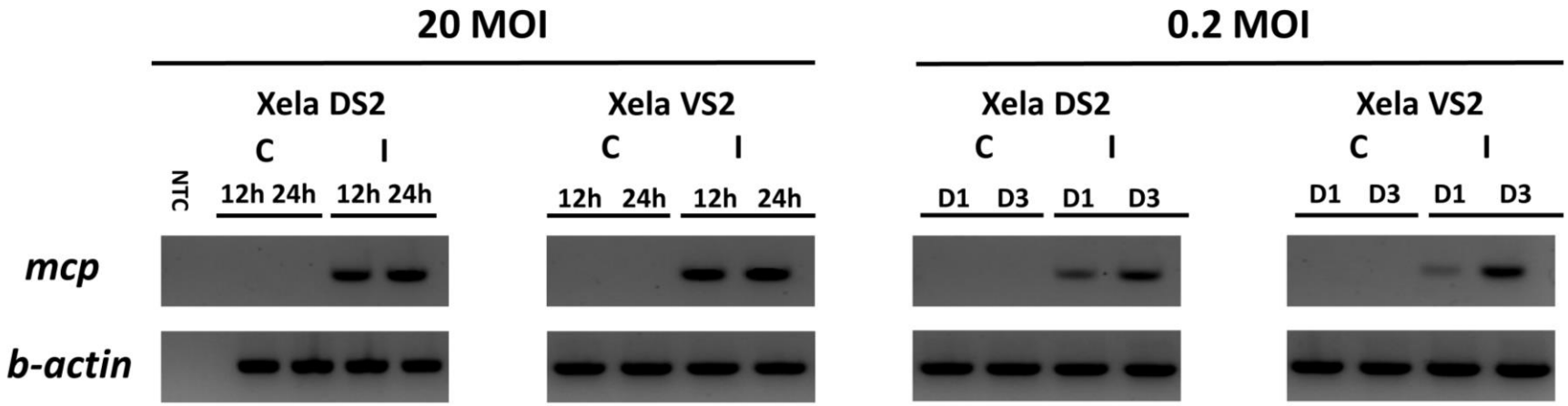

Figure 3.2. FV3 major capsid protein transcripts are detected in Xela DS2 and Xela VS2 after FV3 infection. Gel electrophoresis image from RT-PCR of no template control (NTC), Xela DS2 and Xela VS2 non-infected control (C) and FV3 infected (I) cells at a multiplicity of infection (MOI) of 20 or 0.2 for FV3 major capsid protein (*mcp*) at 12 and 24 hpi or at 1 (D1) and 3 (D3) dpi, respectively. Detection of *b-actin* (*actb)* transcripts was used as an endogenous control.

infected with FV3. At earlier passages (30-50) of Xela DS2 and Xela VS2 (Fig. 3.3), FV3 viral titre appears to increase in a time-dependent and dose-dependent manner. At day 0, FV3 titres are below the limit of detection for both cell lines infected with FV3 at a MOI of 0.2 (Fig. 3.3). Titre values appear to reach a plateau by day 7, achieving $\log_{10}(TCID_{50}/mL)$ values of 6.5 ± 0.3 and 6.5 ± 0.1 for Xela DS2 and Xela VS2, respectively, with these titres persisting till day 14 (Fig. 3.3). When challenged with FV3 MOI of 20, viral particles were detected as early as day 0, with titre values of 3.3 ± 0.1 and 3.4 ± 0.1 for Xela DS2 and Xela VS2 respectively. Titres peaked by day 3 persisted up to day 5, reaching 6.5 ± 0.1 in Xela DS2 and 6.2 ± 0.4 in Xela VS2 at 5 dpi (Fig. 3.3). Similar peak viral titres were achieved in Xela DS2 and Xela VS2 by 5 dpi across varying FV3 MOIs (Fig. 3.3).

The loss of Xela DS2 and Xela VS2 cell adherence upon FV3 infection was identified as a characteristic FV3-induced CPE, wherein Alamar Blue assay was used to monitor the degree of loss in cellular adherence due to FV3 infection. Data was expressed as a fold-change relative to blank wells absent of cells, thus representing a case of complete loss in cell adherence (Fig. 3.4). Therefore, a value of 1.0 would infer that all cells in the treatment lost adherence, and anything greater than 1.0 suggests active cellular metabolic activity from any remaining adherent cells. Both Xela DS2 (Fig. 3.4A) and Xela VS2 (Fig. 3.4B) showed similar trends, wherein there is a clear dose-dependent and time-dependent decrease in the number of adherent cells as confirmed by two-way ANOVA analysis. There were no significant differences between values in cells challenged with FV3 at MOI ≤ 0.02, and time-dependent decreases in cell adherence in cells challenge with FV3 at MOI ≥ 0.2. Overall, the loss of cell adherence can be used as a proxy to monitor FV3-induced CPE in Xela DS2 and Xela VS2 which can be monitored using a resazurin assay.

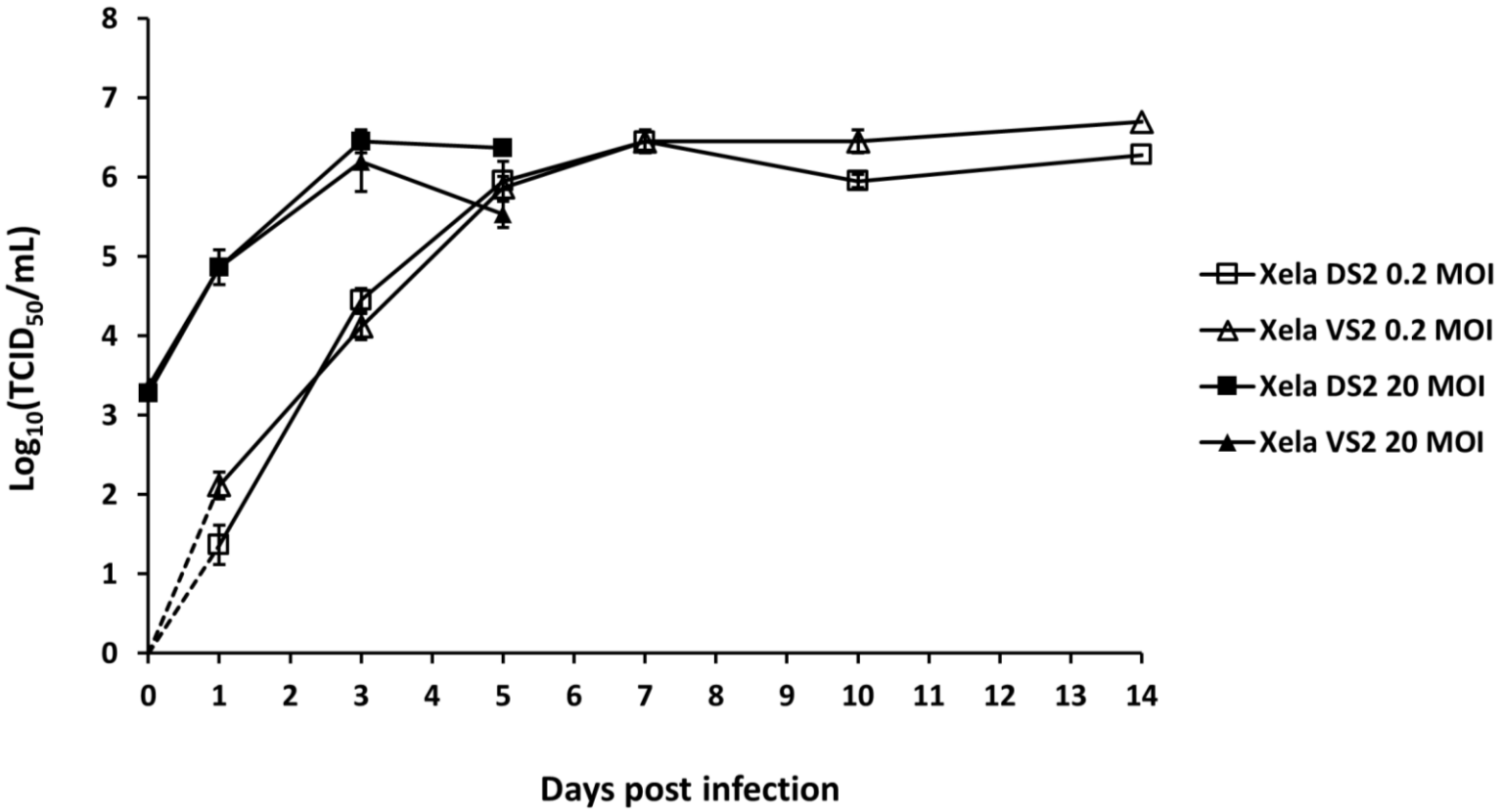

Figure 3.3. Xela DS2 and Xela VS2 are permissible to viral replication at early passages. Early passages (passages 30-50) of Xela DS2 and Xela VS2 cell line were infected with FV3 at a MOI of 20 or 0.2 and cell culture media collected over 5 or 14 days, respectively. Cell culture media from FV2-infected Xela DS2 and Xela VS2 were serially diluted and applied to a 96-well plate containing monolayer of EPC cells. EPC monolayers were scored for cytopathic effects (CPE) after 7 days to determine the $TCID_{50}$/mL. Dashed lines represent projected $TCID_{50}$/mL values as no CPE was observed at day 0 for Xela DS2 or Xela VS2 cells infected at MOI of 0.2. CPE were not observed in cell culture media from non-infected Xela DS2 and Xela VS2 cell lines at any time point. Data represent the mean ± standard error, n = 3 independent experiments.

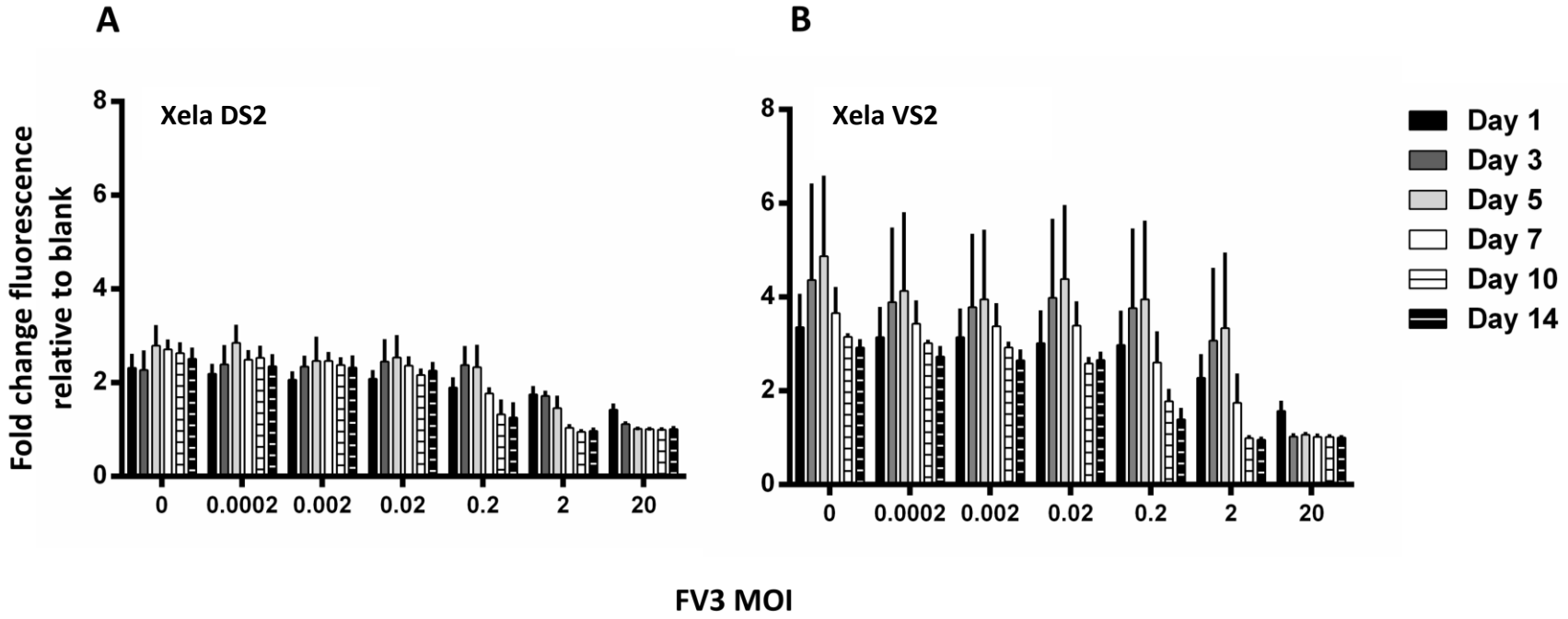

Figure 3.4. Xela DS2 and Xela VS2 lose adherence in response to infection with FV3. Early passages of (A) Xela DS2 and (B) Xela VS2 cell line were infected with FV3 at MOI of 20, 2, 0.2, 0.02, 0.002, and 0.0002 and CPE was monitored over 14 days via Alamar Blue assay using a BioTek Synergy H1 plate reader. Data is expressed as a fold change of fluorescence relative to blank wells which are representative of wells absent of adherent or suspension cells. Data represent the mean ± standard error, n = 7 independent experiments.

3.3.2. Xela DS2 and Xela VS2 maintain susceptibility to FV3 at higher passages

To assess the effect of FV3 challenge on Xela DS2 and Xela VS2 at later passages (129-139), cells were exposed to a range of FV3 MOIs and cells monitored for CPE using phase contrast microscopy over 7 days. While non-infected Xela DS2 (Fig. 3.5A) and Xela VS2 (Fig. 3.5B) cell monolayers become slightly more compact with time, no changes in cell morphology or adherence associated with CPE were observed. In general, both Xela DS2 (Fig. 3.5A) and Xela VS2 (Fig. 3.5B) exhibited similar dose- and time-dependent CPE following FV3 infection, characterized by cell contraction and loss of adherence to the cell culture vessel resulting in large floating cell clumps in the cell culture media. Xela DS2 exhibited signs of CPE, characterized by loss of cell adherence, by day 1 at MOIs of 20 and 2, by day 3 at MOI of 0.2, and by day 5 at MOI of 0.02 (Fig. 3.5A). For Xela VS2, initial signs of CPE were observed by day 1 for MOIs of 20 and 2, and by day 3 at MOIs of 0.2 and 0.02 (Fig. 3.5B). In contrast to higher MOIs, no CPE were observed when Xela DS2 (Fig. 3.5A) or Xela VS2 (Fig. 3.5B) were challenge with FV3 at MOI 0.002. These morphological observations at higher MOIs were accompanied with increasing viral titre values in a time-dependent and dose-dependent manner (Fig. 3.6). No viral particles were detected in non-FV3 treated samples. Viral particles were detected as early as day 0 for Xela DS2 at MOI of 0.02, 0.2, 2, and 20 (Fig. 3.6A) and for VS2 at MOI of 0.002, 0.02, 0.2, 2, and 20 (Fig. 3.5B). These viral titres increase in a time-dependent manner with viral titre levels peaking at day 5-7 post infection (Fig. 3.6), reaching a maximal titre similar to that observed in the early passage cells (Fig. 3.3). While Xela DS2 and Xela VS2 largely support viral replication, FV3 appears unable to effectively replicate at MOI of 0.002 (Fig. 3.6).

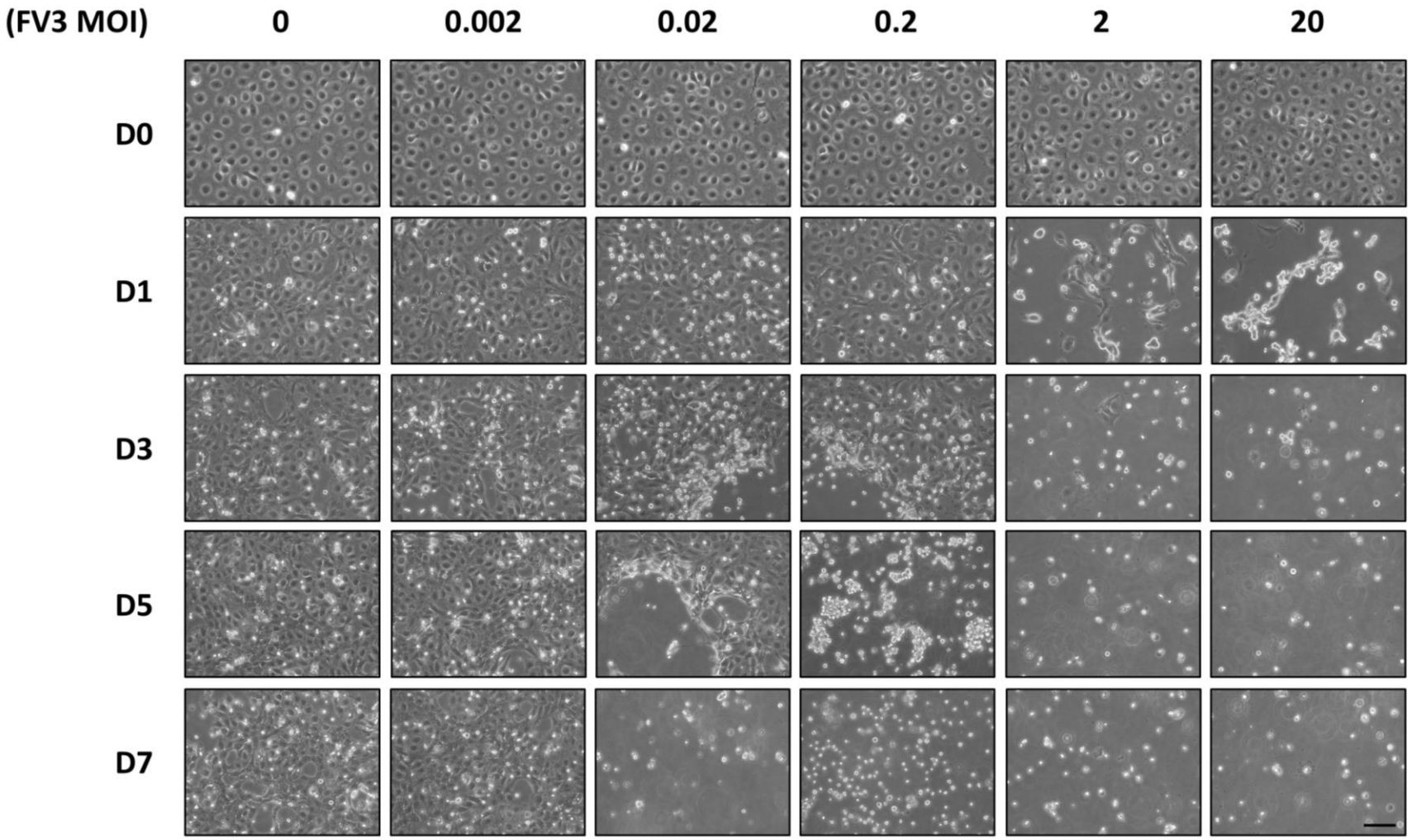

Figure 3.5A. Effect of FV3 challenge on Xela DS2 morphology. Phase contrast images of Xela DS2 following challenge with FV3 at MOIs of 0, 0.002, 0.02, 0.2, 2, or 20, monitored over 7 days. Images were taken at 200× magnification using a Leica DMi1 microscope, scale bar is 100 µM. Images are representative of four independent trials.

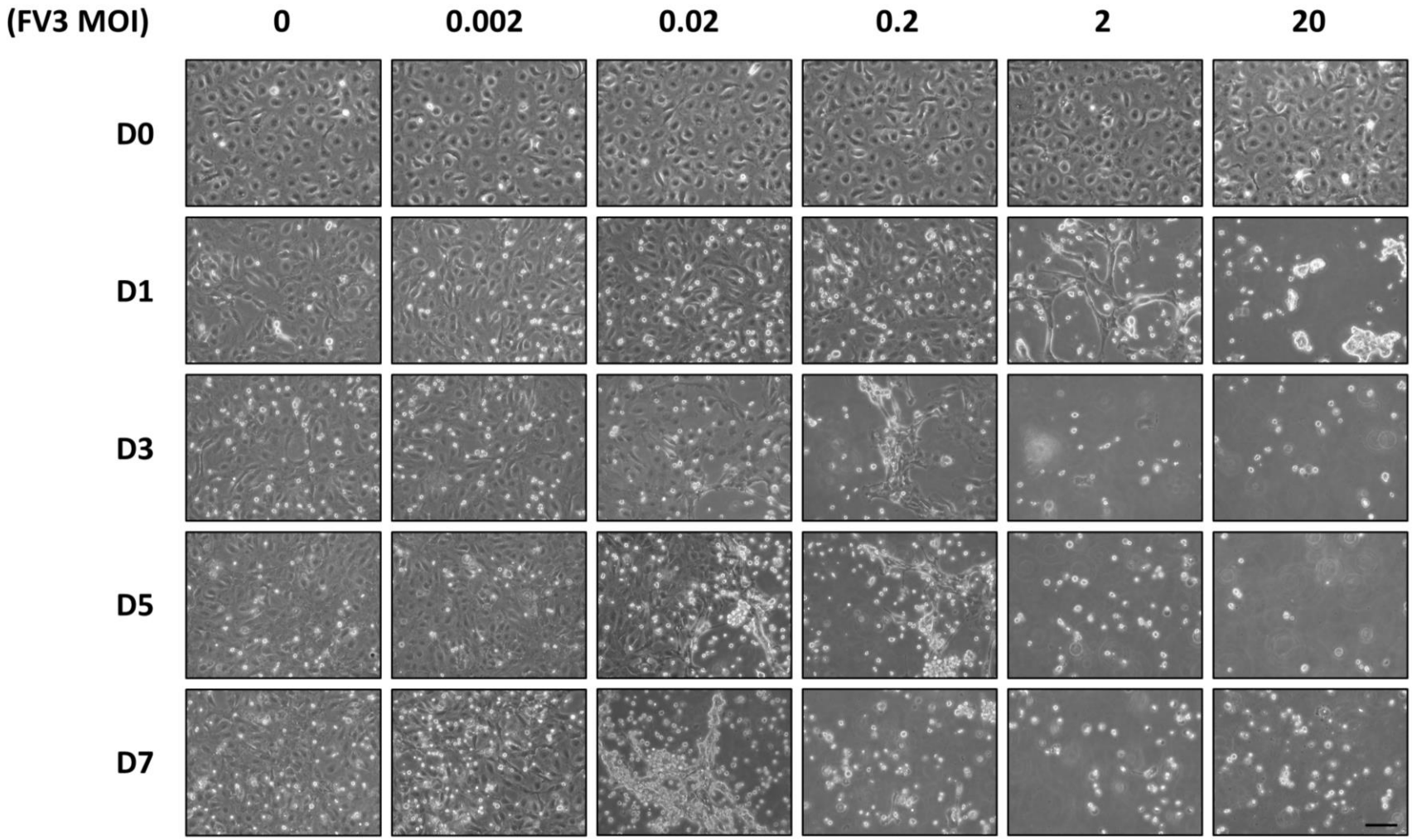

Figure 3.5B. Effect of FV3 challenge on Xela VS2 morphology. Phase contrast images of Xela VS2 following challenge with FV3 at MOIs of 0, 0.002, 0.02, 0.2, 2, or 20, monitored over 7 days. Images were taken at 200× magnification using a Leica DMi1 microscope, scale bar is 100 µM. Images are representative of four independent trials.

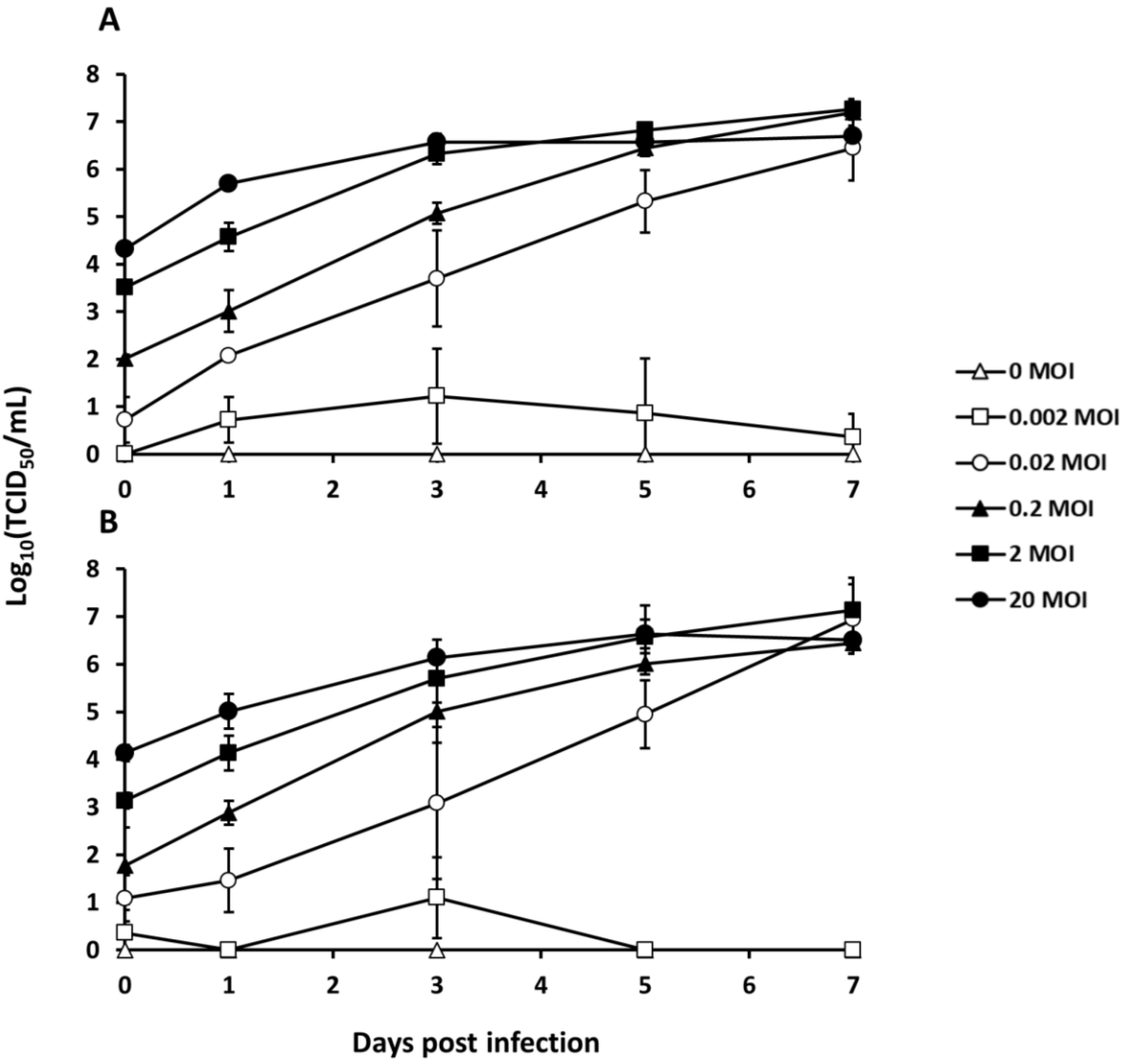

Figure 3.6. Xela DS2 and Xela VS2 are permissible to viral replication across a range of MOIs. Viral titres in cell culture media from (A) Xela DS2 and (B) Xela VS2 following infection with FV3 at MOIs of 0, 0.002, 0.02, 0.2, 2, and 20, performed at passages 129-139 and 134-139 for Xela DS2 and Xela VS2 respectively. Cell culture media collected from FV3-infected cells were serially diluted and applied to EPC monolayers and scored for cytopathic effects after 7 days to determine the $TCID_{50}$/mL. Cytopathic effects were not observed in cell culture media from non-infected Xela DS2 and Xela VS2 cell lines at any time point. Data represent the mean ± standard error, n = 4 independent experiments.

3.3.3. Xela DS2 and Xela VS2 do not initiate antiviral or proinflammatory transcript upregulation when challenged with UV-inactivated FV3 or FV3

Xela DS2 and Xela VS2 were monitored for changes in cellular morphology over 72 h following exposure to Xela low serum media alone or containing 1 µg/mL poly(I:C), UV-inactivated FV3 at MOI of 2, or FV3 at MOI of 2. The cell monolayer appears to become slightly more compact for the non-treated control cells in Xela DS2 (Fig. 3.7A) and Xela VS2 (Fig. 3.7B). For both Xela DS2 and Xela VS2, initial loss of cell adherence is observed by 6 h in poly(I:C) treated cells, with cells continuing to lose adherence up to 72 h (Fig. 3.7). There is an initial change in cellular morphology upon UV-FV3 and FV3 challenge at 6 h in Xela DS2 and Xela VS2, as cell monolayers appear more disordered (Fig. 3.7). Loss of adherence is observed by 24 h in UV-FV3 and FV3 challenged cells, which progresses up to 72 h where not many cells remain adherent (Fig. 3.7).

I wanted to determine whether FV3, in an active or inactivated state, was able to promote an antiviral response in Xela DS2 and Xela VS2. RT-qPCR was performed to monitor any changes in antiviral transcript levels in Xela DS2 and Xela VS2 challenged with FV3 and UV-FV3 at MOI of 2, using treatment of Xela DS2 and Xela VS2 with 1 µg/mL poly(I:C) as a positive control (Fig. 3.8). No significant changes in *ifn1* or *mx2* transcript levels relative to time-matched controls occurred in Xela DS2 (Fig. 3.8A, C) or Xela VS2 (Fig. 3.8B, D) over the 72 h period, regardless of treatment. There appeared to be a significant effect of poly(I:C) treatment only on Xela DS2 *ifn1* expression ($p = 0.0062$), but there was no time-dependent effect ($p = 0.9485$) or significant interaction between time and treatment ($p = 0.9935$). However, significantly higher *pkr* transcript levels were detected in Xela DS2 (Fig. 3.8E) and Xela VS2 (Fig. 3.8F) in poly(I:C) stimulated cells ($p < 0.0001$) and decreased in a time-dependent manner by 72 h post-treatment ($p < 0.0001$). No changes

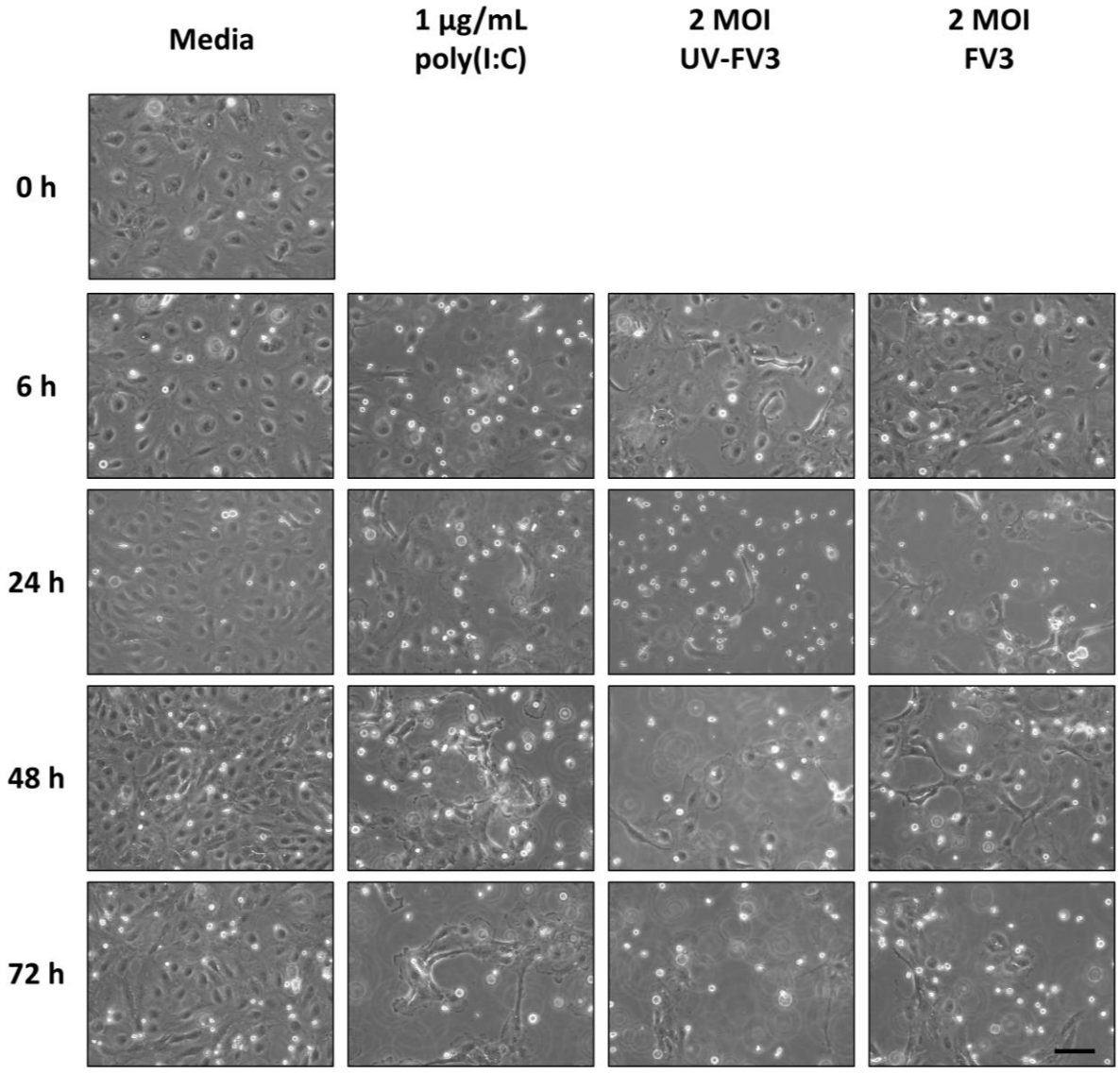

Figure 3.7A. Xela DS2 lose adherence when treated with poly(I:C), UV-inactivated FV3 or FV3. Phase-contrast images of Xela DS2 when treated with media alone, 1 µg/mL poly(I:C), UV-inactivated FV3 at MOI of 2, and FV3 at MOI of 2. Cellular morphology was monitored at 0, 6, 24, 48, and 72 hpi by capturing phase contrast images. Images were taken at 200× magnification using a Leica DMi1 microscope, scale bar is 100 µm. Images shown are representative of four independent trials.

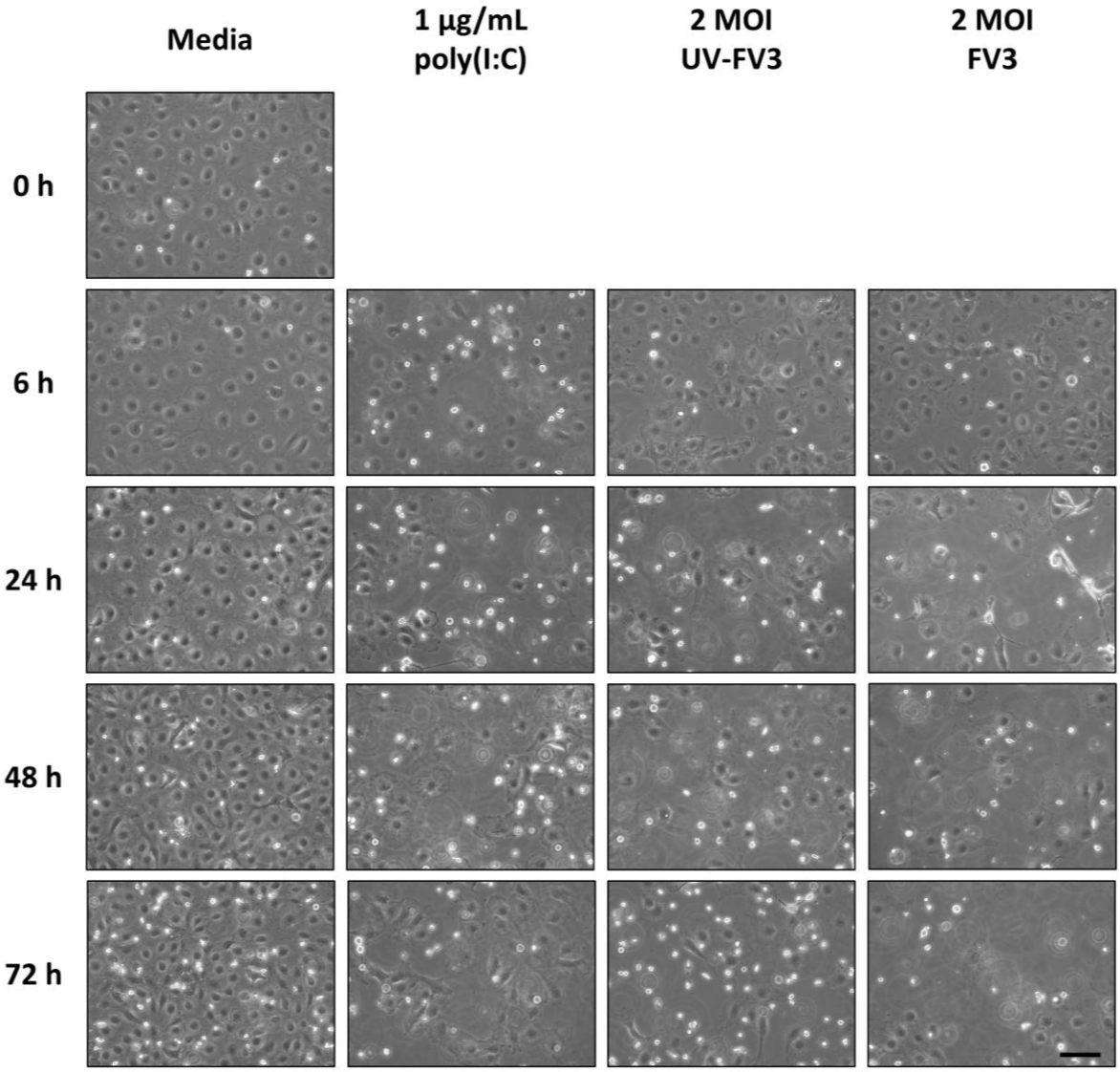

Figure 3.7B. Xela VS2 lose adherence when treated with poly(I:C), UV-inactivated FV3 or FV3. Phase-contrast images of Xela VS2 when treated with media alone, 1 µg/mL poly(I:C), UV-inactivated FV3 at MOI of 2, and FV3 at MOI of 2. Cellular morphology was monitored at 0, 6, 24, 48, and 72 hpi by capturing phase contrast images. Images were taken at 200× magnification using a Leica DMi1 microscope, scale bar is 100 µm. Images shown are representative of four independent trials.

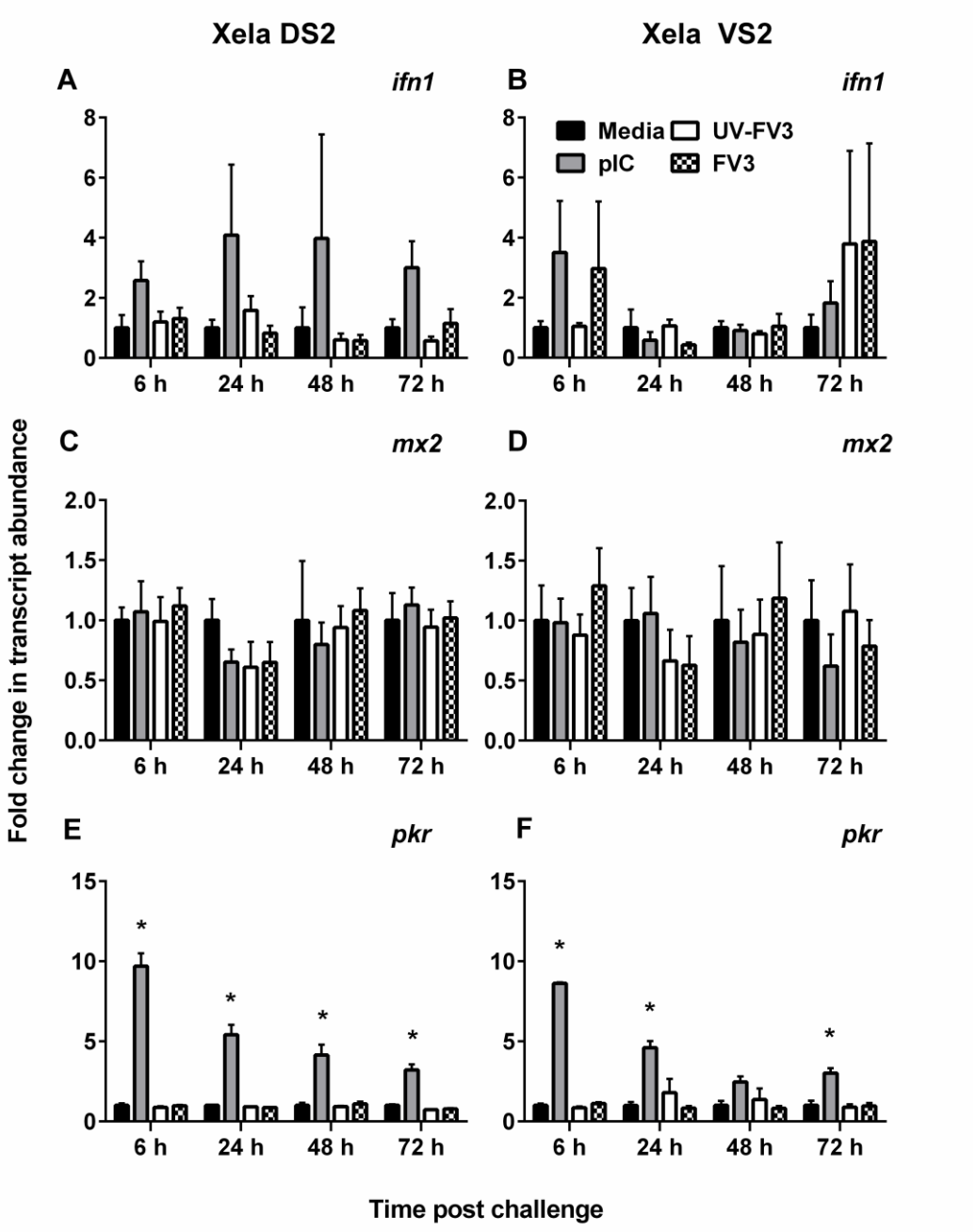

Figure 3.8. Xela DS2 and Xela VS2 do not upregulate antiviral transcripts following challenge with UV-inactivated FV3 or FV3. RT-qPCR was performed using cDNA generated from non-treated (media), 1 µg/mL poly I:C treated (pIC), UV-FV3 challenged at MOI of 2 and FV3 infected at MOI of 2 Xela DS2 or Xela VS2 cells to determine relative transcript levels of *ifn1*, *mx2*, and *pkr*. For all experiments, transcript levels from treated samples were normalized to time-matched, non-treated control. Data represent the mean ± standard error, n = 4 independent experiments. Asterisks (*) indicate significant differences in transcript levels relative to the time-matched control, determined by a two-way ANOVA and Holm-Sidak post-hoc test ($p < 0.05$).

in *pkr* transcript levels were observed in UV-FV3 and FV3 challenged cells. I then assessed whether Xela DS2 and Xela VS2 initiate proinflammatory programs in response to FV3. I previously demonstrated that Xela DS2 and Xela VS2 upregulate proinflammatory transcripts in response to 10 µg/mL poly(I:C) stimulation (Chapter 2, Section 2.3.6). A similar response is observed when Xela DS2 and Xela VS2 are treated with 1 µg/mL of poly(I:C), wherein a significant upregulation in *il1* (Fig. 3.8A, B), *tnf* (Fig. 3.9C, D), *il8* (Fig. 3.9E, 3F), and *ikb* (Fig. 3.9G, H) transcript levels are seen. Although Xela DS2 and Xela VS2 can sense and initiate proinflammatory programs upon poly(I:C) stimulation, UV-FV3 or FV3 challenge does not appear to induce Xela DS2 and Xela VS2 proinflammatory gene expressions (Fig. 3.8).

3.3.4. UV-inactivated FV3 is not capable of replication in Xela DS2 or Xela VS2

To verify that UV-FV3 was inactivated and incapable of replicating in Xela DS2 and Xela VS2, I assessed viral transcription and viral titres in Xela DS2 and Xela VS2 challenged with UV-FV3. Transcripts for *mcp* were detected in FV3 infected EPC cells (positive control), and in infected Xela DS2 and Xela VS2 cells but was not detectable in UV-FV3 FV3 challenged samples (Fig. 3.10A). Inactivation of UV-FV3 was further confirmed by performing titre analysis on collected cell supernatants. Although CPE were observed from incubation with UV-FV3 supernatants, 2-way ANOVA analysis unveiled that there is no change in these titre values over time. Meanwhile, titre values from FV3-treated supernatants increase in a time-dependent manner and is always significantly higher than UV-FV3 treated titres. The presence of CPE in EPC monolayers treated with UV-FV3 supernatant is likely a similar effect as observed when Xela DS2 and Xela VS2 underwent CPE in response to UV-FV3 challenge. It was concluded that FV3 aliquots were effectively inactivated by UV irradiation

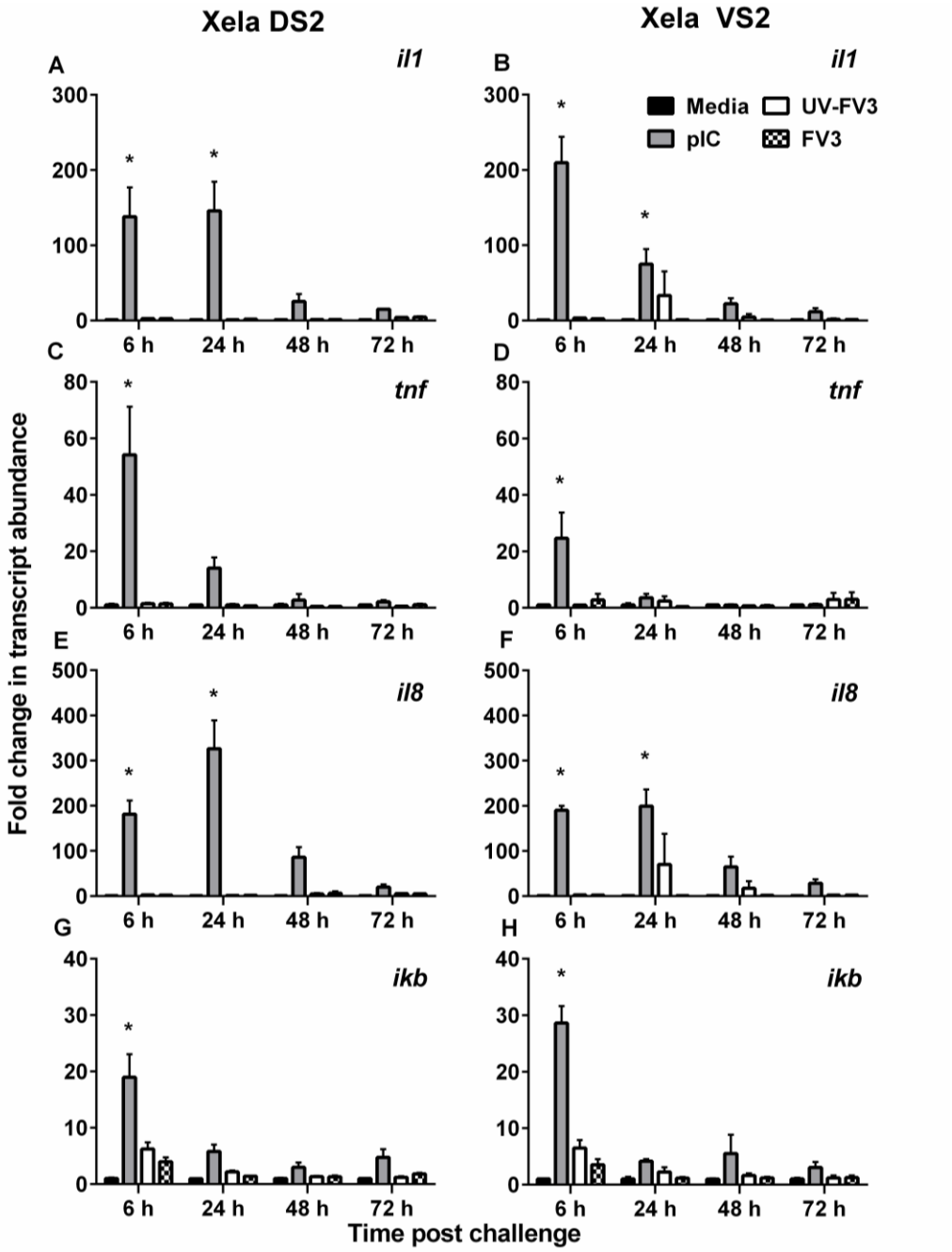

Figure 3.9. Xela DS2 and Xela VS2 do not initiate proinflammatory programs following addition of UV-inactivated FV3 or FV3. RT-qPCR was performed on cDNA generated from non-treated (media), 1 µg/mL poly I:C treated (pIC), UV-FV3 challenged at MOI of 2 and FV3 infected at MOI of 2 Xela DS2 or Xela VS2 cells to determine relative transcript levels of *il1*, *tnf*, *il8*, and *ikb*. For all experiments, transcript expression from treated samples was normalized to time matched non-treated control. Data represent the mean ± standard error, n = 4 independent experiments. Significant differences (*) indicate significant upregulation in transcript expression relative to the time matched control, determined by a two-way ANOVA and Holm-Sidak post-hoc test ($p < 0.05$).

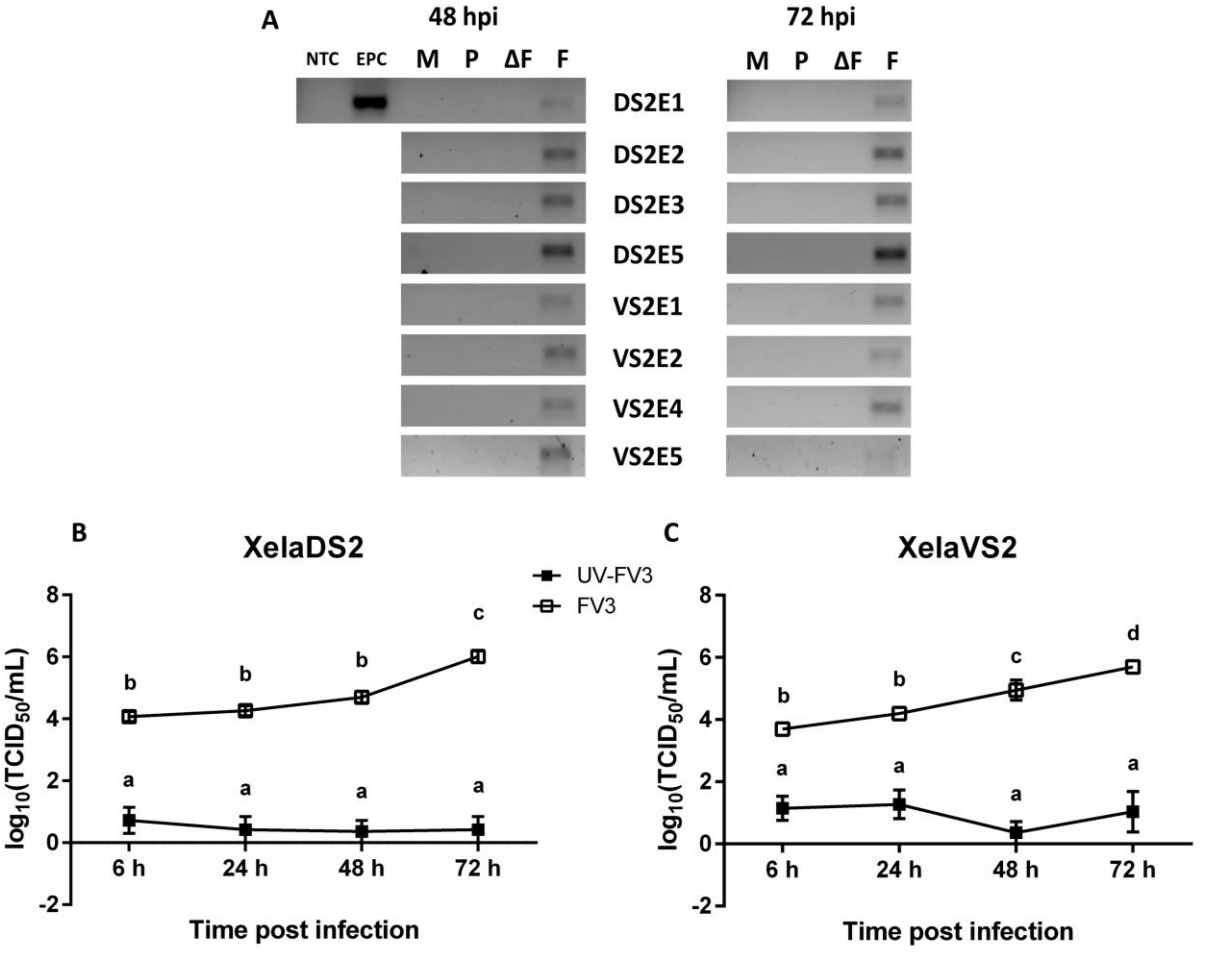

Figure 3.10. Confirmation of UV-FV3 inactivation via RT-PCR and titre analysis. (A) Gel electrophoresis image from RT-PCR of no template control (NTC), Xela DS2 and Xela VS2 non-infected control (M), poly(I:C) treated (P), UV-FV3 challenged at MOI of 2 (ΔF) and FV3 infected at MOI of 2 (F) cells for FV3 *mcp* at 48 and 72 hpi. EPC cells infected with FV3 at MOI of 2 was used as a positive control. Cell culture media was collected across all treatments at all time points for Xela DS2 (B) and Xela VS2 (C), serially diluted and applied to EPC monolayers and scored for cytopathic effects after 7 days to determine the $TCID_{50}$/mL. Cytopathic effects were not observed in cell culture media from non-infected or poly(I:C) stimulated Xela DS2 and Xela VS2 cell lines at any time point, with minimal cytopathic effects observed in UV-FV3 challenged cells. Data represent the mean ± standard error, n = 4 independent experiments. Significant differences were determined by a one-way ANOVA and a Tukey's post-hoc test ($p < 0.05$), wherein like lettering indicates no statistical significance between groups.

as viral replication is inhibited, demonstrated by the absence of viral transcript production in tandem with no increasing viral titre.

3.3.5. Evaluating poly(I:C) cytotoxicity in Xela DS2 and Xela VS2

Prior to selection of a poly(I:C) dosage to test the effect of poly(I:C) pre-treatment on FV3 infection, I first ascertained whether poly(I:C) treatment is cytotoxic to Xela DS2 and Xela VS2. This was done through a trypan blue exclusion assay under the principle that live cells have intact cellular membranes which would exclude trypan blue, while dead cells have an impaired cellular membrane thus allowing for the uptake of trypan blue (Strober, 2001). For Xela DS2, there is a significant dose-dependent relationship of poly(I:C) treatment with cell viability ($p = 0.0002$). While there are no significant differences between 0, 10, 50, or 100 ng/mL poly(I:C) treatment, there is a significant decrease in percent cell viability Xela DS2 cells treated with 1,000 ng/mL ($p = 0.0027$) or 10,000 ng/mL ($p = 0.0005$) relative to the non-treated control (Fig. 3.11A). Similarly, a significant dose-dependent relationship was observed in Xela VS2 ($p < 0.0001$), wherein treatment of cells with 1,000 ng/mL ($p < 0.0001$) or 10,000 ng/mL ($p < 0.0001$) poly(I:C) yielded a significant decrease in percent cell viability relative to the non-treated control (Fig. 3.11B). Although further confirmation is required, it appears that poly(I:C) is more cytotoxic to Xela VS2 than Xela DS2 based on the difference in magnitude of percent cell viability between the two cell lines at the higher poly(I:C) dosages (Fig. 3.11).

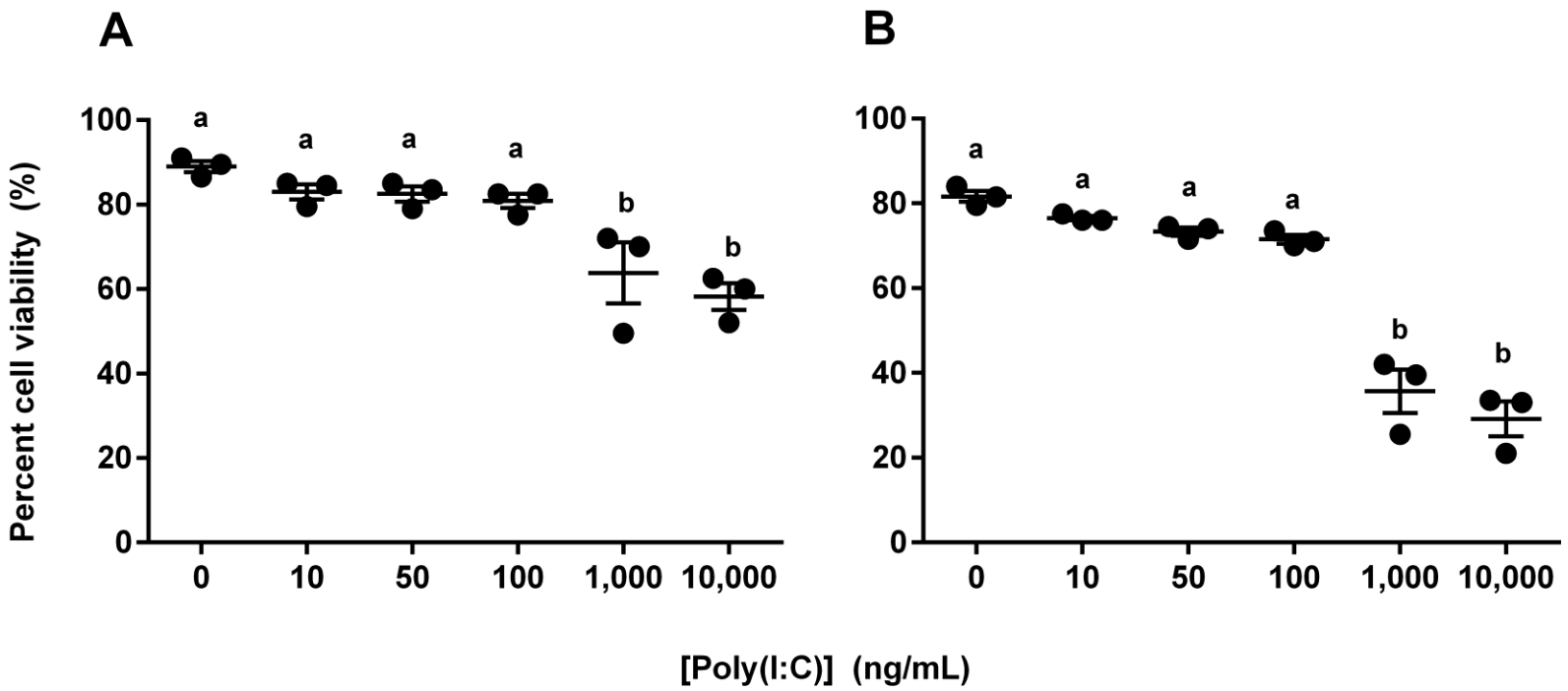

Figure 3.11. High concentrations of poly(I:C) appear cytotoxic to Xela DS2 and Xela VS2. Viability of (A) Xela DS2 and (B) Xela VS2 cells that had lost adherence to the culture vessel were assessed 24 hpt with 0, 10, 50, 100, 1,000, or 10,000 ng/mL poly(I:C) using Trypan blue. Suspension cells were collected from cell culture media by centrifugation, mixed 1:1 with trypan blue and cell viability assessed on a hemocytometer under brightfield microscopy, wherein a total of 200 cells were enumerated. Data represent the mean ± standard error, n = 3 independent experiments. Significant differences were determined by a one-way ANOVA and a Tukey's post-hoc test ($p < 0.05$), wherein like lettering indicates no statistical significance between groups.

3.3.6. Poly(I:C) pre-treatment confers partial protection against FV3-induced CPE in Xela DS2 and Xela VS2

To assess the potential effects of poly(I:C) pre-treatment on FV3-induced CPE in Xela DS2 and Xela VS2, cells were pre-treated with 0 ng/mL, 10 ng/mL, 50 ng/mL or 100 ng/mL for 24 h before FV3 infection (MOI of 2) and viability of adherent and suspension cells assessed over 5 dpi. These poly(I:C) concentrations were selected because they were not cytotoxic to Xela DS2 or Xela VS2 and did not affect cell adherence to the tissue culture vessel. NucBlue Live staining was used to visualize the number of adherent cells in wells of the tissue culture vessel. No change in the cell population is seen in Xela DS2 (Fig. 3.12A) or Xela VS2 (Fig. 3.12B) in poly(I:C) treated, non-infected cells over the 5 d experiment. Minor CPE (loss of cell adherence, thus decreasing the presence of stained nuclei) was observed on day 3 for Xela DS2 (Fig. 3.11A) at 0 and 10 ng/mL pre-treatment, while CPE was observed at all poly(I:C) concentrations for Xela VS2 with 100 ng/mL being the least severe (Fig. 3.12B). By day 5, clear CPE was observed in FV3 infected cells with no poly(I:C) pre-treatment as there was a complete loss in the presence of NucBlue Live-stained nuclei, but adherence was unaffected in both Xela DS2 (Fig. 3.12A) and Xela VS2 (Fig. 3.12B) for all poly(I:C) treated, non-infected wells. Nonetheless, poly(I:C) pre-treatment was able to mitigate FV3-induced CPE in a dose-dependent manner, at 100 or 50 ng/mL poly(I:C) in Xela DS2 (Fig. 3.12A) and 100 ng/mL for Xela VS2 (Fig. 3.12B). This trend was identical in phase contrast images of cells, wherein there was a poly(I:C) dose-dependent protection against FV3-induced CPE in both Xela DS2 (Fig. 3.13A) and Xela VS2 (Fig. 3.13B) monolayers. Additionally, cellular morphology appears unchanged between control wells, poly(I:C) treated wells, and FV3 infected wells where no CPE was observed.

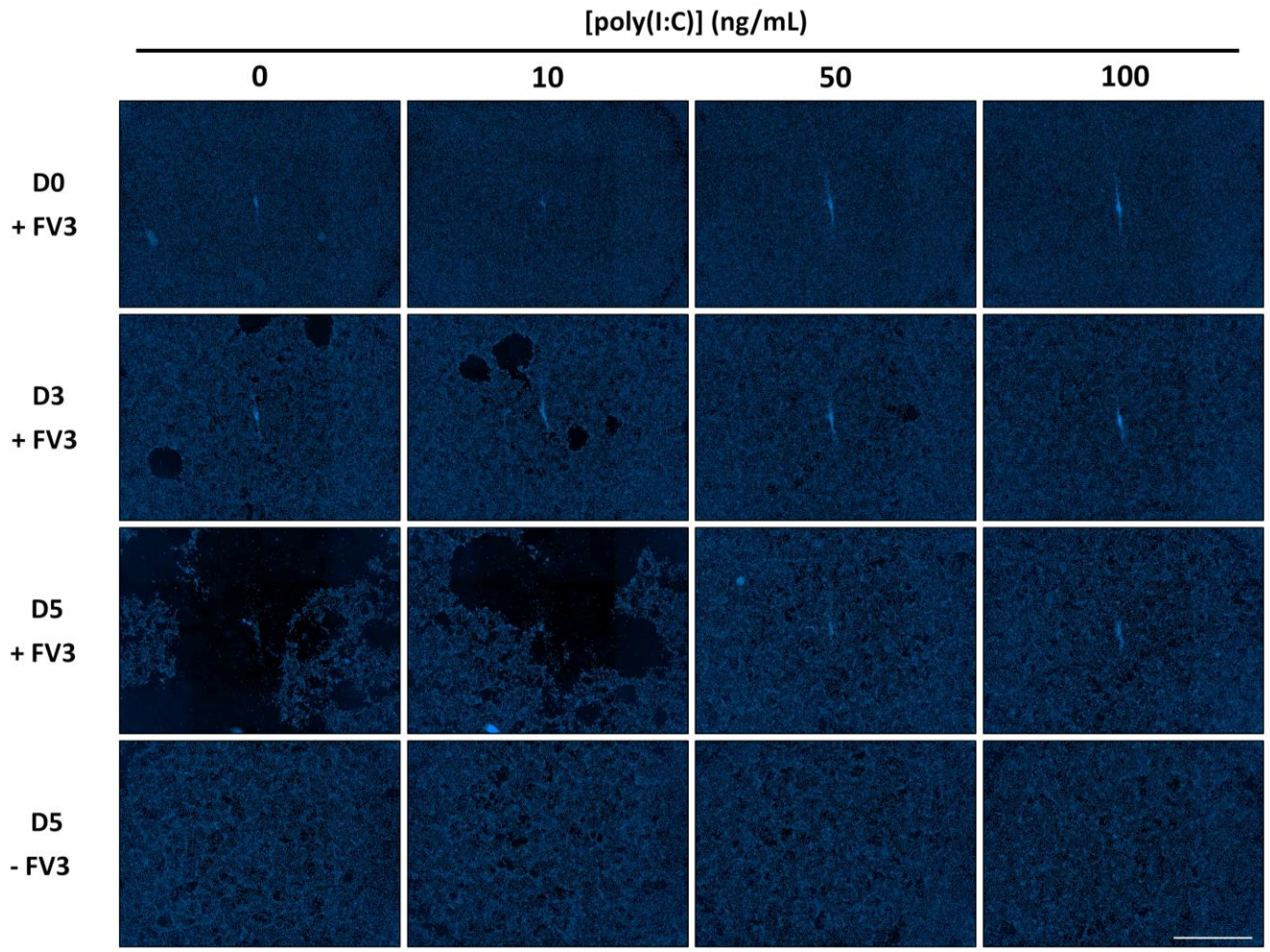

Figure 3.12A. Pre-treatment of Xela DS2 with poly(I:C) mitigate FV3-induced cytopathic effects. Fluorescence microscopy of NucBlue Live-stained Xela DS2 pre-treated with 0, 10, 50, or 100 ng/mL poly(I:C) for 24 h followed by FV3 infection at MOI of 2. Cellular morphology was monitored 0, 3, and 5 dpi. The BioTek Cytation 5 imaging reader was used to capture sixteen 40 × images in a single well, stitched together with Gen5 software; scale bar is 200 µm. Images shown are representative of four independent trials.

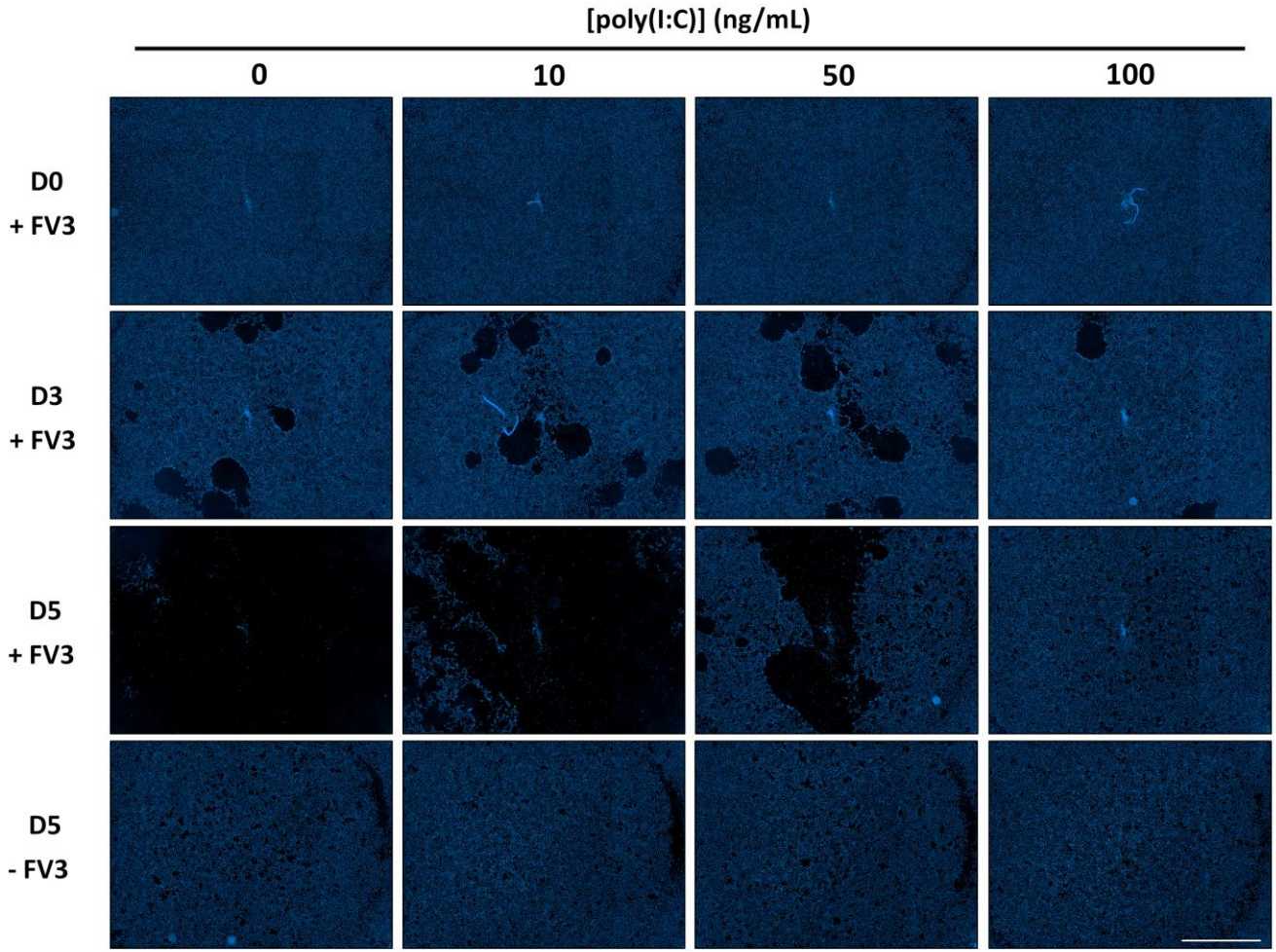

Figure 3.12B. Pre-treatment of Xela VS2 with poly(I:C) mitigate FV3-induced cytopathic effects. Fluorescence microscopy of NucBlue Live-stained Xela VS2 pre-treated with 0, 10, 50, or 100 ng/mL poly(I:C) for 24 h followed by FV3 infection at MOI of 2. Cellular morphology was monitored 0, 3, and 5 dpi. The BioTek Cytation 5 imaging reader was used to capture sixteen 40 × images in a single well, stitched together with Gen5 software; scale bar is 200 µm. Images shown are representative of four independent trials.

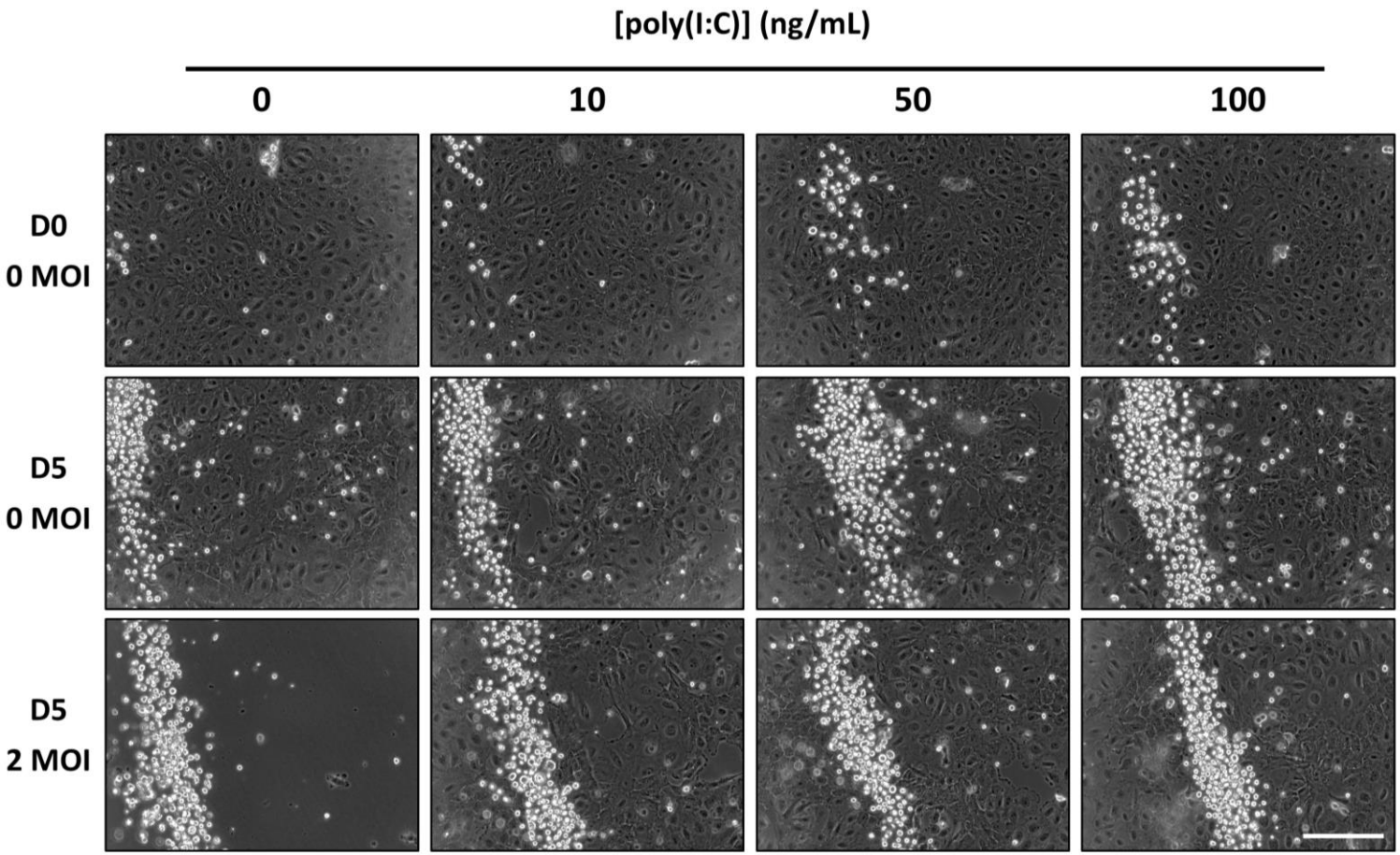

Figure 3.13A. Monitoring Xela DS2 morphology from poly(I:C) pre-treatment followed by FV3 infection. Phase-contrast microscopy of Xela DS2 cells pre-treated with 0, 10, 50, or 100 ng/mL poly(I:C) for 24 h followed by FV3 infection at MOI of 2. Cellular morphology was monitored 0, 3, and 5 dpi using the BioTek Cytation 5 imaging reader; scale bar is 50 µm. Images shown are representative of four independent trials.

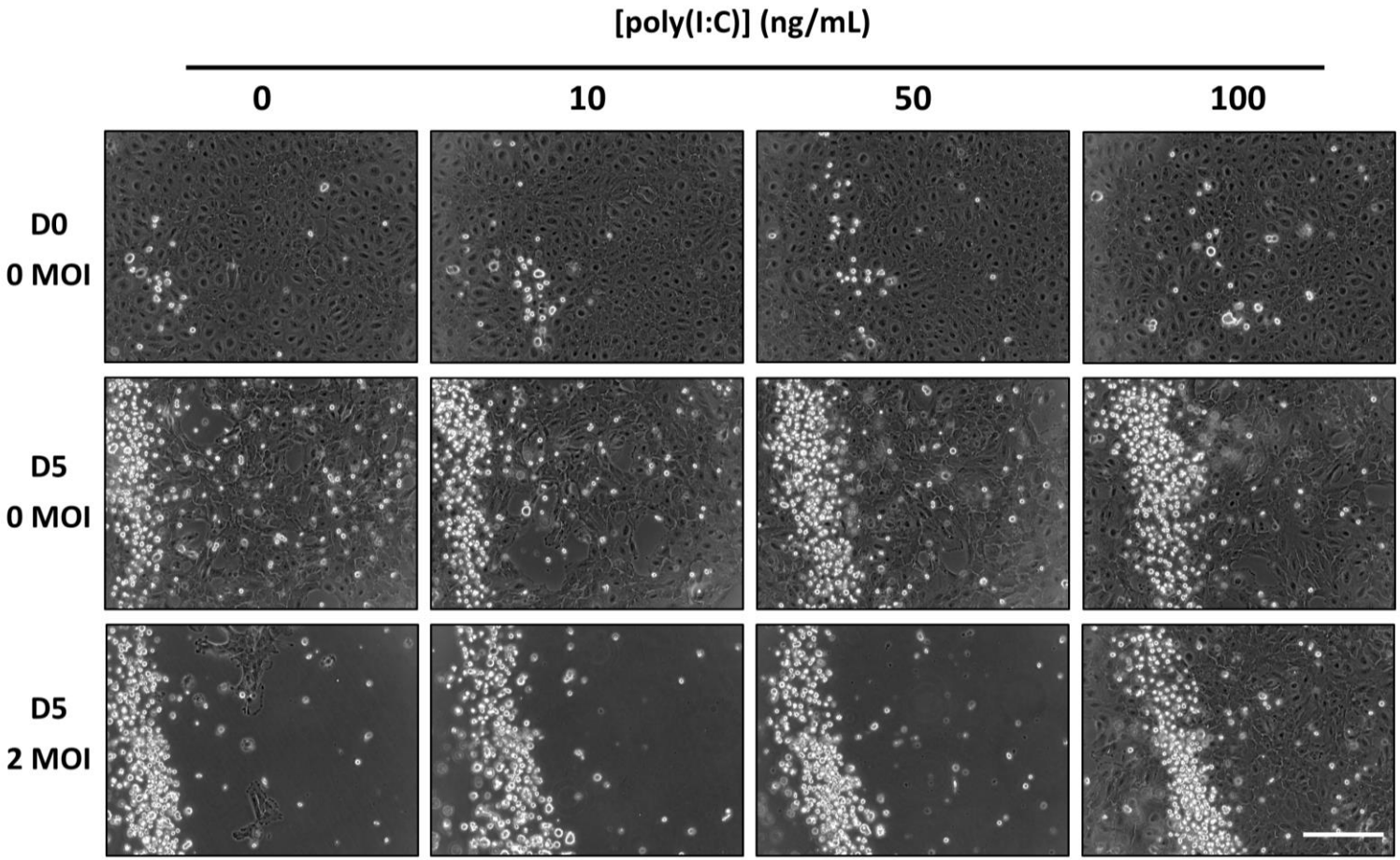

Figure 3.13B. Monitoring Xela VS2 morphology from poly(I:C) pre-treatment followed by FV3 infection. Phase-contrast microscopy of Xela VS2 cells pre-treated with 0, 10, 50, or 100 ng/mL poly(I:C) for 24 h followed by FV3 infection at MOI of 2. Cellular morphology was monitored 0, 3, and 5 dpi using the BioTek Cytation 5 imaging reader; scale bar is 50 µm. Images shown are representative of four independent trials.

In order to quantify the FV3-induced loss of cell adherence, the number of remaining adherent Xela DS2 (Fig. 3.14A) and Xela VS2 (Fig. 3.14B) cells were counted via NucBlue Live-stained nuclei enumeration, to determine the relative cell count ratio. Two-way ANOVA analysis indicated that there was a significant effect due to time ($p < 0.0001$) and poly(I:C) pre-treatment concentration ($p < 0.0001$), accompanied with a significant interaction between theses two factors ($p < 0.0001$), on Xela DS2 and Xela VS2 adherence monitored through NucBlue Live-stained nuclei enumeration. It appears that while there is no significant change in cell number among control wells and poly(I:C) treated, non-infected wells, poly(I:C) pre-treatment helps mitigate FV3-induced CPE in Xela DS2 (Fig. 3.14A) and Xela VS2 (Fig. 3.14B), in a dose-dependent manner. Furthermore, Xela DS2 appears more sensitive and better capable of conferring protection to FV3 challenge upon poly(I:C) pre-treatment than Xela VS2. While 100 and 50 ng/mL poly(I:C) pre-treatment appears to completely mitigate FV3-induced CPE in Xela DS2 (Fig. 3.14A), Xela VS2 was completely protected only when pre-treated with 100 ng/mL poly(I:C) (Fig. 3.14B).

These effects were further confirmed by using resazurin assay as a proxy to infer the presence of viable adherent cells and thus monitor the degree of loss in cell adherence. Two-way ANOVA analysis indicated that there was a significant effect due to time ($p = 0.0004$ for Xela DS2, $p < 0.0001$ for Xela VS2) and poly(I:C) pre-treatment concentration ($p = 0.0159$ for Xela DS2, $p = 0.0002$ for Xela VS2), accompanied with a significant interaction between theses two factors ($p = 0.0308$ for Xela DS2, $p < 0.0001$ for Xela VS2), on Xela DS2 and Xela VS2 adherence monitored via resazurin assay. For both Xela DS2 (Fig. 3.14C) and Xela VS2 (Fig. 3.14D), there was no significant change in relative absorbance ratio values across all poly(I:C) treated, non-infected cells. Overall, it appears as though the trend in resazurin

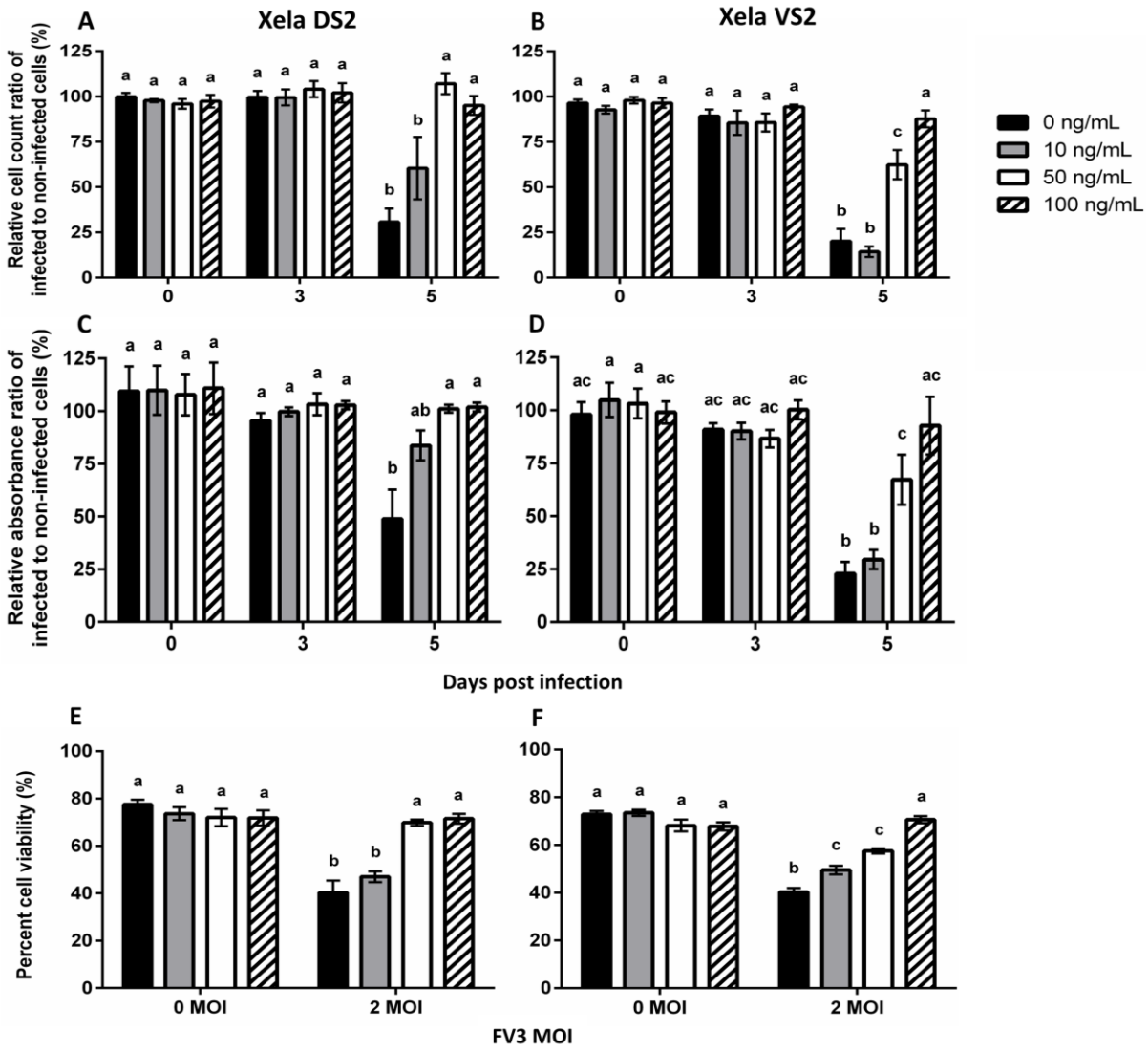

Figure 3.14. Pre-treatment of Xela DS2 and Xela VS2 with poly(I:C) mitigates FV3-induced loss in cell adherence. Xela DS2 and Xela VS2 cells were pre-treated with 0, 10, 50, or 100 ng/mL poly(I:C) for 24 h before infecting cells with FV3 at MOI of 2 alongside non-treated controls. On 0, 3, and 5 dpi, cell culture media was removed and adherent Xela DS2 (A) and Xela VS2 (B) NucBlue Live-stained nuclei were enumerated using the Cytation 5 plate reader. Resazurin assay was also performed on Xela DS2 (C) and Xela VS2 (D) to monitor metabolic-based viability. Data represent the mean ± standard error, n = 3 independent experiments. The viability of non-adherent cells were monitored at 5 dpi via trypan blue exclusion assay in (E) Xela DS2 and (F) Xela VS2. Data represent the mean ± standard error, n = 4 independent experiments. Significant differences were determined by a two-way ANOVA and a Tukey's post-hoc test ($p < 0.05$) for all tests, wherein like lettering indicates no statistical significance between groups.

assay data is similar to the observed changes in morphology and nuclei counts: pre-treatment with 50 and 100 ng/mL poly(I:C) is able to abrogate FV3-induced CPE in Xela DS2 (Fig. 3.14C) while 100 ng/mL poly(I:C) abrogates FV3-induced CPE in Xela VS2 (Fig. 3.14D).

Trypan blue exclusion assay was also performed to assess the effect of FV3 challenge on suspension cell viability, as the assessment of these cells would have been excluded from DAPI-staining counts and resazurin assay experiments. Two-way ANOVA analysis indicated that there was a significant effect due to both FV3 ($p < 0.0001$) and poly(I:C) pre-treatment concentration ($p = 0.0005$ for Xela DS2, $p < 0.0001$ for Xela VS2) on Xela DS2 and Xela VS2 FV3-induced CPE, accompanied with a significant interaction between these two factors ($p < 0.0001$). In general, FV3 seems to impact Xela DS2 (Fig. 3.14E) and Xela VS2 (Fig. 3.14F) suspension cell viability, but poly(I:C) pre-treatment is able to mitigate this effect in a dose-dependent manner. As such, both the adherent and suspension Xela DS2 and Xela VS2 cells respond to poly(I:C) pre-treatment by conferring partial resistance to FV3-induced CPE.

3.3.7. Poly(I:C) pre-treatment limits FV3 viral replication in Xela DS2 and Xela VS2

To determine whether poly(I:C) pre-treatment limits FV3 replication, Xela DS2 or Xela VS2 were pre-treated with low serum media alone or containing 100 ng/mL poly(I:C) for 24 h prior to infection of cells with FV3. Viral titre analysis was performed on sample supernatants at 0, 3 and 5 dpi (Fig. 3.15). Two-way ANOVA analysis indicated that there was a significant effect due to time ($p < 0.0001$) and poly(I:C) pre-treatment concentration ($p < 0.0001$ for Xela DS2, $p = 0.0106$ for Xela VS2), accompanied with a significant interaction between theses two factors ($p < 0.0001$ for Xela DS2, $p = 0.0063$ for Xela VS2), on Xela DS2 and Xela VS2 viral titre from poly(I:C) pre-treatment. Poly(I:C) pre-treatment at

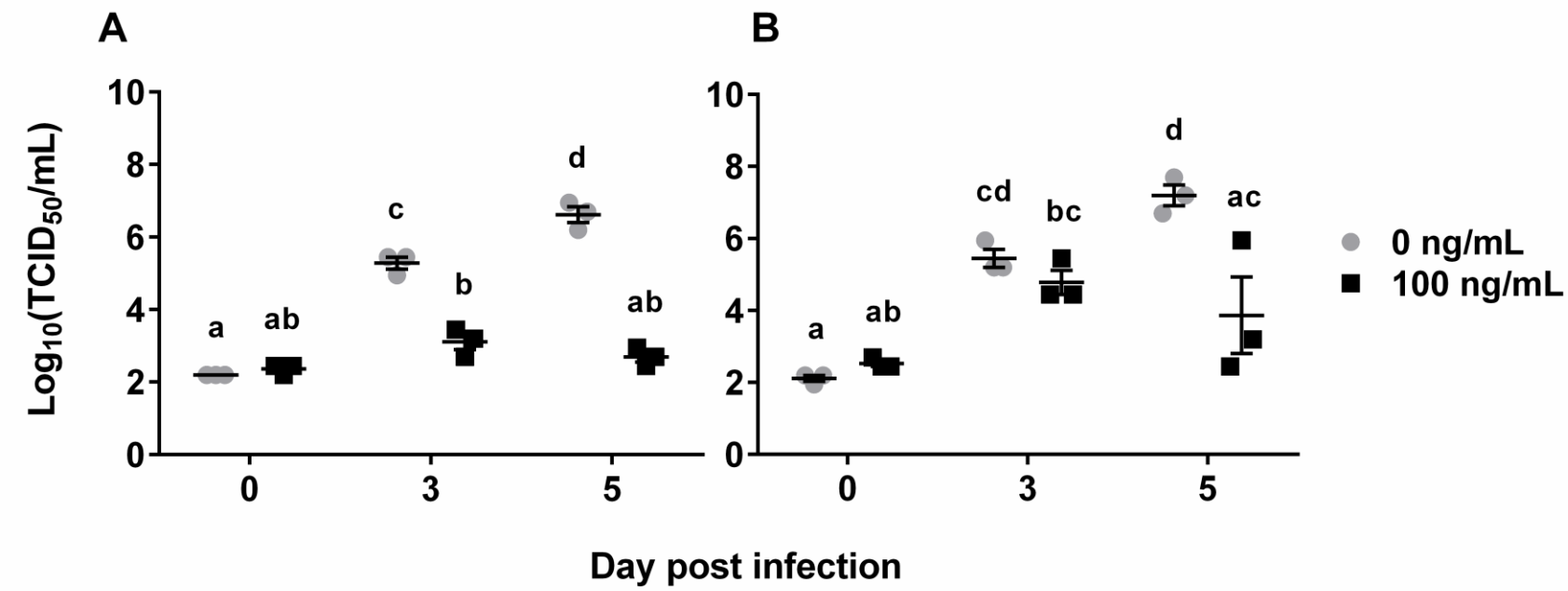

Figure 3.15. Poly(I:C) pre-treatment reduces viral titre in Xela DS2 and Xela VS2. Cell culture media was collected from (A) Xela DS2 and (B) Xela VS2 when pre-treated with 0 or 100 ng/mL poly(I:C) then challenged with FV3 at MOI of 2, at 0, 3, and 5 days post infection. Cell supernatants were serially diluted then applied to a 96-well plate containing a monolayer of EPC cells. Monolayers were scored for cytopathic effects after 7 days determine the $TCID_{50}$/mL. Data represent the mean ± standard error, n = 3 independent experiments. Significant differences were determined by a two-way ANOVA and a Tukey's post-hoc test ($p < 0.05$), wherein like lettering indicates no statistical significance between groups.

100 ng/mL is able to limit FV3 replication in both Xela DS2 (Fig. 3.15A) and Xela VS2 (Fig. 3.15B), which is in accordance with the observed trends from changes in cell morphology and analysis of FV3-induced CPE wherein 100 ng/mL poly(I:C) pre-treatment completely abrogated FV3-induced CPE. While the viral titre from non-poly(I:C) pre-treated Xela DS2 (Fig. 3.15A) and Xela VS2 (Fig. 3.15B) increased in a time-dependent manner, there was no significant difference in titre levels between cells pre-treated with 100 ng/mL poly(I:C) at day 5 and cells from non-poly(I:C) pre-treated cells at day 0. However, for Xela VS2 (Fig. 3.15B), there was a significant increase in the day 3 poly(I:C) pre-treated viral titre value relative to day 0 non-poly(I:C) pre-treated cells which then decreased back to baseline value (Fig. 3.15B).

3.4. Discussion

3.4.1. Xela DS2 and Xela VS2 are permissive to FV3 and support viral replication

Xela DS2 and Xela VS2 cells infected with FV3 exhibit CPE wherein cells appear to shrink and contract then lose adherence to the cell culture vessel. This has also been observed in mammalian and fish cell lines, as well as the *X. laevis* A6 kidney epithelial cell line (Chinchar et al., 2003; Pham et al., 2015). A number of studies have identified apoptosis as a mechanism of cell death upon cellular FV3 infection in a various cell lines across vertebrates (Chinchar et al., 2003; Morales et al., 2010; Pham et al., 2015). However, other cell lines appear to lose viability through non-apoptosis driven mechanisms (Jancovich et al., 2015). While the mechanisms of cell death in FV3-infected Xela DS2 and Xela VS2 was not examined in this study, preliminary assessments of cell viability using trypan blue suggest the loss of membrane integrity and could be indicative of late apoptotic cells or pyroptosis. Regardless of the mechanism of cell death following FV3 infection, the loss of cell

adherence can be used as a proxy to estimate viral infection via a resazurin assay, wherein the degree of metabolic activity is proportional to the number of remaining viable cells that are adherent to the tissue culture vessel. Although metabolic activity may be altered in response to external stimuli leading to a potential under-representation of cell populations, decreases in metabolic function would indicate a negative impact on cellular health in general (Rampersad, 2012). In these situations, it is recommended that the resazurin assay is coupled with an additional assay to generate a more accurate prediction of the system, such as directly monitoring cell numbers (Rampersad, 2012). As such, coupling the resazurin assay with NucBlue Live-stained nuclei enumeration is an effective measure of FV3-induced CPE in terms of the loss of cellular adherence. Further studies are required to understand how/if Xela DS2 and Xela VS2 metabolism is impacted from poly(I:C) and/or FV3 treatment, the mechanism of the loss of cellular adherence, and confirmation of whether these cells are undergoing cell death.

Xela DS2 and Xela VS2 appear equally permissible to FV3, supporting viral transcription and replication in a dose and time-dependent manner. While Xela DS2 and Xela VS2 are generally susceptible to FV3 at higher MOIs ($\geq$ 0.02), no CPE is observed when infected with FV3 MOI of 0.002. This suggests that Xela DS2 and Xela VS2 have viral restriction to FV3. Interestingly at this lower MOI, infectious particles are detected earlier in infection which then appears to be cleared with time, although further investigation is required. Increases in viral titre and the detection of *mcp* in infected Xela DS2 and Xela VS2 show that these cell lines are permissive to FV3 alongside mammalian and fish cells used in FV3 studies (Ariel et al., 2009; Braunwald et al., 1985; Pham et al., 2015; Vo et al., 2019a), albeit to varying degrees. The viral titre plateau for a number of rainbow trout cell lines was

reported at $log_{10}(TCID_{50}/mL)$ 4-5, versus Xela DS2 and Xela VS2 at $log_{10}(TCID_{50}/mL)$ 6-7, and EPC at $log_{10}(TCID_{50}/mL)$ 8-9 (Ariel et al., 2009; Pham et al., 2015) demonstrating the different replicative capacity of FV3 across cell lines. To my knowledge, the lower limit tolerance of cell lines to FV3 has not been previously studied. By showing that Xela DS2 and Xela VS2 are permissible to FV3 infection, it is likely that individual frog skin epithelial cells are susceptible to FV3, allowing infection to propagate through the skin. Further studies must be conducted to better elucidate the various mechanisms performed in the FV3-frog skin epithelial cell interaction, wherein Xela DS2 and Xela VS2 serve as suitable models.

3.4.2. Xela DS2 and Xela VS2 do not upregulate antiviral or proinflammatory genes in response to FV3

While Xela DS2 and Xela VS2 can recognize, are permissive to and support FV3 viral replication, they appear to be unable to initiate antiviral or proinflammatory programs in the presence of FV3. Similarly, both cell lines failed to initiate these programs in response to UV-FV3, yet UV-FV3 is unable to undergo viral replication. Although I cannot rule out the upregulation of other antiviral genes, such as the ~30 other *ifn* transcripts (Sang et al., 2016; Wendel et al., 2018), the ~1000 ISGs, or other proinflammatory cytokines, my results suggest FV3 is likely enacting immunoevasion strategies of these frogs skin epithelial-like cell lines. FV3 is known for shutting down macromolecular synthesis in mammalian and fish cell lines (Goorha and Granoff, 1974), and select viral genes have been identified as possessing immune evasion properties against mammalian, fish, and amphibian (kidney A6) cell lines (Andino Fde et al., 2015; Jacques et al., 2017). This has also been shown to occur in cells challenged with FV3 that was heat-treated or UV-inactivated (Williams, 1996), which may explain the similar response between FV3 and UV-FV3 challenged Xela DS2 and Xela VS2. It is currently theorized that FV3 carries a capsid protein that is responsible for the

rapid shutdown of host antiviral pathways (Jacques et al., 2017; Rothenburg et al., 2011). While there is no documentation of the effect of UV inactivation of FV3 immunoevasion ability, I predict that UV inactivation does not impact FV3's ability to elicit immunoevasion strategies since the protein would remain intact. Although further study is required, it appears as though the ability for FV3 to elicit immunoevasion strategies and induce total shutdown of host cellular machinery may be no different in Xela DS2 and Xela VS2. To my knowledge, this is the first report of potential immunoevasion elicited by FV3 in isolated frog skin epithelial-like cells, yet further studies must be conducted to further elucidate the FV3-frog skin epithelial cell interaction.

3.4.3. Poly(I:C) pre-treatment of Xela DS2 and Xela VS2 mitigate FV3 replication

Xela DS2 and Xela VS2 appear to have a dose-dependent response to poly(I:C) treatment, wherein treatment at 10 µg/mL appears to yield a greater fold-change in gene expression for all transcripts studied (see Chapter 2, Sections 2.3.5 – 2.3.6) relative to treatment at 1 µg/mL (see Section 3.3.3). Regardless of treatment with 10 or 1 µg/mL poly(I:C), a significant number of Xela DS2 and Xela VS2 lose adherence, and only a single preliminary trypan blue exclusion assay with 10 µg/m poly(I:C) treatment demonstrated that cells were likely dying. Analysis of Xela DS2 and Xela VS2 cytotoxicity to poly(I:C) uncovered the degree of sensitivity of these cells to poly(I:C) exposure. Of the poly(I:C) concentrations studied, only those ≤ 100 ng/mL did not induce significant cellular cytotoxicity. Xela DS2 and Xela VS2 are then included among cell lines which respond to low poly(I:C) dose (Poynter et al., 2019; Tohyama et al., 2005), opposed to those which have been studied in concentrations ranges which would otherwise be cytotoxic to Xela DS2 and Xela VS2 (Kumar et al., 2006; Ritter et al., 2005). Given this sensitivity, it is important that

future studies involving the use of poly(I:C) as an immunostimulant in Xela DS2 and Xela VS2 are performed at low dosage levels. It was observed that treatment of mammalian neonatal keratinocyte cells with 25,000 ng/mL poly(I:C) induced cell death via pyroptosis (Lian et al., 2012). I have already demonstrated that Xela DS2 and Xela VS2 have a robust proinflammatory response when treated with poly(I:C), which is a known hallmark of pyroptotic cells—programmed cell death induced by a high inflammation state (Bergsbaken et al., 2009). As such, it is possible that Xela DS2 and Xela VS2 undergo pyroptosis in response to high dose poly(I:C) treatment but must be further studied to be confirmed.

In response to poly(I:C) pre-treatment, both Xela DS2 and Xela VS2 demonstrated a protective effect against FV3-induced CPE at low poly(I:C) levels (≤ 100 ng/mL) in a dose-dependent manner, in tandem with limiting the capability for FV3 to replicate. Given that poly(I:C) is a known Type I IFN inducer, and my current gene expression studies (see Chapter 2 Section 2.3.5; Chapter 3 Section 3.3.3) demonstrate that *ifn1* and ISG transcripts are being upregulated in Xela DS2 and Xela VS2, it is likely that poly(I:C) stimulation induces an antiviral program in these cells to better prepare and protect from FV3 infection. This induction and protective effect appears to be stronger in Xela DS2 than Xela VS2, due to its ability to induce a protective effect at lower poly(I:C) levels. When these cells were previously exposed to a high dose of 10 µg/mL poly(I:C), most Xela DS2 innate immune transcripts examined were upregulated sooner than those in Xela VS2 (see Chapter 2, section 2.3.5). It is proposed that this sensitivity is being captured, as the 24 h pre-treatment period may be enough time to induce a protective antiviral state in Xela DS2 but not as effective in Xela VS2. However, the exact mechanism to confer resistance to FV3 infection due to poly(I:C) pre-treatment is not known and should be further investigated. Nonetheless, the

initial poly(I:C)-induced immunogenic burst was enough to allow for not only protection of the cell monolayer and limiting/reducing viral titre , but also for the reduction in the number of non-viable suspension Xela DS2 and Xela VS2 cells when challenged with FV3 demonstrating complete resistance to FV3 cytopathicity. It is important to note that the trypan blue exclusion assay may provide inference about whether cells are live or dead, but further analysis is required to support my findings such as exploring mechanisms of cell death.

Previous studies on FV3 infection, as well as infection with other aquatic viruses, in fish cells have shown that poly(I:C) pre-treatment effectively mitigates viral-induced CPE in tandem with limiting viral replication (Lisser et al., 2017; Poynter and DeWitte-Orr, 2018; Poynter et al., 2019). However, my findings are the first study to demonstrate the effectiveness of an immunostimulant on mitigating FV3-induced CPE and limiting viral replication in isolated frog skin epithelial-like cells. Although FV3 may elicit immunoevasion properties to inhibit the induction of an antiviral program in Xela DS2 and Xela VS2, which is consistent with the literature (Andino Fde et al., 2015; Jacques et al., 2017), my research shows evidence that FV3 is unable to break an antiviral program at not only the tissue level (Wendel et al., 2017), but also the cellular level. In conclusion, frog skin epithelial cells are permissive to FV3 as seen by CPE and inability to initiate antiviral and proinflammatory programs, but CPE can be mitigated when treated with an immunostimulant that induces an antiviral program in the host.

Chapter 4: Conclusions and Future Directions

4.1. Overview and significance of findings

Despite being faced with declines in amphibian populations wherein FV3 is believed to be a driving force (Daszak et al., 2003; Stuart et al., 2004), FV3-cellular interactions and mechanisms of infection in frog cells, such as eliciting immunoevasion strategies or induction of cell death, remain poorly understood. Frog skin is an important interface between the frog's external and internal environment and is likely the first organ to encounter environmental pathogens, with surface layer epithelial cells acting as an important physical barrier limiting entry (Varga et al., 2019). However, the role of frog skin epithelial cells in recognizing and responding to FV3 is unknown. My thesis focuses on bridging this knowledge gap through the generation of novel *X. laevis* skin epithelial-like cell lines, Xela DS2 and Xela VS2. These cell lines were characterized after establishment, and with successive passages became stable cell lines for the *in vitro* study of isolated frog skin epithelial cells. Treatment of Xela DS2 and Xela VS2 with poly(I:C) (an analogue of viral dsRNA), although cytotoxic at high doses, induces transcript expression of antiviral and proinflammatory genes, demonstrating the ability of frog skin epithelial cells to sense and respond to viral dsRNA. The induction of this complement of genes was not observed when Xela DS2 and Xela VS2 are challenged with FV3 or UV-FV3, leading to obvious signs of cytopathicity characterized by cell contraction and subsequent loss of cellular adherence properties. Nonetheless, FV3-induced CPE and replication were capable of being mitigated in Xela DS2 and Xela VS2 with poly(I:C) pre-treatment. The implications of my findings are further discussed below, accompanied with potential future directions this work can be taken based on my results.

4.2. Frog skin epithelial cells are capable of recognizing and responding to extracellular viral dsRNA

Treatment of Xela DS2 and Xela VS2 with poly(I:C) induces morphological changes and robust increases in immune gene transcripts. There is a clear dose-dependent sensitivity of Xela DS2 and Xela VS2 to poly(I:C), where relatively high doses (≥ 1000 ng/mL) induces the loss of cellular adherence and appears to be cytotoxic. This alone shows that Xela DS2 and Xela VS2 are capable of the extracellular recognition and response to dsRNA, potentially through a SR family member (DeWitte-Orr et al., 2010; Limmon et al., 2008; Vo et al., 2019b), which is a feature not present in all cell types demonstrating the sensitivity of frog skin epithelial cells to extracellular dsRNA. In relation to the whole animal, skin shedding is common in amphibians for maintaining optimal physiological performance or in response to stress such as pathogen insult (Pessier, 2002; Weldon et al., 1993). As such, the loss of cellular adherence in Xela DS2 and Xela VS2 of may be reflective of skin shedding in response to external stimuli but needs to be further investigated. Nonetheless, poly(I:C) treatment of Xela DS2 and Xela VS2 induces the upregulation of antiviral (*ifn1, pkr)*, and proinflammatory (*tnf*, *il1*, *il8)* genes, although the mechanism and specific PRR engagement is not known. The induction of these set of genes is dose-dependent, as treatment with poly(I:C) at 10 µg/mL (Chapter 2) yields a greater magnitude fold-change in gene expression for all transcripts studied than compared to treatment with 1 µg/mL (Chapter 3). To my knowledge, this work is the first study to confirm the ability for isolated frog skin epithelial-like cells to sense and respond to a viral dsRNA analogue, as seen by potent upregulation of antiviral and proinflammatory gene transcripts under poly(I:C) treatment. Whether increased transcript levels correspond to protein synthesis of these targets in Xela DS2 and Xela VS2 is unknown. Similarly, poly(I:C) treatment of mammalian epithelial cell cultures resulted in

marked upregulation of *TNF*, *IL-1β*, *IL-8*, *IFN1* and *Mx* gene expression and protein production (Kinoshita et al., 2009; Kumar et al., 2006). The upregulation of key proinflammatory cytokines *tnf* and *il1* was also observed in the teleost epithelial cell line EPC when treated with poly(I:C) (Holopainen et al., 2012). These suggest potential conservation of the ability for epithelial cells across species to recognize and respond to dsRNA.

4.3. Immunoevasion properties of FV3 are retained in frog skin epithelial cells, but can be overcome with prior induction of antiviral programs

Xela DS2 and Xela VS2 are shown to be permissive to FV3 and viral replication, as seen by CPE, detection of viral *mcp* transcripts, and time and dose-dependent increases in viral titre in infected cells. These cell lines also incur CPE from UV-FV3 treatment, but without accompanying increase in titre levels or *mcp* detection. Although Xela DS2 and Xela VS2 demonstrate the ability to recognize FV3 and UV-FV3, there was no change in antiviral *ifn1*, *mx2*, *pkr* and proinflammatory *tnf*, *il1*, *il8*, and *ikb* transcript levels. The ability for FV3, whether active or UV-inactivated, to shut-down cellular molecular synthesis and elicit immune evasion strategies in mammalian and fish cells (Andino Fde et al., 2015; Chen et al., 2011; Goorha and Granoff, 1974; Jacques et al., 2017) appears to be conserved in Xela DS2 and Xela VS2. This may in part be due to the contribution of FV3 genes which have been identified as eliciting immune evasion strategies against mammalian, fish, and amphibian cells (Andino Fde et al., 2015; Jacques et al., 2017). Such genes include 18K, 52L, 64R, and viF2α (Andino Fde et al., 2015; Chen et al., 2011; Jacques et al., 2017). Nonetheless, I have demonstrated that pre-treatment of Xela DS2 and Xela VS2 with poly(I:C) allows for initial upregulation of proinflammatory and antiviral programs which effectively mitigate FV3-induced CPE and limits viral replication from occurring. My studies thus show that while

FV3 is capable of host macromolecular shutdown and immune evasion, FV3 does not appear to be able to break an antiviral state once already induced.

FV3 possesses a 100 kb genome which is composed of 95-100 ORFs as identified in in wild isolate strains (Morrison et al., 2014), but the exact function of each corresponding protein is unkown. The most well documented FV3 immune invasion protein is vIF2α, sharing homology with eukaryotic initiation factor 2α, and is an agonist to host-cell PKR (Rothenburg et al., 2011). Yet unlike other ranaviruses, the N-terminal PKR binding domain appears truncated in FV3 vIF2α, rendering the role of vIF2α unknown in FV3 (Chen et al., 2011). Nonetheless, vIF2α-knockout mutant FV3 strains was still met with decreased levels of infectivity as well as viral titres levels (Chen et al., 2011). So while the role of FV3 vIF2α remains to be confirmed, it will be assumed that its immune evasion strategy is PKR-dependent like other ranaviruses. Suppression of PKR would render the cell incapable of halting viral transcripts from undergoing transcription, so if there were an overabundance of PKR initially present, the cells could potentially overcome agonistic vIF2α. As such, one potential mechanism of protection from poly(I:C) pre-treatment may be that Xela DS2 and Xela VS2 produce PKR in an overabundance to limit vIF2α-mediated effects, wherein Xela DS2 may be more efficient at sooner producing PKR than Xela VS2. Many alternative proteins may exist which suppress host immune responses, such as 18K, 52L, and 64R (Jacques et al., 2017), but the function of these proteins must be better elucidated first.

4.4. Novel frog skin epithelial-like cell lines for use as *in vitro* models

While a handful of *X. laevis* cell lines do currently exist, they do not necessarily provide a system to study the initial interaction between the environment and amphibian. With the generation of Xela DS2 and Xela VS2, which are epithelial-like in nature, we can

now begin to elucidate this interaction and better understand the role of skin epithelial cells in frog host defence to a number of threats. Although Xela DS2 and Xela VS2 have been generated for their use in understanding the role of frog skin epithelial cells in sensing and responding to viral PAMPs and interaction with FV3, their use is not limited to these applications. Indeed, these cell lines can be utilized to answer a wide range of questions, such as understanding the impact of various stressors on frog skin epithelial cell immune mechanisms or barrier integrity in relation to the whole animal. Extensive studies have been conducted to better understand the impacts of our changing environment on frog populations, and have concluded that amphibians are sensitive to changes in temperature, increased UV radiation, and environmental stressors like chemical contaminants (Blaustein et al., 2010b; Hayes et al., 2002; Kerby et al., 2010; Todd et al., 2011). These demonstrate that stressors may render a host immunocompromised and susceptible to infection with a virulent pathogen (Blaustein et al., 2010a; Blaustein et al., 2003; Sifkarovski et al., 2014). Thus, Xela DS2 and Xela VS2 can be used to monitor the potential effects of multiple stressors on frog skin epithelial cells, such as use in toxicity screens. For example, atrazine exposure affected larval and adult *X. laevis* antiviral immunity, which can now be studied at the cellular level using Xela DS2 and Xela VS2 (Sifkarovski et al., 2014). Furthermore, since these cell lines are epithelial-like in nature and the expression of cellular junctions at the transcript level was identified, we can begin to look at how the expression of these junctions, and thus barrier integrity, may be impacted from environmental stressors. Yet, further *in vitro* analysis for the identification of these junction proteins in Xela DS2 and Xela VS2 must be performed to confirm that these cell lines are epithelial cells, and not just epithelial-like.

Immunoevasion mechanisms by FV3 can be confirmed in Xela DS2 and Xela VS2; although this can be studied in other cell lines as seen in A6 (Andino Fde et al., 2015), this would allow for the further elucidation of molecular mechanisms of FV3 immune evasion at the frog skin epithelial barrier. I propose this is important to look at because while many cell lines are highly susceptible to FV3 infection, Xela DS2 and Xela VS2 are currently the only cell lines which reports a lower limit resistance to FV3 infection which may be controlled by cellular antiviral mechanisms. This was seen by a net reduction of viral titres over time with FV3 infection at MOI of 0.002. As such, overall study of Xela DS2 and Xela VS2 with FV3 at MOI $\leq$ 0.002 should be investigated to see whether ISGs and thus viral restriction genes are being turned on in the host, and may be useful in understanding the kinetics between viral and host gene transcripts and how one may outcompete the other. It is clear that the decline in amphibian species is due to a combination of factors, but there are limited studies showing this multi-factorial impact on amphibian hosts (Longo and Zamudio, 2017; Rollins-Smith, 2017; Sifkarovski et al., 2014). Thus, the generation of Xela DS2 and Xela VS2 will act as important *in vitro* system for studying amphibian host-pathogen interactions at the skin epithelial interface in tandem with the impact of our changing environment. Xela DS2 and Xela VS2 will prove to be novel models for better understanding the interface between a frog and its environment.

4.5. Future Directions

4.5.1. Mechanism of Xela DS2 and Xela VS2 cell death from FV3 challenge

While CPE was observed in Xela DS2 and Xela VS2 in response to poly(I:C), UV-FV3, and FV3, the mechanism of cell death is unknown. The uptake of trypan blue by cells with a compromised cell integrity indicates that the cell is non-viable but does not unveil the

mechanism of cellular death. As such, the decrease in Xela DS2 and Xela VS2 viability from poly(I:C) or FV3 treatment should be further explored in order to understand what programs are being initiated in the host cell. For poly(I:C), a study found that cell death was induced in mammalian keratinocytes from high-dose poly(I:C) treatment via pyroptosis (Lian et al., 2012). Pyroptosis is a form of programmed cell death which, in mammals, is partly dependent on the caspase-1-dependent induction and activation of IL-1β and IL-18 (Bergsbaken et al., 2009). I previously demonstrated that high-dose poly(I:C) is potent to Xela DS2 and Xela VS2, yielding a strong upregulation in proinflammatory transcripts including *il1*. As such, Xela DS2 and Xela VS2 should be monitored for pyroptosis upon poly(I:C) treatment. For FV3, numerous studies have already identified that cells undergo apoptosis upon FV3 challenge, regardless if the cell is of mammalian, fish, or amphibian origin (Chinchar et al., 2003; Morales et al., 2010; Pham et al., 2015). Whether Xela DS2 and Xela VS2 undergo apoptosis from FV3 infection must be confirmed. Although the viability of Xela DS2 and Xela VS2 suspension cells from UV-FV3 treatment was not monitored, apoptosis was found to be induced in mammalian and fish cells regardless if treated with FV3, heat-inactivated FV3, or UV-FV3 (Chinchar et al., 2003), suggesting that this may be the same for isolated frog skin epithelial cells but requires confirmation. Elucidating the mechanism of cell death from these treatments in Xela DS2 and Xela VS2 will help to better understand the FV3-frog skin epithelial cell interaction and how FV3 may bypass the skin barrier at the cellular level.

4.5.2. Screening Xela DS2 and Xela VS2 for the expression of dsRNA and dsDNA sensors and pattern recognition receptors

The ability for Xela DS2 and Xela VS2 to recognize poly(I:C), FV3, and UV-FV3 is a good indication that these cells possess dsRNA sensors and PRRs necessary for at least the

recognition of extracellular pathogenic particles. Previously, SR-As have been shown to sense and bind dsRNA in mammalian, fish, and frog cells and are believed to be important in FV3 binding and mediating cell entry (DeWitte-Orr et al., 2010; Limmon et al., 2008; Vo et al., 2019a; Vo et al., 2019b). As such, SR family expression, identification and activity in Xela DS2 and Xela VS2 may help infer how these cells recognize poly(I:C) and FV3. These studies have also highlighted the importance of SRs in mediating cellular entry of poly(I:C) and FV3 (DeWitte-Orr et al., 2010; Vo et al., 2019a). The presence of internal dsRNA PRRs in Xela DS2 and Xela VS2 should also be investigated. It is known that dsRNA is produced during the FV3 life cycle (Doherty et al., 2016), yet the interaction between intracellular dsRNA sensors and FV3-derived dsRNA in frogs remains unknown. A number of internal cellular PRRs have previously been identified in mammalian and fish models which recognize viral dsRNA, including endosomal TLR3, cytosolic MDA5, RIG-I, and NLRs (Poynter et al., 2015; Zhou et al., 2014). The screening of Xela DS2 and Xela VS2 for viral dsRNA sensors would be insightful in understanding which members are potentially responsible for the recognition and response to viral pathogens.

While a number of cytoplasmic DNA sensors exist (Paludan and Bowie, 2013), a novel cytosolic DNA sensor has recently been identified which is comprised of two parts: PAMP-recognizing cyclic GMP-AMP synthase (cGAS) and cell signalling Stimulator of Interferon Genes (STING), creating the cGAS-STING system (Diner et al., 2013; Sun et al., 2013). This system is well documented in mediating the recognition of cytosolic dsDNA (from virus, bacteria, or necrotic cells) by cGAS to catalyze ATP and GTP to 2',3'-cGAMP, then activating STING which is the member responsible for the induction of NF-κB and IRF3 (Chen et al., 2016). A recent study has elucidated the role of dsDNA poxvirus immune

nucleases (poxins) in inhibiting the cGAS-STING system leading to 2',3'-cGAMP degradation, thus eliciting immune evasion strategies (Eaglesham et al., 2019). Additionally, RNase III nuclease has been identified in the ranavirus *Ambyostoma tigrinum* virus, and although noted to be involved in suppressing fish cellular immunity, the impact of this or other viral nucleases on the cGAS-STING system is unknown. As such, it would be interesting to see whether novel nucleases are encoded by the FV3 genome, or other ranaviruses, which may be used to elicit immunoevasion strategies through bypassing the cGAS-STING system.. This may be a potential mechanism being utilized by FV3 to elicit immunoevasion in Xela DS2 and Xela VS2; release of putative nucleases by FV3 may inhibit host cGAS-STING-like system, suppressing the initiation of antiviral and proinflammatory pathways. This would be circumvented by poly(I:C) pre-treatment as Xela DS2 and Xela VS2 become challenged with FV3 when the systems are already well into the induction of antiviral and proinflammatory programs, successfully inhibiting viral replication. However, this is just speculation, confirmation of these events would begin with the identification of cGAS-STING system expression in Xela DS2 and Xela VS2, and identification of putative nucleases in FV3. Overall, the ability for Xela DS2 and Xela VS2 to induce antiviral and proinflammatory programs appear to be turned off from FV3 and UV-FV3 treatment, wherein mechanisms of immunoevasion should be further explored.

4.5.3. Effect of poly(I:C) post-treatment on FV3 infection and replication in Xela DS2 and Xela VS2

Pre-treatment of Xela DS2 and Xela VS2 with poly(I:C) resulted in the reduction of FV3-induced CPE and effectively limited FV3 replication, demonstrating that regardless of how immunoevasive FV3 is known to be, it is unable to break an antiviral program (Chapter 3). My studies demonstrate that FV3 is capable of eliciting immunoevasion and shutdown of

macromolecular synthesis in Xela DS2 and Xela VS2 although the exact mechanism is not well understood. It is currently believed that part of this suppression is due to the overabundance of viral transcripts which outcompete host transcripts in protein production (Jancovich et al., 2015). As such, treatment of Xela DS2 and Xela VS2 with poly(I:C) following FV3 infection should be explored to see whether these cells are then able to overcome FV3's immunoevasive strategies. Theoretically, post-treatment wtih poly(I:C) will upregulate Xela DS2 and Xela VS2 proinflammatory and antiviral gene expression, potentially mitigation the competition between viral and host transcripts dependent on the kinetics of the isolated system. So, while immediate FV3 CPE and replication may occur, it is assumed that post-treatment will allow for recovery of FV3-induced CPE and still limit, but not necessarily eliminate, FV3 replication. This phenomenon should be further investigated to better understand the *in vitro* FV3-frog skin epithelial cell model so that future preventative measures on mitigating FV3 infection *in vivo* can be explored.

4.5.4. Comparison of Xela DS2 and Xela VS2 to primary skin epithelial cells

My findings are insightful for better understanding the role of isolated frog skin epithelial cells in FV3 infection, however while cell lines can be predictive of *in vivo* mechanisms, they are not necessarily indicative. It is common for cell lines to undergo genetic changes over time which go unnoticed, potentiating inconsistency in results dependent on the passage range used (Kaur and Dufour, 2012). Although similarities may be carried over across passages, any differences must be kept into consideration when making conclusions. As such, it would be important to compare the FV3-frog skin epithelial cell interaction in Xela DS2 and Xela VS2 to that of primary frog skin cultures alongside other properties, such as expression of molecular markers and response to dsRNA.

4.5.5. Evaluating the impacts of environmental stress on the ability of Xela DS2 and Xela VS2 to initiate antiviral and proinflammatory programs

Xela DS2 and Xela VS2 can be used as an *in vitro* tool for the screening of environmental factors or agents that can influence frog skin epithelial cell immunity, with focus on susceptibility to FV3. These include anthropogenic stressors such as chemical contaminants from agents like pesticides or fertilizers, and environmental impacts due to climate change such as increased global temperatures and decreased dissolved oxygen levels in aquatic communities. The presence of chemical contaminants may impair immunity and can reduce chemical skin defences (Davidson et al., 2007; Gilbertson et al., 2003). Compared to mammalian skin, frog skin has significantly greater uptake potential of xenobiotics that can bioconcentrate and may be detrimental to frog health (Blaustein et al., 2003; Quaranta et al., 2009; Van Meter et al., 2014). Chemical contaminants can also impact host immune function resulting in altered host resistance to pathogens. Exposure to pesticides, such as atrazine, has been shown to influence antiviral immunity in larval and adult frogs that led to increased susceptibility to FV3 invasion and susceptibility (De Jesús Andino et al., 2017; Pochini and Hoverman, 2017; Sifkarovski et al., 2014), which should be further investigated in Xela DS2 and Xela VS2. Xela DS2 and Xela VS2 are suitable *in vitro* models for performing wide-scale toxicity screening to monitor the effects of chemical contaminants, individually and in tandem, on frog skin epithelial cells.

Effects due to climate change are already predicted to be drastic where over the next century, global average annual temperatures are projected to rise 1.1-6.4°C by 2100 and the magnitude and frequency of extreme weather events is also projected to increase (Field et al., 2012; Lawler et al., 2009; Solomon et al., 2007). As a physiological system, the immune system in frogs may be impacted by changes in temperature outside of the hosts' thermal

optimum, yielding altered immune functions as observed in mammalian and fish models (Abram et al., 2017; Bouma et al., 2010). While it was shown that Xela DS2 and Xela VS2 are capable of supporting growth in across a wide range of temperatures (Chapter 2), the ability for these cells to recognize and respond to an immunostimulant at different temperatures should be explored. Furthermore, pathogens are also temperature dependent, wherein the optimal temperature for FV3 replication is 29°C and incubation at 37°C renders FV3 non-permissive (Tripier et al., 1977). While my data show that Xela DS2 and Xela VS2 are permissive to FV3 infection at 26°C, two possible outcomes are possible when considering temperature changes: (a) at lower temperatures, Xela DS2 and Xela VS2 may be immunosuppressed thus increasing FV3 susceptibility at MOIs $\leq$ 0.002, or (b) at higher temperatures, such as the FV3 replication optimum of 29°C, may too demonstrate heightened susceptibility of frog skin epithelial cells to infection. FV3 susceptibility of Xela DS2 and Xela VS2 in changing temperatures should be investigated, as long-term changes in climate patterns may contribute to a compromised immune response in the frog host, leading to greater FV3 susceptibility and host mortality.

References

Abram, Q.H., Dixon, B., Katzenback, B.A., 2017. Impacts of Low Temperature on the Teleost Immune System. *Biology* 6, 39.

Alexopoulou, L., Holt, A.C., Medzhitov, R., Flavell, R.A., 2001. Recognition of double-stranded RNA and activation of NF-κB by Toll-like receptor 3. *Nature* 413, 732-738.

Alsharifi, M., Mullbacher, A., Regner, M., 2008. Interferon type I responses in primary and secondary infections. *Immunol Cell Biol* 86, 239-245.

Altschul, S.F., Gish, W., Miller, W., Myers, E.W., Lipman, D.J., 1990. Basic local alignment search tool. *J Mol Biol* 215, 403-410.

AmphibiaWeb, accessed 2019.Available online at: www.amphibiaweb.org

Andino Fde, J., Grayfer, L., Chen, G., Chinchar, V.G., Edholm, E.S., Robert, J., 2015. Characterization of Frog Virus 3 knockout mutants lacking putative virulence genes. *Virology* 485, 162-170.

Anizet, M., Huwe, B., Pays, A., Picard, J., 1981. Characterization of a new cell line, XL2, obtained from *Xenopus laevis* and determination of optimal culture conditions. *In Vitro Cell Dev-Pl* 17, 267-274.

Ariel, E., Nicolajsen, N., Christophersen, M.-B., Holopainen, R., Tapiovaara, H., Bang Jensen, B., 2009. Propagation and isolation of ranaviruses in cell culture. *Aquaculture* 294, 159-164.

Artis, D., 2008. Epithelial-cell recognition of commensal bacteria and maintenance of immune homeostasis in the gut. *Nat Rev Immunol* 8, 411-420.

Baggiolini, M., Walz, A., Kunkel, S.L., 1989. Neutrophil-activating peptide-1/interleukin 8, a novel cytokine that activates neutrophils. *J Clin Invest* 84, 1045-1049.

Bartenschlager, R., Cosset, F.-L., Lohmann, V., 2010. Hepatitis C virus replication cycle. *J Hepatol* 53, 583-585.

Beard, K.H., Vogt, K.A., Kulmatiski, A., 2002. Top-down effects of a terrestrial frog on forest nutrient dynamics. *Oecologia* 133, 583-593.

Bergsbaken, T., Fink, S.L., Cookson, B.T., 2009. Pyroptosis: host cell death and inflammation. *Nat Rev Microbiol* 7, 99.

Bird, S., Zou, J., Wang, T., Munday, B., Cunningham, C., Secombes, C.J., 2002. Evolution of interleukin-1β. *Cytokine Growth F Rev* 13, 483-502.

Birkedal-Hansen, H., Munksgaard, E.C., Hansen, I.L., Nellemann, K., Gay, R., 1982. Multiple Collagen Gene Expression with Type III Predominance in Rat Mucosal Keratinocytes. *Collagen Rel Res* 2, 287-300.

Blaustein, A., Walls, S., Bancroft, B., Lawler, J., Searle, C., Gervasi, S., 2010a. Direct and Indirect Effects of Climate Change on Amphibian Populations. *Diversity* 2, 281-313.

Blaustein, A.R., Romansic, J.M., Kiesecker, J.M., Hatch, A.C., 2003. Ultraviolet radiation, toxic chemicals and amphibian population declines. *Div Dist* 9, 123-140.

Blaustein, A.R., Walls, S.C., Bancroft, B.A., Lawler, J.J., Searle, C.L., Gervasi, S.S., 2010b. Direct and indirect effects of climate change on amphibian populations. *Diversity* 2, 281-313.

Bols, N.C., Pham, P.H., Dayeh, V.R., Lee, L.E.J. 2017. Invitromatics, invitrome, and invitroomics: introduction of three new terms for in vitro biology and illustration of their use with the cell lines from rainbow trout. *In Vitro Cell Dev Biol Anim* 53, 383-405.

Bonjardim, C.A., Ferreira, P.C., Kroon, E.G., 2009. Interferons: signaling, antiviral and viral evasion. *Immunol Let* 122, 1-11.

Bouma, H.R., Carey, H.V., Kroese, F.G., 2010. Hibernation: the immune system at rest? *J Leukoc Biol* 88, 619-624.

Braff, M.H., Zaiou, M., Fierer, J., Nizet, V., Gallo, R.L., 2005. Keratinocyte Production of Cathelicidin Provides Direct Activity against Bacterial Skin Pathogens. *Infect Immun* 73, 6771.

Braunwald, J., Nonnenmacher, H., Tripier-Darcy, F., 1985. Ultrastructural and biochemical study of frog virus 3 uptake by BHK-21 cells. *J Gen Virol* 66, 283-293.

Brewer, D.B., 1967. The fibroblast. *Proc R Soc Med* 60, 778-781.

Brunner, J.L., Schock, D.M., Collins, J.P., 2007. Transmission dynamics of the amphibian ranavirus *Ambystoma tigrinum* virus. *Dis Aquat Organ* 77, 87-95.

Buller, R.M., Palumbo, G.J., 1991. Poxvirus pathogenesis. *Microbiol Rev* 55, 80.

Cano, A., Perez-Moreno, M.A., Rodrigo, I., Locascio, A., Blanco, M.J., del Barrio, M.G., Portillo, F., Nieto, M.A., 2000. The transcription factor snail controls epithelial-mesenchymal transitions by repressing E-cadherin expression. *Nat Cell Biol* 2, 76-83.

Chang, D.J., Hwang, Y.S., Cha, S.W., Chae, J.P., Hwang, S.H., Hahn, J.H., Bae, Y.C., Lee, H.S., Park, M.J., 2010. Xclaudin 1 is required for the proper gastrulation in Xenopus laevis. *Biochem Bioph Res Co* 397, 75-81.

Chaw, S.Y., Abdul Majeed, A., Dalley, A.J., Chan, A., Stein, S., Farah, C.S., 2012. Epithelial to mesenchymal transition (EMT) biomarkers – E-cadherin, beta-catenin, APC and Vimentin – in oral squamous cell carcinogenesis and transformation. *Oral Oncol* 48, 997-1006.

Che, J., Chen, H.M., Yang, J.X., Jin, J.Q., Jiang, K., Yuan, Z.Y., Murphy, R.W., Zhang, Y.P., 2012. Universal COI primers for DNA barcoding amphibians. *Mol Ecol Res* 12, 247-258.

Chen, G., Ward, B.M., Yu, K.H., Chinchar, V.G., Robert, J., 2011. Improved knockout methodology reveals that frog virus 3 mutants lacking either the 18K immediate-early gene or the truncated vIF-2alpha gene are defective for replication and growth in vivo. *J Virol* 85, 11131-11138.

Chen, Q., Sun, L., Chen, Z.J., 2016. Regulation and function of the cGAS–STING pathway of cytosolic DNA sensing. *Nat Immunol* 17, 1142.

Chinchar, V.G., 2002. Ranaviruses (family *Iridoviridae*): emerging cold-blooded killers. *Arch Virol* 147, 447-470.

Chinchar, V.G., Bryan, L., Wang, J., Long, S., Chinchar, G.D., 2003. Induction of apoptosis in frog virus 3-infected cells. *Virology* 306, 303-312.

Chinchar, V.G., Yu, K.H., Jancovich, J.K., 2011. The molecular biology of frog virus 3 and other iridoviruses infecting cold-blooded vertebrates. *Viruses* 3, 1959-1985.

Chu, P.G., Weiss, L.M., 2002. Keratin expression in human tissues and neoplasms. *Histopathology* 40, 403-439.

Cone, R.A., 2009. Barrier properties of mucus. *Adv Drug Deliver Rev* 61, 75-85.

Covello, J.M., Bird, S., Morrison, R.N., Battaglene, S.C., Secombes, C.J., Nowak, B.F., 2009. Cloning and expression analysis of three striped trumpeter (*Latris lineata*) pro-inflammatory cytokines, TNF-alpha, IL-1beta and IL-8, in response to infection by the ectoparasitic, Chondracanthus goldsmidi. *Fish Shellfish Immunol* 26, 773-786.

Coyne, C.B., Gambling, T.M., Boucher, R.C., Carson, J.L., Johnson, L.G., 2003. Role of claudin interactions in airway tight junctional permeability. *Am J Physiol Lung Cell Mol Physiol* 285, L1166-1178.

Creely, J.J., Commers, P.A., Haralson, M.A., 1988. Synthesis of Type III Collagen by Cultured Kidney Epithelial Cells. *Connect Tissue Res* 18, 107-122.

Dai, X., Sayama, K., Tohyama, M., Shirakata, Y., Yang, L., Hirakawa, S., Tokumaru, S., Hashimoto, K., 2008. The NF-κB, p38 MAPK and STAT1 pathways differentially regulate the dsRNA-mediated innate immune responses of epidermal keratinocytes. *Int Immunol* 20, 901-909.

Daszak, P., Cunningham, A.A., Hyatt, A.D., 2003. Infectious disease and amphibian population declines. *Divers Distrib* 9, 141-150.

Davidson, C., Benard, M.F., Shaffer, H.B., Parker, J.M., O'Leary, C., Conlon, J.M., Rollins-Smith, L.A., 2007. Effects of chytrid and carbaryl exposure on survival, growth and skin peptide defenses in foothill yellow-legged frogs. *Envir Sci Technol* 41, 1771-1776.

De Bosscher, K., Vanden Berghe, W., Haegeman, G., 2003. The Interplay between the Glucocorticoid Receptor and Nuclear Factor-κB or Activator Protein-1: Molecular Mechanisms for Gene Repression. *Endo Rev* 24, 488-522.

De Jesús Andino, F., Lawrence, B.P., Robert, J., 2017. Long term effects of carbaryl exposure on antiviral immune responses in *Xenopus laevis*. *Chemosphere* 170, 169-175.

Der, S.D., Zhou, A., Williams, B.R.G., Silverman, R.H., 1998. Identification of genes differentially regulated by interferon α, β, or γ using oligonucleotide arrays. *P Natl A Sci* 95, 15623.

DeWitte-Orr, S.J., Collins, S.E., Bauer, C.M., Bowdish, D.M., Mossman, K.L., 2010. An accessory to the 'Trinity': SR-As are essential pathogen sensors of extracellular dsRNA, mediating entry and leading to subsequent type I IFN responses. *PLoS Pathogens* 6, e1000829.

Dieudonne, A., Torres, D., Blanchard, S., Taront, S., Jeannin, P., Delneste, Y., Pichavant, M., Trottein, F., Gosset, P., 2012. Scavenger receptors in human airway epithelial cells: role in response to double-stranded RNA. *PloS One* 7, e41952.

Dimri, G.P., Lee, X., Basile, G., Acosta, M., Scott, G., Roskelley, C., Medrano, E.E., Linskens, M., Rubelj, I., Pereira-Smith, O., et al., 1995. A biomarker that identifies senescent human cells in culture and in aging skin in vivo. *P Natl A Sci USA* 92, 9363-9367.

Dinarello, C.A., 1996. Biologic basis for interleukin-1 in disease. *Blood* 87, 2095-2147.

Dinarello, C.A., 2000. Proinflammatory cytokines. *Chest* 118, 503-508.

Diner, E.J., Burdette, D.L., Wilson, S.C., Monroe, K.M., Kellenberger, C.A., Hyodo, M., Hayakawa, Y., Hammond, M.C., Vance, R.E., 2013. The innate immune DNA sensor cGAS produces a noncanonical cyclic dinucleotide that activates human STING. *Cell Rep* 3, 1355-1361.

Doherty, L., Poynter, S.J., Aloufi, A., DeWitte-Orr, S.J., 2016. Fish viruses make dsRNA in fish cells: characterization of dsRNA production in rainbow trout (*Oncorhynchus mykiss*) cells infected with viral haemorrhagic septicaemia virus, chum salmon reovirus and frog virus 3. *J Fish Dis* 39, 1133-1137.

Dolcet, X., Llobet, D., Pallares, J., Matias-Guiu, X., 2005. NF-kB in development and progression of human cancer. *Virchows Arch* 446, 475-482.

Duffus, A.L.J., Pauli, B.D., Wozney, K., Brunetti, C.R., Berrill, M., 2008. Frog virus 3-like infections in aquatic amphibian communities. *J Wild Dis* 44, 109-120.

Duffus, A.L.J., Waltzek, T.B., Stöhr, A.C., Allender, M.C., Gotesman, M., Whittington, R.J., Hick, P., Hines, M.K., Marschang, R.E., 2015. Distribution and Host Range of Ranaviruses, in: Gray, M.J., Chinchar, V.G. (Eds.), Ranaviruses: Lethal Pathogens of Ectothermic Vertebrates. *Springer International Publishing*, pp. 9-57.

DuRant, S.E., Hopkins, W.A., 2008. Amphibian predation on larval mosquitoes. *Can J Zool* 86, 1159-1164.

Eaglesham, J.B., Pan, Y., Kupper, T.S., Kranzusch, P.J., 2019. Viral and metazoan poxins are cGAMP-specific nucleases that restrict cGAS–STING signalling. *Nature* 566, 259-263.

Farquhar, M.G., Palade, G.E., 1963. Junctional complexes in various epithelia. *J Cell Biol* 17, 375-412.

Farquhar, M.G., Palade, G.E., 1965. Cell junctions in amphibian skin. *J Cell Biol* 26, 263-291.

Field, C.B., Barros, V., Stocker, T.F., Dahe, Q., 2012. Managing the Risks of Extreme Events and Disasters to Advance Climate Change Adaptation: Special Report of the Intergovernmental Panel on Climate Change. *Cambridge University Press*.

Figiel, S., Vasseur, C., Bruyere, F., Rozet, F., Maheo, K., Fromont, G., 2017. Clinical significance of epithelial-mesenchymal transition markers in prostate cancer. *Hum Pathol* 61, 26-32.

Fink, K., Grandvaux, N., 2013. STAT2 and IRF9. *JAK-STAT* 2, e27521.

Forzán, M.J., Jones, K.M., Ariel, E., Whittington, R.J., Wood, J., Markham, R.J.F., Daoust, P.-Y., 2017. Pathogenesis of Frog Virus 3 (Ranavirus, *Iridoviridae*) Infection in Wood Frogs (*Rana sylvatica*). *Vet Pathol* 54, 531-548.

Franke, W.W., Schmid, E., Osborn, M., Weber, K., 1978. Different intermediate-sized filaments distinguished by immunofluorescence microscopy. *Proc Natl Acad Sci USA* 75, 5034-5038.

Furuse, M., Fujita, K., Hiiragi, T., Fujimoto, K., Tsukita, S., 1998. Claudin-1 and -2: novel integral membrane proteins localizing at tight junctions with no sequence similarity to occludin. *J Cell Biol* 141, 1539-1550.

Furuse, M., Hata, M., Furuse, K., Yoshida, Y., Haratake, A., Sugitani, Y., Noda, T., Kubo, A., Tsukita, S., 2002. Claudin-based tight junctions are crucial for the mammalian epidermal barrier: a lesson from claudin-1-deficient mice. *J Cell Biol* 156, 1099-1111.

Furuse, M., Hirase, T., Itoh, M., Nagafuchi, A., Yonemura, S., Tsukita, S., Tsukita, S., 1993. Occludin: a novel integral membrane protein localizing at tight junctions. *J Cell Biol* 123, 1777-1788.

Gantress, J., Maniero, G.D., Cohen, N., Robert, J., 2003. Development and characterization of a model system to study amphibian immune responses to iridoviruses. *Virology* 311, 254-262.

Ghosh, S., May, M.J., Kopp, E.B., 1998. NF-κB and related proteins: Evolutionarily Conserved Mediators of Immune Responses. *Ann Rev Immunol* 16, 225-260.

Gilbertson, M.K., Haffner, G.D., Drouillard, K.G., Albert, A., Dixon, B., 2003. Immunosuppression in the northern leopard frog (*Rana pipiens*) induced by pesticide exposure. *Environ Tox Chem* 22, 101-110.

Gomez, D., Sunyer, J.O., Salinas, I., 2013. The mucosal immune system of fish: The evolution of tolerating commensals while fighting pathogens. *Fish Shellfish Immunol* 35, 1729-1739.

Goorha, R., Granoff, A., 1974. Macromolecular synthesis in cells infected by frog virus 3: I. Virus-specific protein synthesis and its regulation. *Virology* 60, 237-250.

Gray, M.J., Miller, D.L., Hoverman, J.T., 2009. Ecology and pathology of amphibian ranaviruses. *Dis Aquta Organ* 87, 243-266.

Gray, M.J., Miller, D.L., Schmutzer, A.C., Baldwin, C.A., 2007. Frog virus 3 prevalence in tadpole populations inhabiting cattle-access and non-access wetlands in Tennessee, USA. *Dis Aquat Organ* 77, 97-103.

Greer, A.L., Berrill, M., Wilson, P.J., 2005. Five amphibian mortality events associated with ranavirus infection in south central Ontario, Canada. *Dis Aquat Organ* 67, 9-14.

Groulx, J.F., Gagne, D., Benoit, Y.D., Martel, D., Basora, N., Beaulieu, J.F., 2011. Collagen VI is a basement membrane component that regulates epithelial cell-fibronectin interactions. Matrix biology : *J Int Soc Matrix Bio* 30, 195-206.

Haller, O., Kochs, G., 2011. Human MxA protein: an interferon-induced dynamin-like GTPase with broad antiviral activity. *J Interferon Cytokine Res* 31, 79-87.

Haller, O., Staeheli, P., Schwemmle, M., Kochs, G., 2015. Mx GTPases: dynamin-like antiviral machines of innate immunity. *Trends Microbiol* 23, 154-163.

Hamel, R., Dejarnac, O., Wichit, S., Ekchariyawat, P., Neyret, A., Luplertlop, N., Perera-Lecoin, M., Surasombatpattana, P., Talignani, L., Thomas, F., Cao-Lormeau, V.-M., Choumet, V., Briant, L., Desprès, P., Amara, A., Yssel, H., Missé, D., 2015. Biology of Zika Virus Infection in Human Skin Cells. *J Virol* 89, 8880.

Haslam, I.S., Roubos, E.W., Mangoni, M.L., Yoshizato, K., Vaudry, H., Kloepper, J.E., Pattwell, D.M., Maderson, P.F., Paus, R., 2014. From frog integument to human skin: dermatological perspectives from frog skin biology. *Biol Rev Camb Philos Soc* 89, 618-655.

Hausmann, J.C., Wack, A.N., Allender, M.C., Cranfield, M.R., Murphy, K.J., Barrett, K., Romero, J.L., Wellehan, J.F.X., Blum, S.A., Zink, M.C., Bronson, E., 2015. Experimental challenge study of FV3-like ranavirus infection in previously FV3-like ranavirus infected eastern box turtles (*Terrapene carolina* carolina) to assess infection and survival. *J Zoo Wild Med* 46, 732-746.

Hayashi, M., Ninomiya, Y., Hayashi, K., Linsenmayer, T.F., Olsen, B.R., Trelstad, R.L., 1988. Secretion of collagen types I and II by epithelial and endothelial cells in the developing chick cornea demonstrated by in situ hybridization and immunohistochemistry. *Development* 103, 27.

Hayes, C.N., Chayama, K., 2017. Interferon stimulated genes and innate immune activation following infection with hepatitis B and C viruses. *J Med Virol* 89, 388-396.

Hayes, T.B., Collins, A., Lee, M., Mendoza, M., Noriega, N., Stuart, A.A., Vonk, A., 2002. Hermaphroditic, demasculinized frogs after exposure to the herbicide atrazine at low ecologically relevant doses. *Proc Nat Acad Sci USA* 99, 5476-5480.

Hewitt, K.J., Agarwal, R., Morin, P.J., 2006. The claudin gene family: expression in normal and neoplastic tissues. *BMC Cancer* 6, 186.

Hinther, A., Bromba, C.M., Wulff, J.E., Helbing, C.C., 2011. Effects of triclocarban, triclosan, and methyl triclosan on thyroid hormone action and stress in frog and mammalian culture systems. *Environ Sci Technol* 45, 5395-5402.

Holopainen, R., Tapiovaara, H., Honkanen, J., 2012. Expression analysis of immune response genes in fish epithelial cells following ranavirus infection. *Fish Shellfish Immunol* 32, 1095-1105.

Hosper, N.A., van den Berg, P.P., de Rond, S., Popa, E.R., Wilmer, M.J., Masereeuw, R., Bank, R.A., 2013. Epithelial-to-mesenchymal transition in fibrosis: collagen type I expression is highly upregulated after EMT, but does not contribute to collagen deposition. *Exp Cell Res* 319, 3000-3009.

Ishii, A., Kawasaki, M., Matsumoto, M., Tochinai, S., Seya, T., 2007. Phylogenetic and expression analysis of amphibian *Xenopus* Toll-like receptors. *Immunogenetics* 59, 281-293.

Itahana, K., Campisi, J., Dimri, G.P., 2007. Methods to detect biomarkers of cellular senescence: The senescence-associated β-galactosidase assay, *Methods Mol Biol*, pp. 21-31.

Jacques, R., Edholm, E.-S., Jazz, S., Odalys, T.-L., Francisco, D.J.A., 2017. *Xenopus*-FV3 host-pathogen interactions and immune evasion. *Virology* 511, 309-319.

Jancovich, J.K., Qin, Q., Zhang, Q.-Y., Chinchar, V.G., 2015. Ranavirus Replication: Molecular, Cellular, and Immunological Events, in: Gray, M.J., Chinchar, V.G. (Eds.), Ranaviruses: Lethal Pathogens of Ectothermic Vertebrates. *Springer International Publishing* pp. 105-139.

Jelaso, A.M., Acevedo, S., Dang, T., Lepere, A., Ide, C.F., 1998. Interleukin-1beta and its type 1 receptor are expressed in developing neural circuits in the frog, *Xenopus laevis. J Comp Neurol* 394, 242-251.

Kalluri, R., Weinberg, R.A., 2009. The basics of epithelial-mesenchymal transition. *J Clinic Invest* 119, 1420-1428.

Kärber, G., 1931. Beitrag zur kollektiven Behandlung pharmakologischer Reihenversuche. Naunyn-Schmiedebergs Archiv für experimentelle Pathologie und Pharmakologie 162, 480-483.

Kaur, G., Dufour, J.M., 2012. Cell lines: Valuable tools or useless artifacts. *Spermatogenesis* 2, 1-5.

Kawasaki, T., Kawai, T., 2014. Toll-Like Receptor Signaling Pathways. *Front Immunol* 5.

Kay, B.K., Peng, H.B., 1992. *Xenopus laevis*: Practical Uses in Cell and Molecular Biology. *Elsevier Science*.

Kerby, J.L., Richards-Hrdlicka, K.L., Storfer, A., Skelly, D.K., 2010. An examination of amphibian sensitivity to environmental contaminants: are amphibians poor canaries? *Ecol Lett* 13, 60-67.

Kim, J.M., Eckmann, L., Savidge, T.C., Lowe, D.C., Witthoft, T., Kagnoff, M.F., 1998. Apoptosis of human intestinal epithelial cells after bacterial invasion. *J Clinic Invest* 102, 1815-1823.

Kinoshita, H., Takai, T., Le, T.A., Kamijo, S., Wang, X.L., Ushio, H., Hara, M., Kawasaki, J., Vu, A.T., Ogawa, T., Gunawan, H., Ikeda, S., Okumura, K., Ogawa, H., 2009. Cytokine milieu modulates release of thymic stromal lymphopoietin from human keratinocytes stimulated with double-stranded RNA. *J Allergy Clin Immunol* 123, 179-186.

Knudson, D.L., Tinsley, T.W., 1974. Replication of a nuclear polyhedrosis virus in a continuous cell culture of Spodoptera frugiperda: purification, assay of infectivity, and growth characteristics of the virus. *J Virol* 14, 934-944.

Köllisch, G., Kalali, B.N., Voelcker, V., Wallich, R., Behrendt, H., Ring, J., Bauer, S., Jakob, T., Mempel, M., Ollert, M., 2005. Various members of the Toll-like receptor family contribute to the innate immune response of human epidermal keratinocytes. *Immunology* 114, 531-541.

Kopfnagel, V., Wittmann, M., Werfel, T., 2011. Human keratinocytes express AIM2 and respond to dsDNA with IL-1β secretion. *Exp Dermatol* 20, 1027-1029.

Koubourli, D.V., Wendel, E.S., Yaparla, A., Ghaul, J.R., Grayfer, L., 2017. Immune roles of amphibian (*Xenopus laevis*) tadpole granulocytes during Frog Virus 3 ranavirus infections. *Dev Comp Immunol* 72, 112-118.

Krause, C.D., Pestka, S., 2005. Evolution of the Class 2 cytokines and receptors, and discovery of new friends and relatives. *Pharmacol Therapeut* 106, 299-346.

Kumar, A., Zhang, J., Yu, F.-S.X., 2006. Toll-like receptor 3 agonist poly(I:C)-induced antiviral response in human corneal epithelial cells. *Immunology* 117, 11-21.

Larsen, E.H., Ramløv, H., 2013. Role of cutaneous surface fluid in frog osmoregulation. *Comp Biochem and Physiol* 165, 365-370.

Lawler, J.J., Shafer, S.L., White, D., Kareiva, P., Maurer, E.P., Blaustein, A.R., Bartlein, P.J., 2009. Projected climate-induced faunal change in the Western Hemisphere. *Ecology* 90, 588-597.

Lawrence, T., 2009. The nuclear factor NF-kappaB pathway in inflammation. *Cold Spring Harb Perspect Biol* 1, a001651.

Lesbarreres, D., Balseiro, A., Brunner, J., Chinchar, V.G., Duffus, A., Kerby, J., Miller, D.L., Robert, J., Schock, D.M., Waltzek, T., Gray, M.J., 2012. Ranavirus: past, present and future. *Biol Lett* 8, 481-483.

Levi, G., Gumbiner, B., Thiery, J.P., 1991. The distribution of E-cadherin during *Xenopus laevis* development. *Development* 111, 159-169.

Li, H., Liu, B.L., Gao, L.Z., Chen, H.L., 2004. Studies on bullfrog skin collagen. *Food Chem* 84, 65-69.

Lian, L.H., Milora, K.A., Manupipatpong, K.K., Jensen, L.E., 2012. The double-stranded RNA analogue polyinosinic-polycytidylic acid induces keratinocyte pyroptosis and release of IL-36γ. *J Inest Dermatol*132, 1346-1353.

Lillywhite, H.B., 2006. Water relations of tetrapod integument. *J Exp Biol* 209, 202.

Lillywhite, H.B., Licht, P., 1975. A comparative study of integumentary mucous secretions in amphibians. *Comp Biochem Physiol* 51, 937-941.

Limmon, G.V., Arredouani, M., McCann, K.L., Minor, R.A.C., Kobzik, L., Imani, F., 2008. Scavenger receptor class-A is a novel cell surface receptor for double-stranded RNA. T*he FASEB Journal* 22, 159-167.

Lisser, G.J., Vo, N.T.K., DeWitte-Orr, S.J., 2017. Delineating the roles of cellular and innate antiviral immune parameters mediating ranavirus susceptibility using rainbow trout cell lines. *Virus Res* 238, 114-123.

Liu, Y., Yu, S., Chai, Y., Zhang, Q., Yang, H., Zhu, Q., 2012. Lipopolysaccharide-induced gene expression of interleukin-1 receptor-associated kinase 4 and interleukin-1beta in roughskin sculpin (*Trachidermus fasciatus*). *Fish Shellfish Immunol* 33, 690-698.

Locksley, R.M., Killeen, N., Lenardo, M.J., 2001. The TNF and TNF receptor superfamilies: integrating mammalian biology. *Cell* 104, 487-501.

Longhi, M.P., Trumpfheller, C., Idoyaga, J., Caskey, M., Matos, I., Kluger, C., Salazar, A.M., Colonna, M., Steinman, R.M., 2009. Dendritic cells require a systemic type I interferon

response to mature and induce CD4+ Th1 immunity with poly IC as adjuvant. *J Exp Med* 206, 1589-1602.

Longo, A.V., Zamudio, K.R., 2017. Temperature variation, bacterial diversity and fungal infection dynamics in the amphibian skin. *Mol Ecol* 26, 4787-4797.

Madeira, F., Park, Y.M., Lee, J., Buso, N., Gur, T., Madhusoodanan, N., Basutkar, P., Tivey, A.R.N., Potter, S.C., Finn, R.D., Lopez, R., 2019. The EMBL-EBI search and sequence analysis tools APIs in 2019. *Nucleic Acids Res* 47, W636-W641.

Martin, O.C., Gunawardane, R.N., Iwamatsu, A., Zheng, Y., 1998. Xgrip109: a gamma tubulin-associated protein with an essential role in gamma tubulin ring complex (gammaTuRC) assembly and centrosome function. *J Cell Biol* 141, 675-687.

Martins, K.A., Bavari, S., Salazar, A.M., 2015. Vaccine adjuvant uses of poly-IC and derivatives. *Expert Rev Vaccines* 14, 447-459.

Matsumoto, M., Seya, T., 2008. TLR3: Interferon induction by double-stranded RNA including poly(I:C). *Adv Drug Deliv Rev* 60, 805-812.

Matsuyoshi, N., Imamura, S., 1997. Multiple Cadherins Are Expressed in Human Fibroblasts. *Biochem Biophy Res Commun* 235, 355-358.

Menco, B.P., 1980. Qualitative and quantitative freeze-fracture studies on olfactory and nasal respiratory structures of frog, ox, rat, and dog. I. A general survey. *Cell Tissue Res* 207, 183-209.

Mendez, M.G., Kojima, S., Goldman, R.D., 2010. Vimentin induces changes in cell shape, motility, and adhesion during the epithelial to mesenchymal transition. *FASEB J: Fed Am Soc Exper Biol* 4, 1838-1851.

Michel, M., Torok, N., Godbout, M.J., Lussier, M., Gaudreau, P., Royal, A., Germain, L., 1996. Keratin 19 as a biochemical marker of skin stem cells in vivo and in vitro: keratin 19 expressing cells are differentially localized in function of anatomic sites, and their number varies with donor age and culture stage. *J Cell Sci* 109 , 1017-1028.

Miller, D.L., Rajeev, S., Gray, M.J., Baldwin, C.A., 2007. Frog Virus 3 Infection, Cultured American Bullfrogs. *Emerg Infect Dis* 13, 342-343.

Miskulin, M., Dalgleish, R., Kluve-Beckerman, B., Rennard, S.I., Tolstoshev, P., Brantly, M., Crystal, R.G., 1986. Human type III collagen gene expression is coordinately modulated with the type I collagen genes during fibroblast growth. *Biochemistry* 25, 1408-1413.

Miyata, K., Ose, K., 2012. Thyroid Hormone-disrupting Effects and the Amphibian Metamorphosis Assay. *J Toxicol Pathol* 25, 1-9.

Moll, R., Franke, W.W., Schiller, D.L., Geiger, B., Krepler, R., 1982. The catalog of human cytokeratins: Patterns of expression in normal epithelia, tumors and cultured cells. *Cell* 31, 11-24.

Morales, H.D., Abramowitz, L., Gertz, J., Sowa, J., Vogel, A., Robert, J., 2010. Innate immune responses and permissiveness to ranavirus infection of peritoneal leukocytes in the frog *Xenopus laevis*. *J Virol* 84, 4912-4922.

Morales, H.D., Robert, J., 2007. Characterization of primary and memory CD8 T-cell responses against ranavirus (FV3) in *Xenopus laevis*. *J Virol* 81, 2240-2248.

Morrison, E.A., Garner, S., Echaubard, P., Lesbarrères, D., Kyle, C.J., Brunetti, C.R., 2014. Complete genome analysis of a frog virus 3 (FV3) isolate and sequence comparison with isolates of differing levels of virulence. *Virol J* 11, 46.

Munoz, W.A., Kloc, M., Cho, K., Lee, M., Hofmann, I., Sater, A., Vleminckx, K., McCrea, P.D., 2012. Plakophilin-3 is required for late embryonic amphibian development, exhibiting roles in ectodermal and neural tissues. *PloS One* 7, e34342.

Murshid, A., Gong, J., Ahmad, R., Borges, T.J., Calderwood, S.K., 2015. Scavenger receptor SREC-I promotes double stranded RNA-mediated TLR3 activation in human monocytes. *Immunobiology* 220, 823-832.

Nestle, F.O., Di Meglio, P., Qin, J.-Z., Nickoloff, B.J., 2009. Skin immune sentinels in health and disease. *Nat Rev Immunol* 9, 679.

Niessen, C.M., 2007. Tight Junctions/Adherens Junctions: Basic Structure and Function. *J Invest Dermatol* 127, 2525-2532.

Ohji, M., SundarRaj, N., Hassell, J.R., Thoft, R.A., 1994. Basement membrane synthesis by human corneal epithelial cells in vitro. *Invest Ophthalmol Vis Sci* 35, 479-485.

Paludan, Søren R., Bowie, Andrew G., 2013. Immune Sensing of DNA. *Immunity* 38, 870-880.

Pasparakis, M., Haase, I., Nestle, F.O., 2014. Mechanisms regulating skin immunity and inflammation. *Nat Rev Immunol* 14, 289.

Pessier, A.P., 2002. An overview of amphibian skin disease. *Semin Avian Exotic Pet Med* 11, 162-174.

Petricevich, V.L., Palomares, L.A., Gonzalez, M., Ramirez, O.T., 2001. Parameters that determine virus adsorption kinetics: toward the design of better infection strategies for the insect cell - baculovirus expression system. *Enzyme Microb Technol* 29, 52-61.

Pham, P., Huang, Y., Mosser, D., Bols, N., 2015. Use of cell lines and primary cultures to explore the capacity of rainbow trout to be a host for frog virus 3 (FV3). *In Vitro Cell Dev Biol An* 51, 894-904.

Pham, P.H., Jung, J., Bols, N.C., 2011. Using 96-well tissue culture polystyrene plates and a fluorescence plate reader as tools to study the survival and inactivation of viruses on surfaces. *Cytotechnology* 63, 385-397.

Pilla-Moffett, D., Barber, M.F., Taylor, G.A., Coers, J., 2016. Interferon-Inducible GTPases in Host Resistance, Inflammation and Disease. *J Mol Biol* 428, 3495-3513.

Plotkowski, M., Bajolet-Laudinat, O., Puchelle, E., 1993. Cellular and molecular mechanisms of bacterial adhesion to respiratory mucosa. *Eur Respir J* 6, 903-916.

Pochini, K.M., Hoverman, J.T., 2017. Reciprocal effects of pesticides and pathogens on amphibian hosts: The importance of exposure order and timing. *Environ Pollut* 221, 359-366.

Poynter, S., Lisser, G., Monjo, A., DeWitte-Orr, S., 2015. Sensors of Infection: Viral Nucleic Acid PRRs in Fish. *Biology* 4, 460-493.

Poynter, S.J., DeWitte-Orr, S.J., 2018. Understanding Viral dsRNA-Mediated Innate Immune Responses at the Cellular Level Using a Rainbow Trout Model. *Front Immunol* 9.

Poynter, S.J., Leis, E.M., DeWitte-Orr, S.J., 2019. In vitro transcribed dsRNA limits viral hemorrhagic septicemia virus (VHSV)-IVb infection in a novel fathead minnow (*Pimephales promelas*) skin cell line. *Fish Shellfish Immunol* 86, 403-409.

Proksch, E., Brandner, J.M., Jensen, J.-M., 2008. The skin: an indispensable barrier. *Exp Dermatol* 17, 1063-1072.

Pudney, M., Varma, M., Leake, C., 1973. Establishment of a cell line (XTC-2) from the South African clawed toad, *Xenopus laevis*. *Experientia 29*, 466-467.

Purna Sai, K., Babu, M., 2001. Studies on Rana tigerina skin collagen. Comparative Biochemistry and Physiology Part B: *Biochem Mol Bio* 128, 81-90.

Quaranta, A., Bellantuono, V., Cassano, G., Lippe, C., 2009. Why amphibians are more sensitive than mammals to xenobiotics. *PloS One* 4, e7699.

Rafferty, K.A., 1969. Mass Culture of Amphibian Cells: Methods and Observations Concerning Stability of Cell Type, in: Mizell, M. (Ed.), Biology of Amphibian Tumors. Springer Berlin Heidelberg, Berlin, Heidelberg, pp. 52-81.

Rafferty, K.A., Jr., 1965. The cultivation of inclusion-associated viruses from Lucke tumor frogs. *Ann NY Acad Sci* 126, 3-21.

Raghow, R., Thompson, J.P., 1989. Molecular mechanisms of collagen gene expression. *Mol Cell Biochem* 86, 5-18.

Rampersad, S.N., 2012. Multiple applications of Alamar Blue as an indicator of metabolic function and cellular health in cell viability bioassays. *Sensors* (Basel) 12, 12347-12360.

Ramsey, J.P., Reinert, L.K., Harper, L.K., Woodhams, D.C., Rollins-Smith, L.A., 2010. Immune defenses against *Batrachochytrium dendrobatidis*, a fungus linked to global amphibian declines, in the South African clawed frog, *Xenopus laevis*. *Infect Immun* 78, 3981-3992.

Rausch, D., Simpson, S., 1988. In vivo test system for tumor production by cell lines derived from lower vertebrates. *In Vitro Cell Develop Bio* 24, 217-222.

Ricard-Blum, S., 2011. The collagen family. *Cold Spring Harb Perspect Biol* 3, a004978.

Ringø, E., Løvmo, L., Kristiansen, M., Bakken, Y., Salinas, I., Myklebust, R., Olsen, R.E., Mayhew, T.M., 2010. Lactic acid bacteria vs. pathogens in the gastrointestinal tract of fish: A review. *Aquacult Res* 41, 451-467.

Ritter, M., Mennerich, D., Weith, A., Seither, P., 2005. Characterization of Toll-like receptors in primary lung epithelial cells: strong impact of the TLR3 ligand poly(I:C) on the regulation of Toll-like receptors, adaptor proteins and inflammatory response. *J Inflamm* (Lond) 2, 16.

Robert, J., accessed 2015. Primers available for *Xenopus laevis* research. Available online at: https://www.urmc.rochester.edu/microbiology-immunology/xenopus-laevis/primers.aspx as of September 2019

Robert, J., Abramowitz, L., Gantress, J., Morales, H.D., 2007. *Xenopus laevis*: a possible vector of Ranavirus infection? *J Wild Dis* 43, 645-652.

Robert, J., George, E., De Jesús Andino, F., Chen, G., 2011. Waterborne infectivity of the Ranavirus frog virus 3 in *Xenopus laevis. Virology* 417, 410-417.

Robert, J., Grayfer, L., Edholm, E.S., Ward, B., De Jesús Andino, F., 2014. Inflammation-induced reactivation of the ranavirus Frog Virus 3 in asymptomatic *Xenopus laevis. PloS One* 9, e112904.

Robert, J., Guiet, C., Du Pasquier, L., 1994. Lymphoid tumors of *Xenopus laevis* with different capacities for growth in larvae and adults. *Dev Immunol* 3, 297-307.

Robert, J., Morales, H., Buck, W., Cohen, N., Marr, S., Gantress, J., 2005. Adaptive immunity and histopathology in frog virus 3-infected *Xenopus. Virology* 332, 667-675.

Rollins-Smith, L.A., 2017. Amphibian immunity-stress, disease, and climate change. *Dev Comp Immunol* 66, 111-119.

Rothenburg, S., Chinchar, V.G., Dever, T.E., 2011. Characterization of a ranavirus inhibitor of the antiviral protein kinase PKR. *BMC Micro* 11, 56.

Sakaguchi, D.S., Moeller, J.F., Coffman, C.R., Gallenson, N., Harris, W.A., 1989. Growth cone interactions with a glial cell line from embryonic Xenopus retina. *Dev Biol* 134, 158-174.

Sang, Y., Liu, Q., Lee, J., Ma, W., McVey, D.S., Blecha, F., 2016. Expansion of amphibian intronless interferons revises the paradigm for interferon evolution and functional diversity. *Sci Rep* 6, 29072.

Schock, D.M., Bollinger, T.K., Chinchar, V.G., Jancovich, J.K., Collins, J.P., 2008. Experimental evidence that amphibian ranaviruses are multi-host pathogens. *Copeia*, 133-143.

Schoggins, J.W., Rice, C.M., 2011. Interferon-stimulated genes and their antiviral effector functions. *Curr Opin Virol* 1, 519-525.

Sen, G.C., Ransohoff, R.M., 1993. Interferon-induced antiviral actions and their regulation. *Adv Virus Res* 42, 57-102.

Shahin, S.H., Blankemeyer, J.T., 1989. Demonstration of gap junctions in frog skin epithelium. *Am J Physiol* 257, C658-C664.

Showell, C., Conlon, F.L., 2009. The western clawed frog (*Xenopus tropicalis*): an emerging vertebrate model for developmental genetics and environmental toxicology. *Cold Spring Harb Protoc* pdb.emo131.

Sifkarovski, J., Grayfer, L., De Jesus Andino, F., Lawrence, B.P., Robert, J., 2014. Negative effects of low dose atrazine exposure on the development of effective immunity to FV3 in *Xenopus laevis*. *Dev Comp Immunol* 47, 52-58.

Silverman, R.H., 2007. Viral encounters with 2',5'-oligoadenylate synthetase and RNase L during the interferon antiviral response. *J Virol* 81, 12720-12729.

Smith, S.J., Kotecha, S., Towers, N., Latinkic, B.V., Mohun, T.J., 2002. XPOX2-peroxidase expression and the XLURP-1 promoter reveal the site of embryonic myeloid cell development in *Xenopus*. *Mech Develop* 117, 173-186.

Solomon, S., Qin, D., Manning, M., Averyt, K., Marquis, M., 2007. Climate change 2007-the physical science basis: Working group I contribution to the fourth assessment report of the IPCC. *Cambridge University Press*.

Sperandio, B., Fischer, N., Sansonetti, P.J., 2015. Mucosal physical and chemical innate barriers: Lessons from microbial evasion strategies. *Semin Immunol* 27, 111-118.

Stannard, W., O'Callaghan, C., 2006. Ciliary function and the role of cilia in clearance. Journal of aerosol medicine : *J Int Sco Aerosol Med* 19, 110-115.

Strober, W., 2001. Trypan blue exclusion test of cell viability. *Curr Protoc Immunol* Appendix 3, Appendix 3B.

Stuart, S.N., Chanson, J.S., Cox, N.A., Young, B.E., Rodrigues, A.S.L., Fischman, D.L., Waller, R.W., 2004. Status and trends of amphibian declines and extinctions worldwide. *Science* 306, 1783-1786.

Suhrbier, A., Garrod, D., 1986. An investigation of the molecular components of desmosomes in epithelial cells of five vertebrates. *J Cell Sci* 81, 223-242.

Sun, F., Zhang, Y.B., Liu, T.K., Gan, L., Yu, F.F., Liu, Y., Gui, J.F., 2010. Characterization of fish IRF3 as an IFN-inducible protein reveals evolving regulation of IFN response in vertebrates. *J Immunol* 185, 7573-7582.

Sun, L., Wu, J., Du, F., Chen, X., Chen, Z.J., 2013. Cyclic GMP-AMP Synthase Is a Cytosolic DNA Sensor That Activates the Type I Interferon Pathway. *Science* 339, 786.

Todd, B.D., Bergeron, C.M., Hepner, M.J., Hopkins, W.A., 2011. Aquatic and terrestrial stressors in amphibians: A test of the double jeopardy hypothesis based on maternally and trophically derived contaminants. *Environ Tox Chem* 30, 2277-2284.

Tohyama, M., Dai, X., Sayama, K., Yamasaki, K., Shirakata, Y., Hanakawa, Y., Tokumaru, S., Yahata, Y., Yang, L., Nagai, H., Takashima, A., Hashimoto, K., 2005. dsRNA-mediated innate immunity of epidermal keratinocytes. *Biochem Bioph Res* 335, 505-511.

Toledo, R.C., Jared, C., 1995. Cutaneous granular glands and amphibian venoms. *Comp Biochem Physiol* 111, 1-29.

Tosi, M.F., 2005. Innate immune responses to infection. *J Allergy Clin Immun* 116, 241-249.

Tripier, F., Braunwald, J., Markovic, L., Kirn, A., 1977. Frog virus 3 morphogenesis: effect of temperature and metabolic inhibitors. *J Gen Virol* 37, 39-52.

Tsukita, S., Furuse, M., 1999. Occludin and claudins in tight-junction strands: leading or supporting players? *Trends Cell Biol* 9, 268-273.

Tucker, S.J., Tannahill, D., Higgins, C.F., 1992. Identification and developmental expression of the *Xenopus laevis* cystic fibrosis transmembrane conductance regulator gene. *Hum Mol Genet* 1, 77-82.

Van Meter, R.J., Glinski, D.A., Hong, T., Cyterski, M., Henderson, W.M., Purucker, S.T., 2014. Estimating terrestrial amphibian pesticide body burden through dermal exposure. *Environ Pollut* 193, 262-268.

van Roy, F., Berx, G., 2008. The cell-cell adhesion molecule E-cadherin. *Cell Mol Life Sci* : CMLS 65, 3756-3788.

Varga, J.F.A., Bui-Marinos, M.P., Katzenback, B.A., 2019. Frog Skin Innate Immune Defences: Sensing and Surviving Pathogens. *Front Immunol* 9.

Vilcek, J., 2003. Novel interferons. *Nat Immunol* 4, 8-9.

Villaro, A.C., Rovira, J., Bodegas, M.E., Burrell, M.A., Sesma, P., 1998. Relationship between epithelial and connective tissues in the stomach of the frog *Rana temporaria* during metamorphosis: an ultrastructural study. *Tissue Cell* 30, 427-445.

Vo, N.T.K., Guerreiro, M., Yaparla, A., Grayfer, L., DeWitte-Orr, S.J., 2019a. Class A Scavenger Receptors Are Used by Frog Virus 3 During Its Cellular Entry. *Viruses* 11.

Vo, N.T.K., Moore, L.C., Leis, E., DeWitte-Orr, S.J., 2019b. Class A scavenger receptors mediate extracellular dsRNA sensing, leading to downstream antiviral gene expression in a novel American toad cell line, BufoTad. *Dev Comp Immunol* 92, 140-149.

Vuorio, T., Mäkelä, J., Kähäri, V.M., Vuorio, E., 1987. Coordinated regulation of type I and type III collagen production and mRNA levels of pro α1(I) and pro α2(I) collagen in cultured morphea fibroblasts. *Arch Dermatol Res* 279, 154-160.

Wack, A., Terczyńska-Dyla, E., Hartmann, R., 2015. Guarding the frontiers: the biology of type III interferons. *Nat Immunol* 16, 802.

Warner, A.E., 1985. The role of gap junctions in amphibian development. *J Embryol Exp Morph* 89 Suppl, 365-380.

Weber, F., Wagner, V., Rasmussen, S.B., Hartmann, R., Paludan, S.R., 2006. Double-stranded RNA is produced by positive-strand RNA viruses and DNA viruses but not in detectable amounts by negative-strand RNA viruses. *J Virol* 80, 5059-5064.

Weldon, P.J., Demeter, B.J., Rosscoe, R., 1993. A Survey of Shed Skin-Eating (Dermatophagy) in Amphibians and Reptiles. *J Herpetol* 27, 219-228.

Wendel, E.S., Yaparla, A., Koubourli, D.V., Grayfer, L., 2017. Amphibian (*Xenopus laevis*) tadpoles and adult frogs mount distinct interferon responses to the Frog Virus 3 ranavirus. *Virology* 503, 12-20.

Wendel, E.S., Yaparla, A., Melnyk, M.L.S., Koubourli, D.V., Grayfer, L., 2018. Amphibian (*Xenopus laevis*) Tadpoles and Adult Frogs Differ in Their Use of Expanded Repertoires of Type I and Type III Interferon Cytokines. *Viruses* 10.

Wilkins, C., Gale, M., 2010. Recognition of viruses by cytoplasmic sensors. *Curr Op Immunol* 22, 41-47.

Williams, B.R., 1999. PKR; a sentinel kinase for cellular stress. *Oncogene* 18, 6112-6120.

Williams, T., 1996. The iridoviruses. *Adv Virus Res* 46, 345-412.

Winton, J., Batts, W., deKinkelin, P., LeBerre, M., Bremont, M., Fijan, N., 2010. Current lineages of the epithelioma papulosum cyprini (EPC) cell line are contaminated with fathead minnow, *Pimephales promelas*, cells. *J Fish Dis* 33, 701-704.

Yang, J., Wheeler, S.E., Velikoff, M., Kleaveland, K.R., LaFemina, M.J., Frank, J.A., Chapman, H.A., Christensen, P.J., Kim, K.K., 2013. Activated alveolar epithelial cells initiate fibrosis through secretion of mesenchymal proteins. *Am J Pathol* 183, 1559-1570.

Yap, A.S., Brieher, W.M., Gumbiner, B.M., 1997. Molecular and functional analysis of cadherin-based adherens junctions. *Annu Rev Cell Dev Biol* 13, 119-146.

Yoneyama, M., Fujita, T., 2010. Recognition of viral nucleic acids in innate immunity. *Rev Med Virol* 20, 4-22.

Young, B.E., Lips, K.R., Reaser, J.K., Ibáñez, R., Salas, A.W., Cedeño, J.R., Coloma, L.A., Ron, S., La Marca, E., Meyer, J.R., Muñoz, A., Bolaños, F., Chaves, G., Romo, D., 2001. Population Declines and Priorities for Amphibian Conservation in Latin America. *Conserv Biol* 15, 1213-1223.

Ysebrant de Lendonck, L., Martinet, V., Goriely, S., 2014. Interferon regulatory factor 3 in adaptive immune responses. *Cell Mol Life Sci* : CMLS 71, 3873-3883.

Zamanian-Daryoush, M., Mogensen, T.H., DiDonato, J.A., Williams, B.R.G., 2000. NF-κB Activation by Double-Stranded-RNA-Activated Protein Kinase (PKR) Is Mediated through NF-κB-Inducing Kinase and IκB Kinase. *Mol Cell Biol* 20, 1278.

Zelova, H., Hosek, J., 2013. TNF-alpha signalling and inflammation: interactions between old acquaintances. *Inflamm Res* 62, 641-651.

Zhou, A., Li, S., Wu, J., Khan, F.A., Zhang, S., 2014. Interplay between microRNAs and host pathogen recognition receptors (PRRs) signaling pathways in response to viral infection. *Virus Res* 184, 1-6.

Appendix A – DNA Barcoding MSA for Xela DS2

```
HM991335.1          TGAACCTCTGTACACGGAGCTACAATCCGCCGCCTATTACTCGGCCACCTTACCTGTGGC        5400
XelaDS2COI-11       ------------------------------------------------------------        0
XelaDS2COI-22       ------------------------------------------------------------        0
XelaDS2COI-10b      ------------------------------------------------------------        0
XelaDS2COI-5        ------------------------------------------------------------        0
XelaDS2COI-10       ------------------------------------------------------------        0
XelaDS2COI-9        ------------------------------------------------------------        0
XelaDS2COI-21       ------------------------------------------------------------        0
XelaVS2COI-1        ------------------------------------------------------------        0
XelaDS2COI-26       ------------------------------------------------------------        0
XelaDS2COI-15       ------------------------------------------------------------        0
XelaDS2COI-25       ------------------------------------------------------------        0

HM991335.1          AATTACTCGTTGATTATTCTCAACAAATCACAAAGACATTGGCACCCTTTACTTAGTTTT        5460
XelaDS2COI-11       ----------------TTTTCTACTAATCATAAAGATATCGGCACCCTTTACTTAGTTTT        44
XelaDS2COI-22       ----------------TTCTCTACAAATCATAAAGACATCGGCACCCTTTACTTAGTTTT        44
XelaDS2COI-10b      ----------------TTCTCAACTAACCACAAAGATATCGGCACCCTTTACTTAGTTTT        44
XelaDS2COI-5        -----------------TTTCTACTAATCATAAAGATATCGGCACCCTTTACTTAGTTTT        43
XelaDS2COI-10       ----------------TTTTCTACTAATCATAAAGATATCGGCACCCTTTACTTAGTTTT        44
XelaDS2COI-9        ----------------TTCTCTACTAATCATAAAGATATCGGCACCCTTTACTTAGTTTT        44
XelaDS2COI-21       ----------------TTCTCTACTAATCATAAAGATATCGGCACCCTTTACTTAGTTTT        44
XelaVS2COI-1        ------------------------------------------------------------        0
XelaDS2COI-26       ----------------TTTTCAACAAACCACAAAGACATCGGCACCCTTTACTTAGTTTT        44
XelaDS2COI-15       ----------------TTTTCTACTAATCACAAAGATATCGGCACCCTTTACTTAGTTTT        44
XelaDS2COI-25       ----------------------------------------TCACCCTTTACTTAGTTTT        19

HM991335.1          TGGTGCTTGAGCAGGGATGGTCGGAACCGCTCTTAGCTTATTAATTCGAGCTGAACTTAG        5520
XelaDS2COI-11       TGGTGCTTGAGCAGGGATGGTCGGAACCGCTCTTAGCTTATTAATTCGAGCTGAACTTAG        104
XelaDS2COI-22       TGGTGCTTGAGCAGGGATGGTCGGAACCGCTCTTAGCTTATTAATTCGAGCTGAACTTAG        104
XelaDS2COI-10b      TGGTGCTTGAGCAGGGATGGTCGGAACCGCTCTTAGCTTATTAATTCGAGCTGAACTTAG        104
XelaDS2COI-5        TGGTGCTTGAGCAGGGATGGTCGGAACCGCTCTTAGCTTATTAATTCGAGCTGAACTTAG        103
XelaDS2COI-10       TGGTGCTTGAGCAGGGATGGTCGGAACCGCTCTTAGCTTATTAATTCGAGCTGAACTTAG        104
XelaDS2COI-9        TGGTGCTTGAGCAGAGATGGTCGGAACCGCTCTTAGCTTATTAATTCGAGCTGAACTTAG        104
XelaDS2COI-21       TGGTGCTTGAGCAGGGATGGTCGGAACCGCTCTTAGCTTATTAATTCGAGCTGAACTTAG        104
XelaVS2COI-1        ----------------------GAACCGCTCTTAGCTTATTAATTCGAGCTGAACTTAG        37
XelaDS2COI-26       TGGTGCTTGAGCAGGGATGGTCGGAACCGCTCTTAGCTTATTAATTCGAGCTGAACTTAG        104
XelaDS2COI-15       TGGTGCTTGAGCAGGGATGGTCGGAACCGCTCTTAGCTTATTAATTCGAGCTGAACTTAG        104
XelaDS2COI-25       TGGTGCTTGAGCAGGGATGGTCGGAACCGCTCTTAGCTTATTAATTCGAGCTGAACTTAG        79
                                    ************************************

HM991335.1          CCAGCCCGGAACACTACTTGGAGATGACCAAATTTATAATGTTATCGTTACAGCACATGC        5580
XelaDS2COI-11       CCAGCCCGGAACACTACTTGGAGATGACCAAATTTATAATGTTATCGTTACAGCACATGC        164
XelaDS2COI-22       CCAGCCCGGAACACTACTTGGAGATGACCAAATTTATAATGTTATCGTTACAGCACATGC        164
XelaDS2COI-10b      CCAGCCCGGAACACTACTTGGAGATGACCAAATTTATAATGTTATCGTTACAGCACATGC        164
XelaDS2COI-5        CCAGCCCGGAACACTACTTGGAGATGACCAAATTTATAATGTTATCGTTACAGCACATGC        163
XelaDS2COI-10       CCAGCCCGGAACACTACTTGGAGATGACCAAATTTATAATGTTATCGTTACAGCACATGC        164
XelaDS2COI-9        CCAGCCCGGAACACTACTTGGAGATGACCAAATTTATAATGTTATCGTTACAGCACATGC        164
XelaDS2COI-21       CCAGCCCGGAACACTACTTGGAGATGACCAAATTTATAATGTTATCGTTACAGCACATGC        164
XelaVS2COI-1        CCAGCCCGGAACACTACTTGGAGATGACCAAATTTATAATGTTATCGTTACAGCACATGC        97
XelaDS2COI-26       CCAGCCCGGAACACTACTTGGAGATGACCAAATTTATAATGTTATCGTTACAGCACATGC        164
XelaDS2COI-15       CCAGCCCGGAACACTACTTGGAGATGACCAAATTTATAATGTTATCGTTACAGCACATGC        164
XelaDS2COI-25       CCAGCCCGGAACACTACTTGGAGATGACCAAATTTATAATGTTATCGTTACAGCACATGC        139
                    ************************************************************

HM991335.1          TTTTATTATAATTTTCTTCATAGTCATGCCTATTATAATCGGTGGATTTGGGAACTGATT        5640
XelaDS2COI-11       TTTTATTATAATTTTCTTCATAGTCATGCCTATTATAATCGGTGGATTTGGGAACTGATT        224
XelaDS2COI-22       TTTTATTATAATTTTCTTCATAGTCATGCCTATTATAATCGGTGGATTTGGGAACTGATT        224
XelaDS2COI-10b      TTTTATTATAATTTTCTTCATAGTCATGCCTATTATAATCGGTGGATTTGGGAACTGATT        224
XelaDS2COI-5        TTTTATTATAATTTTCTTCATAGTCATGCCTATTATAATCGGTGGATTTGGGAACTGATT        223
XelaDS2COI-10       TTTTATTATAATTTTCTTCATAGTCATGCCTATTATAATCGGTGGATTTGGGAACTGATT        224
XelaDS2COI-9        TTTTATTATAATTTTCTTCATAGTCATGCCTATTATAATCGGTGGATTTGGGAACTGATT        224
XelaDS2COI-21       TTTTATTATAATTTTCTTCATAGTCATGCCTATTATAATCGGTGGATTTGGGAACTGATT        224
```

```
XelaVS2COI-1        TTTTATTATAATTTTCTTCATAGTCATGCCTATTATAATCGGTGGATTTGGGAACTGATT        157
XelaDS2COI-26       TTTTATTATAATTTTCTTCATAGTCATGCCTATTATAATCGGTGGATTTGGGAACTGATT        224
XelaDS2COI-15       TTTTATTATAATTTTCTTCATAGTCATGCCTATTATAATCGGTGGATTTGGGAACTGATT        224
XelaDS2COI-25       TTTTATTATAATTTTCTTCATAGTCATGCCTATTATAATCGGTGGATTTGGGAACTGATT        199
                    ************************************************************

HM991335.1          AGTTCCATTAATAATTGGAGCCCCAGATATAGCATTTCCGCGAATAAATAATATAAGCTT        5700
XelaDS2COI-11       AGTTCCATTAATAATTGAAGCCCCAGATATAGCATTTCCGCGAATAAATAATATAAGCTT        284
XelaDS2COI-22       AGTTCCATTAATAATTGGAGCCCCAGATATAGCATTTCCGCGAATAAATAATATAAGCTT        284
XelaDS2COI-10b      AGTTCCATTAATAATTGGAGCCCCAGATATAGCATTTCCGCGAATAAATAATATAAGCTT        284
XelaDS2COI-5        AGTTCCATTAATAATTGGAGCCCCAGATATAGCATTTCCGCGAATAAATAATATAAGCTT        283
XelaDS2COI-10       AGTTCCATTAATAATTGGAGCCCCAGATATAGCATTTCCGCGAATAAATAATATAAGCTT        284
XelaDS2COI-9        AGTTCCATTAATAATTGGAGCCCCAGATATAGCATTTCCGCGAATAAATAATATAAGCTT        284
XelaDS2COI-21       AGTTCCATTAATAATTGGAGCCCCAGATATAGCATTTCCGCGAATAAATAATATAAGCTT        284
XelaVS2COI-1        AGTTCCATTAATAATTGGAGCCCCAGATATAGCATTTCCGCGAATAAATAATATAAGCTT        217
XelaDS2COI-26       AGTTCCATTAATAATTGGAGCCCCAGATATAGCATTTCCGCGAATAAATAATATAAGCTT        284
XelaDS2COI-15       AGTTCCATTAATAATTGGAGCCCCAGATATAGCATTTCCGCGAATAAATAATATAAGCTT        284
XelaDS2COI-25       AGTTCCATTAATAATTGGAGCCCCAGATATAGCATTTCCGCGAATAAATAATATAAGCTT        259
                    ***************** ******************************************

HM991335.1          TTGACTTCTTCCCCCATCATTTCTTTTATTACTAGCATCATCTGGGGTTGAAGCAGGAGC        5760
XelaDS2COI-11       TTGACTTCTTCCCCCATCATTTCTTTTATTACTAGCATCATCTGGGGTTGAAGCAGGAGC        344
XelaDS2COI-22       TTGACTTCTTCCCCCATCATTTCTTTTATTACTAGCATCATCTGGGGTTGAAGCAGGAGC        344
XelaDS2COI-10b      TTGACTTCTTCCCCCATCATTTCTTTTATTACTAGCATCATCTGGGGTTGAAGCAGGAGC        344
XelaDS2COI-5        TTGACTTCTTCCCCCATCATTTCTTTTATTACTAGCATCATCTGGGGTTGAAGCAGGAGC        343
XelaDS2COI-10       TTGACTTCTTCCCCCATCATTTCTTTTATTACTAGCATCATCTGGGGTTGAAGCAGGAGC        344
XelaDS2COI-9        TTGACTTCTTCCCCCATCATTTCTTTTATTACTAGCATCATCTGGGGTTGAAGCAGGAGC        344
XelaDS2COI-21       TTGACTTCTTCCCCCATCATTTCTTTTATTACTAGCATCATCTGGGGTTGAAGCAGGAGC        344
XelaVS2COI-1        TTGACTTCTTCCCCCATCATTTCTTTTATTACTAGCATCATCTGGGGTTGAAGCAGGAGC        277
XelaDS2COI-26       TTGACTTCTTCCCCCATCATTTCTTTTATTACTAGCATCATCTGGGGTTGAAGCAGGAGC        344
XelaDS2COI-15       TTGACTTCTTCCCCCATCATTTCTTTTATTACTAGCATCATCTGGGGTTGAAGCAGGAGC        344
XelaDS2COI-25       TTGACTTCTTCCCCCATCATTTCTTTTATTACTAGCATCATCTGGGGTTGAAGCAGGAGC        319
                    ************************************************************

HM991335.1          CGGAACAGGTTGAACTGTGTACCCGCCTTTAGCTGGAAACCTAGCACATGCTGGAGCATC        5820
XelaDS2COI-11       CGGAACAGGTTGAACTGTGTACCCGCCTTTAGCTGGAAACCTAGCACATGCTGGAGCATC        404
XelaDS2COI-22       CGGAACAGGTTGAACTGTGTACCCGCCTTTAGCTGGAAACCTAGCACATGCTGGAGCATC        404
XelaDS2COI-10b      CGGAACAGGTTGAACTGTGTACCCGCCTTTAGCTGGAAACCTAGCACATGCTGGAGCATC        404
XelaDS2COI-5        CGGAACAGGTTGAACTGTGTACCCGCCTTTAGCTGGAAACCTAGCACATGCTGGAGCATC        403
XelaDS2COI-10       CGGAACAGGTTGAACTGTGTACCCGCCTTTAGCTGGAAACCTAGCACATGCTGGAGCATC        404
XelaDS2COI-9        CGGAACAGGTTGAACTGTGTACCCGCCTTTAGCTGGAAACCTAGCACATGCTGGAGCATC        404
XelaDS2COI-21       CGGAACAGGTTGAACTGTGTACCCGCCTTTAGCTGGAAACCTAGCACATGCTGGAGCATC        404
XelaVS2COI-1        CGGAACAGGTTGAACTGTGTACCCGCCTTTAGCTGGAAACCTAGCACATGCTGGAGCATC        337
XelaDS2COI-26       CGGAACAGGTTGAACTGTGTACCCGCCTTTAGCTGGAAACCTAGCACATGCTGGAGCATC        404
XelaDS2COI-15       CGGAACAGGTTGAACTGTGTACCCGCCTTTAGCTGGAAACCTAGCACATGCTGGAGCATC        404
XelaDS2COI-25       CGGAACAGGTTGAACTGTGTACCCGCCTTTAGCTGGAAACCTAGCACATGCTGGAGCATC        379
                    ************************************************************

HM991335.1          AGTTGACCTAACAATTTTCTCCCTTCACTTAGCTGGTATTTCATCTATTTTAGGAGCAAT        5880
XelaDS2COI-11       AGTTGACCTAACAATTTTCTCCCTTCACTTAGCTGGTATTTCATCTATTTTAGGAGCAAT        464
XelaDS2COI-22       AGTTGACCTAACAATTTTCTCCCTTCACTTAGCTGGTATTTCATCTATTTTAGGAGCAAT        464
XelaDS2COI-10b      AGTTGACCTAACAATTTTCTCCCTTCACTTAGCTGGTATTTCATCTATTTTAGGAGCAAT        464
XelaDS2COI-5        AGTTGACCTAACAATTTTCTCCCTTCACTTAGCTGGTATTTCATCTATTTTAGGAGCAAT        463
XelaDS2COI-10       AGTTGACCTAACAATTTTCTCCCTTCACTTAGCTGGTATTTCATCTATTTTAGGAGCAAT        464
XelaDS2COI-9        AGTTGACCTAACAATTTTCTCCCTTCACTTAGCTGGTATTTCATCTATTTTAGGAGCAAT        464
XelaDS2COI-21       AGTTGACCTAACAATTTTCTCCCTTCACTTAGCTGGTATTTCATCTATTTTAGGAGCAAT        464
XelaVS2COI-1        AGTTGACCTAACAATTTTCTCCCTTCACTTAGCTGGTATTTCATCTATTTTAGGAGCAAT        397
XelaDS2COI-26       AGTTGACCTAACAATTTTCTCCCTTCACTTAGCTGGTATTTCATCTATTTTAGGAGCAAT        464
XelaDS2COI-15       AGTTGACCTAACAATTTTCTCCCTTCACTTAGCTGGTATTTCATCTATTTTAGGAGCAAT        464
XelaDS2COI-25       AGTTGACCTAACAATTTTCTCCCTTCACTTAGCTGGTATTTCATCTATTTTAGGAGCAAT        439
                    ************************************************************

HM991335.1          TAACTTCATCACAACAACAATTAACATAAAACCACCAGCTATATCTCAATACCAAACCCC        5940
XelaDS2COI-11       TAACTTCATCACAACAACAATTAACATAAAACCACCAGCTATATCTCAATACCAAACCCC        524
XelaDS2COI-22       TAACTTCATCACAACAACAATTAACATAAAACCACCAGCTATATCTCAATACCAAACCCC        524
```

```
XelaDS2COI-10b      TAACTTCATCACAACAACAATTAACATAAAACCACCAGCTATATCTCAATACCAAACCCC        524
XelaDS2COI-5        TAACTTCATCACAACAACAATTAACATAAAACCACCAGCTATATCTCAATACCAAACCCC        523
XelaDS2COI-10       TAACTTCATCACAACAACAATTAACATAAAACCACCAGCTATATCTCAATACCAAACCCC        524
XelaDS2COI-9        TAACTTCATCACAACAACAATTAACATAAAACCACCAGCTATATCTCAATACCAAACCCC        524
XelaDS2COI-21       TAACTTCATCACAACAACAATTAACATAAAACCACCAGCTATATCTCAATACCAAACCCC        524
XelaVS2COI-1        TAACTTCATCACAACAACAATTAACATAAAACCACCAGCTATATCTCAATACCAAACCCC        457
XelaDS2COI-26       TAACTTCATCACAACAACAATTAACATAAAACCACCAGCTATATCTCAATACCAAACCCC        524
XelaDS2COI-15       TAACTTCATCACAACAACAATTAACATAAAACCACCAGCTATATCTCAATACCAAACCCC        524
XelaDS2COI-25       TAACTTCATCACAACAACAATTAACATAAAACCACCAGCTATATCTCAATACCAAACCCC        499
                    ************************************************************

HM991335.1          ACTATTTGTTTGATCAGTATTAATCACAGCTGTACTTTTACTTCTTTCTCTTCCTGTCTT       6000
XelaDS2COI-11       ACTATTTGTTTGATCAGTATTAATCACAGCTGTACTTTTACTTCTTTCTCTTCCTGTCTT        584
XelaDS2COI-22       ACTATTTGTTTGATCAGTATTAATCACAGCTGTACTTTTACTTCTTTCTCTTCCTGTCTT        584
XelaDS2COI-10b      ACTATTTGTTTGATCAGTATTAATCACAGCTGTACTTTTACTTCTTTCTCTTCCTGTCTT        584
XelaDS2COI-5        ACTATTTGTTTGATCAGTATTAATCACAGCTGTACTTTTACTTCTTTCTCTTCCTGTCTT        583
XelaDS2COI-10       ACTATTTGTTTGATCAGTATTAATCACAGCTGTACTTTTACTTCTTTCTCTTCCTGTCTT        584
XelaDS2COI-9        ACTATTTGTTTGATCAGTATTAATCACAGCTGTACTTTTACTTCTTTCTCTTCCTGTCTT        584
XelaDS2COI-21       ACTATTTGTTTGATCAGTATTAATCACAGCTGTACTTTTACTTCTTTCTCTTCCTGTCTT        584
XelaVS2COI-1        ACTATTTGTTTGATCAGTATTAATCACAGCTGTACTTTTACTTCTTTCTCTTCCTGTCTT        517
XelaDS2COI-26       ACTATTTGTTTGATCAGTATTAATCACAGCTGTACTTTTACTTCTTTCTCTTCCTGTCTT        584
XelaDS2COI-15       ACTATTTGTTTGATCAGTATTAATCACAGCTGTACTTTTACTTCTTTCTCTTCCTGTCTT        584
XelaDS2COI-25       ACTATTTGTTTGATCAGTATTAATCACAGCTGTACTTTTACTTCTTTCTCTTCCTGTCTT        559
                    ************************************************************

HM991335.1          AGCCGCAGGAATCACAATGTTATTAACAGATCGTAATCTGAATACAACTTTCTTTGACCC       6060
XelaDS2COI-11       AGCCGCAGGAATCACAATGTTATTAACAGATCGTAATCTGAATACAACTTTCTTTGACCT        644
XelaDS2COI-22       AGCCGCAGGAATCACAATGTTATTAACAGATCGTAATCTGAATACAACTTTCTTTGACCC        644
XelaDS2COI-10b      AGCCGCAGGAATCACAATGTTATTAACAGATCGTAATCTGAATACAACTTTCTTTGACCC        644
XelaDS2COI-5        AGCCGCAGGAATCACAATGTTATTAACAGATCGTAATCTGAATACAACTTTCTTTGACCC        643
XelaDS2COI-10       AGCCGCAGGAATCACAATGTTATTAACAGATCGTAATCTGAATACAACTTTCTTTGACCC        644
XelaDS2COI-9        AGCCGCAGGAATCACAATGTTATTAACAGATCGTAATCTGAATACAACTTTCTTTGACCC        644
XelaDS2COI-21       AGCCGCAGGAATCACAATGTTATTAACAGATCGTAATCTGAATACAACTTTCTTTGACCC        644
XelaVS2COI-1        AGCCGCAGGAATCACAATGTTATTAACAGATCGTAATCTGAATACAACTTTCTTTGACCC        577
XelaDS2COI-26       AGCCGCAGGAATCACAATGTTATTAACAGATCGTAATCTGAATACAACTTTCTTTGACCC        644
XelaDS2COI-15       AGCCGCAGGAATCACAATGTTATTAACAGATCGTAATCTGAATACAACTTTCTTTGACCC        644
XelaDS2COI-25       AGCCGCAGGAATCACAATGTTATTAACAGATCGTAATCTGAATACAACTTTCTTTGACCC        619
                    ************************************************************

HM991335.1          TGCCGGAGGAGGTGACCCAGTACTTTACCAACACCTGTTCTGATTCTTTGGGCACCCAGA       6120
XelaDS2COI-11       TGCCGGAGGAGGTGACCCAGTACTTTACCAACACCTGTTCTGATTCTTCGGCCA------        698
XelaDS2COI-22       TGCCGGAGGAGGTGACCCAGTACTTTACCAACACCTGTTCTGATTCTTTGGCCATCCTGA        704
XelaDS2COI-10b      TGCCGGAGGAGGTGACCCAGTACTTTACCAACACCTGTTCTGATTTTTTGGCCATCCTGA        704
XelaDS2COI-5        TGCCGGAGGAGGTGACCCAGTACTTTACCAACACCTGTTCTGATTTTTTGGCCATCCTGA        703
XelaDS2COI-10       TGCCGGAGGAGGTGACCCAGTACTTTACCAACACCTGTTCTGATTTTTTGGCCATCCCGA        704
XelaDS2COI-9        TGCCGGAGGAGGTGACCCAGTACTTTACCAACACCTGTTCTGATTTTTCGGCCATCCTGA        704
XelaDS2COI-21       TGCCGGAGGAGGTGACCCAGTACTTTACCAACACCTGTTCTGATTTTTCGGCCATCCTGA        704
XelaVS2COI-1        TGCCGGAGGAGGTGACCCAGTACTTTACCAACACCTGTTCTGATTCTTCGGCCACCCCGA        637
XelaDS2COI-26       TGCCGGAGGAGGTGACCCAGTACTTTACCAACACCTGTTCTGATTCTTTGGTCACCCTGA        704
XelaDS2COI-15       TGCCGGAGGAGGTGACCCAGTACTTTACCAACACCTGTTCTGATTCTTCGGTCACCCCGA        704
XelaDS2COI-25       TGCCGGAGGAGGTGACCCAGTACTTTACCAACACCTGTTCTGATTCTTTGGTCACCCCGA        679
                    ******************************************** ** ** **

HM991335.1          AGTGTACATTCTTATCTTACCAGGGTTTGG--CATGATCTCCCATATCGTAACTTATTAC       6178
XelaDS2COI-11       ------------------------------------------------------------        698
XelaDS2COI-22       GGT---------------------------------------------------------        707
XelaDS2COI-10b      GGT---------------------------------------------------------        707
XelaDS2COI-5        GGTA--------------------------------------------------------        707
XelaDS2COI-10       GGT---------------------------------------------------------        707
XelaDS2COI-9        GGTACTTTTACTTCTTTCTCTTCCTGTCTTAGCCGCAGGAATCACAATGTTATTAACAGA       764
XelaDS2COI-21       GGTACTTTTACTTCTTTCTCTTCCTGTCTTAGCCGCAGGAATCACAATGTTATTAACAGA       764
XelaVS2COI-1        GGTA--------------------------------------------------------        641
XelaDS2COI-26       GGT---------------------------------------------------------        707
XelaDS2COI-15       GGT---------------------------------------------------------        707
XelaDS2COI-25       GGT---------------------------------------------------------        682
```

```
HM991335.1          TCAGGAAA----AAAAGAACCTTTCGGCTATATAGGAATAGTCTGGGCAATAATATCAAT        6234
XelaDS2COI-11       ------------------------------------------------------------        698
XelaDS2COI-22       ------------------------------------------------------------        707
XelaDS2COI-10b      ------------------------------------------------------------        707
XelaDS2COI-5        ------------------------------------------------------------        707
XelaDS2COI-10       ------------------------------------------------------------        707
XelaDS2COI-9        TCGTAATCTGAATACAACTTTCTTTGACCCTGCCGGAGGAGGTGACCCAGTACTTTACCA        824
XelaDS2COI-21       TCGTAATCTGAATACAACTTTCTTTGACCCTGCCGGAGGAGGTGACCCAGTACTTTACCA        824
XelaVS2COI-1        ------------------------------------------------------------        641
XelaDS2COI-26       ------------------------------------------------------------        707
XelaDS2COI-15       ------------------------------------------------------------        707
XelaDS2COI-25       ------------------------------------------------------------        682

HM991335.1          TGGACTTCTAGGCTTTATTGTCTGAGCCCATCACATATTTACGGTTGATCTAAACGTAGA        6294
XelaDS2COI-11       ------------------------------------------------------------        698
XelaDS2COI-22       ------------------------------------------------------------        707
XelaDS2COI-10b      ------------------------------------------------------------        707
XelaDS2COI-5        ------------------------------------------------------------        707
XelaDS2COI-10       ------------------------------------------------------------        707
XelaDS2COI-9        ACACCTGTTCTGATTTTTTGGC----------------------------------------        846
XelaDS2COI-21       ACACCTGTTCTGATTTTTTGGC----------------------------------------        846
XelaVS2COI-1        ------------------------------------------------------------        641
XelaDS2COI-26       ------------------------------------------------------------        707
XelaDS2COI-15       ------------------------------------------------------------        707
XelaDS2COI-25       ------------------------------------------------------------        682
```

Appendix B – DNA Barcoding MSA for Xela VS2

```
XelaVS2COI-3b      ------------------------------------------------------------ 0
XelaVS2COI-4b      ------------------------------------------------------------ 0
HM991335.1         TGAACCTCTGTACACGGAGCTACAATCCGCCGCCTATTACTCGGCCACCTTACCTGTGGC 5400
XelaVS2COI-2b      ------------------------------------------------------------ 0
XelaVS2COI-11      ------------------------------------------------------------ 0
XelaVS2COI-7       ------------------------------------------------------------ 0
XelaVS2COI-2       ------------------------------------------------------------ 0
XelaVS2COI-3       ------------------------------------------------------------ 0
XelaVS2COI-4       ------------------------------------------------------------ 0
XelaVS2COI-1       ------------------------------------------------------------ 0
XelaVS2COI-6       ------------------------------------------------------------ 0


XelaVS2COI-3b      ----------------TTTTCAACTAATCATAAAGATATCGGCACCCTTTACTTAGTTTT 44
XelaVS2COI-4b      ----------------TTTTCAACTAATCATAAAGATATCGGCACCCTTTACTTAGTTTT 44
HM991335.1         AATTACTCGTTGATTATTCTCAACAAATCACAAAGACATTGGCACCCTTTACTTAGTTTT 5460
XelaVS2COI-2b      -----------------TCTCAACAAACCATAAAGACATCGGCACCCTTTACTTAGTTTT 43
XelaVS2COI-11      -----------------TCTCAACAAACCATAAAGACATCGGCACCCTTTACTTAGTTTT 43
XelaVS2COI-7       -----------------TTTCAACAAATCATAAAGACATCGGCACCCTTTACTTAGTTTT 43
XelaVS2COI-2       ----------------TTTTCTACAAATCATAAAGACATCGGCACCCTTTACTTAGTTTT 44
XelaVS2COI-3       ----------------TTTTCTACAAATCATAAAGACATCGGCACCCTTTACTTAGTTTT 44
XelaVS2COI-4       ------------GGTCTTCTCAACTAATCACAAAGATATCGGCACCCTTTACTTAGTTTT 48
XelaVS2COI-1       ------------------------------------------------------------ 0
XelaVS2COI-6       -----------------TCTCAACAAACCACAAAGATATCGGCACCCTTTACTTAGTTTT 43


XelaVS2COI-3b      TGGTGCTTGAGCAGGGATGGTCGGAACCGCTCTTAGCTTATTAATTCGAGCTGAACTTAG 104
XelaVS2COI-4b      TGGTGCTTGAGCAGGGATGGTCGGAACCGCTCTTAGCTTATTAATTCGAGCTGAACTTAG 104
HM991335.1         TGGTGCTTGAGCAGGGATGGTCGGAACCGCTCTTAGCTTATTAATTCGAGCTGAACTTAG 5520
XelaVS2COI-2b      TGGTGCTTGAGCAGGGATGGTCGGAACCGCTCTTAGCTTATTAATTCGAGCTGAACTTAG 103
XelaVS2COI-11      TGGTGCTTGAGCAGGGATGGTCGGAACCGCTCTTAGCTTATTAATTCGAGCTGAACTTAG 103
XelaVS2COI-7       TGGTGCTTGAGCAGGGATGGTCGGAACCGCTCTTAGCTTATTAATTCGAGCTGAACTTAG 103
XelaVS2COI-2       TGGTGCTTGAGCAGGGATGGTCGGAACCGCTCTTAGCTTATTAATTCGAGCTGAACTTAG 104
XelaVS2COI-3       TGGTGCTTGAGCAGGGATGGTCGGAACCGCTCTTAGCTTATTAATTCGAGCTGAACTTAG 104
XelaVS2COI-4       TGGTGCTTGAGCAGGGATGGTCGGAACCGCTCTTAGCTTATTAATTCGAGCTGAACTTAG 108
XelaVS2COI-1       ----------------------GAACCGCTCTTAGCTTATTAATTCGAGCTGAACTTAG 37
XelaVS2COI-6       TGGTGCTTGAGCAGGGATGGTCGGAACCGCTCTTAGCTTATTAATTCGAGCTGAACTTAG 103
                                         ********************************** 


XelaVS2COI-3b      CCAGCCCGGAACACTACTTGGAGATGACCAAATTTATAATGTTATCGTTACAGCACATGC 164
XelaVS2COI-4b      CCAGCCCGGAACACTACTTGGAGATGACCAAATTTATAATGTTATCGTTACAGCACATGC 164
HM991335.1         CCAGCCCGGAACACTACTTGGAGATGACCAAATTTATAATGTTATCGTTACAGCACATGC 5580
XelaVS2COI-2b      CCAGCCCGGAACACTACTTGGAGATGACCAAATTTATAATGTTATCGTTACAGCACATGC 163
XelaVS2COI-11      CCAGCCCGGAACACTACTTGGAGATGACCAAATTTATAATGTTATCGTTACAGCACATGC 163
XelaVS2COI-7       CCAGCCCGGAACACTACTTGGAGATGACCAAATTTATAATGTTATCGTTACAGCACATGC 163
XelaVS2COI-2       CCAGCCCGGAACACTACTTGGAGATGACCAAATTTATAATGTTATCGTTACAGCACATGC 164
XelaVS2COI-3       CCAGCCCGGAACACTACTTGGAGATGACCAAATTTATAATGTTATCGTTACAGCACATGC 164
XelaVS2COI-4       CCAGCCCGGAACACTACTTGGAGATGACCAAATTTATAATGTTATCGTTACAGCACATGC 168
XelaVS2COI-1       CCAGCCCGGAACACTACTTGGAGATGACCAAATTTATAATGTTATCGTTACAGCACATGC 97
XelaVS2COI-6       CCAGCCCGGAACACTACTTGGAGATGACCAAATTTATAATGTTATCGTTACAGCACATGC 163
                   ************************************************************ 


XelaVS2COI-3b      TTTTATTATAATTTTCTTCATAGTCATGCCTATTATAATCGGTGGATTTGGGAACTGATT 224
XelaVS2COI-4b      TTTTATTATAATTTTCCTCATAGTCATGCCTATTATAATCGGTGGATTTGGGAACTGATT 224
HM991335.1         TTTTATTATAATTTTCTTCATAGTCATGCCTATTATAATCGGTGGATTTGGGAACTGATT 5640
XelaVS2COI-2b      TTTTATTATAATTTTCTTCATAGTCATGCCTATTATAATCGGTGGATTTGGGAACTGATT 223
XelaVS2COI-11      TTTTATTATAATTTTCTTCATAGTCATGCCTATTATAATCGGTGGATTTGGGAACTGATT 223
XelaVS2COI-7       TTTTATTATAATTTTCTTCATAGTCATGCCTATTATAATCGGTGGATTTGGGAACTGATT 223
XelaVS2COI-2       TTTTATTATAATTTTCTTCATAGTCATGCCTATTATAATCGGTGGATTTGGGAACTGATT 224
XelaVS2COI-3       TTTTATTATAATTTTCTTCATAGTCATGCCTATTATAATCGGTGGATTTGGGAACTGATT 224
XelaVS2COI-4       TTTTATTATAATTTTCTTCATAGTCATGCCTATTATAATCGGTGGATTTGGGAACTGATT 228
XelaVS2COI-1       TTTTATTATAATTTTCTTCATAGTCATGCCTATTATAATCGGTGGATTTGGGAACTGATT 157
XelaVS2COI-6       TTTTATTATAATTTTCTTCATAGTCATGCCTATTATAATCGGTGGATTTGGGAACTGATT 223
                   *************** ****************************************** 
```

```
XelaVS2COI-3b      AGTTCCATTAATAATTGGAGCCCCAGATATAGCATTTCCGCGAATAAATAATATAAGCTT 284
XelaVS2COI-4b      AGTTCCATTAATAATTGGAGCCCCAGATATAGCATTTCCGCGAATAAATAATATAAGCTT 284
HM991335.1         AGTTCCATTAATAATTGGAGCCCCAGATATAGCATTTCCGCGAATAAATAATATAAGCTT 5700
XelaVS2COI-2b      AGTTCCATTAATAATTGGAGCCCCAGATATAGCATTTCCGCGAATAAATAATATAAGCTT 283
XelaVS2COI-11      AGTTCCATTAATAATTGGAGCCCCAGATATAGCATTTCCGCGAATAAATAATATAAGCTT 283
XelaVS2COI-7       AGTTCCATTAATAATTGGAGCCCCAGATATAGCATTTCCGCGAATAAATAATATAAGCTT 283
XelaVS2COI-2       AGTTCCATTAATAATTGGAGCCCCAGATATAGCATTTCCGCGAATAAATAATATAAGCTT 284
XelaVS2COI-3       AGTTCCATTAATAATTGGAGCCCCAGATATAGCATTTCCGCGAATAAATAATATAAGCTT 284
XelaVS2COI-4       AGTTCCATTAATAATTGGAGCCCCAGATATAGCATTTCCGCGAATAAATAATATAAGCTT 288
XelaVS2COI-1       AGTTCCATTAATAATTGGAGCCCCAGATATAGCATTTCCGCGAATAAATAATATAAGCTT 217
XelaVS2COI-6       AGTTCCATTAATAATTGGAGCCCCAGATATAGCATTTCCGCGAATAAATAATATAAGCTT 283
                   ************************************************************

XelaVS2COI-3b      TTGACTTCTTCCCCCATCATTTCTTTTATTACTAGCATCATCTGGGGTTGAAGCAGGAGC 344
XelaVS2COI-4b      TTGACTTCTTCCCCCATCATTTCTTTTATTACTAGCATCATCTGGGGTTGAAGCAGGAGC 344
HM991335.1         TTGACTTCTTCCCCCATCATTTCTTTTATTACTAGCATCATCTGGGGTTGAAGCAGGAGC 5760
XelaVS2COI-2b      TTGACTTCTTCCCCCATCATTTCTTTTATTACTAGCATCATCTGGGGTTGAAGCAGGAGC 343
XelaVS2COI-11      TTGACTTCTTCCCCCATCATTTCTTTTATTACTAGCATCATCTGGGGTTGAAGCAGGAGC 343
XelaVS2COI-7       TTGACTTCTTCCCCCATCATTTCTTTTATTACTAGCATCATCTGGGGTTGAAGCAGGAGC 343
XelaVS2COI-2       TTGACTTCTTCCCCCATCATTTCTTTTATTACTAGCATCATCTGGGGTTGAAGCAGGAGC 344
XelaVS2COI-3       TTGACTTCTTCCCCCATCATTTCTTTTATTACTAGCATCATCTGGGGTTGAAGCAGGAGC 344
XelaVS2COI-4       TTGACTTCTTCCCCCATCATTTCTTTTATTACTAGCATCATCTGGGGTTGAAGCAGGAGC 348
XelaVS2COI-1       TTGACTTCTTCCCCCATCATTTCTTTTATTACTAGCATCATCTGGGGTTGAAGCAGGAGC 277
XelaVS2COI-6       TTGACTTCTTCCCCCATCATTTCTTTTATTACTAGCATCATCTGGGGTTGAAGCAGGAGC 343
                   ************************************************************

XelaVS2COI-3b      CGGAACAGGTTGAACTGTGTACCCGCCTTTAGCTGGAAACCTAGCACATGCTGGAGCATC 404
XelaVS2COI-4b      CGGAACAGGTTGAACTGTGTACCCGCCTTTAGCTGGAAACCTAGCACATGCTGGAGCATC 404
HM991335.1         CGGAACAGGTTGAACTGTGTACCCGCCTTTAGCTGGAAACCTAGCACATGCTGGAGCATC 5820
XelaVS2COI-2b      CGGAACAGGTTGAACTGTGTACCCGCCTTTAGCTGGAAACCTAGCACATGCTGGAGCATC 403
XelaVS2COI-11      CGGAACAGGTTGAACTGTGTACCCGCCTTTAGCTGGAAACCTAGCACATGCTGGAGCATC 403
XelaVS2COI-7       CGGAACAGGTTGAACTGTGTACCCGCCTTTAGCTGGAAACCTAGCACATGCTGGAGCATC 403
XelaVS2COI-2       CGGAACAGGTTGAACTGTGTACCCGCCTTTAGCTGGAAACCTAGCACATGCTGGAGCATC 404
XelaVS2COI-3       CGGAACAGGTTGAACTGTGTACCCGCCTTTAGCTGGAAACCTAGCACATGCTGGAGCATC 404
XelaVS2COI-4       CGGAACAGGTTGAACTGTGTACCCGCCTTTAGCTGGAAACCTAGCACATGCTGGAGCATC 408
XelaVS2COI-1       CGGAACAGGTTGAACTGTGTACCCGCCTTTAGCTGGAAACCTAGCACATGCTGGAGCATC 337
XelaVS2COI-6       CGGAACAGGTTGAACTGTGTACCCGCCTTTAGCTGGAAACCTAGCACATGCTGGAGCATC 403
                   ************************************************************

XelaVS2COI-3b      AGTTGACCTAACAATTTTCTCCCTTCACTTAGCTGGTATTTCATCTATTTTAGGAGCAAT 464
XelaVS2COI-4b      AGTTGACCTAACAATTTTCTCCCTTCACTTAGCTGGTATTTCATCTATTTTAGGAGCAAT 464
HM991335.1         AGTTGACCTAACAATTTTCTCCCTTCACTTAGCTGGTATTTCATCTATTTTAGGAGCAAT 5880
XelaVS2COI-2b      AGTTGACCTAACAATTTTCTCCCTTCACTTAGCTGGTATTTCATCTATTTTAGGAGCAAT 463
XelaVS2COI-11      AGTTGACCTAACAATTTTCTCCCTTCACTTAGCTGGTATTTCATCTATTTTAGGAGCAAT 463
XelaVS2COI-7       AGTTGACCTAACAATTTTCTCCCTTCACTTAGCTGGTATTTCATCTATTTTAGGAGCAAT 463
XelaVS2COI-2       AGTTGACCTAACAATTTTCTCCCTTCACTTAGCTGGTATTTCATCTATTTTAGGAGCAAT 464
XelaVS2COI-3       AGTTGACCTAACAATTTTCTCCCTTCACTTAGCTGGTATTTCATCTATTTTAGGAGCAAT 464
XelaVS2COI-4       AGTTGACCTAACAATTTTCTCCCTTCACTTAGCTGGTATTTCATCTATTTTAGGAGCAAT 468
XelaVS2COI-1       AGTTGACCTAACAATTTTCTCCCTTCACTTAGCTGGTATTTCATCTATTTTAGGAGCAAT 397
XelaVS2COI-6       AGTTGACCTAACAATTTTCTCCCTTCACTTAGCTGGTATTTCATCTATTTTAGGAGCAAT 463
                   ************************************************************

XelaVS2COI-3b      TAACTTCATCACAACAACAATTAACATAAAACCACCAGCTATATCTCAATACCAAACCCC 524
XelaVS2COI-4b      TAACTTCATCACAACAACAATTAACATAAAACCACCAGCTATATCTCAATACCAAACCCC 524
HM991335.1         TAACTTCATCACAACAACAATTAACATAAAACCACCAGCTATATCTCAATACCAAACCCC 5940
XelaVS2COI-2b      TAACTTCATCACAACAACAATTAACATAAAACCACCAGCTATATCTCAATACCAAACCCC 523
XelaVS2COI-11      TAACTTCATCACAACAACAATTAACATAAAACCACCAGCTATATCTCAATACCAAACCCC 523
XelaVS2COI-7       TAACTTCATCACAACAACAATTAACATAAAACCACCAGCTATATCTCAATACCAAACCCC 523
XelaVS2COI-2       TAACTTCATCACAACAACAATTAACATAAAACCACCAGCTATATCTCAATACCAAACCCC 524
XelaVS2COI-3       TAACTTCATCACAACAACAATTAACATAAAACCACCAGCTATATCTCAATACCAAACCCC 524
XelaVS2COI-4       TAACTTCATCACAACAACAATTAACATAAAACCACCAGCTATATCTCAATACCAAACCCC 528
XelaVS2COI-1       TAACTTCATCACAACAACAATTAACATAAAACCACCAGCTATATCTCAATACCAAACCCC 457
XelaVS2COI-6       TAACTTCATCACAACAACAATTAACATAAAACCACCAGCTATATCTCAATACCAAACCCC 523
                   ************************************************************
```

```
XelaVS2COI-3b      ACTATTTGTTTGATCAGTATTAATCACAGCTGTACTTTTACTTCTTTCTCTTCCTGTCTT 584
XelaVS2COI-4b      ACTATTTGTTTGATCAGTATTAATCACAGCTGTACTTTTACTTCTTTCTCTTCCTGTCTT 584
HM991335.1         ACTATTTGTTTGATCAGTATTAATCACAGCTGTACTTTTACTTCTTTCTCTTCCTGTCTT 6000
XelaVS2COI-2b      ACTATTTGTTTGATCAGTATTAATCACAGCTGTACTTTTACTTCTTTCTCTTCCTGTCTT 583
XelaVS2COI-11      ACTATTTGTTTGATCAGTATTAATCACAGCTGTACTTTTACTTCTTTCTCTTCCTGTCTT 583
XelaVS2COI-7       ACTATTTGTTTGATCAGTATTAATCACAGCTGTACTTTTACTTCTTTCTCTTCCTGTCTT 583
XelaVS2COI-2       ACTATTTGTTTGATCAGTATTAATCACAGCTGTACTTTTACTTCTTTCTCTTCCTGTCTT 584
XelaVS2COI-3       ACTATTTGTTTGATCAGTATTAATCACAGCTGTACTTTTACTTCTTTCTCTTCCTGTCTT 584
XelaVS2COI-4       ACTATTTGTTTGATCAGTATTAATCACAGCTGTACTTTTACTTCTTTCTCTTCCTGTCTT 588
XelaVS2COI-1       ACTATTTGTTTGATCAGTATTAATCACAGCTGTACTTTTACTTCTTTCTCTTCCTGTCTT 517
XelaVS2COI-6       ACTATTTGTTTGATCAGTATTAATCACAGCTGTACTTTTACTTCTTTCTCTTCCTGTCTT 583
                   ************************************************************

XelaVS2COI-3b      AGCCGCAGGAATCACAATGTTATTAACAGATCGTAATCTGAATACAACTTTCTTTGACCC 644
XelaVS2COI-4b      AGCCGCAGGAATCACAATGTTATTAACAGATCGTAATCTGAATACAACTTTCTTTGACCC 644
HM991335.1         AGCCGCAGGAATCACAATGTTATTAACAGATCGTAATCTGAATACAACTTTCTTTGACCC 6060
XelaVS2COI-2b      AGCCGCAGGAATCACAATGTTATTAACAGATCGTAATCTGAATACAACTTTCTTTGACCC 643
XelaVS2COI-11      AGCCGCAGGAATCACAATGTTATTAACAGATCGTAATCTGAATACAACTTTCTTTGACCC 643
XelaVS2COI-7       AGCCGCAGGAATCACAATGTTATTAACAGATCGTAATCTGAATACAACTTTCTTTGACCC 643
XelaVS2COI-2       AGCCGCAGGAATCACAATGTTATTAACAGATCGTAATCTGAATACAACTTTCTTTGACCC 644
XelaVS2COI-3       AGCCGCAGGAATCACAATGTTATTAACAGATCGTAATCTGAATACAACTTTCTTTGACCC 644
XelaVS2COI-4       AGCCGCAGGAATCACAATGTTATTAACAGATCGTAATCTGAATACAACTTTCTTTGACCC 648
XelaVS2COI-1       AGCCGCAGGAATCACAATGTTATTAACAGATCGTAATCTGAATACAACTTTCTTTGACCC 577
XelaVS2COI-6       AGCCGCAGGAATCACAATGTTATTAACAGATCGTAATCTGAATACAACTTTCTTTGACCC 643
                   ************************************************************

XelaVS2COI-3b      TGCCGGAGGAGGTGACCCAGTACTTTACCAACACCTGTTCTGATTTTTTGGTCATCCTGA 704
XelaVS2COI-4b      TGCCGGAGGAGGTGACCCAGTACTTTACCAACACCTGTTCTGATTTTTCGGCCATCCTGA 704
HM991335.1         TGCCGGAGGAGGTGACCCAGTACTTTACCAACACCTGTTCTGATTCTTTGGGCACCCAGA 6120
XelaVS2COI-2b      TGCCGGAGGAGGTGACCCAGTACTTTACCAACACCTGTTCTGATTCTTTGGCCATCCTGA 703
XelaVS2COI-11      TGCCGGAGGAGGTGACCCAGTACTTTACCAACACCTGTTCTGATTCTTTGGCCATCCTGA 703
XelaVS2COI-7       TGCCGGAGGAGGTGACCCAGTACTTTACCAACACCTGTTCTGATTCTTCGGTCACCCTGA 703
XelaVS2COI-2       TGCCGGAGGAGGTGACCCAGTACTTTACCAACACCTGTTCTGATTCTTCGGTCACCCCGA 704
XelaVS2COI-3       TGCCGGAGGAGGTGACCCAGTACTTTACCAACACCTGTTCTGATTCTTCGGTCACCCCGA 704
XelaVS2COI-4       TGCCGGAGGAGGCGACCCAGTACTTTACCAACACCTGTTCTGATTCTTCGGCCACCCCGA 708
XelaVS2COI-1       TGCCGGAGGAGGTGACCCAGTACTTTACCAACACCTGTTCTGATTCTTCGGCCACCCCGA 637
XelaVS2COI-6       TGCCGGAGGAGGTGACCCAGTACTTTACCAACACCTGTTCTGATTCTTCGGCCACCCCGA 703
                   *********** ******************************** ** ** ** ** **

XelaVS2COI-3b      GGT---------------------------------------------------------- 707
XelaVS2COI-4b      AGT---------------------------------------------------------- 707
HM991335.1         AGTGTACATTCTTATCTTACCAGGGTTTGGCATGATCTCCCATATCGTAACTTATTACTC 6180
XelaVS2COI-2b      GGT---------------------------------------------------------- 706
XelaVS2COI-11      GGT---------------------------------------------------------- 706
XelaVS2COI-7       GGTA--------------------------------------------------------- 707
XelaVS2COI-2       GGT---------------------------------------------------------- 707
XelaVS2COI-3       GGTAGACC----------------------------------------------------- 712
XelaVS2COI-4       AGTA--------------------------------------------------------- 712
XelaVS2COI-1       GGTA--------------------------------------------------------- 641
XelaVS2COI-6       GGTA--------------------------------------------------------- 707
                    **
```

Appendix C – Sequence confirmation of molecular markers

β-actin
S: AGGAGATGAAGCTCAAAGCAA
AS: GTTACACCATCACCTGAGTCC
AS Compliment: GGACTCAGGTGATGGTGTAAC

(1) Xela-Bactin-1-M13For

Description	Max score	Total score	Query cover	E value	Ident	Accession
Xenopus laevis actin, beta L homeolog (actb.L), mRNA	574	574	99%	4e-160	100%	gil1070257615|NM_001088953.2
PREDICTED: Xenopus laevis actin, beta L homeolog (actb.L), transcript variant X1, mRNA	574	574	99%	4e-160	100%	gil1069389028|XM_018234172.1
Xenopus laevis hypothetical protein MGC52661, mRNA (cDNA clone MGC:85343 IMAGE:6876400), complete cds	574	574	99%	4e-160	100%	gil54035187|BC084121.1
Xenopus laevis hypothetical protein MGC52661, mRNA (cDNA clone MGC:52661 IMAGE:4681586), complete cds	574	574	99%	4e-160	100%	gil27735426|BC041203.1
Xenopus laevis cytoplasmic beta actin mRNA, complete cds	574	574	99%	4e-160	100%	gil3348130|AF079161.1

Xenopus laevis actin, beta L homeolog (actb.L), mRNA
Sequence ID: gil1070257615|NM_001088953.2 Length: 1658 Number of Matches: 1

Range 1: 219 to 536 GenBank Graphics Next Match Previous Match

Score	Expect	Identities	Gaps	Strand
574 bits(636)	4e-160	318/318(100%)	0/318(0%)	Plus/Plus

```
Query  1    AGGAGATGAAGCTCAAAGCAAAAGAGGTATTCTTACACTCAAATATCCAATTGAACATGG  60
            ||||||||||||||||||||||||||||||||||||||||||||||||||||||||||||
Sbjct  219  AGGAGATGAAGCTCAAAGCAAAAGAGGTATTCTTACACTCAAATATCCAATTGAACATGG  278

Query  61   CATTGTCACCAACTGGGATGATATGGAGAAGATCTGGCATCACACCTTCTACAATGAACT  120
            ||||||||||||||||||||||||||||||||||||||||||||||||||||||||||||
Sbjct  279  CATTGTCACCAACTGGGATGATATGGAGAAGATCTGGCATCACACCTTCTACAATGAACT  338

Query  121  GCGAGTGGCACCAGAAGAACACCCAGTGCTGCTCACAGAAGCACCCCTGAATCCTAAAGC  180
            ||||||||||||||||||||||||||||||||||||||||||||||||||||||||||||
Sbjct  339  GCGAGTGGCACCAGAAGAACACCCAGTGCTGCTCACAGAAGCACCCCTGAATCCTAAAGC  398

Query  181  TAACAGGGAGAAGATGACACAGATAATGTTCGAGACCTTTAACACTCCAGCTATGTATGT  240
            ||||||||||||||||||||||||||||||||||||||||||||||||||||||||||||
Sbjct  399  TAACAGGGAGAAGATGACACAGATAATGTTCGAGACCTTTAACACTCCAGCTATGTATGT  458

Query  241  TGCCATCCAAGCTGTGTTGTCCCTGTATGCATCTGGTCGTACCACTGGTATTGTCATGGA  300
            ||||||||||||||||||||||||||||||||||||||||||||||||||||||||| |||
Sbjct  459  TGCCATCCAAGCTGTGTTGTCCCTGTATGCATCTGGTCGTACCACTGGTATTGTCATGGA  518

Query  301  CTCAGGTGATGGTGTAAC  318
            ||||||||||||||||||
Sbjct  519  CTCAGGTGATGGTGTAAC  536
```

Match for β-actin sequence

Col1A1
S: ATTCAACGGACCCTCTGGAC
AS: ATCTTCAGGTCACGGCAGGT
AS Compliment:
ACCTGCCGTGACCTGAAGAT

(12) Xela-Col1A1_user-added

Description	Max score	Total score	Query cover	E value	Ident	Accession
Xenopus laevis collagen, type I, alpha 1 S homeolog (col1a1.S), mRNA	529	624	100%	2e-146	100%	gi|1069984408|NM_001087352.2
Xenopus laevis collagen, type I, alpha 1, mRNA (cDNA clone MGC:52532 IMAGE:5572094), complete cds	529	624	100%	2e-146	100%	gi|29436388|BC049829.1
Xenopus laevis COL1A1 mRNA for type I collagen alpha 1, complete cds	506	552	100%	2e-139	95%	gi|7670049|AB034701.1
PREDICTED: Xenopus laevis collagen alpha-1(I) chain (LOC108700840), mRNA	484	586	100%	7e-133	97%	gi|1069390231|XM_018234828.1
Xenopus tropicalis collagen, type I, alpha 1 (col1a1), mRNA	425	560	100%	6e-115	94%	gi|58332411|NM_001011005.1

Xenopus laevis collagen, type I, alpha 1 S homeolog (col1a1.S), mRNA

Sequence ID: gi|1069984408|NM_001087352.2 **Length:** 5717 **Number of Matches:** 3

Range 1: 3456 to 3844 GenBank Graphics ▼ Next Match ▲ Previous Match

Score	Expect	Identities	Gaps	Strand
529 bits(586)	2e-146	389/389(100%)	0/389(0%)	Plus/Plus

```
Query  1     GTCCATCTGGTGCTTCTGGTCCTGCTGGTCCAAGAGGTCCCCCTGGATCTTCTGGCAATC  60
             ||||||||||||||||||||||||||||||||||||||||||||||||||||||||||||
Sbjct  3456  GTCCATCTGGTGCTTCTGGTCCTGCTGGTCCAAGAGGTCCCCCTGGATCTTCTGGCAATC  3515

Query  61    CTGGTAAAGATGGTTCTAATGGTCTGCCAGGACCTATTGGTCCCCCTGGTCCACGTGGTC  120
             ||||||||||||||||||||||||||||||||||||||||||||||||||||||||||||
Sbjct  3516  CTGGTAAAGATGGTTCTAATGGTCTGCCAGGACCTATTGGTCCCCCTGGTCCACGTGGTC  3575

Query  121   GTACTGGTGATGTtggtcctgctggtccccctggacctcctggtcctcctggtcctcctg  180
             ||||||||||||||||||||||||||||||||||||||||||||||||||||||||||||
Sbjct  3576  GTACTGGTGATGTTGGTCCTGCTGGTCCCCCTGGACCTCCTGGTCCTCCTGGTCCTCCTG  3635

Query  181   gCCAATCAGGTGGTGGATTCGACTTCAGCTTCATGCCTCAGCCACCTCAGGAGAAATCTC  240
             ||||||||||||||||||||||||||||||||||||||||||||||||||||||||||||
Sbjct  3636  GCCAATCAGGTGGTGGATTCGACTTCAGCTTCATGCCTCAGCCACCTCAGGAGAAATCTC  3695

Query  241   ATGATGGCCGCTTCTACCGTGCTGATGATGCCAATGTAATGCGCGACCGTGACCTGGAAG  300
             ||||||||||||||||||||||||||||||||||||||||||||||||||||||||||||
Sbjct  3696  ATGATGGCCGCTTCTACCGTGCTGATGATGCCAATGTAATGCGCGACCGTGACCTGGAAG  3755

Query  301   TTGACTCCACCCTCAAGAGTCTGAGCAAACAGATCGAAAACATCCGCAGCCCAGAGGGTA  360
             ||||||||||||||||||||||||||||||||||||||||||||||||||||||||||||
Sbjct  3756  TTGACTCCACCCTCAAGAGTCTGAGCAAACAGATCGAAAACATCCGCAGCCCAGAGGGTA  3815

Query  361   CCAGAAAGAACCCAGCCCGCACCTGCCGT  389
             |||||||||||||||||||||||||||||
Sbjct  3816  CCAGAAAGAACCCAGCCCGCACCTGCCGT  3844
```

Col1A1
S: ATTCAACGGACCCTCTGGAC
AS: ATCTTCAGGTCACGGCAGGT
AS Compliment:
ACCTGCCGTGACCTGAAGAT

(12) Xela-Col1A1_user-added

Confirmation that direct sequencing did not capture 5’ end of the amplicon

Collagen type I A2
S: AGCGTGGCTATCCTGGAAAC
AS: ATTCACCACCAAAGCCACCA
AS Compliment: TGGTGGCTTTGGTGGTGAAT

(9) Xela-Col1A2-1-M13For

Description	Max score	Total score	Query cover	E value	Ident	Accession
Xenopus laevis collagen type I alpha 2 L homeolog (col1a2.L), mRNA	915	1136	99%	0.0	100%	gi|147898762|NM_001087258.1
PREDICTED: Xenopus laevis collagen, type 1, alpha 2 L homeolog (col1a2.L), transcript variant X2, mRNA	906	1084	99%	0.0	99%	gi|1069362862|XM_018266289.1
PREDICTED: Xenopus laevis collagen, type 1, alpha 2 L homeolog (col1a2.L), transcript variant X1, mRNA	906	1084	99%	0.0	99%	gi|1069362860|XM_018266288.1
PREDICTED: Xenopus laevis collagen alpha-2(I) chain-like (LOC108719903), transcript variant X2, mRNA	796	1115	99%	0.0	95%	gi|1069368293|XM_018269186.1
PREDICTED: Xenopus laevis collagen alpha-2(I) chain-like (LOC108719903), transcript variant X1, mRNA	796	1115	99%	0.0	95%	gi|1069368291|XM_018269185.1

Xenopus laevis collagen type I alpha 2 L homeolog (col1a2.L), mRNA
Sequence ID: gi|147898762|NM_001087258.1 Length: 4428 Number of Matches: 6
▸See 1 more title(s)

Range 1: 2892 to 3398 GenBank Graphics ▼ Next Match ▲ Previous Match

Score	Expect	Identities	Gaps	Strand
915 bits(1014)	0.0	507/507(100%)	0/507(0%)	Plus/Plus

```
Query  1     AGCGTGGCTATCCTGGAAACAGTGGCCCTGCTGGATCTCTTGGTGCTTCTGGAGCTCCAG  60
Sbjct  2892  AGCGTGGCTATCCTGGAAACAGTGGCCCTGCTGGATCTCTTGGTGCTTCTGGAGCTCCAG  2951
Query  61    GAGCTGTTGGCCCTGCTGGAAAATCAGGAAACCGTGGGGAACCTGGTCCTGTTGGTCCTG  120
Sbjct  2952  GAGCTGTTGGCCCTGCTGGAAAATCAGGAAACCGTGGGGAACCTGGTCCTGTTGGTCCTG  3011
Query  121   CTGGAGTTGTTGGTCCTGCTGGTCCCAGAGGCCCAGCTGGAATTCAAGGTGGTCGTGGTG  180
Sbjct  3012  CTGGAGTTGTTGGTCCTGCTGGTCCCAGAGGCCCAGCTGGAATTCAAGGTGGTCGTGGTG  3071
Query  181   ACAAGGGTGAAGCTGGTGAGAAGGGAGCTAGAGGTTTGGATGGACGCAAAGGACATAATG  240
Sbjct  3072  ACAAGGGTGAAGCTGGTGAGAAGGGAGCTAGAGGTTTGGATGGACGCAAAGGACATAATG  3131
Query  241   GTTTACAAGGTCTCCCTGGTCCTGCTGGTTCTCCAGGAGAAACAGGTCCTGCTGGTACCA  300
Sbjct  3132  GTTTACAAGGTCTCCCTGGTCCTGCTGGTTCTCCAGGAGAAACAGGTCCTGCTGGTACCA  3191
Query  301   ATGGTCCATCTGGCCCACGGGGTCCAGCTGGCCCATCCGGCCCTCCAGGCAAAGAAGGAC  360
Sbjct  3192  ATGGTCCATCTGGCCCACGGGGTCCAGCTGGCCCATCCGGCCCTCCAGGCAAAGAAGGAC  3251
Query  361   GTTCTGGACACAGTGGTACTATCGGTCCAGTTGGTCTTCGTGGTCCTGCTGGTCACCAAG  420
Sbjct  3252  GTTCTGGACACAGTGGTACTATCGGTCCAGTTGGTCTTCGTGGTCCTGCTGGTCACCAAG  3311
Query  421   GTCCTGCTGGTCCTCCTGGACCACCTGGTCTTCCTGGTCTTCCTGGCTCATCTGGTGGTG  480
Sbjct  3312  GTCCTGCTGGTCCTCCTGGACCACCTGGTCTTCCTGGTCTTCCTGGCTCATCTGGTGGTG  3371
Query  481   GATATGATGGTGGCTTTGGTGGTGAAT  507
Sbjct  3372  GATATGATGGTGGCTTTGGTGGTGAAT  3398
```

Range 2: 2411 to 2478 GenBank Graphics ▼ Next Match ▲ Previous Match ▲ First Match

Score	Expect	Identities	Gaps	Strand
46.4 bits(50)	0.80	51/68(75%)	0/68(0%)	Plus/Plus

```
Query  249   GGTCTCCCTGGTCCTGCTGGTTCTCCAGGAGAAACAGGTCCTGCTGGTACCAATGGTCCA  308
Sbjct  2411  GGTTTCCCTGGTCCTGCTGGAAGAACTGGTGCTCCTGGCCCTGCTGGTACTGTTGGTCCT  2470
Query  309   TCTGGCCC  316
Sbjct  2471  TCTGGCCC  2478
```

Range 3: 2993 to 3051 GenBank Graphics ▼ Next Match ▲ Previous Match ▲ First Match

Score	Expect	Identities	Gaps	Strand
44.6 bits(48)	2.8	45/59(76%)	0/59(0%)	Plus/Plus

```
Query  255   CCTGGTCCTGCTGGTTCTCCAGGAGAAACAGGTCCTGCTGGTACCAATGGTCCATCTGG  313
Sbjct  2993  CCTGGTCCTGTTGGTCCTGCTGGAGTTGTTGGTCCTGCTGGTCCCAGAGGCCCAGCTGG  3051
```

Range 4: 3146 to 3204 GenBank Graphics ▼ Next Match ▲ Previous Match ▲ First Match

Score	Expect	Identities	Gaps	Strand
44.6 bits(48)	2.8	45/59(76%)	0/59(0%)	Plus/Plus

```
Query  102   CCTGGTCCTGTTGGTCCTGCTGGAGTTGTTGGTCCTGCTGGTCCCAGAGGCCCAGCTGG  160
Sbjct  3146  CCTGGTCCTGCTGGTTCTCCAGGAGAAACAGGTCCTGCTGGTACCAATGGTCCATCTGG  3204
```

Range 5: 2032 to 2109 GenBank Graphics ▼ Next Match ▲ Previous Match ▲ First Match

Score	Expect	Identities	Gaps	Strand
42.8 bits(46)	9.7	56/78(72%)	0/78(0%)	Plus/Plus

```
Query  68    TGGCCCTGCTGGAAAATCAGGAAACCGTGGGGAACCTGGTCCTGTTGGTCCTGCTGGAGT  127
Sbjct  2032  TGGCCATGCTGGAGAATATGGTAACCAAGGAAGAGATGGTTCTCGTGGTCCTGCTGGTGC  2091
Query  128   TGTTGGTCCTGCTGGTCC  145
Sbjct  2092  TTCCGGTGCTCCTGGTCC  2109
```

Range 6: 2591 to 2658 GenBank Graphics ▼ Next Match ▲ Previous Match ▲ First Match

Score	Expect	Identities	Gaps	Strand
42.8 bits(46)	9.7	50/68(74%)	0/68(0%)	Plus/Plus

```
Query  402   GGTCCTGCTGGTCACCAAGGTCCTGCTGGTCCTCCTGGACCACCTGGTCTTCCTGGTCTT  461
Sbjct  2591  GGTCCATCTGGTGAATCTGGTCCTGCTGGTGCTCCTGGCGCTTCTGGTCCTTCTGGTGTC  2650
Query  462   CCTGGCTC  469
Sbjct  2651  CTTGGTTC  2658
```

Primer sequences not detected in second to sixth alignment matches.

Match for Col1A2 sequence

Collagen type III
S: CTGGTGGTCGTGGTATTGTT
AS: TTAGATCCTGGTGGTCCTCTT
AS Compliment: AAGAGGACCACCAGGATCTAA

(7) Xela-ColIII-1-M13For

Description	Max score	Total score	Query cover	E value	Ident	Accession
Xenopus laevis collagen, type III, alpha 1 (Ehlers-Danlos syndrome type IV, autosomal dominant) S homeolog (col3a1.S), mRNA	1034	1123	99%	0.0	99%	gi|147905731|NM_001090075.1
PREDICTED: Xenopus laevis collagen alpha-1(III) chain-like (LOC108701482), mRNA	839	930	99%	0.0	92%	gi|1069392944|XM_018236216.1
Xenopus tropicalis collagen, type III, alpha 1 (Ehlers-Danlos syndrome type IV, autosomal dominant) (col3a1), mRNA	827	1012	99%	0.0	92%	gi|218847779|NM_001142907.1
PREDICTED: Nanorana parkeri collagen type IV alpha 3 chain (COL4A3), mRNA	484	532	98%	1e-132	79%	gi|1072253194|XM_018556079.1
PREDICTED: Castor canadensis collagen type III alpha 1 chain (Col3a1), mRNA	352	458	88%	5e-93	75%	gi|1147282182|XM_020167065.1

PREDICTED: Xenopus laevis collagen alpha-1(III) chain-like (LOC108701482), mRNA
Sequence ID: gi|1069392944|XM_018236216.1 Length: 5300 Number of Matches: 3

Range 1: 3018 to 3594 GenBank Graphics ▼ Next Match ▲ Previous Match

Score	Expect	Identities	Gaps	Strand
839 bits(930)	0.0	532/577(92%)	0/577(0%)	Plus/Plus

```
Query  2     CTGGTGGTCGTGGTATTGTTCGATTGCCTGGTTTACAAGGCAGACCAGGTGCTCCTGGCC  61
Sbjct  3018  CTGGTGGTCGTGGTATTGTTCGATTGCCTGGCTTACAAGGCAGAGCAGGTGCTCCTGGCA  3077
Query  62    TTTCAGGTTCTAAGGGTGAGGATGGAAAACCTGGTACCAATGGATCTCCTGGTGAACGTG  121
Sbjct  3078  TTCCAGGTTCAAAGGGCGAGGATGGAAAACCTGGTTCCAATGGATCTCCTGGTGAACGTG  3137
Query  122   GTCCTGCTGGTGCTCCTGGACCTGCTGGGCTTAATGGTGCACCTGGTGAAAGTGGCAGAG  181
Sbjct  3138  GTCTTGCTGGTTCTCCTGGGCCTGCCGGGCTTAATGGTGCTCCTGGGGAAAGTGGAAGAG  3197
Query  182   ATGGTAATTCTGGTTCTGATGGTTTGCCTGGACGTGATGGTTCCCATGGTCCTAAAGGAG  241
Sbjct  3198  ATGGCAATTCTGGTTCTGATGGTTTGCCTGGACGTGATGGTTCCTCTGGTCCTAAAGGAG  3257
Query  242   ATAGGGGTGAAAACGGATCTCCAGGTGCTCCTGGAGCTCCAGGCCATCCTGGTGCTCCCG  301
Sbjct  3258  ATCGGGGTGAAAATGGATCTCCAGGTTCTAATGGAGCTCCAGGTCATCCTGGTGCTCCAG  3317
Query  302   GTCCTGTTGGCCCAGCTGGAAAGCCTGGAGATAGAGGAGAAACTGGTCCGGCTGGTCTTT  361
Sbjct  3318  GTCCTGTTGGCCCAGCTGGAAAGTCGGGAGATAGAGGAGAAACTGGTCCATCTGGTCCTG  3377
Query  362   CAGGCCCTTCTGGCCCTGCTGGTGCTCGCGGTGCTCCTGGGGCCCAAGGACCACGTGGTG  421
Sbjct  3378  CAGGCCCTGCTGGCTCTGCTGGTGCTCGTGGTGCTCCTGGTCCCCAAGGATCACGTGGTG  3437
Query  422   ACAAAGGTGAAGCTRGTGAGCGTGGTACAAATGGAATCAAAGGTCATCGTGGTCATCCTG  481
Sbjct  3438  ATAAAGGTGAAGCTGGTGAGCGTGGTACAAATGGAATGAAAGGTCATCGTGGTCATCCTG  3497
Query  482   GTAATCCTGGTTTACCTGGTCCTCCTGGATCTTCAGGAGAACAAGGTACTGCTGGAAGCC  541
Sbjct  3498  GTAATCCTGGTTTACCTGGTCCTCCTGGATCTCCAGGAGAACAAGGTACTGCAGGAAGCC  3557
Query  542   AAGGTCCACAGGGCCCAAGAGGACCACCAGGATCTAA  578
Sbjct  3558  AAGGCCAACAGGGTCCAAGAGGACCACCAGGCTCTAA  3594
```

Range 2: 2776 to 2818 GenBank Graphics ▼ Next Match ▲ Previous Match ▲ First Match

Score	Expect	Identities	Gaps	Strand
46.4 bits(50)	0.92	36/43(84%)	0/43(0%)	Plus/Plus

```
Query  471   TGGTCATCCTGGTAATCCTGGTTTACCTGGTCCTCCTGGATCT  513
Sbjct  2776  TGGTTTTCCTGGTACTCGCGGGTTGCCTGGTCCTCCTGGATCT  2818
```

Range 3: 1310 to 1415 GenBank Graphics ▼ Next Match ▲ Previous Match ▲ First Match

Score	Expect	Identities	Gaps	Strand
44.6 bits(48)	3.2	75/108(69%)	2/108(1%)	Plus/Plus

```
Query  301   GGTCCTGTTGGCCCAGCTGGAAAGCCTGGAGATAGAGGAGAAACTGGTCCGGCTGGTCTT  360
Sbjct  1310  GGTCCTCCTGGTAGAGACGGAAATCCAGGCAACAAAGGAGAAGTGGGTCCCGGTGGTATA  1369
Query  361   TCAGGCCCTTCTGGCCCTGCTGGTGCTCGCGGTGCTCCTGGGGCCCAA  408
Sbjct  1370  CCTGGTGCTCCTGGACTGGCTGGTGCTCGTGGTCCACCT--GGCCCAA  1415
```

Primer sequences not detected in second and third alignment match

Match for Collagen type III sequence

CK 5
S: GTCATCAGCTCTGGAGGCAA
AS: TGCACAGACAATGCTTGAGAG
AS Compliment: CTCTCAAGCATTGTCTGTGCA

(4) Xela-CK5-3-M13For

Description	Max score	Total score	Query cover	E value	Ident	Accession
Xenopus laevis keratin 5, gene 5 L homeolog (krt5.5.L), mRNA	909	909	99%	0.0	99%	NM_001085584.1
Xenopus laevis larval keratin, mRNA (cDNA clone MGC:197259 IMAGE:9093918), complete cds	856	856	99%	0.0	98%	BC170532.1
PREDICTED: Xenopus tropicalis keratin 5, gene 5 (krt5.5), mRNA	368	368	64%	8e-98	87%	XM_002935730.2
Xenopus laevis keratin 5, gene 6 S homeolog (krt5.6.S), mRNA	335	335	83%	8e-88	82%	NM_001097714.1

Xenopus laevis keratin 5, gene 5 L homeolog (krt5.5.L), mRNA
Sequence ID: NM_001085584.1 **Length:** 2406 **Number of Matches:** 1
▶ See 1 more title(s)

Range 1: 1521 to 2021 GenBank Graphics ▼ Next Match ▲ Previous M

Score	Expect	Identities	Gaps	Strand
909 bits(492)	0.0	498/501(99%)	0/501(0%)	Plus/Plus

```
Query  1     GTCATCAGCTCTGGAGGCAAAAGTTCCCTaggaggaggaggaggaggTGGATCTGGAGCA  60
             ||||||||||||||||||||||||||||| ||||||||||||||||||||||||||||
Sbjct  1521  GTCATCAGCTCTGGAGGCAAAAGTTCCCTACGAGGAGGAGGAGGAGGTGGATCTGGAGCA  1580

Query  61    GGCTTCGGCTTtggaagtggtggtggaggctttggtggaagtggtggtggagccttcagt  120
             |||||||||||| |||||||||||||||||| |||||||||||||||||||||||||||
Sbjct  1581  GGCTTCGGCTTTGGAAGTGGTGGTGGAGGCTTCGGTGGAAGTGGTGGTGGAGCCTTCAGT  1640

Query  121   ggaagtggtggtggagcctttggtggaagtggtggcagtgcctttggtggcagtggcctt  180
             ||||||||||||||||||||||||||||||||||||||||||||||||||||||||||||
Sbjct  1641  GGAAGTGGTGGTGGAGCCTTTGGTGGAAGTGGTGGCAGTGCCTTTGGTGGCAGTGGCCTT  1700

Query  181   tcctttggcTCAGGAGGTGGCGGATTCAGCTCCTCAAGCTCCTCATTTGGTGGTGGCGTC  240
             ||||||||| ||||||||||||||||||||||||||||||||||||||||||||||||||
Sbjct  1701  TCCTTTGGCTCAGGAGGTGGCGGATTCAGCTCCTCAAGCTCCTCATTTGGTGGTGGCGTC  1760

Query  241   AGCAGCGGTGTGAGATTTTCTTCCAGCAAGTCCAGCTACAGGAGTTAATCAAGTCATGAA  300
             ||||||||||||||||||||||||||||||||||||||||||||||||||||||||||||
Sbjct  1761  AGCAGCGGTGTGAGATTTTCTTCCAGCAAGTCCAGCTACAGGAGTTAATCAAGTCATGAA  1820

Query  301   ATGAGGCAAATATCAGTGCCCAGAACACAATAATTCATTGCCTGTTAATACAGATACTGC  360
             ||||||||||||||||||||||||||||||||||||||||||||||||||||||||||||
Sbjct  1821  ATGAGGCAAATATCAGTGCCCAGAACACAATAATTCATTGCCTGTTAATACAGATACTGC  1880

Query  361   GCTTTCAGTTGCTGTAAACATTCTGTTCTGCAGATCCCATCCTCATGACTTTCTCTTTAA  420
             |||||||||||||||||||||||||||||||||||||||||||||||||||||||||||
Sbjct  1881  GCTTTCAGTTGCTGTAAACATTCTGTTCTGCAGATCCCATCCTCATGACTTTCTCTTTTA  1940

Query  421   AGCAAACACATGTTTCCACTAAGGCTTTTCCGCAATAAGGTGCTGTCATTCCATACTTGT  480
             ||||||||||||||||||||||||||||||||||||||||||||||||||||||||||||
Sbjct  1941  AGCAAACACATGTTTCCACTAAGGCTTTTCCGCAATAAGGTGCTGTCATTCCATACTTGT  2000

Query  481   CTCTCAAGCATTGTCTGTGCA  501
             |||||||||||||||||||||
Sbjct  2001  CTCTCAAGCATTGTCTGTGCA  2021
```

Match for CK5 sequence

CK 14
S: TTTTGACCGGTGGCACTTCT
AS: CAACTCCCACACTGGACCTG
AS Compliment: CAGGTCCAGTGTGGGAGTTG

(5) Xela-CK14-1-M13For (A)

Xenopus laevis keratin 14, type I L homeolog (krt14.L), mRNA
Sequence ID: gi|1070257542|NM_001166441.2 Length: 1762 Number of Matches: 1

Range 1: 624 to 1310 GenBank Graphics

Score	Expect	Identities	Gaps	Strand
1234 bits(1368)	0.0	686/687(99%)	0/687(0%)	Plus/Plus

```
Query  1     TTTTGACCGGTGGCACTTCTGTTACATCATCAGATTCCTCTGCCCCAGTCAACTATGAAC  60
             ||||||||||||||||||||||||||||||||||||||||||||||||||||||||||||
Sbjct  624   TTTTGACCGGTGGCACTTCTGTTACATCATCAGATTCCTCTGCCCCAGTCAACTATGAAC  683

Query  61    TTCAGCTGACAGATCTTAGAAACACAGTTGAGAGTCTAACTTTAGAAAACGTTAGATACG  120
             ||||||||||||||||||||||||||||||||||||||||||||||||||||||||||||
Sbjct  684   TTCAGCTGACAGATCTTAGAAACACAGTTGAGAGTCTAACTTTAGAAAACGTTAGATACG  743

Query  121   AGATTGAACTTGACAACATCAGAGGAGCAGCTGAAGAGCTTAAGACTAAGTATGAACTAG  180
             |||||||||||||||||||||||||||||||||||||||||| ||||||||||||||||||
Sbjct  744   AGATTGAACTTGACAACATCAGAGGAGCAGCTGAAGAGCTTAAGACCAAGTATGAACTAG  803

Query  181   AATTGGGAGTGAAATACCAACTGGACACAGATATTGCTGCAATGAAAAGGGATATTGAAA  240
             ||||||||||||||||||||||||||||||||||||||||||||||||||||||||||||
Sbjct  804   AATTGGGAGTGAAATACCAACTGGACACAGATATTGCTGCAATGAAAAGGGATATTGAAA  863

Query  241   CTGCTACTGATTTACGTACCACACTAGAACAAAGGTTTACCTCTGCACTGGATGATCTTG  300
             ||||||||||||||||||||||||||||||||||||||||||||||||||||||||||||
Sbjct  864   CTGCTACTGATTTACGTACCACACTAGAACAAAGGTTTACCTCTGCACTGGATGATCTTG  923

Query  301   ATTTCCTAAAGAAGACACATGAAGAGGAAATCACCACACTACAGAGCAAGCTGGGTGCTA  360
             ||||||||||||||||||||||||||||||||||||||||||||||||||||||||||||
Sbjct  924   ATTTCCTAAAGAAGACACATGAAGAGGAAATCACCACACTACAGAGCAAGCTGGGTGCTA  983

Query  361   CATCTGACACCTCTGTATCTCTTATTGAAGTGGATGCTGTTAAATCATTTGACCTCACCA  420
             ||||||||||||||||||||||||||||||||||||||||||||||||||||||||||||
Sbjct  984   CATCTGACACCTCTGTATCTCTTATTGAAGTGGATGCTGTTAAATCATTTGACCTCACCA  1043

Query  421   CTGCATTAAACAAACTGAGAGCAGAATATGAAAAATCTGTTCAGCAGCATAAAGAAGATG  480
             ||||||||||||||||||||||||||||||||||||||||||||||||||||||||||||
Sbjct  1044  CTGCATTAAACAAACTGAGAGCAGAATATGAAAAATCTGTTCAGCAGCATAAAGAAGATG  1103

Query  481   CAGAAGCCTACTTTAGAGCCAAGATTGAAGAAATAAGCAGTGAATCAGCAAAAACGTCAG  540
             ||||||||||||||||||||||||||||||||||||||||||||||||||||||||||||
Sbjct  1104  CAGAAGCCTACTTTAGAGCCAAGATTGAAGAAATAAGCAGTGAATCAGCAAAAACGTCAG  1163

Query  541   AAGTTGTGGCCACGGTTAAAACAGAAATTGCATCCACAAAGAAAGAATTGCAGACATATA  600
             ||||||||||||||||||||||||||||||||||||||||||||||||||||||||||||
Sbjct  1164  AAGTTGTGGCCACGGTTAAAACAGAAATTGCATCCACAAAGAAAGAATTGCAGACATATA  1223

Query  601   ACTCAGAACTACAGTCACTTCTTTCAGTGAATTACACACTTGAAAGCAGCTTGGCTGAAG  660
             ||||||||||||||||||||||||||||||||||||||||||||||||||||||||||||
Sbjct  1224  ACTCAGAACTACAGTCACTTCTTTCAGTGAATTACACACTTGAAAGCAGCTTGGCTGAAG  1283

Query  661   TAGTAGCCAGGTCCAGTGTGGGAGTTG  687
             |||||||||||||||||||||||||||
Sbjct  1284  TAGTAGCCAGGTCCAGTGTGGGAGTTG  1310
```

Match for CK14 sequence

	Max score	Total score	Query cover	E value	Ident	Accession
Xenopus laevis keratin 14, type I L homeolog (krt14.L), mRNA	1234	1234	100%	0.0	99%	gi|1070257542|NM_001166441.2
Xenopus laevis ouro2 mRNA for Ouroboros 2, complete cds	1234	1234	100%	0.0	99%	gi|260063817|AB299973.1
PREDICTED: Xenopus tropicalis thread biopolymer filament subunit gamma-like (LOC100489129), mRNA	996	996	99%	0.0	92%	gi|1062909489|XM_018094882.1
PREDICTED: Nanorana parkeri thread biopolymer filament subunit gamma-like (LOC108797612), mRNA	594	594	99%	1e-165	79%	gi|1072277461|XM_018569234.1
PREDICTED: Latimeria chalumnae thread biopolymer filament subunit gamma-like (LOC102360182), mRNA	282	282	97%	8e-72	70%	gi|557004528|XM_006004090.1

CK 19
S: CCAAGTCGGTGGACAAATTA
AS: CCATAACGGGCTTCTGTTT
AS Compliment: AAACAGAAGCCCGTTATGG

(6) Xela-CK19-1-M13For

Description	Max score	Total score	Query cover	E value	Ident	Accession
Xenopus laevis keratin 19 L homeolog (krt19.L), mRNA	565	565	100%	2e-157	99%	gi|148232402|NM_001091523.1
PREDICTED: Xenopus laevis keratin 19, type I L homeolog (krt19.L), transcript variant X1, mRNA	547	547	100%	6e-152	98%	gi|1069389200|XM_018234265.1
Xenopus tropicalis finished cDNA, clone TGas121l05	419	419	99%	2e-113	90%	gi|77621515|CR761861.2
PREDICTED: Xenopus tropicalis keratin 19, type I (krt19), transcript variant X1, mRNA	416	416	99%	2e-112	89%	gi|1062938298|XM_012971580.2
Xenopus tropicalis keratin 19 (krt19), mRNA	416	416	99%	2e-112	89%	gi|45360454|NM_203587.1

Xenopus laevis keratin 19 L homeolog (krt19.L), mRNA

Sequence ID: gi|148232402|NM_001091523.1 **Length:** 1545 **Number of Matches:** 1

▶ See 1 more title(s)

Range 1: 778 to 1093 GenBank Graphics ▼ Next Match ▲ Previous Match

Score	Expect	Identities	Gaps	Strand
565 bits(626)	2e-157	315/316(99%)	0/316(0%)	Plus/Plus

```
Query  1     CCAAGTCGGTGGACAAATTACGTTGAAGTGGATGCGGCGCCAACGGTGGACATTACTAA  60
             ||||||||||||||||||||||||||||||||||||||||||||||||||||||||||||
Sbjct  778   CCAAGTCGGTGGACAAATTACGTTGAAGTGGATGCGGCGCCAACGGTGGACATTACTAA  837

Query  61    GAGATTGACAGAAATGAGAGACCAGTATGAGCTCCTGGCAGAAAAGAACCGCAGAGATGC  120
             ||||||||||||||||||||||||||||||||||||||||||||||||||||||||||||
Sbjct  838   GAGATTGACAGAAATGAGAGACCAGTATGAGCTCCTGGCAGAAAAGAACCGCAGAGATGC  897

Query  121   AGAGGAATGGTTCTTCGCACAGTCCGAGGAGTTGAACAAAGAAGTGGCAACCCATACAGA  180
             ||||||||||||||||||||||||||||||||||||||||||||||||||||||||||||
Sbjct  898   AGAGGAATGGTTCTTCGCACAGTCCGAGGAGTTGAACAAAGAAGTGGCAACCCATACAGA  957

Query  181   ACAGATTCAGACCAGCAAATCGGAGATCACAGACCTGAGACGCACAATCCAGGGTCTGGA  240
             ||||||||||||||||||||||||||||||||||||||||||||||||||||||||||||
Sbjct  958   ACAGATTCAGACCAGCAAATCGGAGATCACAGACCTGAGACGCACAATCCAGGGTCTGGA  1017

Query  241   AATAGAATTGCAGTCACAGCTCAGCATGAAAGCCGCATTGGAAAACACACTTGGGCAAAC  300
             ||||||||||||||||||||||||||||||||||||||||||||||||| ||||||||||
Sbjct  1018  AATAGAATTGCAGTCACAGCTCAGCATGAAAGCCGCATTGGAAAACACACTGGGGCAAAC  1077

Query  301   AGAAGCCCGTTATGGA  316
             ||||||||||||||||
Sbjct  1078  AGAAGCCCGTTATGGA  1093
```

Match for CK19 sequence

Vimentin
S: CTGTCGGAAGCTGCTAATC
AS: CAACCTGTCCATCTCTTGTC
AS Compliment: GACAAGAGATGGACAGGTTG

(10) Xela-Vimentin-1-M13For

D	Max score	Total score	Query cover	E value	Ident	Accession
Xenopus laevis vimentin 4, mRNA (cDNA clone MGC:53233 IMAGE:5543495), complete cds	839	839	99%	0.0	99%	gi|28277304|BC045233.1
Xenopus laevis vimentin S homeolog (vim.S), mRNA	830	830	99%	0.0	99%	gi|148221984|NM_001087438.1
X. laevis Vim4 mRNA for vimentin	827	827	99%	0.0	99%	gi|65208|X16844.1
Xenopus laevis vimentin L homeolog (vim.L), mRNA	738	738	99%	0.0	95%	gi|148232219|NM_001087439.1
Xenopus laevis vimentin 1, mRNA (cDNA clone MGC:53668 IMAGE:4888155), complete cds	738	738	99%	0.0	95%	gi|28278762|BC045052.1

Xenopus laevis vimentin S homeolog (vim.S), mRNA
Sequence ID: gi|148221984|NM_001087438.1 Length: 1787 Number of Matches: 1
▸See 1 more title(s)

Range 1: 929 to 1396 GenBank Graphics ▼ Next Match ▲ Previous Match

Score	Expect	Identities	Gaps	Strand
830 bits(920)	0.0	465/468(99%)	0/468(0%)	Plus/Plus

```
Query  2     CTGTCGGAAGCTGCTAATCGCAACAATGAAGCTCTGCGTCAGGCTAAGCAGGATACCAAT  61
             ||||||||||||||||||| ||||||||||||||||||||||||||||||||||||||||
Sbjct  929   CTGTCGGAAGCTGCTAATCGCAACAATGAAGCTCTGCGTCAGGCTAAGCAGGATACCAAT  988

Query  62    GACTACCGCAGACAGATCCAGACTCTAACCTGCGAGATTGATGCAATGAAAGGATCTAAC  121
             ||||||||||||||||||||||||||||||||||||||||||||||||||||||||||||
Sbjct  989   GACTACCGCAGACAGATCCAGACTCTAACCTGCGAGATTGATGCAATGAAAGGATCTAAC  1048

Query  122   GAGTCTTACGAACGCCAAATGCGAGAAATGGAGGAGAACTTTGCCCTTGAAGCTGCTAAT  181
             ||||||||||||||||||||||||||||||||||||||||||||||||||||||||||||
Sbjct  1049  GAGTCTTACGAACGCCAAATGCGAGAAATGGAGGAGAACTTTGCCCTTGAAGCTGCTAAT  1108

Query  182   TATCAGGACACTATTCAACGGCTGCAAGAGGAGATCCAGAACATGAAGGAGGAGATGTCT  241
             |||||||||||||||||||| |||||||||| ||||||||||||||||||||||||||||
Sbjct  1109  TATCAGGACACTATTCAACGCCTGCAAGAGGAAATCCAGAACATGAAGGAGGAGATGTCT  1168

Query  242   CGGCACCTGAGAGAGTACCAGGATCTGCTCAATGTTAAGATGGCTCTTGATATTGAAATT  301
             ||||||||||||||||||||||||||||||||||||||||||||||||||||||||| |||
Sbjct  1169  CGGCACCTGAGAGAGTACCAGGATCTGCTCAATGTTAAGATGGCTCTTGATATTGAGATT  1228

Query  302   GCTACTTACAGGAAACTCCTGGAGGGAGAGGAGAGCAGAATTACCATTCCTGTACATTCC  361
             ||||||||||||||||||||||||||||||||||||||||||||||||||||||||||||
Sbjct  1229  GCTACTTACAGGAAACTCCTGGAGGGAGAGGAGAGCAGAATTACCATTCCTGTACATTCC  1288

Query  362   TTTTCTACAATGAGCCTGAGAGAAACCAACCGCGATTCTCACCCAGTGGACACTCATTCC  421
             ||||||||||||||||||||||||||||||||||||||||||||||||||||||||||||
Sbjct  1289  TTTTCTACAATGAGCCTGAGAGAAACCAACCGCGATTCTCACCCAGTGGACACTCATTCC  1348

Query  422   AAACGCACTCTGCTCATCAAGACTGTGGAGACAAGAGATGGACAGGTT  469
             ||||||||||||||||||||||| ||||||||||||||||||||||
Sbjct  1349  AAACGCACTCTGCTCATCAAGACTGTGGAGACAAGAGATGGACAGGTT  1396
```

Match for Vimentin sequence

CDH 1
S: ACAGTGAAGGGTTTGGACTATG
AS: CACCAGTCAGCTCTGCTTTAT
AS Compliment:
ATAAAGCAGAGCTGACTGGTG

(A01) Xela-CDH1-1-M13For

Description	Max score	Total score	Query cover	E value	Ident	Accession
PREDICTED: Xenopus laevis cadherin 1, type 1 S homeolog (cdh1.S), transcript variant X1, mRNA	1045	1045	100%	0.0	99%	gi|1069350080|XM_018259321.1
Xenopus laevis (clone: XTCAD-1) cadherin gene, complete cds	1045	1045	100%	0.0	99%	gi|609636|L29057.1
Xenopus laevis cadherin 1, type 1 S homeolog (cdh1.S), mRNA	1045	1045	100%	0.0	99%	gi|288557368|NM_001172232.1
X.laevis mRNA for E-cadherin	962	962	100%	0.0	97%	gi|455529|X75454.1
PREDICTED: Xenopus tropicalis cadherin 1, type 1, E-cadherin (epithelial) (cdh1), mRNA	847	847	100%	0.0	92%	gi|1062888027|XM_002935997.4

PREDICTED: Xenopus laevis cadherin 1, type 1 S homeolog (cdh1.S), transcript variant X1, mRNA
Sequence ID: gi|1069350080|XM_018259321.1 **Length:** 3055 **Number of Matches:** 1

Range 1: 1153 to 1736 GenBank Graphics ▼ Next Match ▲ Previous Match

Score	Expect	Identities	Gaps	Strand
1045 bits(1158)	0.0	582/584(99%)	0/584(0%)	Plus/Plus

```
Query  1     ACAGTGAAGGGTTTGGACTATGAGCTGAAGAAGCAGTATATTCTCTCAGTCATTGTGACA  60
             ||||||||||||||||||||||||||||||||||||||||||||||||||||||||||||
Sbjct  1153  ACAGTGAAGGGTTTGGACTATGAGCTGAAGAAGCAGTATATTCTGTCAGTCATTGTGACA  1212

Query  61    AACAAAGCTAACTTTTCTGTTCCACTGCAAACTTCAACTGCAACGGTGACTGTATCTGTC  120
             ||||||||||||||||||||||||||||||||||||||||||||||||||||||||||||
Sbjct  1213  AACAAAGCTAACTTTTCTGTTCCACTGCAAACTTCAACTGCAACGGTGACTGTATCTGTC  1272

Query  121   GAAGATGTAAACGAAGCCCCAATATTTTTACCACCAGTGAAAGAAGTTTCTGTGTCAGAG  180
             ||||||||||||||||||||||||||||||||||||||||||||||||||||||||||||
Sbjct  1273  GAAGATGTAAACGAAGCCCCAATATTTTTACCACCAGTGAAAGAAGTTTCTGTGTCAGAG  1332

Query  181   GATCTTCCCAGTGGCCAAGTTGTTGCTACCTATACCGCACAGGATCCAGACAAGGAACAG  240
             ||||||||||||||||||||||||||||||||||||||||||||||||||||||||||||
Sbjct  1333  GATCTTCCCAGTGGCCAAGTTGTTGCTACCTATACCGCACAGGATCCAGACAAGGAACAG  1392

Query  241   AACCAGAAGATAACTTACGTCATTGGAAATGACCCAGCAGGGTGGGTGTCGGTAAACAAA  300
             ||||||||||||||||||||||||||||||||||||||||||||||||||||||||||||
Sbjct  1393  AACCAGAAGATAACTTACGTCATTGGAAATGACCCAGCAGGGTGGGTGTCGGTAAACAAA  1452

Query  301   GATAATGGGATTGTCACTGGAAATGGCAATTTGGATCGGGAATCAAAATTTGTGCTAAAC  360
             ||||||||||||||||||||||||||||||||||||||||||||||||||||||||||||
Sbjct  1453  GATAATGGGATTGTCACTGGAAATGGCAATTTGGATCGGGAATCAAAATTTGTGCTAAAC  1512

Query  361   AACACCTACAAAGTCATAATCCTGGCTGCTGACAGTGGCTCTCCTTCAGCCACTGGGACT  420
             ||||||||||||||||||||||||||||||||||||||||||||||||||||||||||||
Sbjct  1513  AACACCTACAAAGTCATAATCCTGGCTGCTGACAGTGGCTCTCCTTCAGCCACTGGGACT  1572

Query  421   GGAACCCTTGTGCTTAATCTCCTTGATGTTAATGATAATGGACCATTTTTGGAGCCCCAA  480
             ||||||||||||||||||||||||||||||||||||||||||||||||||||||||||||
Sbjct  1573  GGAACCCTTGTGCTTAATCTCCTTGATGTTAATGATAACGGACCATTTTTGGAGCCCCAA  1632

Query  481   CAAGAAAGTTTCTGCCAGAAGGATCCAGGCTTTCGTGTATTTACTATCATTGACAGAGAT  540
             ||||||||||||||||||||||||||||||||||||||||||||||||||||||||||||
Sbjct  1633  CAAGAAAGTTTCTGCCAGAAGGATCCAGGCTTTCGTGTATTTACTATCATTGACAGAGAT  1692

Query  541   CTCTCCCCTAACACATACCCGTATAAAGCAGAGCTGACTGGTGA  584
             ||||||||||||||||||||||||||||||||||||||||||||
Sbjct  1693  CTCTCCCCTAACACATACCCGTATAAAGCAGAGCTGACTGGTGA  1736
```

Match for CDH1 sequence

CLDN 1
S:CTGGGCTGGATTGGGTTTATAG
AS: CTACTCCAACCTTTGCCTTCTT
AS Compliment:
AAGAAGGCAAAGGTTGGAGTAG

(8) Xela-CLDN1-4-M13For

Description	Max score	Total score	Query cover	E value	Ident	Accession
PREDICTED: Xenopus laevis claudin-1-like (LOC108716970), mRNA	843	843	99%	0.0	99%	gi|1069357925|XM_018263594.1
Xenopus laevis claudin 1 S homeolog (cldn1.S), mRNA	767	767	99%	0.0	96%	gi|148222887|NM_001085976.1
Xenopus tropicalis claudin 1 (cldn1), mRNA	735	735	99%	0.0	95%	gi|62751356|NM_001015704.1
PREDICTED: Nanorana parkeri claudin 1 (CLDN1), mRNA	437	437	99%	1e-118	81%	gi|1072245017|XM_018576390.1
CTED: Chelonia mydas claudin 1 (CLDN1), mRNA	185	185	92%	1e-42	70%	gi|591366095|XM_007057847.1

PREDICTED: Xenopus laevis claudin-1-like (LOC108716970), mRNA

Sequence ID: gi|1069357925|XM_018263594.1 **Length:** 2828 **Number of Matches:** 1

Range 1: 242 to 711 GenBank Graphics ▼ Next Match ▲ Previous Match

Score	Expect	Identities	Gaps	Strand
843 bits(934)	0.0	469/470(99%)	0/470(0%)	Plus/Plus

```
Query  1    CTGGGCTGGATTGGGTTTATAGTATGTATTGCAATCCCTCAATGGAAAATGTCATCGTTT  60
            ||||||||||||||||||||| ||||||||||||||||||||||||||||||||||||
Sbjct  242  CTGGGCTGGATTGGGTTTATAGTATGTATTGCAATCCCTCAATGGAAAATGTCATCGTTT  301

Query  61   GCTGGGGATGCCATTATCACAGCACAGATAACCTATGAAGGACTCTGGATGTCTTGTGTA  120
            ||||||||||||||||||||||||||||||||||||||||||||||||||||||||||||
Sbjct  302  GCTGGGGATGCCATTATCACAGCACAGATAACCTATGAAGGACTCTGGATGTCTTGTGTA  361

Query  121  ATGCAGAGCACAGGGCAGATGCAGTGTAAATCCTTTGACTCATTGCTGAAGATGGACAGC  180
            ||||||||||||||||||||||||||||||||||||||||||||||||||||||||||||
Sbjct  362  ATGCAGAGCACAGGGCAGATGCAGTGTAAATCCTTTGACTCATTGCTGAAGATGGACAGC  421

Query  181  ACTATGCAGGCCACCCGAGCACTGATGATCTGTGGGATTCTTGTTGGTTTCTTTGCAATG  240
            ||||||||||||||||||||||||||||||||||||||||||||||||||||||||||||
Sbjct  422  ACTATGCAGGCCACCCGAGCACTGATGATCTGTGGGATTCTTGTTGGTTTCTTTGCAATG  481

Query  241  TGTATTGCTGCAGTAGGGATGAAATGCTTGACATGTCTTCAAGATGATGAAGTAAAGAAG  300
            ||||||||||||||||||||||||||||||||||||||||||||||||||| |||||||
Sbjct  482  TGTATTGCTGCAGTAGGGATGAAATGCTTGACATGTCTTCAAGATGATGAAGTAAAGAAG  541

Query  301  GCAAAGGTTGGAGTAGTGGGTGGAGCACTCTTCATTGTTGCTGGTCTCTGTGTTTTGATA  360
            |||||||||||||||| ||||||||||||||||||||||||||||||||||||||||||
Sbjct  542  GCAAAGGTTGGAGTAGTGGGTGGAGCACTCTTCATTGTTGCTGGTCTCTGTGTTTTGATA  601

Query  361  GCAACAAGCTGGTATGGAAATAAAATCGCAAAGGATTTTTACAATGTGTTCACACCAACC  420
            ||||||||||||||||||||||||||||||||||||||||||||||||||||||||||||
Sbjct  602  GCAACAAGCTGGTATGGAAATAAAATCGCAAAGGATTTTTACAATGTGTTCACACCAACC  661

Query  421  AATTCTAAATATGAGTTTGGTCCTGCCTTATTTATTGGATGGGCTGGAGC  470
            ||||||||||||||||||||||||||||||||||||||||||||||||| ||
Sbjct  662  AATTCTAAATATGAGTTTGGTCCTGCCTTATTTATTGGATGGGCTGGGGC  711
```

```
CLDN1_AS1       ------------------------------------------------------------
CLDN1_S1        CTGGGCTGGATTGGGTTTATAG------------------------------------
759195_XelaCLDN1 CTGGGCTGGATTGGGTTTATAGTATGTATTGCAATCCCTCAATGGAAAATGTCATCGTTT

CLDN1_AS1       ------------------------------------------------------------
CLDN1_S1        ------------------------------------------------------------
759195_XelaCLDN1 GCTGGGGATGCCATTATCACAGCACAGATAACCTATGAAGGACTCTGGATGTCTTGTGTA

CLDN1_AS1       ------------------------------------------------------------
CLDN1_S1        ------------------------------------------------------------
759195_XelaCLDN1 ATGCAGAGCACAGGGCAGATGCAGTGTAAATCCTTTGACTCATTGCTGAAGATGGACAGC

CLDN1_AS1       ------------------------------------------------------------
CLDN1_S1        ------------------------------------------------------------
759195_XelaCLDN1 ACTATGCAGGCCACCCGAGCACTGATGATCTGTGGGATTCTTGTTGGTTTCTTTGCAATG

CLDN1_AS1       ----------------------------------------------------AAGAAG
CLDN1_S1        ------------------------------------------------------------
759195_XelaCLDN1 TGTATTGCTGCAGTAGGGATGAAATGCTTGACATGTCTTCAAGATGATGAAGTAAAGAAG

CLDN1_AS1       GCAAAGGTTGGAGTAG------------------------------------------
CLDN1_S1        ------------------------------------------------------------
759195_XelaCLDN1 GCAAAGGTTGGAGTAGTGGGTGGAGCACTCTTCATTGTTGCTGGTCTCTGTGTTTTGATA

CLDN1_AS1       ------------------------------------------------------------
CLDN1_S1        ------------------------------------------------------------
759195_XelaCLDN1 GCAACAAGCTGGTATGGAAATAAAATCGCAAAGGATTTTTACAATGTGTTCACACCAACC

CLDN1_AS1       ----------------------------------------------------
CLDN1_S1        ----------------------------------------------------
759195_XelaCLDN1 AATTCTAAATATGAGTTTGGTCCTGCCTTATTTATTGGATGGGCTGGAGCA
```

CLDN 3
S:GGATGGATAGGAAGTGTGGTATG
AS: GTTGACCTGGCAGCTGTATAA
AS Compliment:
TTATACAGCTGCCAGGTCAAC

(C01) Xela-CLDN3-1-M13For

	Description	Max score	Total score	Query cover	E value	Ident	Accession
☐	Xenopus laevis claudin 3 L homeolog (cldn3.L), mRNA	1016	1016	99%	0.0	100%	gi|148227414|NM_001093931.1
☐	Xenopus tropicalis claudin 3 (cldn3), mRNA	801	801	100%	0.0	91%	gi|54020931|NM_001005709.1
☐	PREDICTED: Xenopus laevis claudin-3-like (LOC108709321), mRNA	787	787	97%	0.0	92%	gi|1069331042|XM_018249057.1
☐	PREDICTED: Nanorana parkeri claudin 3 (CLDN3), mRNA	520	520	95%	2e-143	81%	gi|1072262721|XM_018561247.1
☐	Xenopus tropicalis claudin 4, mRNA (cDNA clone MGC:197488 IMAGE:9040019), complete cds	381	381	91%	1e-101	76%	gi|213624187|BC170761.1

Xenopus laevis claudin 3 L homeolog (cldn3.L), mRNA
Sequence ID: gi|148227414|NM_001093931.1 Length: 2908 Number of Matches: 1
See 1 more title(s)

Range 1: 421 to 983 GenBank Graphics Next Match Previous Match

Score	Expect	Identities	Gaps	Strand
1016 bits(1126)	0.0	563/563(100%)	0/563(0%)	Plus/Plus

```
Query  2    GGATGGATAGGAAGTGTGGTATGCTGCGCTTTACCTATGTGGAGAGTAACTGCCTTCATT  61
            ||||||||||||||||||||||||||||||||||||||||||||||||||||||||||||
Sbjct  421  GGATGGATAGGAAGTGTGGTATGCTGCGCTTTACCTATGTGGAGAGTAACTGCCTTCATT  480

Query  62   GGAAACAACATTGTCGTTGCCCAAACTATTTGGGAAGGACTGTGGATGAACTGTGTGGTG  121
            ||||||||||||||||||||||||||||||||||||||||||||||||||||||||||||
Sbjct  481  GGAAACAACATTGTCGTTGCCCAAACTATTTGGGAAGGACTGTGGATGAACTGTGTGGTG  540

Query  122  CAGAGCACGGGGCAAATGCAATGCAAAGTGTATGACTCGCTATTAGCTCTTCCTCAAGAT  181
            ||||||||||||||||||||||||||||||||||||||||||||||||||||||||||||
Sbjct  541  CAGAGCACGGGGCAAATGCAATGCAAAGTGTATGACTCGCTATTAGCTCTTCCTCAAGAT  600

Query  182  CTTCAGGCAGCTCGCGCCCTGATTGTGATCTCAATTGTAATTGCTGTGCTGGGAGTTCTC  241
            ||||||||||||||||||||||||||||||||||||||||||||||||||||||||||||
Sbjct  601  CTTCAGGCAGCTCGCGCCCTGATTGTGATCTCAATTGTAATTGCTGTGCTGGGAGTTCTC  660

Query  242  ATTTCAATCATTGGTGCTAAGTGCACAAATTGTGTTCAGGATGAGTCAGCTAAAGCCAAA  301
            ||||||||||||||||||||||||||||||||||||||||||||||||||||||||||||
Sbjct  661  ATTTCAATCATTGGTGCTAAGTGCACAAATTGTGTTCAGGATGAGTCAGCTAAAGCCAAA  720

Query  302  ATTATGATTGTGTCTGGAGTTATTTTTATCCTTGCTGGACTGATGACACTTATCCCTGTG  361
            ||||||||||||||||||||||||||||||||||||||||||||||||||||||||||||
Sbjct  721  ATTATGATTGTGTCTGGAGTTATTTTTATCCTTGCTGGACTGATGACACTTATCCCTGTG  780

Query  362  TCCTGGTCTGCAAACACTATAATCCGTGATTTCTACAATCCTTTGGTAGTGGATGCACAA  421
            ||||||||||||||||||||||||||||||||||||||||||||||||||||||||||||
Sbjct  781  TCCTGGTCTGCAAACACTATAATCCGTGATTTCTACAATCCTTTGGTAGTGGATGCACAA  840

Query  422  AAGAGAGAGCTTGGCTCCTCAATGTACCTTGGATGGGCAGCCTCTGCTCTTCTTATGCTT  481
            ||||||||||||||||||||||||||||||||||||||||||||||||||||||||||||
Sbjct  841  AAGAGAGAGCTTGGCTCCTCAATGTACCTTGGATGGGCAGCCTCTGCTCTTCTTATGCTT  900

Query  482  GGAGGAGCAATGCTCTGCTGTTCTTGCCCCCCAAAAGACAAGTACCCTCCTTCAAGAGTG  541
            ||||||||||||||||||||||||||||||||||||||||||||||||||||||||||||
Sbjct  901  GGAGGAGCAATGCTCTGCTGTTCTTGCCCCCCAAAAGACAAGTACCCTCCTTCAAGAGTG  960

Query  542  GCTTATACAGCTGCCAGGTCAAC  564
            |||||||||||||||||||||||
Sbjct  961  GCTTATACAGCTGCCAGGTCAAC  983
```

Match for CLDN3 sequence

OCLN
S: CTTCTGGATCGGCTTTCTACAC
AS: GGCAGACTCTCCTCCTGTATTA
AS Compliment:
TAATACAGGAGGAGAGTCTGCC

(D01) Xela-OCLN-1-M13For

Description	Max score	Total score	Query cover	E value	Ident	Accession
Synthetic construct Xenopus laevis MGC81923 protein, mRNA (cDNA clone MGC:81923 IMAGE:7009477), complete cds	1052	1052	99%	0.0	99%	gi|51704032|BC081061.1
PREDICTED: Xenopus laevis occludin-like (LOC108717687), transcript variant X2, mRNA	1034	1034	99%	0.0	99%	gi|1069314444|XM_018264949.1
PREDICTED: Xenopus laevis occludin-like (LOC108717687), transcript variant X1, mRNA	1034	1034	99%	0.0	99%	gi|1069314442|XM_018264940.1
Xenopus laevis occludin S homeolog (ocln.S), mRNA	874	874	99%	0.0	93%	gi|147900541|NM_001088474.1
PREDICTED: Xenopus laevis occludin S homeolog (ocln.S), transcript variant X2, mRNA	868	868	99%	0.0	93%	gi|1069317306|XM_018234248.1

Xenopus laevis occludin S homeolog (ocln.S), mRNA

Sequence ID: gi|147900541|NM_001088474.1 Length: 1821 Number of Matches: 1

See 1 more title(s)

Range 1: 584 to 1173 GenBank Graphics Next Match Previous Match

Score	Expect	Identities	Gaps	Strand
874 bits(968)	0.0	548/590(93%)	3/590(0%)	Plus/Plus

```
Query  1     CTTCTGGATCGGCTTTCTACACCAGATTGTGTCAATATGCAACCAGTTCTATTCCCCAG  60
             ||||||||||||||||||||||||||||||| |||||||||||||||||||||||||||
Sbjct  584   CTTCTGGATCGGCTTTCTACACCAGATTGTGTCCATATGCAACCAGTTCTATTCCCCGG  643

Query  61    TACAAACCGGAGTATTTGTGAATCAATATCTTTATCACTACTGTGTGGTAGAGCCCCAAG  120
             ||||||| ||||| ||||| ||||||||||||||||||||||||||||||||||||||||
Sbjct  644   TACAAACTGGAGTGTTTGTTAATCAATATCTTTATCACTACTGTGTGGTAGAGCCCCAAG  703

Query  121   AGGCAATTGCCATAGTCCTGGGGTTCTTGATTGTTGTGGCCTTTGCCATTATTATATTCT  180
             ||||||||| |||||||| ||||||||||||||||||||||||||||||||| ||||||
Sbjct  704   AGGCAATTGCAATAGTCCTTGGGTTCTTGATTGTTGTGGCCTTTGCCATTATTATCTTCT  763

Query  181   TTGCTGTAAAAACCCGAAAAAAGATCGGTCAGTATGGCAAAGCAAACATCCTCTGGAAGA  240
             |||||||||| ||||| |||||||||   |||||||||| ||||||||||||||||||||
Sbjct  764   TTGCTGTAAAGACCCGGAAAAAAGATCAACCAGTATGGCAAAACAAACATCCTCTGGAAGA  823

Query  241   AAAACCACGTTCATGAAGATGGAGATCCTCAAGTTGAACAATGGGTTAAAAATGTAACTG  300
             |||||||| || |||||||||| ||||||||||||||||||||||||||||||| |||||
Sbjct  824   AAAACCACATTTATGAAGATGGGGATCCTCAAGTTGAACAATGGGTTAAAAATGTAGCTG  883

Query  301   CAACTTCAGCACCTGCCTTGTCTGATTACAATGAGAAAACCAATGGCTCAGTAGCGGACT  360
               || |||||||||||||||||||||||||||| ||| | |||| || ||||||||||
Sbjct  884   AAAATTCAGCACCTGCCTTGTCTGATTACAATGAAAAAGTCGATGGTTCTGTAGCGGACT  943

Query  361   ATAGAAGTGGATATGGGGTTCAGGCTTACCCATCTCAG---AACATCTCTCATCCGATAC  417
             |||||||| | |||||||||| || |||||||| |||   |||||||||||||||||||
Sbjct  944   ATAGAAGTGCAAATGGGGTTCAAGCCTACCCATCACAGAACAACATCTCTCATCCGATAG  1003

Query  418   CAGAGGAGGAGTTGCCTTTGAAAGAAGACTATGGAATGTCCCCACGTGCTTACAGCAGTA  477
             |||||||||||||||||||||||||||||||||||||||||||||||| ||||||||||
Sbjct  1004  CAGAGGAGGAGTTGCCTTTGAAAGAAGACTATGGAATGTCCCCACGTCATTACAGCAGTA  1063

Query  478   GTTCCGATGCCACAAGCAAGAAGGCGCCTCCTAAGAAGCGGCCAGGAAAGCCCAGGAGGT  537
             |||| |||||||| |||||| ||||||||||||||||||||||||||||||||||||||
Sbjct  1064  GTTCTGATGCCACAACCAAGAAAGCGCCTCCTAAGAAGCGGCCAGGAAAGCCCAGGAGGT  1123

Query  538   CCGACATTGATACCAATGAAGGAGGCTATAATACAGGAGGAGAGTCTGCC  587
             ||||| |||||||||||||||||| ||||||||||||||||||||||||
Sbjct  1124  CCGACCTTGATACCAATGAAGGAGGTTATAATACAGGAGGAGAGTCTGCC  1173
```

Match for OCLN sequence

Appendix D – Sequence confirmation of antiviral and proinflammatory genes

EF1a
S: GTTCATTTACCGCACAGGTTATC
AS: CGGCGATCAATCTTCTCCTT
AS Compliment:
AAGGAGAAGATTGATCGCCG

(E01+F01) Xela-EF1a-1)-6)-M13For

Description	Max score	Total score	Query cover	E value	Ident	Accession
Xenopus laevis eukaryotic translation elongation factor 1 alpha 1 L homeolog (eef1a1.L), mRNA	241	241	99%	4e-60	100%	gi|148233182|NM_001087442.1
X. laevis EF-1alpha mRNA for elongation factor 1-alpha	241	241	99%	4e-60	100%	gi|64654|X55324.1
PREDICTED: Xenopus laevis elongation factor 1-alpha, somatic form (LOC108704161), transcript variant X9, mRNA	223	223	99%	1e-54	97%	gi|1069304764|XM_018240577.1
PREDICTED: Xenopus laevis elongation factor 1-alpha, somatic form (LOC108704161), transcript variant X8, mRNA	223	223	99%	1e-54	97%	gi|1069304762|XM_018240576.1
PREDICTED: Xenopus laevis elongation factor 1-alpha, somatic form (LOC108704161), transcript variant X7, mRNA	223	223	99%	1e-54	97%	gi|1069304760|XM_018240575.1

Xenopus laevis eukaryotic translation elongation factor 1 alpha 1 L homeolog (eef1a1.L), mRNA
Sequence ID: gi|148233182|NM_001087442.1 Length: 1730 Number of Matches: 1
See 1 more title(s)

Range 1: 1059 to 1191 GenBank Graphics Next Match Previous Match

Score	Expect	Identities	Gaps	Strand
241 bits(266)	4e-60	133/133(100%)	0/133(0%)	Plus/Plus

```
Query  1     GTTCATTTACCGCACAGGTTATCATCCTGAACCACCCAGGCCAGATTGGTGCTGGATATG  60
             ||||||||||||||||||||||||||||||||||||||||||||||||||||||||||||
Sbjct  1059  GTTCATTTACCGCACAGGTTATCATCCTGAACCACCCAGGCCAGATTGGTGCTGGATATG  1118

Query  61    CCCCTGTGTTGGATTGTCACACTGCTCACATTGCTTGCAAGTTTGCTGAGCTCAAGGAGA  120
             ||||||||||||||||||||||||||||||||||||||||||||||||||||||||||||
Sbjct  1119  CCCCTGTGTTGGATTGTCACACTGCTCACATTGCTTGCAAGTTTGCTGAGCTCAAGGAGA  1178

Query  121   AGATTGATCGCCG  133
             |||||||||||||
Sbjct  1179  AGATTGATCGCCG  1191
```

```
753123EF1a-1   ------------------------------------------------------------
753124EF1a-6   ------------------------------------------------------------
NM_001087442.1 TGACAACGTTGGTTTTAACGTCAAGAACGTATCTGTGAAGGACGTCCGTCGTGGCAACGT

753123EF1a-1   ----------------------------------GTTCATTTACCGCACAGGTTAT
753124EF1a-6   ----------------------------------GTTCATTTACCGCACAGGTTAT
NM_001087442.1 TGCTGGTGACAGCAAGAATGACCCACCAATGGAAGCTGTTCATTTACCGCACAGGTTAT
                                                  **********************

753123EF1a-1   CATCCTGAATCACCCAGGCCAGATTGGTGCTGGATATGCCCCTGTGTTGGATTGCCACAC
753124EF1a-6   CATCCTGAACCACCCAGGCCAGATTGGTGCTGGATATGCCCCTGTGTTGGATTGTCACAC
NM_001087442.1 CATCCTGAACCACCCAGGCCAGATTGGTGCTGGATATGCCCCTGTGTTGGATTGTCACAC
               ********* ********************************************* *****

753123EF1a-1   TGCTCACATTGCTTGCAAGTTTGCTGAGCTAAAGGAGAAGATTGATCGCCGA--------
753124EF1a-6   TGCTCACATTGCTTGCAAGTTTGCTGAGCTCAAGGAGAAGATTGATCGCCGA--------
NM_001087442.1 TGCTCACATTGCTTGCAAGTTTGCTGAGCTCAAGGAGAAGATTGATCGCCGTTCTGGTAA
               ***************************** ********************

753123EF1a-1   ------------------------------------------------------------
753124EF1a-6   ------------------------------------------------------------
NM_001087442.1 GAAACTGGAAGACAATCCCAAGTTCCTGAAGTCTGGTGATGCTGCCATTGTTGACATGAT
```

Match for EF1a sequence

IFN type I
S: GCTGCTCCTGCTCAGTCTCA
AS: GAAAGCCTTCAGGATCTGTGTGT
AS Compliment:
ACACACAGATCCTGAAGGCTTTC

(G01) Xela-IFNtypeI-5-M13For

Description	Max score	Total score	Query cover	E value	Ident	Accession
Xenopus laevis isolate ifn6 type I interferon 6 gene, complete cds	143	143	100%	4e-31	99%	gi|1042727086|KU594566.1
Xenopus laevis type I interferon (IFN) mRNA, complete cds	143	143	100%	4e-31	99%	gi|597437485|KF597522.1
Xenopus laevis isolate ifn7 type I interferon 7 gene, complete cds	138	138	98%	2e-29	98%	gi|1042727088|KU594567.1
Xenopus laevis isolate ifn4 type I interferon 4 gene, complete cds	134	134	100%	2e-28	96%	gi|1042727082|KU594564.1
Xenopus tropicalis isolate ifn7 type I interferon 7 gene, complete cds	134	134	100%	2e-28	96%	gi|1042726988|KU594517.1

Xenopus laevis type I interferon (IFN) mRNA, complete cds

Sequence ID: gi|597437485|KF597522.1 **Length:** 829 **Number of Matches:** 1

Range 1: 72 to 172 GenBank Graphics ▼ Next Match ▲ Previous Match

Score	Expect	Identities	Gaps	Strand
178 bits(196)	3e-41	100/101(99%)	0/101(0%)	Plus/Plus

```
Query  1    TGCTGCTCCTGCTCAGTCTCACGTCTATTGTCCATTCCCAAAGCTGCAAATGGCTTCACC  60
            ||||||||||||||||||||| ||||||||||||||||||||| ||||||||||||||||
Sbjct  72   TGCTGCTCCTGCTCAGTCTCACGTCTATTGTCCATTCCCAAAGTTGCAAATGGCTTCACC  131

Query  61   CCAAACAAGAATATCTCAACACACAGATCCTGAAGGCTTTC  101
            |||||||||||||||||||||||||||||||||||||||||
Sbjct  132  CCAAACAAGAATATCTCAACACACAGATCCTGAAGGCTTTC  172
```

Match for IFN type I sequence

Mx2
S: GGAACGCCGCACTTGCAGAA
AS: CGATTAATCCTGGCACCTCC
AS Compliment:
GGAGGTGCCAGGATTAATCG

(C02) Xela-Mx2-3-M13For

Description	Max score	Total score	Query cover	E value	Ident	Accession
PREDICTED: Xenopus laevis dynamin 2 L homeolog (dnm2.L), transcript variant X1, mRNA	508	508	99%	4e-143	100%	XM_018250537.1
Xenopus laevis dynamin 2 L homeolog (dnm2.L), mRNA	503	503	99%	2e-141	99%	NM_001089804.1
PREDICTED: Xenopus laevis dynamin-2 (LOC108703474), transcript variant X3, mRNA	431	431	99%	8e-120	95%	XM_018239603.1
PREDICTED: Xenopus laevis dynamin-2 (LOC108703474), transcript variant X2, mRNA	431	431	99%	8e-120	95%	XM_018239602.1
PREDICTED: Xenopus laevis dynamin-2 (LOC108703474), transcript variant X1, mRNA	431	431	99%	8e-120	95%	XM_018239601.1

PREDICTED: Xenopus laevis dynamin 2 L homeolog (dnm2.L), transcript variant X1, mRNA

Sequence ID: XM_018250537.1 **Length:** 2968 **Number of Matches:** 1

Range 1: 971 to 1245 GenBank Graphics ▼ Next Match ▲ Previous Match

Score	Expect	Identities	Gaps	Strand
508 bits(275)	4e-143	275/275(100%)	0/275(0%)	Plus/Plus

```
Query  2     GGAACGCCGCACTTGCAGAAATCGCTCAACCAGCAACTAACCAATCACATCCGAGACACA  61
             ||||||||||||||||||||||||||||||||||||||||||||||||||||||||||||
Sbjct  971   GGAACGCCGCACTTGCAGAAATCGCTCAACCAGCAACTAACCAATCACATCCGAGACACA  1030

Query  62    CTGCCTGCCCTGCGCAACAAACTGCAGAGCCAATTGCTGTCTCTGGAGAAGGAAGTAGAG  121
             ||||||||||||||||||||||||||||||||||||||||||||||||||||||||||||
Sbjct  1031  CTGCCTGCCCTGCGCAACAAACTGCAGAGCCAATTGCTGTCTCTGGAGAAGGAAGTAGAG  1090

Query  122   GAATATAAGAACTTCCGGCCAGATGACCCCACGAGGAAAACCAAAGCTCTGCTGCAAATG  181
             ||||||||||||||||||||||||||||||||||||||||||||||||||||||||||||
Sbjct  1091  GAATATAAGAACTTCCGGCCAGATGACCCCACGAGGAAAACCAAAGCTCTGCTGCAAATG  1150

Query  182   GTCCAACAGTTTGGAGTGGATTTTGAGAAAAGGATTGAGGGCTCCGGAGATCAAGTGGAT  241
             ||||||||||||||||||||||||||||||||||||||||||||||||||||||||||||
Sbjct  1151  GTCCAACAGTTTGGAGTGGATTTTGAGAAAAGGATTGAGGGCTCCGGAGATCAAGTGGAT  1210

Query  242   ACTCTGGAGCTTTCAGGAGGTGCCAGGATTAATCG  276
             |||||||||||||||||||||||||||||||||||
Sbjct  1211  ACTCTGGAGCTTTCAGGAGGTGCCAGGATTAATCG  1245
```

Match for Mx2 sequence

PKR
S: GCTCACCGGCGGGATTA
AS: TTCAACTTTATTCATGCGTGCTATG
AS Compliment:
CATAGCACGCATGAATAAAGTTGAA

(D02) Xela-PKR-3-M13For

Description	Max score	Total score	Query cover	E value	Ident	Accession
PREDICTED: Xenopus laevis eukaryotic translation initiation factor 2 alpha kinase 2 L homeolog (eif2ak2.L), transcript variant X6, mRNA	189	189	100%	2e-47	100%	XM_018261547.1
PREDICTED: Xenopus laevis eukaryotic translation initiation factor 2 alpha kinase 2 L homeolog (eif2ak2.L), transcript variant X5, mRNA	189	189	100%	2e-47	100%	XM_018261546.1
PREDICTED: Xenopus laevis eukaryotic translation initiation factor 2 alpha kinase 2 L homeolog (eif2ak2.L), transcript variant X4, mRNA	189	189	100%	2e-47	100%	XM_018261545.1
PREDICTED: Xenopus laevis eukaryotic translation initiation factor 2 alpha kinase 2 L homeolog (eif2ak2.L), transcript variant X3, mRNA	189	189	100%	2e-47	100%	XM_018261544.1
PREDICTED: Xenopus laevis eukaryotic translation initiation factor 2 alpha kinase 2 L homeolog (eif2ak2.L), transcript variant X2, mRNA	189	189	100%	2e-47	100%	XM_018261543.1

PREDICTED: Xenopus laevis eukaryotic translation initiation factor 2 alpha kinase 2 L homeolog (eif2ak2.L), transcript variant X6, mRNA

Sequence ID: XM_018261547.1 **Length:** 1913 **Number of Matches:** 1

Range 1: 1407 to 1508 GenBank Graphics ▼ Next Match ▲ Previous Match

Score	Expect	Identities	Gaps	Strand
189 bits(102)	2e-47	102/102(100%)	0/102(0%)	Plus/Plus

```
Query  1     GCTCACCGGCGGGATTAAAAGAGGAGTATCTCTTCATAGGAATGGAGTGGTGTGAAAAAG  60
             ||||||||||||||||| ||||||||||||||||||||||||||||||||||||||||||
Sbjct  1407  GCTCACCGGCGGGATTAAAAGAGGAGTATCTCTTCATAGGAATGGAGTGGTGTGAAAAAG  1466

Query  61    GAACTTTAGAAAGCTGGATAGCACGCATGAATAAAGTTGAAA  102
             |||||||||||||||||||||||||||||||||||||||||||
Sbjct  1467  GAACTTTAGAAAGCTGGATAGCACGCATGAATAAAGTTGAAA  1508
```

Match for PKR sequence

IkB
S: TATCCGCCGTTCATACAAGGA
AS: GATTTCGTGTTGCTCGGT
AS Compliment:
ACCGAGCAACACGAAATC

(B02) Xela-IkB-1-M13For

Description	Max score	Total score	Query cover	E value	Ident	Accession
Xenopus laevis NFKB inhibitor alpha L homeolog (nfkbia.L), mRNA	183	183	100%	6e-43	100%	gi|148230966|NM_001093529.1
Xenopus tropicalis NFKB inhibitor alpha (nfkbia), mRNA	136	136	99%	8e-29	90%	gi|52345605|NM_001004851.1
Xenopus tropicalis finished cDNA, clone TNeu099d12	136	136	99%	8e-29	90%	gi|77625825|CR760347.2
Xenopus laevis nuclear factor of kappa light polypeptide gene enhancer in B-	132	132	100%	1e-27	89%	gi|148237831|NM_001095781.1
PREDICTED: Pelodiscus sinensis nuclear factor of kappa light polypeptide g	64.4	64.4	62%	4e-07	83%	gi|558137813|XM_006117798.1

Xenopus laevis NFKB inhibitor alpha L homeolog (nfkbia.L), mRNA

Sequence ID: gi|148230966|NM_001093529.1 **Length:** 1562 **Number of Matches:** 1

▶ See 1 more title(s)

Range 1: 414 to 514 GenBank Graphics ▼ Next Match ▲ Previous Match

Score	Expect	Identities	Gaps	Strand
183 bits(202)	6e-43	101/101(100%)	0/101(0%)	Plus/Plus

```
Query  1    TATCCGCCGTTCATACAAGGACCATTGCTACCTGAACAAACAGAATAATCTTCACCAGAC  60
            ||||||||||||||||||||||||||||||||||||||||||||||||||||||||||||
Sbjct  414  TATCCGCCGTTCATACAAGGACCATTGCTACCTGAACAAACAGAATAATCTTCACCAGAC  473

Query  61   AGCACTACATCTGGCAGTAATCACCGAGCAACACGAAATCA  101
            |||||||||||||||||||||||||||||||||||||||||
Sbjct  474  AGCACTACATCTGGCAGTAATCACCGAGCAACACGAAATCA  514
```

Match for IkB sequence

IL-1B
S: CATTCCCATGGAGGGCTACA
AS: TGACTGCCACTGAGCAGCAT
AS Compliment:
ATGCTGCTCAGTGGCAGTCA

(H01) Xela-IL1B-3-M13For

Description	Max score	Total score	Query cover	E value	Ident	Accession
Xenopus laevis interleukin-1-beta, mRNA (cDNA clone MGC:197246 IMAGE	181	181	100%	3e-45	100%	gi|213624007|BC170519.1
Xenopus laevis interleukin-1-beta, mRNA (cDNA clone IMAGE:6954778), pa	181	181	100%	3e-45	100%	gi|62185796|BC092346.1
Xenopus laevis interleukin 1 beta S homeolog (il1b.S), mRNA	176	176	100%	1e-43	99%	gi|148226411|NM_001085605.1
Xenopus laevis IL-1b gene for interleukin 1 beta	91.5	195	100%	5e-18	100%	gi|40644919|AJ314758.1
Xenopus laevis nuclear receptor corepressor 1 S homeolog (ncor1.S), mRN/	33.7	33.7	28%	1.1	86%	gi|1205914820|NM_001088756.3

Xenopus laevis interleukin 1 beta S homeolog (il1b.S), mRNA

Sequence ID: gi|148226411|NM_001085605.1 **Length:** 1462 **Number of Matches:** 1

See 1 more title(s)

Range 1: 91 to 190 GenBank Graphics Next Match Previous Match

Score	Expect	Identities	Gaps	Strand
176 bits(194)	1e-43	99/100(99%)	0/100(0%)	Plus/Plus

```
Query  1    CATTCCCATGGAGGGCTACAGCGGCGACGATGAAATGTTTTACAGTGATAGCCCATCGGG  60
            ||||||||||||||||||| ||||||||||||||||||||||||||||||||||||||||
Sbjct  91   CATTCCCATGGAGGGCTACAGCGGCGACGATGAAATGTTTTACAGTGATAGCCCATCGGG  150

Query  61   AATGAAGGACGACATGGAAGATGCTGCTCAGTGGCAGTCA  100
            |||||||||||||||| ||||||||||||||||||||||
Sbjct  151  AATGAAGGACGACATGGGAGATGCTGCTCAGTGGCAGTCA  190
```

Match for IL-1B sequence

IL-8
S: CCTATCCATCCCAAGCACATAAA
AS: GATATCGTCCCCACTTGTCAAAG
AS Compliment:
CTTTGACAAGTGGGGACGATATC

(A02) Xela-IL8-3-M13For

Description	Max score	Total score	Query cover	E value	Ident	Accession
Xenopus laevis interleukin-8 (IL-8) mRNA, complete cds	185	185	99%	2e-43	100%	gi|329668213|JF412665.1
Xenopus laevis chemokine (C-X-C motif) ligand 8 L homeolog (cxcl8.L), mRN	185	185	99%	2e-43	100%	gi|148237947|NM_001097106.1
PREDICTED: Xenopus laevis interleukin-8-like (LOC108706769), mRNA	156	156	98%	9e-35	94%	gi|1069319714|XM_018243455.1
PREDICTED: Xenopus tropicalis chemokine (C-X-C motif) ligand 8 (cxcl8), m	152	152	99%	1e-33	93%	gi|1062794282|XM_002942532.4
Xenopus tropicalis finished cDNA, clone TTpA077e08	152	152	99%	1e-33	93%	gi|112808130|CU075899.1

Xenopus laevis interleukin-8 (IL-8) mRNA, complete cds

Sequence ID: gi|329668213|JF412665.1 **Length:** 312 **Number of Matches:** 1

Range 1: 127 to 228 GenBank Graphics ▼ Next Match ▲ Previous Match

Score	Expect	Identities	Gaps	Strand
185 bits(204)	2e-43	102/102(100%)	0/102(0%)	Plus/Plus

```
Query  1    CCTATCCATCCCAAGCACATAAAGAATATCGAGATGATCCCTAAAGGGCCCCACTGCAAA  60
            ||||||||||||||||||||||||||||||||||||||||||||||||||||||||||||
Sbjct  127  CCTATCCATCCCAAGCACATAAAGAATATCGAGATGATCCCTAAAGGGCCCCACTGCAAA  186

Query  61   AACGTGGAAGTCATTGCAACTTTGACAAGTGGGGACGATATC  102
            ||||||||||||||||||||||||||||||||||||||||||
Sbjct  187  AACGTGGAAGTCATTGCAACTTTGACAAGTGGGGACGATATC  228
```

Match for IL-8 sequence

TNFa
S: TGTCAGGCAGGAAAGAAGCA
AS: CAGCAGAGCAAAGAGGATGGT
AS Compliment:
ACCATCCTCTTTGCTCTGCTG

(E02) Xela-TNFa-3-M13For

Description	Max score	Total score	Query cover	E value	Ident	Accession
Xenopus laevis tumor necrosis factor L homeolog (tnf.L), mRNA	183	183	100%	6e-43	100%	gi|168693468|NM_001114778.1
Xenopus tropicalis tumor necrosis factor (tnf), mRNA	159	159	100%	7e-36	95%	gi|165973355|NM_001113671.1
PREDICTED: Xenopus laevis tumor necrosis factor-like (LOC108700235), m	141	141	100%	2e-30	91%	gi|1069387308|XM_018233255.1
PREDICTED: Sorghum bicolor DDB1- and CUL4-associated factor homolog	44.6	44.6	28%	0.40	93%	gi|1205965230|XM_021463187.1
PREDICTED: Sorghum bicolor DDB1- and CUL4-associated factor homolog	44.6	44.6	28%	0.40	93%	gi|1205965229|XM_002448784.2

Xenopus laevis tumor necrosis factor L homeolog (tnf.L), mRNA

Sequence ID: gi|168693468|NM_001114778.1 **Length:** 965 **Number of Matches:** 1

See 1 more title(s)

Range 1: 105 to 205 GenBank Graphics Next Match Previous Match

Score	Expect	Identities	Gaps	Strand
183 bits(202)	6e-43	101/101(100%)	0/101(0%)	Plus/Plus

```
Query  1    TTGTCAGGCAGGAAAGAAGCAACAGGAATTCCACCTGGCGCTTTGTCAGTATCTGTGCAT  60
            ||||||||||||||||||||||||||||||||||||||||||||||||||||||||||||
Sbjct  105  TTGTCAGGCAGGAAAGAAGCAACAGGAATTCCACCTGGCGCTTTGTCAGTATCTGTGCAT  164

Query  61   TCCTGTTATTACTGGGATCCACCATCCTCTTTGCTCTGCTG  101
            |||||||||||||||||||||||||||||||||||||||||
Sbjct  165  TCCTGTTATTACTGGGATCCACCATCCTCTTTGCTCTGCTG  205
```

Match for TNFa sequence